Subleading effects of soft emissions

J.S. Sinninghe Damsté

Subleading effects of soft emissions

A study of next-to-leading power threshold corrections to scattering amplitudes

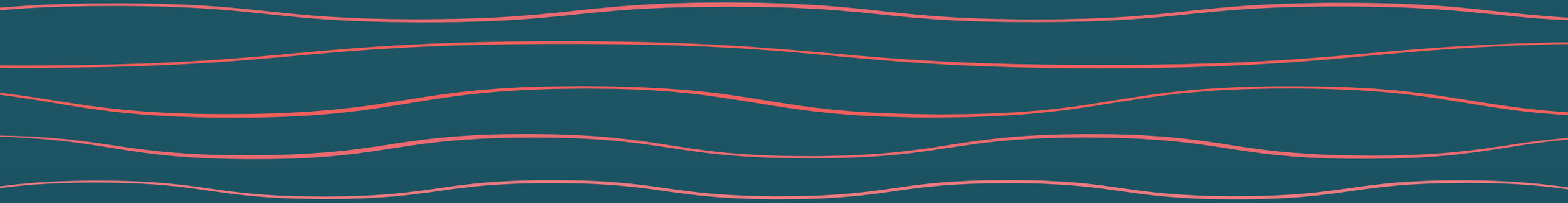

Jort Smede Sinninghe Damsté

Subleading effects of soft emissions

A study of next-to-leading power threshold corrections to scattering amplitudes

ACADEMISCH PROEFSCHRIFT

ter verkrijging van de graad van doctor
aan de Universiteit van Amsterdam
op gezag van de Rector Magnificus
prof. dr. ir. K.I.J. Maex
ten overstaan van een door het College voor Promoties ingestelde comissie,
in het openbaar te verdedigen in de Agnietenkapel
op dinsdag 14 september 2021, te 12.00 uur

door

Jort Smede Sinninghe Damsté

geboren te Schagen

Promotiecommissie

Promotor:	prof. dr. E.L.M.P Laenen	Universiteit van Amsterdam
Copromotor:	dr. W.J. Waalewijn	Universiteit van Amsterdam
Overige leden:	prof. dr. S.C.M. Bentvelsen	Universiteit van Amsterdam
	prof. dr. P.J.G. Mulders	Vrije Universiteit Amsterdam
	dr. M.E.J. Postma	Nikhef
	prof. dr. W.J.P. Beenakker	Universiteit van Amsterdam
	prof. dr. L. Magnea	Università di Torino
	dr. J. de Vries	Universiteit van Amsterdam

Faculteit der Natuurwetenschappen, Wiskunde en Informatica

ISBN:	978 94 6419 269 8
NUR:	925
Geprint door:	Gildeprint - Enschede

Dit werk is ondersteund door het D-ITP consortium, een programma van de Nederlandse Organisatie voor Wetenschappelijk Onderzoek (NWO) gefinancierd door het ministerie van Onderwijs, Cultuur en Wetenschap (OCW). Het promotieonderzoek beschreven in dit proefschrift werd verricht aan de Universiteit van Amsterdam, alsmede aan het Nationaal instituut voor subatomaire fysica (Nikhef).

UNIVERSITEIT VAN AMSTERDAM

Nikhef

Delta Institute for Theoretical Physics

NWO

Contents

List of publications

[1] N. Bahjat-Abbas, J. Sinninghe Damsté, L. Vernazza, and C. D. White, *On next-to-leading power threshold corrections in Drell-Yan production at N^3LO*, *JHEP* **10** (2018) 144, [arXiv:1807.09246].
(Chapter 3)

[2] N. Bahjat-Abbas, D. Bonocore, J. Sinninghe Damsté, E. Laenen, L. Magnea, L. Vernazza, and C. White, *Diagrammatic resummation of leading-logarithmic threshold effects at next-to-leading power*, *JHEP* **11** (2019) 002, [arXiv:1905.13710].
(Chapter 4)

[3] E. Laenen, J. Sinninghe Damsté, L. Vernazza, W. Waalewijn, and L. Zoppi, *Towards all-order factorization of QED amplitudes at next-to-leading power*, *Phys. Rev. D* **103** (2021) 034022, [arXiv:2008.01736].
(Chapter 2)

[4] M. van Beekveld, E. Laenen, J. Sinninghe Damsté, and L. Vernazza, *Next-to-leading power threshold corrections for finite order and resummed colour-singlet cross sections*, *JHEP* **05** (2021) 114, [arXiv:2101.07270].
(Chapter 5)

Chapter 1

Introduction

The boundless curiosity and steady persistence of generations of scientists have resulted in a deep understanding of the world around us. In particle physics these efforts have culminated in a theoretical framework that is elegant and concise, yet capable of describing the varied interactions of matter at the smallest length scales and their often complicated outcomes. In this so-called standard model of particle physics (SM) (a product of the seminal papers [5–8]), all fundamental particles are described in terms of quantum fields, and their interactions are dictated by gauge symmetry.

The model has remarkably few constituents: it distinguishes only a dozen matter particles, four distinct force carriers and the Higgs field.[1] The first category, the fermions, is divided up into three generations of quarks and leptons. The first of these generations contains the most familiar particles, the u- and d-quarks that form protons and neutrons, as well as the electron (e) and its associated neutrino (ν_e), while the second and third generation contain more exotic copies of these. The dynamics of these quantum fields are described by the Lagrangian. In addition to being Lorentz invariant it must be invariant under local gauge transformations, which requires the introduction of gauge fields. This gauge symmetry is a composite of the transformation groups SU(3) and $\mathrm{SU(2)_L} \times \mathrm{U(1)_Y}$, describing quantum chromodynamics (QCD) and electroweak theory respectively. The associated force field, or gauge boson, for the former is the gluon (g), governing the interaction between quarks. The electroweak sector is intertwined with the Higgs field, which is responsible for the spontaneous breaking of the sector's initial symmetry, by attaining a vacuum expectation value (VEV). The residual symmetry group $\mathrm{U(1)_Q}$ describes quantum electrodynamics (QED), with the photon (γ) as gauge boson. In this process, known in full as the Englert-Brout-Higgs-Guralnik-Hagen-Kibble mechanism [9–14], the $W^{\pm}$ and Z bosons associated to the weak interaction obtain masses, while the photon remains massless. In addition, the VEV of the Higgs field gives rise to masses for all matter fields, through Yukawa couplings to fermions.[2] A prediction of this mechanism is the existence of the scalar Higgs boson as the excitation of the field, which was discovered half a century later in the ATLAS and CMS detectors at

[1] This counting excludes anti-particles, which are obtained from their siblings upon the inversion of charges.
[2] Except perhaps the neutrinos, which may get part of their mass from Majorana mass terms.

the Large Hadron Collider (LHC) at CERN [15, 16]. With this spectacular discovery, the standard model is complete.

This intricate yet solid framework enables one to make precise predictions for many observables that can be tested at the LHC or in other experiments (see ref. [17] for an extensive review). The most successful prediction is arguably the value of the anomalous magnetic dipole moment $(g-2)$ of the electron. The theoretical value, relying in part on QED corrections up to five-loops [18], is still consistent with the experimentally measured value [19], with a deviation appearing only in the tenth digit. At the same time high precision experiments are the testing ground for physics *beyond* the standard model (BSM); we are after all aware of phenomena that are not explained within the SM. An important example is baryogenesis, the process in the early universe leading to the observed asymmetry between matter and anti-matter, which requires stronger CP violation than the SM can provide.[3] A second example is the apparent abundance of an invisible form of matter, dark matter (DM), needed to explain an array of astronomical observations. A vast number of different models have been proposed to explain the nature and origin of DM, almost all requiring BSM particles.

In collider experiments a signal for a new particle may emerge as a resonance, provided it is light enough to be produced on-shell. Because of the lack of such clear signals at the LHC after the discovery of the Higgs boson, we must resort to a less direct method for finding new physics effects, namely via loops. In these virtual quantum corrections to scattering processes a new particle would enter regardless of its mass as it is not physically produced (i.e. part of the observable final state), but can still leave an imprint by altering the observables tied to that process, e.g. the production rate of a certain particle as a function of one or more variables. A careful comparison of predictions for such observables from the SM and experimental measurements, as for the value of $g-2$, may thus lead to the discovery of new physics, on the condition that the observed discrepancy is significant. To this end, it is key to have small experimental error margins as well as precise and accurate predictions from theory.

1.1 Challenges for theory predictions

In QED, we may improve predictions by including perturbative corrections to the process at hand, since the coupling e is usually small for the typical energy scale of the process. The coupling strength increases slowly with the scale, and becomes non-perturbative only at extremely high energy scales that are irrelevant for collider physics (the Landau pole, the singularity point of the coupling, lies around 10^{286} eV). Successive corrections are suppressed by increasing powers of the structure constant $\alpha = e^2/4\pi$ (in natural units), such that the inclusion of the first one or two orders in this (asymptotic) series often yields a satisfying result.

[3] CP symmetry implies that the laws of physics are invariant under combined charge conjugation (C) and parity inversion (P). The violation of this symmetry is one of the three so-called Sakharov conditions [20].

For QCD interactions the transition from the non-perturbative to the perturbative regime does lie in the energy range that is probed in collider experiments. The *running* of the coupling is described by the renormalisation group equation (RGE)

$$\mu_R^2 \frac{d\alpha_s(\mu_R^2)}{d\mu_R^2} \equiv \beta(\alpha_s) = -\alpha_s^2(\mu_R^2) \sum_{i=0}^{\infty} b_i \, \alpha_s^i(\mu_R^2), \tag{1.1}$$

which can be solved order by order in α_s. This dependence on the scale at which the coupling is measured has its origin in the renormalisation of the theory, a standard procedure in all quantum field theories in which ultraviolet (UV) divergences, due to the unbounded momentum flow in loop diagrams, are absorbed in the (unobservable) parameters of the Lagrangian. This allows for the computation of finite quantities, but does result in a coupling that depends on the renormalisation scale μ_R.

The interesting consequences this has for the behaviour of QCD are already revealed by considering just the one-loop β-function coefficient b_0. It is given by

$$b_0 = \frac{11C_A - 4\,n_f\,T_R}{12\pi}, \tag{1.2}$$

for n_f active quarks (i.e. roughly those with masses $m < \mu_R$). In the SM $n_f \leq 6$, while $C_A = 3$ and $T_R = 1/2$ for SU(3), such that b_0 is positive. This means that the coupling strength *decreases* with increasing scale, eventually leading to a regime in which quarks and gluons (partons) are asymptotically free [21, 22]. The one-loop solution to eq. (1.1) can be expressed as

$$\alpha_s(\mu_R^2) = \frac{1}{b_0 \ln \frac{\mu_R^2}{\Lambda_{QCD}^2}} \qquad \text{with} \qquad \Lambda_{QCD} = \mu_0 \exp\left[-\frac{1}{2b_0\,\alpha_s(\mu_0^2)}\right], \tag{1.3}$$

showing explicitly the Landau pole at $\mu_R = \Lambda_{\text{QCD}}$, where α_s becomes singular. This scale is determined by measuring the coupling constant at some reference scale μ_0, e.g. the mass of the Z boson. Λ_{QCD} turns out to be of the order of the pion mass, the lightest QCD bound state. Thus, partons interact strongly in the low-energy regime and are confined to hadrons and mesons. The initial state in hadron colliders such as the LHC is therefore highly non-perturbative.

However, the fast-moving beams in colliders and the relative emptiness of a hadron imply that scattering occurs only between individual partons, as is understood since the early days of the parton model [23, 24]. The energy scale Q associated to such partonic scattering is, due to the set-up of the experiment, much higher than the dynamical scale m_p of hadron interactions. This means that hard scattering of partons takes place on a timescale much smaller than interactions internal to each hadron, $1/Q \ll 1/m_p$, such that hadrons, as compound quark and gluon states, are comparatively static from each others perspective. This separation of scales allows for the *factorisation* of cross sections for processes like $p+p \to X$

(for proofs of factorisation see refs. [25–27]):

$$\sigma_{pp\to X}(\tau,\mu_F,\mu_R)=\sum_{i,j}\int_0^1 dx_1\, f_i(x_1,\mu_F)\int_0^1 dx_2\, f_j(x_2,\mu_F)\,\hat{\sigma}_{ij\to X}(Q,\mu_F,\mu_R)\,\delta\left(\tau-x_1\,x_2\right), \tag{1.4}$$

where $f_i(x,\mu_F)$ denotes a parton distribution function (PDF) and $\hat{\sigma}$ the partonic cross section. The PDF gives the probability for finding a parton of flavour i in the proton, carrying a fraction x of the proton's momentum in the longitudinal direction. In this way, predictions can be made by calculating the process-dependent partonic cross section perturbatively, while the non-perturbative effects associated with the partons being part of the hadron, are encoded in the universal PDFs that are instead extracted from data. The delta function imposes momentum conservation by relating the momentum fractions of colliding partons to $\tau = Q^2/S$, the ratio of the invariant mass of the final state and the hadron system.[4]

Roughly speaking, the factorisation scale μ_F separates the two regimes: a gluon emission with a transverse momentum $k_T > \mu_F$ would constitute a perturbative correction to the partonic cross section, while for $k_T < \mu_F$ it is regarded as part of the proton structure. It is therefore not surprising that the RGE for PDFs, which describes the dependence on μ_F, is governed by such emissions. This is captured in the DGLAP evolution equation [28–30]

$$\mu_F^2\frac{df_i(x,\mu_F)}{d\mu_F^2}=\sum_j\frac{\alpha_s(\mu_F^2)}{2\pi}\int_x^1\frac{dz}{z}\,P_{ij}(z)\,f_j\left(\frac{x}{z},\mu_F\right), \tag{1.5}$$

where the (DGLAP) splitting function $P_{ij}(z)$ describes the transition of a parton of type j to type i under the emission of a (anti)quark or gluon. Specifically, it gives the probability (density) that in this transition parton i retains a fraction z of the momentum of parton j, while the remaining energy is carried away by the emitted particle, e.g. a gluon for the lowest order splitting function $P_{qq}^{(1)}(z)$. The evolution of PDFs across energy scales therefore mixes PDFs of quarks, antiquarks and gluons.

We will now turn to the partonic cross section in eq. (1.4), which enjoys the schematic, perturbative expansion

$$\hat{\sigma}=c_0+\alpha_s\,c_1+\alpha_s^2\,c_2+\ldots, \tag{1.6}$$

where successive orders are suppressed since $\alpha_s=\alpha_s(\mu_R^2)$ is small for $\mu_R\sim Q$. The determination of the coefficients c_i is achieved through the evaluation of higher order corrections to the leading order (LO) cross section. In addition to the virtual loop corrections mentioned before, one needs to include real emission corrections at the same order.

A consistent evaluation of these corrections typically leads to great improvements over the LO result. The inclusion of the extra diagrams brings the approximation closer to the all-order perturbation theory estimate, thus providing a more *accurate* prediction of the cross

[4] The invariant mass of the hadron system is a collider parameter, whose power is quantified by $\sqrt{S}$. In chapter 5 we shall use $\sqrt{S}=13$ TeV for numerical results, corresponding to the collision energy in Run 2 of the LHC.

section.[5] Meanwhile, it reduces the prediction's error bands associated to missing higher order corrections. These bands are obtained by varying the factorisation and renormalisation scale (μ_F and μ_R) around the typical scale for the process. In principle, the final result for a physical observable, such as a hadronic cross section, should not depend on either of these scales, since they are introduced for calculational convenience only. Because the perturbative series is truncated at some order, some scale dependent terms will remain, as they are not cancelled by the omitted, higher order contributions. The residual scale dependence therefore probes the size of perturbative corrections beyond the order at which one works, and is commonly used as an estimate of the uncertainty in the theoretical prediction. Computing higher order corrections therefore improves the *precision* of a prediction, too. For many processes and observables next-to-leading order (NLO) or next-to-next-to-leading order (NNLO) predictions are available, with some exceptional results at N^{3}LO, such as the total cross section for single Higgs [31, 32] and Drell-Yan [33] production.

It should be stressed that the validity of the perturbative series in eq. (1.6) relies critically on the implicit assumption that the coefficients c_i are small: if for $\alpha_s \sim 1/10$ the coefficients would scale as $c_i \sim 10^i$, all terms in the series are equally important. In many situations, this is indeed a concern because the coefficients c_i depend on the kinematics of the process and contain logarithms that grow large in certain kinematics limits. Ultimately these contributions are due *soft* and *collinear* singularities, the notion of which is best illustrated with an example.

Consider the emission of an on-shell gluon from a propagating, high-energetic quark with mass m emerging from a hard scattering process H, as shown in fig. 1.1a. The propagator's denominator is given by

$$\frac{1}{(p+k)^2 - m^2} = \frac{1}{2p^0k^0\left(1 - \sqrt{1 - \frac{m^2}{p_0^2}}\cos\theta\right)}, \tag{1.7}$$

where θ is the angle between the spatial momenta $\boldsymbol{p}$ and $\boldsymbol{k}$. Clearly, the propagator divergences in the limit that the photon is low-energetic ($k^0 \to 0$), known as the soft singularity. Additionally we find a singularity for $\theta \to 0$, that is when the photon is emitted parallel, or collinear, to the quark, provided $m = 0$. Since massless quarks are an otherwise convenient and excellent approximation in many QCD calculations, higher order corrections to amplitudes are beset by such infrared (IR) singularities.[6]

To obtain mathematically well-defined results from theories that give rise to singularities

[5] Admittedly, the full calculation of an all-order quantity in perturbation theory is a Platonic Ideal, but for most practical purposes an evaluation of the first few orders suffices to align predictions with experimental data.

[6] For the five lightest quarks $m = 0$ is an often useful approximation since the masses are negligible compared to the typical energy scale at colliders, but for the top quark this is not manifest. This inspired the infinite top mass approximation in which the theory consists of five massless quarks, $n_f = 5$, while the top quark is *integrated out* (it is no longer regarded as a dynamical quantity in the theory), giving rise to effective vertices such as ggh. In some instances also bottom mass effects are taken into account, but in this thesis we adhere to the scheme explained above.

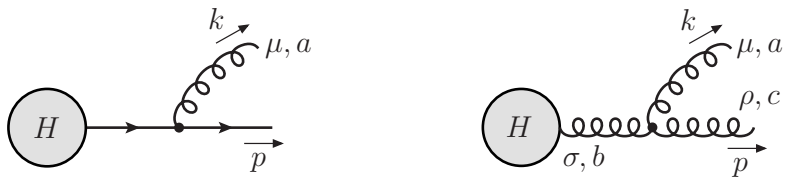

Figure 1.1: *The emission of soft gluon from a highly energetic quark (a) or gluon line (b) extending from a hard interaction H.*

in four-dimensional space-time, we rely on dimensional regularisation. This means that calculations are performed in $d = 4-2\epsilon$ dimensions instead, such that singularities show up as explicit poles in ϵ. This procedure is commonly applied for both IR and UV divergences, where for the latter the resulting poles can subsequently be removed from physical quantities by renormalisation. In this thesis we focus on IR physics and often work with unrenormalised quantities. The origin of a particular pole ϵ may, depending on the context, thus be unclear from the expression alone. In those instances we shall elucidate the singular structure.

According to the Kinoshita-Lee-Nauenberg (KLN) theorem [34, 35], quantum mechanical transition probabilities are IR finite provided one sums over a set of degenerate states. For scattering processes this set is obtained by considering all possible final-state cuts of diagrams contributing to the cross section. In practice this means that all IR poles caused by real and virtual emissions from final state particles cancel, order by order in perturbation theory. For initial state radiation, there will be one residual collinear pole per order in α_s left in the partonic cross section, as the initial state is non-degenerate. With this understanding one may define renormalised PDFs, in which these poles are absorbed, rendering the partonic cross section free of explicit divergences. This procedure is known as mass factorisation.

Even though the partonic cross section then no longer contains explicit poles, the singularities still leave an imprint on the cross section in the form of potentially large logarithms. These terms signal that the real and virtual contributions do not cancel each other entirely, as the phase space for a real gluon emission is limited by the invariant mass of the LO final state, contrary to virtual corrections. They grow large in case the initial state contains just enough energy to produce the particle(s) in LO final state (i.e. it is produced at threshold), since in that case little energy is left for additional radiation, restricting the available phase space even further. The production of the final state near threshold thus forces additional radiation to be soft, which in turn leads to large *threshold logarithms*. In section 1.3 we will discuss the origin of these terms in more detail.

The occurrence of these large logarithms at every order in perturbation theory jeopardises the convergence of the series in eq. (1.6).[7] For observables plagued by these terms, mean-

[7] Note that, depending on the process and observable, other types of logarithms may play a role instead. Examples are the q_T-distribution (transverse momentum) of a final state particle that is plagued by $\log(q_T^2/Q^2)$ terms (with Q the hard scale), and mass effects leading to potentially large $\log(m/Q)$ terms.

ingful predictions can only be obtained if the logarithmic contributions are summed to all orders in α_s. Such *resummed* results may be obtained in a variety of ways, but central to each approach is a simplification of the dynamics causing successive perturbative orders to have a predictable form. In section 1.2 we will introduce the *(next-to-)eikonal approximation* and give a first impression of how this simplification allows for all-order results.

1.2 The (next-to-)eikonal approximation

In the eikonal (E) approximation [36], one expands an amplitude in soft gauge boson momenta and retains only the leading power (LP) terms. A natural improvement is to keep next-to-leading power (NLP) terms as well, which is then, unsurprisingly, referred to as the next-to-eikonal (NE) approximation. To illustrate this, we return to the amplitude depicted in fig. 1.1a, where a high-energetic fermion emanating from a hard scattering process H emits a soft gluon, which for the sake of generality is taken off-shell. Expanding the amplitude in the soft gluon's momentum k^μ yields

$$\begin{aligned}\mathscr{M}^\mu(p,k) &= \bar{u}(p)(ig_s t^a\gamma^\mu)\frac{i(\not{p}+\not{k})+m}{(p+k)^2-m^2}H(p+k)\\ &= -\bar{u}(p)(g_s t^a)\left[\frac{p^\mu}{p\cdot k}+\frac{\gamma^\mu\not{k}}{2p\cdot k}-\frac{p^\mu k^2}{2(p\cdot k)^2}+\dots\right]H(p+k)\,,\end{aligned} \tag{1.8}$$

where the ellipsis denotes terms suppressed by even higher powers of k. When an soft emitted boson is described at NE accuracy, it is sometimes called *next-to-soft* in the literature. This nomenclature is also used sporadically in this thesis. We may express the first NE term in a slightly different way and find

$$\mathscr{M}^\mu_{\mathrm{NE}}(p,k) = -\bar{u}(p)(g_s t^a)\left[\frac{p^\mu}{p\cdot k}-\frac{1}{2}\frac{p^\mu k^2}{(p\cdot k)^2}+\frac{1}{2}\frac{k^\mu}{p\cdot k}+\frac{ik_\nu\Sigma^{\nu\mu}}{p\cdot k}\right]H(p+k)\,. \tag{1.9}$$

If the (next-to-)soft gluon is emitted from a hard gluon line instead, as shown in fig. 1.1b, the NE approximation gives

$$\begin{aligned}\mathscr{M}^\mu_{\mathrm{NE}}(p,k) = -(ig_s f^{abc})\Bigg[&\left(\frac{p^\mu}{p\cdot k}-\frac{1}{2}\frac{p^\mu k^2}{(p\cdot k)^2}+\frac{1}{2}\frac{k^\mu}{p\cdot k}\right)\epsilon^*(p)\cdot H(p+k)\\ &+\frac{ik_\nu(M^{\nu\mu})_{\rho\sigma}}{p\cdot k}\epsilon^{\rho *}(p)H^\sigma(p+k)\Bigg].\end{aligned} \tag{1.10}$$

Eq. (1.9) and eq. (1.10) contain the Lorentz generator for spin one-half and spin one particles respectively, which are defined as

$$\Sigma^{\nu\mu}=\frac{i}{4}[\gamma^\nu,\gamma^\mu] \qquad \text{and} \qquad (M^{\nu\mu})_{\rho\sigma}=i\left(\delta^\nu_\rho\delta^\mu_\sigma-\delta^\mu_\rho\delta^\nu_\sigma\right). \tag{1.11}$$

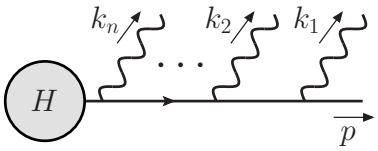

Figure 1.2: *Subsequent emission of n soft photons from a hard fermion.*

We see a clear similarity between the two expressions in eqs. (1.9) and (1.10). Aside from the different colour factor, we note that the eikonal term is in fact identical, showing that a (strictly) soft gluon is insensitive to the spin of the emitter. By writing $p^\mu = |p|n^\mu$, we note a further simplification as the magnitude of the momentum four-vector p^μ cancels between numerator and denominator in this term. In the eikonal approximation the soft gluon is thus only sensitive to the direction n^μ of the emitters momentum. Together with the observed spin independence, we may interpret this as the inability of a soft gluon to resolve any emitter structure, due to its long wavelength. At next-to-leading power we see that the terms become again sensitive to the size of p^μ, such that subsequent emissions start to influence one another by momentum conservation and the emitter recoils. In addition, the last term in both expressions does depend on the spin of the emitter, as signaled by the respective Lorentz generators.

To illustrate the benefits of the simplified dynamics, we study the emission of multiple soft photons. For the emission of n soft photons from a hard fermion line (depicted in fig. 1.2) the amplitude simplifies to[8]

$$\mathscr{M}_{\mathrm{E}}^{\mu_1\cdots\mu_n}(p,k_i) = \bar{u}(p)\, e^n \frac{n^{\mu_1}}{n\cdot k_1}\frac{n^{\mu_2}}{n\cdot(k_1+k_2)}\cdots\frac{n^{\mu_n}}{n\cdot(k_1+\cdots+k_n)} H(p+k_1+\cdots+k_n)\,. \quad (1.12)$$

Note that we consider only the amplitude for a particular ordering of the momentum insertions, while at order e^n there are $n!$ permutations possible. We denote the effect of a certain permutation π on the momentum k_i by $k_{\pi(i)}$. By Bose symmetry all such permutations must contribute equally, therefore we express eq. (1.12) as

$$\begin{aligned}\mathscr{M}_{\mathrm{E}}^{\mu_1\cdots\mu_n}(p,k_i) = \bar{u}(p)\,H(p)\,e^n \prod_{i=1}^{n} n^{\mu_i} \\ \times \frac{1}{n!}\sum_{\pi}\frac{1}{n\cdot k_{\pi(1)}}\frac{1}{n\cdot(k_{\pi(1)}+k_{\pi(2)})}\cdots\frac{1}{n\cdot(k_{\pi(1)}+\cdots+k_{\pi(n)})}\,,\end{aligned} \quad (1.13)$$

where we also drop the dependence of the hard scattering amplitude H on k_i, since we work strictly at LP accuracy. Note that the hard scattering amplitude is now entirely separated from the remainder of the amplitude, which describes the soft emissions. Such a *factorisation* of the amplitude or partonic cross section into *hard* and *soft functions* is key to resummation efforts, and will be frequently observed in what follows.[9] Application of the

[8] For simplicity, we have set the fermions charge $Q = -e$, with e the elementary charge.

[9] Given the initial factorisation of the hadronic cross section into PDFs and the partonic cross section, a further separation of scales in the latter is also referred to as *re*-factorisation.

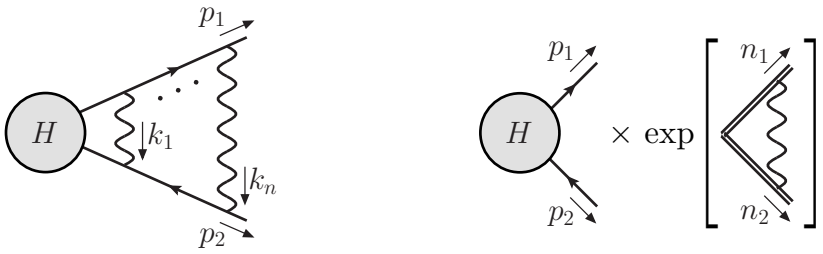

Figure 1.3: *Virtual corrections due to the exchange of n-soft photons between hard fermion* ***(a)****. In the eikonal limit the amplitude factorises into a hard part and a soft factor. Upon summation over all perturbative orders the latter assumes an exponential form depending on the eikonal one-loop contribution only* ***(b)****.*

eikonal identity [37]

$$\sum_{\pi} \frac{1}{n\cdot k_{\pi(1)}} \frac{1}{n\cdot(k_{\pi(1)}+k_{\pi(2)})} \cdots \frac{1}{n\cdot(k_{\pi(1)}+\cdots+k_{\pi(n)})} = \prod_{i=1}^{n} \frac{1}{n\cdot k_i}\,, \tag{1.14}$$

yields

$$\mathscr{M}_{\mathrm{E}}^{\mu_1\cdots\mu_n}(p,k_i) = \bar{u}(p)H(p)\frac{1}{n!}\prod_{i=1}^{n} e\frac{n^{\mu_i}}{n\cdot k_i}\,, \tag{1.15}$$

which makes the decorrelation of the eikonal emissions manifest.

This decoupling is achieved on every fermion leg that may extend from the hard interaction. Therefore, the n-loop virtual amplitude depicted in fig. 1.3a, when summed over all permutations of the exchanged photons, simplifies in the eikonal approximation to

$$\mathscr{M}_{\mathrm{E,\,tot.}}^{(n)}(p_1,p_2) = \bar{u}(p_1)H(p_1,p_2)v(p_2)\frac{1}{n!}\prod_{i=1}^{n}\left(-i\,e^2\right)\int\frac{d^dk_i}{(2\pi)^d}\frac{1}{k_i^2}\frac{1}{n_1\cdot k_i}\frac{1}{n_2\cdot k_i}\,. \tag{1.16}$$

The light-like vectors n_1^μ and n_2^μ denote the direction of the momenta p_1^μ and p_2^μ, and are normalised to $n_1\cdot n_2 = 1$. We note that the expression consists of n-powers of a decoupled one-loop expression, as all momenta k_i are integrated over, and drop the subscript i. Now, a particularly elegant all-order expression can be obtained by summing over all perturbative orders:

$$\begin{aligned}\mathscr{M}_{\mathrm{E}}^{\mathrm{all-order}}(p_1,p_2) &= \bar{u}(p_1)H(p_1,p_2)v(p_2)\sum_{n=0}^{\infty}\frac{1}{n!}\left[-i\,e^2\int\frac{d^dk}{(2\pi)^d}\frac{1}{k^2}\frac{1}{n_1\cdot k}\frac{1}{n_2\cdot k}\right]^n \\ &= \bar{u}(p_1)H(p_1,p_2)v(p_2)\exp\left[-i\,e^2\int\frac{d^dk}{(2\pi)^d}\frac{1}{k^2}\frac{1}{n_1\cdot k^2}\frac{1}{n_2\cdot k}\right].\end{aligned} \tag{1.17}$$

Thus, in the eikonal limit, the soft function assumes an exponential form, allowing one to express the all-order amplitude in terms of a one-loop quantity, see also fig. 1.3b. The simplification of the dynamics thus leads to an impressive increase of the predictive power of the theory. In QCD one must be cautious in re-ordering attachments due to the non-abelian

nature of the theory, but this result may nevertheless be generalised using *webs* [38–40]. A more recent proof of exponentiation using webs relies on the *replica-trick* [41], which forms the basis for the application of webs in a multi-parton scattering context [42, 43]. We will discuss this in more detail in chapter 4. In addition, we will see there that the phase-space integration is also simplified in the eikonal approximation, such that an all-order form for real corrections to cross sections can be derived in a similar fashion.

This exponentiation property thereby lies at the very basis of the resummation of the problematic threshold logarithms, at least at leading power. At the NE level, when NLP corrections are taken into account, the picture becomes somewhat more complicated. However, given that at this level of accuracy important physical aspects are starting to be included in the approximation, one may hope that an NLP description of cross sections offers a significant improvement over a LP one, while maintaining some of the advantages offered by the simplified dynamics. In this thesis we will explore in different contexts the feasibility and importance of providing such NLP descriptions.

1.3 A closer look at threshold logarithms

We shall now elucidate the origin of threshold logarithms with a simple example. We consider a radiative correction to the Drell-Yan (DY) process [44], which is the hadronic production of a lepton pair, via an intermediary vector boson. At LO the partonic interaction is induced by a quark-antiquark pair, and we may take the vector boson to be an off-shell photon. The leptonic part of the process is often neglected in the context of QCD, where only the coloured initial state is susceptible to corrections. Unless stated otherwise, DY thus refers to the (LO) partonic interaction $q(p_1) + \bar{q}(p_2) \to \gamma^*(Q)$. The real correction consists of a gluon that is radiated from either of the quark lines and enters the final state, as shown in fig. 1.4. As we are interested in the structure of threshold logarithms, we impose that the emitted gluon is soft, and apply the NE approximation discussed above.

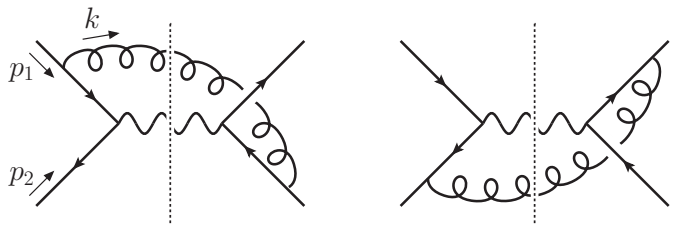

Figure 1.4: *Single real contributions to the DY process. The (conjugate) amplitude is depicted on the left (right) hand side of the final state cut, as indicated by the dashed line. Diagrams in which the gluon attaches to the same fermion leg contribute only at NNLP and are therefore not shown.*

Instead of the full cross section we calculate the *K-factor*, which is the ratio of the higher order cross section (in this case the real contribution to the NLO correction) to the LO cross section. In this way factors relating to the production of the off-shell photon are

divided out, which is convenient since we are mostly interested in the effect of the QCD correction. Finally, we shall work in $d = 4$ dimensions and deal with explicit divergences in an alternative way, to paint a more intuitive picture. In chapter 4 a similar calculation is presented in full, using dimensional regularisation. The real NLO *K*-factor is obtained by integrating the (approximated) squared-amplitude over the gluon's phase space

$$K^{(1)}_{\mathrm{R,NE}} = g_s^2 C_F \int \frac{d^4k}{(2\pi)^3} \frac{s - 2(p_1\cdot k + p_2\cdot k)}{p_1\cdot k\, p_2\cdot k}\, \delta_+(k^2)\, \delta\left(1 - z - \frac{2k\cdot(p_1+p_2)}{s}\right). \tag{1.18}$$

The Dirac delta functions impose the on-shell condition of the emitted gluon and momentum conservation. We have introduced the Mandelstam variable $s = (p_1+p_2)^2 = 2p_1\cdot p_2$, denoting the invariant mass of the quark-antiquark pair, and defined the ratio of the invariant mass of the LO final state and the initial state as $z = Q^2/s$. With this notation, the partonic threshold corresponds to $z \to 1$, so we expect threshold logarithms to appear in terms of the *threshold variable* $(1-z)$. We choose to work in the center-of-mass (CM) frame where $p_1^\mu = \frac{\sqrt{s}}{2}(1,0,0,1)$ and $p_2^\mu = \frac{\sqrt{s}}{2}(1,0,0,-1)$, and express the *K*-factor as

$$\begin{aligned}
K^{(1)}_{\mathrm{R,NE}} &= \frac{g_s^2 C_F}{(2\pi)^3} \int_0^\infty dk^0 \int_{-\infty}^\infty dk^3 \int_0^{2\pi} d\phi \int_0^\infty d|\boldsymbol{k}_\perp|\,|\boldsymbol{k}_\perp| \frac{s - 2\left(\frac{\sqrt{s}}{2}(k^0+k^3) + \frac{\sqrt{s}}{2}(k^0-k^3)\right)}{\left(\frac{\sqrt{s}}{2}\right)^2 (k^0+k^3)(k^0-k^3)} \\
&\quad \times \delta\left(\left(k^0\right)^2 - \boldsymbol{k}_\perp^2 - \left(k^3\right)^2\right) \delta\left(1 - z - \frac{2k^0}{\sqrt{s}}\right) \\
&= \frac{g_s^2 C_F}{\pi^2} \int_0^\infty dk^0 \int_{-\infty}^\infty dk^3 \int_0^\infty d|\boldsymbol{k}_\perp|\,|\boldsymbol{k}_\perp| \frac{1 - 2\frac{k^0}{\sqrt{s}}}{(k^0)^2 - (k^3)^2} \\
&\quad \times \delta\left(\left(k^0\right)^2 - \boldsymbol{k}_\perp^2 - \left(k^3\right)^2\right) \delta\left(1 - z - \frac{2k^0}{\sqrt{s}}\right),
\end{aligned} \tag{1.19}$$

after integration over the azimuth angle ϕ. Integrating over k^3 and rearranging the remaining delta function yields

$$K^{(1)}_{\mathrm{R,NE}} = \left(\frac{\alpha_s}{4\pi}\right) 8 C_F \sqrt{s} \int_0^\infty \frac{dk^0}{k^0} \int_0^{k^0} d|\boldsymbol{k}_\perp| \frac{1 - 2\frac{k^0}{\sqrt{s}}}{|\boldsymbol{k}_\perp|} \frac{1}{\sqrt{1 - \boldsymbol{k}_\perp^2/(k^0)^2}}\, \delta\left(k^0 - \frac{\sqrt{s}}{2}(1-z)\right), \tag{1.20}$$

where we have extracted the typical coupling factor of $(\alpha_s/4\pi)^n$ for an N^{n}LO calculation. We expect the largest contributions in the limit where the emission is collinear in addition to being soft, i.e. for which $|\boldsymbol{k}_\perp| << k^0$. We expand the square root in this regime and keep only the leading term, which is unity. The divergent integral over $|\boldsymbol{k}_\perp|$, representing the collinear singularity observed in eq. (1.7), needs to be regulated to give an interpretable result. As mentioned before, this is usually done in dimensional regularisation, but since our main aim is to derive the dominant logarithmic dependence, we put here a cut-off on the integral, for which we take μ_F. Resolving the remaining integrals we find

$$K^{(1)}_{\mathrm{R,NE}} = \left(\frac{\alpha_s}{4\pi}\right) 8 C_F \sqrt{s} \int_0^\infty dk^0\, \frac{1 - 2\frac{k^0}{\sqrt{s}}}{k^0} \ln\left(\frac{k^0}{\mu_F}\right) \delta\left(k^0 - \frac{\sqrt{s}}{2}(1-z)\right) \tag{1.21}$$

$$= \left(\frac{\alpha_s}{4\pi}\right) 16 C_F \left\{ \left[\frac{\log(1-z)}{1-z} + \frac{1}{1-z} \log\left(\frac{\sqrt{s}/2}{\mu_F}\right) \right] - \left[\log(1-z) + \log\left(\frac{\sqrt{s}/2}{\mu_F}\right) \right] \right\} .$$

The NE approximation of the single real contribution to the *K*-factor has thus provided us with two classes of logarithms, at LP and NLP in the threshold variable $(1-z)$. Although the NLP term is parametrically suppressed with respect to the LP one, both terms diverge for $z \to 1$.[10] When treated properly in dimensional regularisation, the LP term that regulated the collinear divergence will combine with a similar expression in the virtual part of the *K*-factor, and turn the $1/(1-z)$ pole in to a regulated *plus distribution*.

In general, a partonic cross section expanded in the threshold region will then have the following structure:

$$\frac{d\hat{\sigma}}{dz} = \sum_{n=0}^{\infty} \left(\frac{\alpha_s}{4\pi}\right)^n \left\{ \sum_{m=0}^{2n-1} \left[c_{nm}^{(-1)} \left(\frac{\log^m(1-z)}{1-z} \right)_+ + c_{nm}^{(0)} \log^m(1-z) + \dots \right] + c_n^{(\delta)} \delta(1-z) \right\}. \tag{1.22}$$

At each order in α_s we observe towers of the threshold logarithm at both LP and NLP in $(1-z)$, labeled with coefficient $c_{nm}^{(-1)}$ and $c_{nm}^{(0)}$. The highest power of the logarithm, $m = 2n-1$ at the n-th order in perturbation theory, is generated when all real/virtual emissions are maximally soft and collinear, giving rise to the highest number of logarithmically divergent integrations. In addition, we find contributions localised at threshold, with coefficients $c_n^{(\delta)}$. The plus distributions at LP, denoted by the +-subscript, are now *integrably* divergent, just as the NLP terms. The ellipsis denotes terms suppressed by even higher powers of $(1-z)$, which vanish at threshold.

The problematic nature of LP terms was noted already in the early days of QCD (see for example ref. [45]), and it was quickly realised that the leading logarithm (LL), i.e. $\log^{2n-1}(1-z)$ at $\mathcal{O}(\alpha_s^n)$ in eq. (1.22), could be summed up to all orders in perturbation theory to achieve a well-behaved result near threshold [46, 47]. In the seminal papers [48, 49], soft gluon resummation in DY and deep inelastic scattering (DIS) was extended to sub-leading logarithmic accuracy by means of diagrammatic techniques. References [50, 51] showed that soft radiation can be described in terms of Wilson lines, whose exponentiation properties are at the basis of resummation. Later, by means of similar diagrammatic techniques, resummation was extended to more processes, including those with coloured particles in the final state, see e.g. refs. [52–57]. Soft gluon resummation by means of renormalisation-group techniques was studied in refs. [58–60], and this has more recently also been accomplished using effective field theory techniques, specifically using *Soft-Collinear Effective Theory* (SCET) [61–65], see e.g. refs. [66–73]. By now, resummation of soft gluon radiation at LP has been systematically applied to most processes of interest at lepton and hadron colliders.

Much less research has been devoted to the threshold logarithms occurring at NLP. Historically, the effects of those terms have been though less relevant for phenomenology, but

[10] Note that when z is small instead, and the phase space of the gluon is much less constrained, the contribution of the logarithmically enhanced term $\log(1-z)$ is indeed much smaller.

in recent years interest is growing. In chapter 5 we will see that numerical effects of the NLP threshold logarithms are indeed sizeable for a variety of processes and that the resummation of these terms may be key for the refinement of predictions based on (threshold) resummation.

1.4 Next-to-soft theorems

In section 1.2 we have shown that in the (next)-to-eikonal limit amplitudes simplify considerably. At LP we directly noticed the factorisation of an amplitude into functions describing hard and soft interactions. In case of the virtual n-loop amplitude, the decoupling of subsequent soft photon emissions even led to an all-order expression for the latter function, given in terms of the exponential of the one-loop result. In general, factorisation of amplitudes is key for the resummation of threshold logarithms as it organises the various sources of such terms. At NLP, the factorisation structure may generally be more involved, as we will see in chapter 2. The essence of factorisation, the separation of physical effects at different length/energy scales inside one amplitude, remains however unchanged.

In this section we briefly review some of the early work on the factorisation of amplitudes in the (next-to-)eikonal limit. Besides the intrinsic value of understanding the factorisation properties of amplitudes, the eventual resummation of threshold logarithms is the main motivation for such studies, which is why there is a particular focus on the factorisation of radiative amplitudes. Such formulations are also know as *(next-to-)soft theorems*. In practice, they are often derived from the underlying structure of the non-radiative (purely virtual) amplitude, which at LP takes the following schematic form in the presence of n hard particles (see for instance refs. [74, 75]):

$$\mathscr{M}_n = H_n \times S_n \times \prod_{i=1}^{n} \frac{J_i}{\mathscr{J}_i} \,. \tag{1.23}$$

In this equation the jet and soft functions J_j and S describe long-distance collinear and soft virtual radiation in $\mathscr{M}_n$. These functions are universal, i.e. they depend only on the colour and spin quantum numbers of the external states, and determine also the structure of collinear and soft singularities of the elastic amplitude (see eqs. (2.28) and (2.30) for definitions). The hard function captures the high-energetic, short-distance, interaction, and is an IR finite and process-dependent quantity. Note that one must divide each jet by its eikonal version $\mathscr{J}_i$, to avoid the double counting of soft-collinear divergences. The universality of the soft and (eikonal-)jet function suggests that many different processes may be described within a single factorisation framework, which eventually allows for making resummed predictions in a rather efficient manner.

For radiative amplitudes a similar factorisation takes place. A general scattering amplitude with n highly energetic particles carrying momenta p_i, factorises straightforwardly if the emission is from any of the external legs (see fig. 1.5a). This corresponds to the situation as

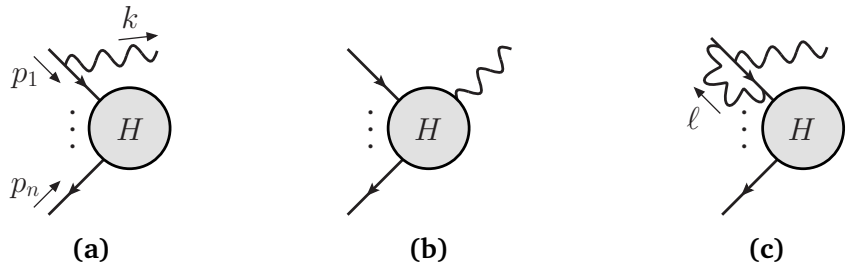

Figure 1.5: *An n-particle scattering amplitude with the emission of an additional soft photon from an external leg (a), from inside the hard scattering (b) or from a collinearly enhanced region (c).*

discussed in section 1.2. For a soft emission from *within* that hard interaction (e.g. when the hard function is loop induced), see fig. 1.5b, the effect of the emission can be expressed in terms of a derivative with respect to the hard momenta p_i acting on the non-radiative function. This is a pure NLP effect, described for massive particles in refs. [76, 77]. Collectively, we will refer to this work as the *LBK theorem*, named after Low, and Burnett and Kroll. Del Duca showed in ref. [78] that this formulation only holds in the region $k^0 \ll m^2/Q$, with Q the centre of mass energy. For $m^2/Q \leq k^0 < m$, the LBK theorem must be extended to account for NLP contributions arising from soft photons emitted from loops in which the exchanged virtual particles have momenta collinear to the external particles.

Fig. 1.5c is a typical example of a diagram that receives such a contribution. Its amplitude is proportional to

$$\begin{aligned}\mathscr{M} &\sim \int \frac{d^d\ell}{(2\pi)^d}\frac{1}{\ell^2}\frac{1}{(\ell+p_1)^2-m^2}\frac{1}{(\ell+p_1-k)^2-m^2} \\ &= \int \frac{d^d\ell}{(2\pi)^d}\int_0^1 dx\int_0^1 dy\,\frac{2x}{[\ell^2-x^2m^2-x(1-x)y\,2p_1\cdot k]^3} \\ &\sim \frac{1}{Q^3}\int \frac{d^d\ell}{(2\pi)^d}\int_0^1 dx\int_0^1 dy\,\frac{2x}{\left[\frac{\ell^2}{Q}-x^2\frac{m^2}{Q}-x(1-x)y\,k^0\right]^3}\,,\end{aligned} \tag{1.24}$$

where we have combined the denominators using the Feynman parameters x and y in the second line, and used $p_1\cdot k \sim Q\,k^0$ in the last line. We see that directly expanding the integrand in the soft photon energy is indeed only safe if $k^0 \ll m^2/Q$. In the massless limit of gauge theories, for which one takes $m/Q \to 0$, an important contribution to this integral arises where $m^2/Q < k^0 \sim \ell^2/Q$. Those virtual collinear modes have a small virtuality, comparable to the energy of the soft photon, while retaining a comparably large momentum component. The resulting contributions are strictly NLP and can be taken into account by a *radiative jet function* [78]. We will give a detailed account of such functions in chapter 2.

The factorisation proposed in ref. [78] was put to the test in ref. [79], where the single-real single-virtual (1R1V) correction to the DY cross section was successfully reproduced at NLP accuracy. This result relies on a one-loop evaluation of the radiative jet function $J_\nu(p_i, k, \bar{n}_i)$,

combined with the central factorisation formula (also valid for off-shell emissions)

$$\mathscr{M}^{\mu}_{(n+1)}(\{p_j\},k) = \sum_{i=1}^{n}\left[q_i\frac{2p_i^{\mu}-k^{\mu}}{2p_i\cdot k-k^2}+q_i G_i^{\nu\mu}\frac{\partial}{\partial p_i^{\nu}}+G_i^{\nu\mu}J_{\nu}(p_i,k,\bar{n}_i)\right]\mathscr{M}_{(n)}(\{p_j\})\,. \quad (1.25)$$

Here $q_i = \pm 1$ for an incoming/outgoing fermion (and vice versa for anti-fermions), while the radiative jet function associated to that leg is further specified by a light-like reference vector $\bar{n}_i^{\mu}$. The partial polarisation tensor $G_i^{\nu\mu}$ is defined through [80]

$$\eta^{\mu\nu} = G^{\mu\nu}+K^{\mu\nu} \qquad \text{with} \qquad K_i^{\mu\nu} = \frac{k^{\mu}(2p_i-k)^{\nu}}{2p_i\cdot k-k^2}\,, \quad (1.26)$$

and is convenient in the derivation of the above result, as the contraction $G_i^{\nu\mu}J_{\nu}(p_i,k,\bar{n}_i)$ is strictly NLP, allowing one to discard k dependence of the hard function at a certain stage. In particular, the one-loop radiative jet function derived in ref. [79] satisfied $G_i^{\nu\mu}J^{(1)}_{\nu}(p_i,k,\bar{n}_i) = J^{(1)}_{\nu}(p_i,k,\bar{n}_i)$, simplifying eq. (1.25) even further. The three different contributions discussed above; emission from either an external leg, from inside the hard function and from a collinearly enhanced region, are thus reflected in the three distinct terms of eq. (1.25). This factorisation framework was later extended to non-abelian theories in ref. [81]. For processes with final state jets the structure is yet more involved, as NLP threshold effects induced by high-energetic final-state radiation come into play [82].

We emphasise that the factorisation formula of eq. (1.25) is based on a LP factorisation picture of the non-radiative amplitude. In order to understand the NLP factorisation properties of the radiative amplitude $\mathscr{M}_{n+1}$ fully, one requires a complete classification of the factorisation structure of the elastic amplitude $\mathscr{M}_n$ at the same level op precision. In chapter 2 we will carry out such a study, again starting for the abelian theory, to put the factorisation of radiative amplitudes on more solid footing.

Other notable contributions to the field include refs. [41, 42, 83], which studied the exponentiation structure of soft radiation at NLP, leading to the notion of *next-to-soft webs*. Moreover, in ref. [84] the universal structure of NLP terms across a range of processes was shown, further shaping our understanding of such terms. In particular, it showed that a next-to-soft emission can be described by applying a kinematic shift to the born level amplitude, while dressing it with an eikonal emission factor. Both developments are key for achieving LL resummation at NLP through diagrammatic methods, as we will see in chapter 4. Finally, we note that there is also a growing body of work on NLP corrections using the SCET formalism. We will comment on corresponding or otherwise relevant SCET studies throughout the subsequent chapters.

1.5 Outline of this thesis

In this thesis we investigate NLP contributions to amplitudes and cross sections, in various ways. In chapter 2, we explore the *all-order* NLP factorisation structure of elastic QED amplitudes and argue, based on a a power-counting analysis, what ingredients are required for such a factorisation. We will see a larger class of (radiative)-jet functions emerge and evaluate contributions from two types as checks on the proposed factorisation formula, at the one- and two-loop level. Indeed, we will see that the factorisation approach presented in that chapter allows for the exact factorisation of amplitudes at NLP, contrary to the formula of eq. (1.25), which only provided compelling results at the cross section level.

In chapter 3 we explore the direction of multiple emissions rather than multiple loops. We do so by calculating the 2R1V correction to Drell-Yan production for the first time at NLP. The method of regions approach employed here allows one to pinpoint the origin of certain threshold logarithms, which provides important data for the future development of factorisation formulae for multi-emission amplitudes.

The results of chapter 3 inspire us, in part, to pursue the resummation of leading-logarithmic terms through an exponentiated *next-to-soft function* in chapter 4. We present an alternative approach as well in which a kinematically shifted cross section needs multiplication by an exponentiated LP soft function only, which may be applied to any colourless n-particle final state. In this fashion, we achieve LL NLP threshold resummation in single Higgs production.

Chapter 5 will explore the numerical effects of NLP terms, both at fixed order and for resummed cross sections. Here we employ the resummation approach developed in chapter 4 for a variety of processes and find that effects of NLP terms are notable. In particular, we see that the inclusion of LL resummation at NLP can have a larger numerical impact than a further improvement of the logarithmic accuracy at LP, e.g. from NNLL' to N3LL.

Due to the somewhat technical character of the work in this thesis, many derivations and ancillary results are presented in appendices to improve readability. For convenience of the reader we have collected the appendices pertaining to a particular chapter at the very end of said chapter. We reflect on the results presented in thesis, as well as on the future research directions they suggest, in chapter 6.

Chapter 2

Towards all-order factorisation of QED amplitudes at NLP

In chapter 1 we noted that beyond LP, a good understanding of the factorisation properties of the non-radiative, or elastic, amplitude is essential in order to describe the factorisation of corresponding radiative amplitudes. The typical example being the radiative jet function [78], which was derived by dressing the LP jet function with a soft emission, and played a key role in the factorisation of the one-loop radiative DY amplitude at NLP accuracy [79]. In this chapter we continue to investigate aspects of factorisation at NLP, and adhere to this philosophy by thoroughly analysing the factorisation structure of the non-radiative amplitude first. In particular, we will focus on the new types of functions that may appear at higher orders in perturbation theory. Given this premise, our first task is thus to determine the analogue of eq. (1.23) at NLP. In the absence of soft radiation, the elastic amplitude would only depend on hard scales. Therefore, following ref. [85], we will first consider the external fermions to have a parametrically small mass m, providing us with a variable for the power expansion. We derive the power counting in section 2.1, which we then generalise to the case of massless particles, and obtain an all-order NLP factorisation formula. In either case new, universal jet functions are required at the NLP level, consisting of *multiple* collinear particles that probe the hard scattering process.

We note that factorisation theorems for amplitudes or cross sections involving soft emissions have also been studied within SCET [61–65]. SCET describes the soft and collinear limits of QCD as separate degrees of freedom, each with their own fields and Lagrangian. An elastic amplitude is encoded in terms of effective n-jet operators and their corresponding short-distance coefficients, which capture the contribution from hard loops. At LP, soft emissions from hard particles can be described by Wilson lines, as in the diagrammatic approach considered throughout this thesis. Beyond LP, these soft emissions follow from time-ordered non-local operators made out of soft and collinear fields, where the power suppression follows either from additional insertions of the power-suppressed soft and collinear Lagrangian, or from subleading operators describing the hard scattering. Within SCET

it is possible to define matrix elements that are equivalent to the radiative jets of the diagrammatic approach [86–88]. Several investigations regarding power corrections have been conducted within SCET, including but not limited to soft gluon corrections, such as studies of the anomalous dimension of power-suppressed operators [89–91], the basis of power-suppressed hard-scattering operators for several processes [92–95] and the application to subtractions at fixed order [96–102]. SCET provides a systematic approach, as each operator and Lagrangian term have by construction a definite power counting. When all operators are included that are consistent with symmetries up to the desired power, this completeness ensures that the resulting factorisation is valid to all orders in the coupling constant. Consequently, factorisation can, at least formally, be extended beyond NLP, by adding more power-suppressed operators.

On the other hand, the diagrammatic approach is often more intuitive compared to the full effective field theory treatment, and also offers a way (as we will see in this chapter) to address so-called endpoint singularities in convolution integrals. These convolutions between ingredients in the factorisation are only well-defined in dimensional regularisation. This poses a challenge for SCET, where one first renormalises each ingredient in the factorisation theorem to derive the renormalisation group equations needed for resummation, causing these convolution integrals to become divergent. (However see refs. [103–105] for recent progress in addressing this issue.) Indeed, in chapter 4 we shall see that the diagrammatic approach allows for a direct way of resumming LLs at NLP by exploiting exponentiation properties of soft radiation and the replica trick [41, 42], and can be carried out within dimensional regularisation. Also beyond LL accuracy, one may hope that the diagrammatic approach will provide an easier path to resummation.

In our analysis of the NLP factorisation ingredients we restrict ourselves to the first non-trivial jet function, which we first calculate for a parametrically small fermion mass up to NLP in section 2.2. Subsequently, we perform checks at one- and two-loop level that validate the obtained jet function and the corresponding part of the factorisation formula. We carry out a similar analysis for single-radiative amplitudes in the massless fermion scenario in section 2.3. We stress that the study presented in this chapter is exploratory in nature, a full characterisation of the radiative jet functions is left to future work. Having in hand the factorisation for both massless and massive fermions would allow the application of our results to a larger class of scattering processes of interest at the LHC, including the production of heavy coloured particles, such as top quarks, or scalar quarks and gluinos in supersymmetry.

2.1 From power counting to factorisation

The factorisation of an n-particle scattering amplitude with emission of a soft photon $\mathscr{M}_{n+1}$ crucially depends on the factorisation properties of the corresponding elastic amplitude $\mathscr{M}_n$. Therefore we start our analysis by extending eq. (1.23) to NLP. Specifically, we set out to obtain a classification of the jet-like structures, consisting of virtual radiation collinear to

any of the n external hard particles, contributing at subleading power. Phrased differently, we wish to derive which jet functions contribute up to NLP in a parametrically small scale, corresponding to a fermion mass or a soft external momentum.

In the following we will distinguish two fermion mass scenarios. One of which is the truly massless theory ($m = 0$), the standard approximation in high energy calculations, where it is well understood that (virtual) collinear effects beyond the LBK theorem play an important role. In the other scenario, we consider fermion masses to be non-zero but parametrically small, and in fact comparable to the scale associated to soft emissions: we assume $m \sim \lambda Q$, such that $p_i \cdot k \sim m^2 \sim \lambda^2 Q^2 \ll Q^2$, where k is a soft momentum. This more intricate small-mass approximation could be of phenomenological importance if soft gluons are emitted from particles with an intermediate-size mass, as mass effects may be comparable in size to the aforementioned collinear effects. Resummation of resulting NLP threshold logarithms (beyond LL accuracy) would, in that case, require a proper understanding of massive radiative jet functions. In addition, this second scenario may prove useful for the resummation of (NLP) logarithmic mass terms, $\log(m/Q)$, even in *non-radiative* processes, where the small fermion mass m and the hard scale Q are the only scales in the problem.

We derive our results by power counting the *pinch surfaces*, that underlie the collinear (and soft) contributions we wish to describe in terms of jet (and soft) functions, for a general QED scattering amplitude. This was done recently for Yukawa theory in ref. [85] for the same two mass scenarios. The pinch surfaces are the solutions of the Landau equations [106] and are represented by reduced diagrams in the Coleman-Norton picture [107]. In these diagrams, all off-shell lines are shrunk to a point, while the on-shell lines are kept and may be organised according to the nature of the singularity they embody, be it soft or collinear. This results in the general reduced diagram of fig. 2.1, in which one distinguishes a soft *blob* containing all lines carrying solely soft momentum, n jets J_i comprised of lines with momenta collinear to the respective external parton and lastly, a hard blob H collecting all contracted, off-shell lines. This picture seems unaltered by the presence of parametrically small fermion masses, because the limit of small m yields the same singular pinch surfaces as the massless theory. In support of this claim, we analysed the QED massive form factor using the method of regions [108–111], finding that soft and collinear modes are sufficient to correctly reproduce the singularity structure in this limit. This analysis is presented in appendix 2.A.

To carry out the power counting we use light-cone coordinates. For each external momentum p_i, we introduce two light-like vectors n_i and $\bar{n}_i$, defined by

$$n_i^\mu = \frac{1}{\sqrt{2}}\left(1, +\frac{\boldsymbol{p}_i}{|\boldsymbol{p}_i|}\right), \qquad \bar{n}_i^\mu = \frac{1}{\sqrt{2}}\left(1, -\frac{\boldsymbol{p}_i}{|\boldsymbol{p}_i|}\right). \tag{2.1}$$

These vectors are normalised such that $n_i \cdot \bar{n}_i = 1$, and by definition $n_i^2 = \bar{n}_i^2 = 0$. In any of these coordinate frames, a generic vector v obeys the Sudakov decomposition

$$v^\mu = v^+ n_i^\mu + v^- \bar{n}_i^\mu + v_{\perp i}^\mu, \tag{2.2}$$

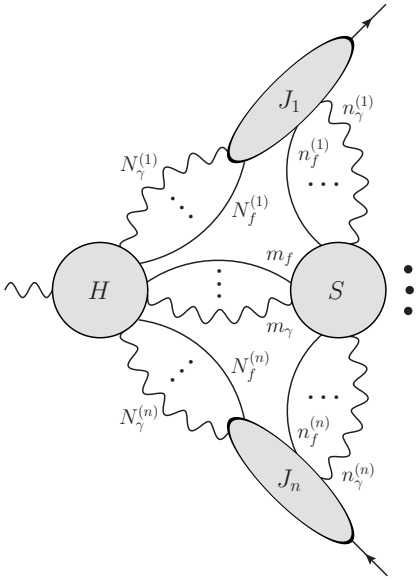

Figure 2.1: *The reduced diagram for a general, vector boson induced QED process with n well-separated hard particles in the final state. Ellipses denote the presence of an arbitrary number of photon/(anti-)fermion lines.*

where $v^+ = v\cdot\bar{n}_i$, $v^- = v\cdot n_i$. A scalar product of two vectors then reads

$$v\cdot w = v^+ w^- + v^- w^+ + v_\perp^\mu w_{\perp\mu}\,. \tag{2.3}$$

Of course, this needs further specification in which of the N collinear directions the decomposition is carried out. We remark that $v_\perp^\mu$ is defined as a four-vector, in which the spatial vector $\boldsymbol{v}_\perp$ is embedded: $v_\perp^\mu = (0, \boldsymbol{v}_\perp, 0)$. The last term in eq. (2.3) is thus equivalent to $v_\perp \cdot w_\perp = -\boldsymbol{v}_\perp \cdot \boldsymbol{w}_\perp$. The latter notation in used in some instances throughout this thesis.

Adopting the notation $k^\mu = (k^+, \boldsymbol{k}_\perp, k^-)$, we associate the following scaling to lines that are soft or collinear to the i-th external leg

$$\text{Soft:} \qquad k^\mu \sim Q\left(\lambda^2, \lambda^2, \lambda^2\right), \qquad\qquad \text{Collinear:} \qquad k^\mu \sim Q\left(1, \lambda, \lambda^2\right), \tag{2.4}$$

in the light-cone coordinate frame corresponding to p_i. The scaling of the normal coordinates parametrises the contribution of soft and collinear lines around the singular surface, which is reached for $\lambda \to 0$. Away from this limit, power counting in λ thus amounts to the ordering of finite contributions of different size and proves to be a valuable technique. We focus on virtual corrections to a hard scattering configuration, for which all invariants $s_{ij} = (p_i + p_j)^2 \sim Q^2$ involving external momenta are large compared to the energy of the radiated soft photon in $\mathscr{M}_{n+1}$. Requiring the soft momentum to be of order λ^2 rather than λ guarantees that the photon is soft with respect to all particles in the elastic amplitude.

Whenever we refer to a NLP quantity in this chapter, we mean that it is suppressed by *up to two* powers in λ with respect to the leading power contribution. This nomenclature originates from strictly massless ($m = 0$) QED where power corrections arise only through

scales associated to soft emissions $p_i \cdot k \sim \lambda^2 Q^2$. In case of parametrically small masses ($m \sim \lambda Q$) power suppressed terms at $\mathcal{O}(\lambda)$ do occur, but we apply the same definition nonetheless.

Using the momentum scaling in eq. (2.4), we start by deriving the *superficial degree of divergence* of a particular reduced diagram $\mathcal{G}$ contained in fig. 2.1, which is simply the λ-scaling of this diagram, $\mathcal{G} \sim \lambda^{\gamma_\mathcal{G}}$. Specifically, we wish to determine how $\gamma_\mathcal{G}$ depends on the structure of $\mathcal{G}$. We will see that, in practice, $\gamma_\mathcal{G}$ can be expressed as function of the number of fermion and photon connections between the hard, soft and collinear subgraphs and, in presence of fermion mass, on the internal structure of the soft subgraph. Such a formula tells us, at any perturbative order, which pinch surfaces contribute up to NLP and guides us in setting up a consistent and complete NLP factorisation framework for QED.[1]

2.1.1 Power counting rules for individual components

In order to derive an expression for $\gamma_\mathcal{G}$ it is convenient to set up a catalogue of the degree of divergence of the individual components first. For massive ($m \sim \lambda Q$) and massless ($m = 0$) QED, these rules vary slightly and we derive them explicitly here.

Given eq. (2.4), the propagator for a collinear, massive fermion scales as

$$\frac{i\,(\not{p} + m)}{p^2 - m^2} \sim \frac{\gamma^- + \lambda^2 \gamma^+ + \lambda \gamma^\perp + \lambda}{\lambda^2} \sim \frac{1}{\lambda^2}\,. \tag{2.5}$$

A massless collinear fermion obeys the same rule as the mass term is subleading in the numerator ($\mathcal{O}(\lambda)$ versus $\mathcal{O}(1)$) and of equal size in the denominator (both $\mathcal{O}(\lambda^2)$). For soft fermion lines a difference does arise; for non-zero mass

$$\frac{i\,(\not{p} + m)}{p^2 - m^2} \sim \frac{\lambda^2 \gamma^- + \lambda^2 \gamma^+ + \lambda^2 \gamma^\perp + \lambda}{\lambda^4 + \lambda^2} \sim \frac{1}{\lambda}\,, \tag{2.6}$$

while for a massless fermion one finds instead

$$\frac{i\,\not{p}}{p^2} \sim \frac{\lambda^2 \gamma^- + \lambda^2 \gamma^+ + \lambda^2 \gamma^\perp}{\lambda^4} \sim \frac{1}{\lambda^2}\,. \tag{2.7}$$

Since we aim at determining the order at which each configuration start contributing, we will only keep track of the most singular contribution to $\gamma_\mathcal{G}$, and discard the subleading terms in eq. (2.5) and (2.6). The singular structure of eq. (2.6) is uncommon because the denominator is not strictly on shell, since $p^2 \sim \lambda^4$ while $m^2 \sim \lambda^2$. In fact, this singularity is entirely determined by the fermion mass. Intuitively, because of their mass, soft fermions are integrated out, an aspect that would be worth investigating from an effective theory

[1] We stress that the power counting analysis performed here is analogous to the one for Yukawa theory, which underlies the results of ref. [85]. Nonetheless, we deem it instructive to show this derivation in detail. We summarise additional results for Yukawa theory in appendix 2.D.

perspective. This momentum configuration, which contributes to the singular structure of scattering amplitudes despite being off shell, bears similarity to Glauber gluons, scaling as $(\lambda^2, \lambda, \lambda^2)$. Our power counting shows that this momentum configuration could affect scattering amplitudes only beyond NLP.

In gauge theories the rules for vector boson vertices depend on the choice of gauge. For power counting purposes, the axial gauge is particularly convenient since non-physical degrees of freedom do not propagate. The latter is a direct consequence of the form of the photon propagator, which reads

$$\Delta^{\mu\nu}(k,r) = \frac{i}{k^2 + i\eta}\left[-\eta^{\mu\nu} + \frac{r^\mu k^\nu + r^\nu k^\mu}{r\cdot k} - \frac{r^2 k^\mu k^\nu}{(r\cdot k)^2}\right], \tag{2.8}$$

with the choice of the reference vector r^μ fixing the gauge. Eq. (2.8) satisfies

$$r_\mu \Delta^{\mu\nu}(k) = 0\,, \tag{2.9}$$

while contracting with the propagating momentum results in

$$k_\mu \Delta^{\mu\nu}(k,r) = i\left(\frac{r^\nu}{r\cdot k} - \frac{r^2 k^\nu}{(r\cdot k)^2}\right), \tag{2.10}$$

which no longer has a pole in k^2. Together, eqs. (2.9) and (2.10) show that scalar and longitudinal polarisations do not propagate in the chosen gauge.

The axial gauge makes it particularly convenient to derive the suppression effects associated to vertices involving gauge bosons [112]. These are effective rules, in the sense that they are not evident from the vertex factor as obtained from the QED Lagrangian, but follow from an interplay with the adjacent lines. To make this concrete, consider the expression for the emission of a photon from a collinear fermion line with momentum p^μ, which is proportional to

$$\left(\not{p} - \not{k}\right)\gamma^\mu \not{p} = -p^2\gamma^\mu + \gamma^\mu \not{k}\not{p} + 2\left(p^\mu - k^\mu\right)\not{p}\,. \tag{2.11}$$

First, we point out that the first two terms are always power suppressed: the first one is per definition of order λ^2, while the second term is of order λ even if the photon emission is collinear, as the dominant component vanishes due to $(\gamma^-)^2 = 0$ (for a soft photon the second term is manifestly of order λ^2). If the photon is soft, $p^\mu \not{p}$ in the third term of eq. (2.11) dominates, being of order λ^0. In that case, no suppression is caused by the vertex. However, if the photon is collinear to the fermion lines extending from the vertex, we can write $p^\mu = \frac{p^+}{k^+}k^\mu + \mathcal{O}(\lambda)$. From eq. (2.10) we then conclude that there is no dominant contribution to on-shell scattering amplitudes from the third term in eq. (2.11). Hence, in axial gauge, a suppression of λ is associated to each emission of a collinear photon from a collinear fermion line. With a different choice of gauge, the presence of longitudinal polarisations would erase this suppression effect of vertices, and individual diagrams would exhibit a harder scaling. In physical observables such polarisations cancel due to *Ward identities*, and the extra λ suppression would become evident when summing over a gauge-invariant set

QED Vertex	Suppression
$\bar{\psi}^{(c)}\gamma^\mu\psi^{(c)}A_\mu^{(c)}$	λ
$\bar{\psi}^{(c)}\gamma^\mu\psi^{(c)}A_\mu^{(s)}$	1
$\bar{\psi}^{(s)}\gamma^\mu\psi^{(c)}A_\mu^{(c)}$ or $\bar{\psi}^{(c)}\gamma^\mu\psi^{(s)}A_\mu^{(c)}$	1
$\bar{\psi}^{(s)}\gamma^\mu\psi^{(s)}A_\mu^{(s)}$	1

Table 2.1: *Power counting rules for QED vertices, depending on the soft or collinear nature of the field. These rules apply to massive and massless fermions alike.*

of diagrams. We summarise the rules for QED vertices in table 2.1.

The scaling of a photon line is determined by the common factor $\frac{1}{k^2}$ in eq. (2.8), and is therefore $\sim \frac{1}{\lambda^2}$ and $\sim \frac{1}{\lambda^4}$ for respectively collinear and soft particles. A further suppression of the degree of divergence results from integration over loop momenta, where the measure $\int d\ell^+ d\ell^- d^2\vec{\ell}_\perp$ provides a suppression of, respectively, λ^4 and λ^8 for collinear and soft loops. These results are, together with the rules for propagators, presented in table 2.2.

	$m=0$	$m\sim\lambda Q$
Collinear fermion	λ^{-2}	
Soft fermion	λ^{-2}	λ^{-1}
Collinear photon	λ^{-2}	
Soft photon	λ^{-4}	
Collinear loop	λ^4	
Soft loop	λ^8	

Table 2.2: *Power counting rules for loop integrals and propagators for photons and fermions. If no rule is specified for $m\sim\lambda Q$, the $m=0$ scaling applies.*

2.1.2 Constructing the overall degree of divergence

We started the derivation of a formula for $\gamma_{\mathscr{G}}$ by obtaining the power counting rules for the basic constituents of any diagram. Here we use these results to obtain power counting formulae for the soft (γ_S) and collinear (γ_{J_i}) sub-diagrams independently. Subsequently, we consider the effect of connections between all sub-diagrams ($\gamma_{S\leftrightarrow H}$,$\gamma_{J_i\leftrightarrow H}$ and $\gamma_{J_i\leftrightarrow S}$) as well as the connections to the external particles ($\gamma^{\text{ext}}_{J_i}$). The degree of divergence of a reduced diagram $\mathscr{G}$ with n-jets will thus be given by

$$\gamma_{\mathscr{G}} = \gamma_S + \gamma_{S\leftrightarrow H} + \sum_{i=1}^{n}\left(\gamma_{J_i} + \gamma_{J_i\leftrightarrow H} + \gamma_{J_i\leftrightarrow S} + \gamma^{\text{ext}}_{J_i}\right), \tag{2.12}$$

We begin with γ_{J_i} and consider a blob of collinear lines, without any external attachments.

According to the rules of table 2.2 the associated degree of divergence is

$$\gamma_{J_i} = -2I + 4L + V, \tag{2.13}$$

where $I = \tilde{I}_f + \tilde{I}_\gamma$ denotes the total number of fermion and photon lines internal to the isolated blob, L the number of loops and V the number of vertices. We use *Euler's identity*

$$L = 1 + \tilde{I}_f + \tilde{I}_\gamma - V, \tag{2.14}$$

and note that diagrams without external legs (i.e. vacuum bubbles) have three internal lines per pair of vertices: $I = \frac{3}{2}V$. As a result, the degree of divergence of a collinear sub-diagram is independent of its internal structure:

$$\gamma_{J_i} = -3V + 4(1 + \tfrac{1}{2}V) + V = 4. \tag{2.15}$$

For the soft sub-diagram one needs to distinguish between the different mass cases. We start with

$$\gamma_S = \begin{cases} -2\tilde{I}_f - 4\tilde{I}_\gamma + 8L & (m = 0) \\ -\tilde{I}_f - 4\tilde{I}_\gamma + 8L & (m \sim \lambda Q) \end{cases}. \tag{2.16}$$

Applying Euler's identity in eq. (2.14) and exploiting the fixed ratio of the number of fermion and photon lines to the number of vertices in a QED vacuum bubble $\tilde{I}_f = 2\tilde{I}_\gamma = V$, we obtain

$$\gamma_S = \begin{cases} = 8 & (m = 0) \\ = 8 + \tilde{I}_f & (m \sim \lambda Q) \end{cases}. \tag{2.17}$$

Next, we must account for the contribution to the overall degree of divergence arising from the connecting lines between hard, soft and jet sub-diagrams of the general reduced diagram in fig. 2.1. Besides the explicit powers of λ associated to lines themselves, they affect the power counting of the disconnected sub-diagrams by splitting internal propagators and adding vertices to both sub-diagrams. In fig. 2.2 we show these effects on a generic sub-diagram A resulting from either a photon or fermion connection to a sub-diagram B, depending on the internal line that is probed. For fermion connections, a fermion anti-fermion pair is inserted to conserve charge in both sub-diagrams.[2] The effect per fermion is simply half that of the combined fermion anti-fermion insertion. An additional suppression effect arises from the loops that are formed in this process.

Consider the connection between a jet and the hard sub-diagram first. A connecting (collinear) photon line adds also a collinear fermion line and an all-collinear QED vertex to the collinear blob, as shown in fig. 2.2a. According to the rules listed in table 2.2 and 2.1, such a connection enhances the degree of divergence by $-2-2+1 = -3$. Each connecting fermion

[2] In principle the charge flow can be more involved and form, for example, a closed loop through the hard, soft and a collinear sub-diagram, or connect to external fermions of opposite charge. These configurations can nevertheless be obtained by applying the basic steps in fig. 2.2.

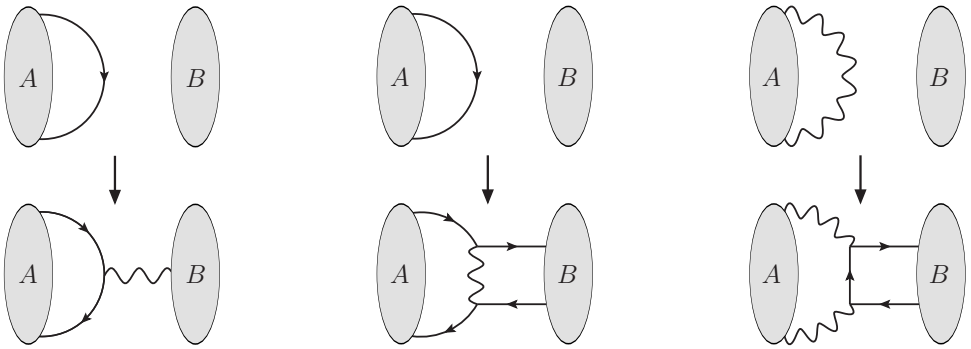

(a) *Photon insertion on a fermion line.*

(b) *Pairwise fermion insertion on a fermion line.*

(c) *Pairwise fermion insertion on a photon line.*

Figure 2.2: *The effect of connecting lines between isolated sub-diagrams A and B on the former.*

line gives the same effect, as found by using the aforementioned procedure: a fermion antifermion pair adds in total four collinear lines and two all-collinear vertices, such that the enhancement of the degree of divergence due to a single fermion line is $\frac{4\times(-2)+2\times(+1)}{2}=-3$. In addition, the $N^{(i)}=N_\gamma^{(i)}+N_f^{(i)}$ connecting lines give rise to $N^{(i)}-1$ collinear loops. Summing up, we find

$$\begin{aligned}\gamma_{J_i\leftrightarrow H} &= -3N_\gamma^{(i)}-3N_f^{(i)}+4(N_\gamma^{(i)}+N_f^{(i)}-1)\\ &= N_\gamma^{(i)}+N_f^{(i)}-4\,.\end{aligned} \tag{2.18}$$

The reduced diagrams considered here are amputated, meaning that there is no propagator, and thus no power counting, associated to the external leg itself. Therefore, connecting the jet to an external fermion leg gives a further enhancement of the degree of divergence of

$$\gamma_{J_i}^{\text{ext}}=\frac{2\times(-2)+2\times(+1)}{2}=-1\,, \tag{2.19}$$

where only the vertices and additional collinear propagators due to the (pairwise) fermion insertion are counted. Similarly, connecting the jet to an external photon gives one additional collinear fermion line an an all-collinear vertex, such that also in this case

$$\gamma_{J_i}^{\text{ext}}=-2+1=-1\,. \tag{2.20}$$

In contrast to $\gamma_{J_i\leftrightarrow H}$ and $\gamma_{J_i}^{\text{ext}}$, the degree of divergence associated to the connection between the soft and hard sub-diagram is not suppressed by vertices since all lines are soft. Therefore, we only need to count the $m_\gamma+m_f$ soft connections themselves, as well as the additional lines created in the soft blob by these insertions (one soft fermion per photon insertion; one soft photon and an additional soft fermion for a pairwise fermion insertion).[3] Including the

[3] The number of soft photon and fermion lines connecting to the hard sub-diagram, denoted by m_γ and m_f, should not be confused with the fermion mass m.

loop suppression, we find

$$\begin{aligned}\gamma_{S\leftrightarrow H} &= (-2-4)m_\gamma + \left(\frac{3\times(-2)-4}{2}\right)m_f + 8(m_\gamma + m_f - 1) \\ &= 2m_\gamma + 3m_f - 8 \qquad (m=0), \qquad (2.21a)\\ \gamma_{S\leftrightarrow H} &= (-1-4)m_\gamma + \left(\frac{3\times(-1)-4}{2}\right)m_f + 8(m_\gamma + m_f - 1) \\ &= 3m_\gamma + \tfrac{9}{2}m_f - 8 \qquad (m\sim\lambda Q). \qquad (2.21b)\end{aligned}$$

Finally, we consider the $n_\gamma^{(i)} + n_f^{(i)}$ connections between the soft sub-diagram and the jets, which affect both the sub-diagrams involved.[4] Also, these connections will form an additional loop by closing a path through H, J_i and S, giving a total of $n_\gamma^{(i)} + n_f^{(i)}$ soft loops. The result is

$$\begin{aligned}\gamma_{J_i\leftrightarrow S} &= -2\overbrace{\left(n_\gamma^{(i)} + n_f^{(i)}\right)}^{\text{collinear effects}} - \overbrace{\left(6n_\gamma^{(i)} + 5n_f^{(i)}\right)}^{\text{soft effects}} + 8\left(n_\gamma^{(i)} + n_f^{(i)}\right) \\ &= n_f^{(i)} \qquad (m=0), \qquad (2.22a)\\ \gamma_{J_i\leftrightarrow S} &= -2\left(n_\gamma^{(i)} + n_f^{(i)}\right) - \left(5n_\gamma^{(i)} + \tfrac{7}{2}n_f^{(i)}\right) + 8\left(n_\gamma^{(i)} + n_f^{(i)}\right) \\ &= n_\gamma^{(i)} + \tfrac{5}{2}n_f^{(i)} \qquad (m\sim\lambda Q). \qquad (2.22b)\end{aligned}$$

Combining ingredients according to eq. (2.12) gives

$$\gamma_{\mathscr{G}} = 2m_\gamma + 3m_f + \sum_{i=1}^{n}\left(N_\gamma^{(i)} + N_f^{(i)} + n_f^{(i)} - 1\right) \qquad (m=0), \qquad (2.23a)$$

$$\gamma_{\mathscr{G}} = \tilde{I}_f + 3m_\gamma + \tfrac{9}{2}m_f + \sum_{i=1}^{n}\left(N_\gamma^{(i)} + N_f^{(i)} + n_\gamma^{(i)} + \tfrac{5}{2}n_f^{(i)} - 1\right) \qquad (m\sim\lambda Q). \qquad (2.23b)$$

We emphasise that the number of internal fermion lines $\tilde{I}_f$ in the soft sub-diagram denotes the number of lines in the *isolated* blob, before connections to the hard and jet functions have been accounted for. It is more intuitive to express this in terms of the total number of internal fermion lines in the amputated soft function, I_f, for which we disregard the actual fermion connections to other blobs, but retain the effect that the connections have on the soft blob itself. Either a single photon attachment or a pairwise (anti-)fermion insertion adds a fermion line to the soft sub-diagram, as indicated in fig. 2.2, giving the relation

$$I_f = \tilde{I}_f + m_\gamma + \tfrac{1}{2}m_f + \sum_i\left(n_\gamma^{(i)} + \tfrac{1}{2}n_f^{(i)}\right). \qquad (2.24)$$

[4]The main difference in power counting compared to Yukawa theory arises from this interaction. In Yukawa theory, each scalar emission from a collinear fermion line is suppressed by a factor of λ, such that power counting rules for all-collinear and all-soft vertices are identical in QED and Yukawa theory. However, vertices for soft-collinear interactions are suppressed by λ in Yukawa theory, but are not suppressed in QED.

Inserting eq. (2.24) in eq. (2.23) gives

$$\gamma_{\mathscr{G}} = 2m_\gamma + 3m_f + \sum_{i=1}^{n} \left(N_\gamma^{(i)} + N_f^{(i)} + n_f^{(i)} - 1 \right) \qquad (m = 0), \tag{2.25a}$$

$$\gamma_{\mathscr{G}} = I_f + 2m_\gamma + 4m_f + \sum_{i=1}^{n} \left(N_\gamma^{(i)} + N_f^{(i)} + 2n_f^{(i)} - 1 \right) \qquad (m \sim \lambda Q), \tag{2.25b}$$

which are the final expressions for the overall degree of divergence for a reduced diagram $\mathscr{G}$ with n-jets. The massless result in eq. (2.25a) is the analogue for n-jet production in QED of the power-counting formulae first derived in refs. [112, 113] for cut vacuum polarisation diagrams and wide-angle scattering amplitudes in a broader class of theories. The massive result in eq. (2.25b) is the equivalent of the equation obtained in ref. [85] for Yukawa theory, which we also re-derived. We present this and other results for Yukawa theory in appendix 2.D.

2.1.3 NLP factorisation of QED amplitudes

Equipped with eq. (2.25), we can determine which reduced diagrams $\mathscr{G}$ contribute up to NLP in λ. For the class of diagrams considered in the previous section, which have an arbitrary number of purely virtual corrections, we see that $\gamma_{\mathscr{G}} \geq 0$, independent of the number of hard particles in the final state. The $\gamma_{\mathscr{G}} = 0$ diagrams contain at most logarithmic singularities, while the $\gamma_{\mathscr{G}} > 0$ are finite and give a vanishing contribution in the $\lambda \to 0$ limit. For small but non-zero values of λ, the $\gamma_{\mathscr{G}} = 0$ diagrams form LP contributions, with the $\gamma_{\mathscr{G}} > 0$ diagrams acting as power corrections.

Eventually, we wish to develop a factorisation formalism that allows one to resum NLP threshold logarithms associated to soft final-state radiation, which requires us to study the factorisation of *radiative* amplitudes. Dressing the non-radiated graphs with a single, soft emission will enhance the degree of divergence by -2, by the splitting of a soft/collinear fermion line.[5] So for these radiative amplitudes, a LP contribution will be $\mathcal{O}(\lambda^{-2})$ instead, with the NLP corrections of $\mathcal{O}(\lambda^0)$.[6] Therefore, we will list all purely virtual reduced diagrams $\mathscr{G}$ characterised by $\gamma_{\mathscr{G}} \leq 2$. Since we study the abelian theory, we restrict our analysis to (anti-)fermions in the final state, although the power counting formulae of eq. (2.25) describe processes involving hard final-state photons as well. As a minimal example we study the amplitude for $\gamma \to f\bar{f}$, but stress that the jet functions that appear there cover the general case of n (anti-)fermions.

[5] For $m \sim \lambda Q$, an emission from a soft fermion would enhance the degree of divergence by -1 instead. However, any non-radiative diagram that allowed for such an emission would contribute only beyond NLP, so we may neglect this subtlety here.

[6] At the cross section level, this still constitutes a logarithmic divergence as the phase space integral over the soft gluon cancels the enhancement of the degree of divergence due to additional propagators in the squared amplitude.

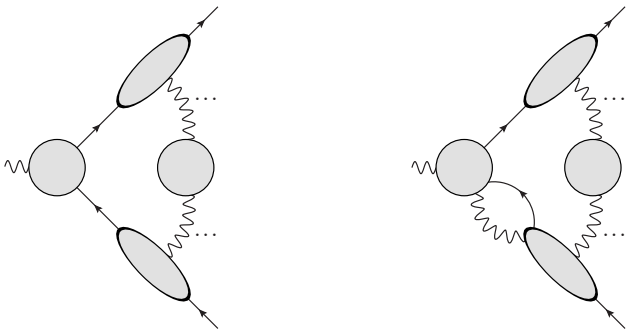

(a) $\gamma = 0$ **(b)** $\gamma = 1$

Figure 2.3: *Reduced diagrams up to* $\gamma = 1$ *for the process* $\gamma \to f\bar{f}$ *. For diagram (b) a similar configuration exists with the double jet connection on the upper leg instead.*

The leading power configuration at $\gamma_{\mathscr{G}} = 0$ is obtained for $N_f^{(i)} = 1$ and $\{N_\gamma^{(i)}, n_f^{(i)}, m_f, m_\gamma, I_f\} = 0$ for all i in eq. (2.25) and is depicted in fig. 2.3a. At $\gamma_{\mathscr{G}} = 1$, the only reduced diagrams allowed by charge conservation are those with one additional photon connection between a jet and the hard sub-diagram, $N_\gamma^{(j)} = 1$ and $N_\gamma^{(i)} = 0$ for all $i \neq j$, as shown in fig. 2.3b. Finally, $\gamma_{\mathscr{G}} = 2$ can follow from a variety of configurations, as indicated in fig. 2.4. We can have a double photon connection from the hard sub-diagram to a jet in addition to the fermion line ($N_\gamma^{(j)} = 2$, fig. 2.4a) or a triple collinear (anti-)fermion connection ($N_f^{(j)} = 3$, fig. 2.4b). Naturally we can have two jets with one extra photon connection as well ($N_\gamma^{(j)} = N_\gamma^{(k\neq j)} = 1$, fig. 2.4c). In addition, there are configurations in which the soft sub-diagram provides the suppression of the degree of divergence. This can be either through a single photon connection to the hard scattering ($m_\gamma = 1$, fig. 2.4d), a double fermion connection to a particular jet ($n_f^{(j)} = 2$, fig. 2.4e) or fermion connections to two different jets ($n_f^{(j)} = n_f^{(k\neq j)} = 1$, fig. 2.4f). The latter two configurations contribute at NLP only in case $m = 0$, while for $m \sim \lambda Q$ eq. (2.25b) yields $\gamma_{\mathscr{G}} = 5$.[7] In either mass scenario, the soft blob may be connected to the jets by an arbitrary number of photons.

Since the reduced diagrams of fig. 2.3 and fig. 2.4 encode all relevant soft and collinear configurations up to NLP, we may immediately cast them into entries in the factorisation formula. Starting at leading power, fig. 2.3a yields the well-known factorisation formula

$$\mathscr{M}^{\mathrm{LP}} = \left(\prod_{i=1}^{n} J_{(f)}(\hat{p}_i) \right) \otimes H(\hat{p}_1, \ldots, \hat{p}_n) S(n_i \cdot n_j), \tag{2.26}$$

where the tensor product $\otimes$ denotes a contraction of spinor indices. The hatted vectors contain only the dominant momentum component

$$\hat{p}_i^\mu = p_i^+ n_i^\mu, \tag{2.27}$$

where the light-cone vector n_i^μ is defined in eq. (2.1). The jet function has the operator

[7] The exception being a single fermion exchanged between the two jets, with no extra soft interactions, which is in fact $\gamma_{\mathscr{G}} = 3$. In eq. (2.25b) one should set $I_f = -1$ in order not to overcount the legs.

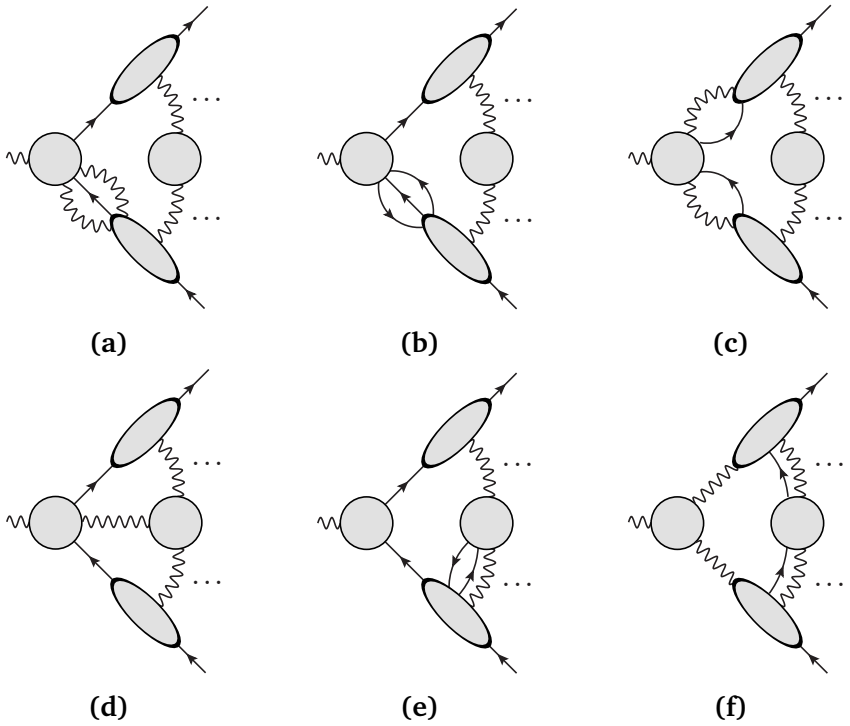

Figure 2.4: *Reduced diagrams contributing at $\gamma = 2$ for $m = 0$. For $m \sim \lambda Q$, diagrams (e) and (f) contribute only beyond* NLP.

definition

$$J_{(f)}(p_i) = \langle p_i | \overline{\psi}(0)\, \Phi_{\bar{n}_i}(0,\infty) | 0 \rangle \,, \tag{2.28}$$

involving a semi-infinite Wilson line in the $\bar{n}_i$ direction

$$\Phi_{\bar{n}_i}(0,\infty) = \exp\left[i\, e \int_0^\infty ds\, \bar{n}_i \cdot A(s\, \bar{n}_i) \right], \tag{2.29}$$

while the soft function S is given by a product of Wilson lines,

$$S(n_i \cdot n_j) = \langle 0 | \prod_{i=1}^{n} \Phi_{n_i}(0,\infty)\, | 0 \rangle \ . \tag{2.30}$$

For simplicity, we assume here that the potential overlap between the soft and collinear regions has already been accounted for in a redefinition of the soft function.[8]

Following the reasoning of ref. [85] for Yukawa theory, we assume that a similar factorisation picture holds at next-to-leading power, with each class of reduced diagrams described by a different jet function. As far as the hard-collinear sector is concerned, this means that the leading power formula in eq. (2.26) is supplemented with four types of contributions,

$$\mathscr{M}^{\text{NLP}}_{\text{coll}} = \sum_{i=1}^{n} \left(\prod_{j \neq i} J^j_{(f)} \right) \left[J^i_{(f\gamma)} \otimes H^i_{(f\gamma)} + J^i_{(f\,\partial\gamma)} \otimes H^i_{(f\,\partial\gamma)} \right] S$$

[8] This results in the so-called *reduced* soft function, see ref. [79].

$$+\sum_{i=1}^{n}\Big(\prod_{j\neq i}J^{j}_{(f)}\Big)J^{i}_{(f\gamma\gamma)}\otimes H^{i}_{(f\gamma\gamma)}S+\sum_{i=1}^{n}\Big(\prod_{j\neq i}J^{j}_{(f)}\Big)J^{i}_{(fff)}\otimes H^{i}_{(fff)}S$$
$$+\sum_{1\leq i\leq j\leq n}\Big(\prod_{k\neq i,j}J^{k}_{(f)}\Big)J^{i}_{(f\gamma)}J^{j}_{(f\gamma)}\otimes H^{ij}_{(f\gamma)(f\gamma)}S\,. \tag{2.31}$$

To improve readability, we suppress the arguments of the factorisation ingredients and introduce the indices i, j, labelling the collinear sectors. We will clarify this notation further momentarily. The first line describes the effect of fig. 2.3b and starts contributing at order λ. This implies that at order λ^2 we may expect a dependence of the hard function on the perpendicular momentum component of the collinear photon emerging from it, which can be re-expressed in terms of the $H^{i}_{(f\partial\gamma)}$ function, as will be shown shortly. The second line describes the classes of diagrams (a) and (b) in fig. 2.4, while diagram (c) corresponds to the third line. These contributions, as well as the $f\partial\gamma$-term, are strictly $\mathcal{O}(\lambda^2)$, which implies that the soft function appearing in those terms is given by the leading-power definition of eq. (2.30). While for massless fermions the same reasoning applies to the $f\gamma$-term, in the massive case the soft function could in principle receive $\mathcal{O}(\lambda)$ corrections. Since we focus on hard-collinear factorisation, we do not explore this possibility in detail. For the same reason, we will not supplement our factorisation formula with terms corresponding to reduced diagrams (d) − (f) with additional connections to the soft function. We leave the identification and investigation of the corresponding terms for future work. Eq. (2.31) is formally identical to the counterpart for massive Yukawa theory [85], as the collinear sectors of the two theories exhibit the same scaling modulo the replacement of scalars with photons.

We now clarify the shorthand index notation. In the simplest non-trivial example of the $f\gamma$-jet and hard functions, we define

$$J^{i}_{(f\gamma)}=J_{(f\gamma)}(p_i-\hat{\ell}_i,\hat{\ell}_i,\epsilon)\,,$$
$$H^{i}_{(f\gamma)}=H_{(f\gamma)}(p_1,\ldots,p_i-\hat{\ell}_i,\ldots,p_n,\hat{\ell}_i,\epsilon)\,. \tag{2.32}$$

The last argument indicates that the factorisation in eq. (2.31) is formulated for unrenormalised amplitudes, i.e. the factorisation ingredients are affected by UV divergences in four dimensions. We employ dimensional regularisation by working in $d=4-2\epsilon$ dimensions instead, such that these divergences are cast into poles in ϵ. The first two arguments of the jet function denote the momentum flowing through the fermion and photon leg, respectively, while in the hard function the index i also specifies which of the n hard momenta has been shifted in presence of the additional collinear emission. In analogy with eq. (2.27), $\hat{\ell}_i^{\mu}=\ell_i^{+}n_i^{\mu}$ denotes the large component of the momentum flowing in the photon leg. In principle, in the spirit of the LP factorisation, one would like to replace p_i with $\hat{p}_i$ in the argument of the hard function, thus neglecting the small components in the external momenta too. This can be done in the massless theory, where the jet functions start contributing at $\mathcal{O}(\lambda^2)$. However, the massive theory allows for odd powers in the λ expansion, so that an overall $\mathcal{O}(\lambda^2)$ term can also originate from an order λ correction from both the hard and a jet function. This effect forces us to retain some subleading components in the argument of eq. (2.32), as will be made clear in the explicit calculation in section 2.2.2. In contrast to

eq. (2.26), the ⊗-product in eq. (2.31) involves, besides spinor index contractions, convolutions over the leading momentum components and additional Lorentz contractions over spacetime indices carried by the photon leg. Explicitly, for the first line of eq. (2.31)

$$\begin{aligned}
&\Big(\prod_{j\neq i} J^j_{(f)}\Big)\Big[J^i_{(f\gamma)}\otimes H^i_{(f\gamma)} + J^i_{(f\partial\gamma)}\otimes H^i_{(f\partial\gamma)}\Big]S \\
&\equiv S(\hat{p}_i\cdot\hat{p}_j,\epsilon)\Big(\prod_{j\neq i} J_{(f)}(p_j,\epsilon)\Big)\int_0^{p_i^+} d\ell_i^+\Big[J^\nu_{(f\gamma)}(p_i-\hat{\ell}_i,\hat{\ell}_i,\epsilon)H_{(f\gamma)\nu}(p_1,\dots,p_i-\hat{\ell}_i,\dots,p_n,\hat{\ell}_i,\epsilon) \\
&\quad + J^{\nu\rho}_{(f\partial\gamma)}(p_i-\hat{\ell}_i,\hat{\ell}_i,\epsilon)H_{(f\partial\gamma)\nu\rho}(p_1,\dots,p_i-\hat{\ell}_i,\dots,p_n,\hat{\ell}_i,\epsilon)\Big]. \qquad (2.33)
\end{aligned}$$

The other terms in eq. (2.31) involve a straightforward generalisation of the notation in eq. (2.32). In presence of more than two legs (e.g. for the $f\gamma\gamma$-term), the corresponding hard function acquires an additional argument, and the momenta p_i are shifted accordingly.

As is clear from eq. (2.33), the hard functions depend only on the large momentum component $\hat{\ell}$ (and not on the full ℓ). However, since we want the NLP formula to be accurate at $\mathcal{O}(\lambda^2)$, we cannot set $\ell^\mu = \hat{\ell}^\mu$ at the level of amplitudes, but we need to keep also its transverse component $\ell^\mu_\perp$. This can be rephrased as a Taylor expansion in the transverse momentum around zero,

$$\begin{aligned}
&\widetilde{H}^i_{(f\gamma)\nu}\big(p_1,\dots,p_n,\ell_i,\epsilon\big) \\
&\quad = \widetilde{H}^i_{(f\gamma)\nu}\big(p_1,\dots,p_n,\hat{\ell}_i,\epsilon\big) + \ell^\rho_\perp\left[\frac{\partial}{\partial\ell^\rho_\perp}\widetilde{H}^i_{(f\gamma)\nu}\big(p_1,\dots,p_n,\ell_i,\epsilon\big)\right]_{\ell_\perp=0} + \mathcal{O}(\lambda^2) \\
&\quad \equiv H_{(f\gamma)\nu}(p_1,\dots,p_i-\hat{\ell}_i,\dots,p_n,\hat{\ell}_i,\epsilon) + \ell^\rho_\perp H_{(f\partial\gamma)\nu\rho}(p_1,\dots,p_i-\hat{\ell}_i,\dots,p_n,\hat{\ell}_i,\epsilon), \qquad (2.34)
\end{aligned}$$

thus identifying the two terms with respectively the $f\gamma$- and $f\partial\gamma$-contributions in eq. (2.31), where by definition the $\ell^\rho_\perp$ in the second term is absorbed in $J^i_{(f\partial\gamma)}$.

In eq. (2.34), we generically denoted with $\widetilde{H}$ the part of the amplitude that is not explicitly described by the soft and collinear functions. In the traditional factorisation approach, this would be obtained via a subtraction algorithm, while in the effective field theory it corresponds to a Wilson coefficient obtained from matching to full QED. Both approaches would require matrix element definitions of the jet functions in eq. (2.31), as well as of the NLP soft function. Gauge invariance of each separate ingredient would then be manifest. This systematic analysis requires further investigation of the interplay between jet functions and (generalised) Wilson lines, which we leave for future work. In absence of an operator definition, we will extract in sec. 2.2.1 the $f\gamma$- and $f\partial\gamma$-jet functions from a generic matrix element, assuming the validity of the picture above. This necessitates in turn a diagrammatic definition of the hard function, of which we will give explicit examples in section 2.2 and 2.3. As a consistency check on this setup, we will show that eq. (2.31) with these functions reproduces the (hard-)collinear region of one-loop (two-loop) diagrams.

Our approach provides important insight into the NLP behaviour of gauge theories. Firstly,

we can explicitly test the categorisation of factorisation ingredients given by the power-counting in eq. (2.23). Secondly, we shed light on some dynamical subtleties that are not fully accounted for by the simpler factorisation theorems presented in refs. [78,79]. Finally, the explicit calculations presented here show how to deal with the endpoint contributions that result from a factorisation structure consisting of convolutions rather than direct products.

2.2 Hard-collinear factorisation for massive fermions

We now turn to the study of some of the ingredients entering the factorisation picture, in the regime where the fermion mass is parametrically small. For definiteness we focus on the $f\gamma$- and $f\partial\gamma$-contributions to our NLP factorisation formula, corresponding to $N_\gamma = 1$ and $N_f = 1$ in eq. (2.23). We calculate these jet functions at one-loop order in section 2.2.1 and validate them as well as the factorisation structure through one- and two-loop calculations in section 2.2.2. The $f\gamma$-term is particularly relevant, according to our power counting formula, as it already contributes at $\mathcal{O}(\lambda)$, for a parametrically small fermion mass. However, the $f\partial\gamma$-term is further suppressed by a power of the transverse momentum component. Thus, to appreciate the interplay between the two functions, we will need to carry out the calculation to $\mathcal{O}(\lambda^2)$. At this order other interesting aspects such as endpoint contributions emerge too. Working at this level of accuracy, and the fact that we consider QED, constitutes an important generalisation of the analogous functions presented in ref. [85] where Yukawa theory was studied. We stress that at $\mathcal{O}(\lambda^2)$ accuracy one also needs the fff- and $f\gamma\gamma$-jet functions, which contribute from two-loop onwards. We leave the calculation of these ingredients for future work.

Although in this section we do not consider external soft radiation, our analysis of the non-radiative factorisation ingredients is an important step towards generalising soft theorems to gauge theories at NLP, in the case of parametrically small masses. In addition, this scenario carries intrinsic interest to collider phenomenology, since precise measurements of cross sections may benefit from classifying and possibly resumming logarithms of small fermion masses at NLP. Examples are charm mass effects in B decays [114], initial-state mass effects in heavy-quark induced processes [115–117], bottom mass effects in Higgs production and decay [103, 118], and $t\bar{t}$ production at a future linear collider, where the top mass could serve as a soft scale. Understanding the NLP factorisation structure is a necessary intermediate step towards resumming such mass effects at this level of accuracy.

2.2.1 The massive $f\gamma$-jet

In the following we carry out an explicit derivation of the one-loop expressions for two of the jet functions that enter the NLP factorisation formula for massive QED, as presented in eq. (2.31). The detailed calculation of these quantities sheds light on the subtleties involved

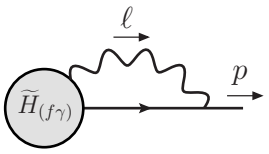

Figure 2.5: *Diagram from which the $f\gamma$- and $f\partial\gamma$-jet functions are extracted.*

beyond leading power. Moreover the functions we extract are process-independent, and could therefore be used in other QED calculations.

To keep expressions compact, we choose a reference frame such that the momentum p^μ of the external particle that defines the jet has no perpendicular component $p^\mu = (p^+, 0, p^-)$, with $p^- \ll p^+$. Unit vectors in the collinear and anti-collinear direction are then denoted by $n^\mu = (1,0,0)$ and $\bar{n}^\mu = (0,0,1)$. We also set the electric charge $Q = -1$. The power counting in eq. (2.23) was derived in axial gauge, which we also use for the jet functions. We will verify that, in a gauge that only allows for physical polarisations, the predicted power counting works on a diagram-by-diagram basis. For simplicity we select light-cone gauge, setting $r^2 = 0$ in eq. (2.8). Furthermore, we choose the reference vector in the anti-collinear direction, $r^\mu = r^- \bar{n}^\mu$. Note that r^- then cancels in the photon propagator in eq. (2.8), leaving

$$\Delta_{\nu\sigma}(\ell) = \frac{i}{\ell^2 + i\eta}\bigg(-\eta_{\nu\sigma} + \frac{\ell_\nu \bar{n}_\sigma + \ell_\sigma \bar{n}_\nu}{\ell\cdot\bar{n}}\bigg). \tag{2.35}$$

We extract the jet functions from the diagram in fig. 2.5. Working in $d = 4-2\epsilon$ dimensions, the corresponding amplitude is given by

$$\mathscr{M}^{(n+1)}_{(f\gamma)}(p) = ie\mu^{2\epsilon}\int \frac{d^{4-2\epsilon}\ell}{(2\pi)^{4-2\epsilon}}\,\frac{\bar{u}(p)N^\nu(p,\ell)}{\big[(p-\ell)^2 - m^2 + i\eta\big]\big[\ell^2 + i\eta\big]}\,\widetilde{H}^{(n)}_{(f\gamma)\nu}\bigg(\frac{\ell^+}{p^+}, \ell_\perp\bigg), \tag{2.36}$$

where μ denotes the renormalisation scale. We have defined the numerator factor

$$N^\nu(p,\ell) = \bigg(-\gamma^\nu + \frac{\not{\ell} r^\nu + \not{r}\ell^\nu}{\ell\cdot r}\bigg)(\not{p} - \not{\ell} + m), \tag{2.37}$$

as well as a generic n-loop hard function $\widetilde{H}^{(n)}_{(f\gamma)\nu}$. We first rearrange its transverse-momentum dependence by Taylor expanding in $\ell^\rho_\perp$, as in eq. (2.34).[9] Retaining terms up to $\mathscr{O}(\lambda)$

$$\begin{aligned}\widetilde{H}^{(n)}_{(f\gamma)\nu}\bigg(\frac{\ell^+}{p^+}, \ell_\perp\bigg) &= \widetilde{H}^{(n)}_{(f\gamma)\nu}\bigg(\frac{\ell^+}{p^+}, 0\bigg) + \ell^\rho_\perp\bigg[\frac{\partial}{\partial \ell^\rho_\perp}\widetilde{H}^{(n)}_{(f\gamma)\nu}\bigg(\frac{\ell^+}{p^+}, \ell_\perp\bigg)\bigg]_{\ell_\perp=0} + \mathscr{O}(\lambda^2)\\ &\equiv H^{(n)}_{(f\gamma)\nu}(x) + \ell^\rho_\perp H^{(n)}_{(f\partial\gamma)\nu\rho}(x) + \mathscr{O}(\lambda^2),\end{aligned} \tag{2.38}$$

[9] We recall that $\ell^\rho_\perp$ denotes the d-dimensional perpendicular component of ℓ^ρ, as defined by means of a Sudakov decomposition: $\ell^\rho = \ell\cdot\bar{n}\, n^\rho + \ell\cdot n\,\bar{n}^\rho + \ell^\rho_\perp$. Similarly we define $\eta^{\nu\rho}_\perp = \eta^{\nu\rho} - n^\nu\bar{n}^\rho - \bar{n}^\nu n^\rho$.

we trade the initial hard function for two objects that depend only on the fraction of the large component of the loop momentum $x = \ell^+/p^+$. Here and in the following we shall suppress the ϵ dependence of the hard and jet functions for brevity. We remind the reader that we deal with unrenormalised quantities throughout this chapter. Comparing eq. (2.36) with the first line of eq. (2.31),

$$\mathscr{M}^{(n+1)}_{(f\gamma)}(p) = \int_0^1 dx \Big[J^{(1)\nu}_{(f\gamma)}(x) H^{(n)}_{(f\gamma)\nu}(x) + J^{(1)\nu\rho}_{(f\partial\gamma)}(x) H^{(n)}_{(f\partial\gamma)\nu\rho}(x) \Big], \tag{2.39}$$

allows us to extract the jet functions,

$$J^{(1)\nu}_{(f\gamma)}(x,p) = iep^+\mu^{2\epsilon} \int \frac{d\ell^- d^{2-2\epsilon}\ell_\perp}{(2\pi)^{4-2\epsilon}} \frac{\bar{u}(p) N^\nu(p,\ell)}{\big[(p-\ell)^2 - m^2 + i\eta\big]\big[\ell^2 + i\eta\big]}, \tag{2.40a}$$

$$J^{(1)\nu\rho}_{(f\partial\gamma)}(x,p) = iep^+\mu^{2\epsilon} \int \frac{d\ell^- d^{2-2\epsilon}\ell_\perp}{(2\pi)^{4-2\epsilon}} \frac{\bar{u}(p) N^\nu(p,\ell)\, \ell_\perp^\rho}{\big[(p-\ell)^2 - m^2 + i\eta\big]\big[\ell^2 + i\eta\big]}. \tag{2.40b}$$

In eq. (2.39), we switched from the dominant loop momentum component ℓ^+ to the momentum fraction x, which determines the convolution between hard and jet functions. The x-integration range is a priori $(-\infty, +\infty)$, but is in fact restricted to $(0,1)$ by noting that the integral over ℓ^- vanishes if the two poles lie on the same side of the integration contour.

In eq. (2.40) the denominators have homogeneous λ-scaling, but the numerator still needs expanding. As expected from the power counting rule for an all-collinear vertex, we find, in axial gauge, that N is $\mathscr{O}(\lambda)$; therefore, the $f\gamma$-jet starts at the same order, while the additional term $\ell_\perp$ causes the $f\partial\gamma$-jet to begin at $\mathscr{O}(\lambda^2)$. Performing the expansion leaves us with three independent numerator structures,

$$1\,, \qquad \ell_\perp^\alpha \ell_\perp^\beta\,, \qquad \ell^-\,. \tag{2.41}$$

The first two lead to straightforward integrals, and follow from closing the integration contour at infinity in the ℓ^- complex plane, evaluating the residue of the integrand at the pole $\ell^- = -\ell_\perp^2/(2\,x\,p^+) - i\eta$, and solving in turn the resulting integral over transverse momentum. The third one is more subtle, since the integrand does not vanish fast enough at the boundary to apply Jordan's lemma. Instead, we can isolate the troublesome term, introduce a Schwinger parameter, and integrate the minus component to a Dirac delta:

$$\begin{aligned}
&\int d\ell^- \frac{1}{-2p^+\ell^-(1-x) + \ell_\perp^2 - xm^2 + i\eta} \\
&\quad = -i \int_0^\infty dt \int d\ell^- \exp\Big[it\big(-2p^+\ell^-(1-x) + \ell_\perp^2 - xm^2\big)\Big] \\
&\quad = -\frac{\pi i}{p^+}\,\delta(1-x) \int_0^\infty \frac{dt}{t} \exp\Big[it\big(\ell_\perp^2 - xm^2\big)\Big].
\end{aligned} \tag{2.42}$$

This endpoint contribution at $x = 1$ corresponds to the limit where the photon leg carries

all the momentum along the +-direction and the fermion line becomes soft.

Results for the integrals relevant to computing eq. (2.40) are collected in eq. (2.94) in appendix 2.B. Having carried them out, we conclude

$$J^{(1)\nu}_{(f\gamma)}(x,p) = -\frac{e}{16\pi^2}\left(\frac{m^2}{4\pi\mu^2}\right)^{-\epsilon}\Gamma(\epsilon)\,\bar{u}(p)\left\{m\,x^{1-2\epsilon}(\not{n}\,n^\nu-\gamma^\nu)\right.$$
$$\left.+\frac{m^2}{p_+}\left[\frac{1}{2(1-\epsilon)}\big(\delta(1-x)-(1-2\epsilon)\,x^{1-2\epsilon}\big)\gamma^\nu\not{n}-2\,x^{-2\epsilon}(1-x)\,\bar{n}^\nu\right]\right\}, \quad (2.43a)$$

$$J^{(1)\nu\rho}_{(f\partial\gamma)}(x,p) = -\frac{e}{16\pi^2}\left(\frac{m^2}{4\pi\mu^2}\right)^{-\epsilon}\Gamma(\epsilon)\,\bar{u}(p)\,\frac{m^2x^{2-2\epsilon}}{2(1-\epsilon)}\left\{\gamma_\perp^\rho(\not{n}\,n^\nu-\gamma^\nu)+\frac{2}{x}\eta_\perp^{\nu\rho}\right\}. \quad (2.43b)$$

These are the one-loop expressions for the $f\gamma$- and $f\partial\gamma$-jet functions in QED, as derived in light-cone gauge. As expected, the $f\gamma$-jet function starts at order $\lambda\sim m/Q$, while the $f\partial\gamma$-jet has pure λ^2 scaling. This is due to the additional factor $\ell_\perp^\rho$, which arises in the expansion of $\widetilde{H}_{(f\gamma)}$ in eq. (2.38), which it absorbs in the definition of eq. (2.39). As a result only the structure $\ell_\perp^\alpha\ell_\perp^\beta$ in eq. (2.41) survives in the numerator. Since m is the only small scale in these functions, the mass expansion coincides with the power expansion.

2.2.2 Testing NLP factorisation with the method of regions

Equipped with the result of eq. (2.43), we will now test the factorisation formula eq. (2.31) in a process with two final-state jet directions, at both one- and two-loop order. Specifically, we wish to see whether this formula reproduces the (hard-)collinear limit of full, unfactorised amplitudes which at face value should be described by the $f\gamma$- and $f\partial\gamma$-jet functions. We will isolate the part of the amplitude that we want to compare with, using the method of regions [108–111]. This is a well-tested tool for calculating amplitudes in kinematic limits where the various scales entering the amplitude are separated in magnitude, thus allowing for a systematic expansion in the ratio of these scales. It is particularly useful for the dissection of loop integrals, by defining regions where the virtual modes have momenta of a certain size as compared to a particular scale in the problem. In this case we use the small ratio of scales $\lambda=\frac{m}{Q}$ to select momentum regions where a virtual photon is hard, soft or collinear to either of the highly energetic particles in the final state. Once the regions have been defined, one may expand the integrand for each region in λ (up to an arbitrary order), which simplifies its structure. The integration is still carried out over the full momentum space, which allows for easy evaluation, but one must be careful not to overcount contributions that appear in multiple regions. For our purposes this is no issue, as each region has a specific associated energy scale (in our case, $(m^2/\mu^2)^{-\epsilon}$ for a collinear region and $(2p_1^+p_2^-/\mu^2)^{-\epsilon}$ for the hard region), which inhibits any cross-talk between such regions. Finally, by summing over all relevant regions, one obtains the result of the full integral up to the chosen order in λ.

With just two jets in the final state, we choose a frame in which the jets are back to back. Given the light-cone decomposition of p_1^μ, we identify the direction collinear to p_2^μ as the

anti-collinear direction. This yields the following regions

$$\begin{aligned} \text{Hard}: \quad & k^\mu \sim Q(1,1,1)\,, & \text{Soft}: \quad & k^\mu \sim Q\left(\lambda^2,\lambda^2,\lambda^2\right), \\ \text{Collinear}: \quad & k^\mu \sim Q\left(1,\lambda,\lambda^2\right), & \text{Anti-collinear}: \quad & k^\mu \sim Q\left(\lambda^2,\lambda,1\right). \end{aligned} \tag{2.44}$$

In the following sections we refrain from considering all regions, but use this tool to extract only the contribution from the collinear (hard-collinear) region of the full amplitude, which is relevant for our one-loop (two-loop) test. For a more detailed discussion, see chapter 3 (in particular section 3.2), where a complete method of regions analysis at NLP is presented for part of the N^{3}LO correction to the DY process.

One-loop test

For one-loop accuracy we calculate the collinear region of fig. 2.6, which should be described by contracting the one-loop $f\gamma$- and $f\partial\gamma$-jet functions with corresponding tree-level hard functions. We will carry out the regions calculation in axial gauge, as we did for the $f\gamma$- and $f\partial\gamma$-jet functions.

The full amplitude for the diagram in fig. 2.6 reads

$$\begin{aligned} \mathscr{M}^{(1)\alpha}(p_1,p_2) &= \int \frac{d^{4-2\epsilon}\ell_1}{(2\pi)^{4-2\epsilon}} \frac{e^3\,\mu^{2\epsilon}\,\bar{u}(p_1)N^{(1)\alpha}(p_i,\ell_1)\,v(p_2)}{\left[\ell_1^2+i\eta\right]\left[(p_1-\ell_1)^2-m^2+i\eta\right]\left[(p_2^2+\ell_1)^2-m^2+i\eta\right]}\,, \\ N^{(1)\alpha}(p_i,\ell_1) &= \gamma^\sigma(\not{p}_1-\not{\ell}_1+m)\gamma^\alpha(-\not{p}_2-\not{\ell}_1+m)\left(-\gamma_\sigma+\frac{\ell_\sigma\,\not{\bar{n}}+\not{\ell}\,\bar{n}_\sigma}{\ell\cdot\bar{n}}\right). \end{aligned} \tag{2.45}$$

The expansion of the integrand in the collinear region is obtained by rescaling the momentum components of both the (collinear) loop momentum and the (anti-)collinear external momenta, according to eq. (2.44). We further exploit our freedom of frame choice to set the perpendicular momentum components of the external momenta to zero. In practice, it is convenient to project onto a single set of light-like vectors in the plus- and minus-direction, using

$$p_1^\mu = \underbrace{p_1\cdot\bar{n}}_{\sim\lambda^0}\,n^\mu + \underbrace{p_1\cdot n}_{\sim\lambda^2}\,\bar{n}^\mu \qquad \text{and} \qquad p_2^\mu = \underbrace{p_2\cdot\bar{n}}_{\sim\lambda^2}\,n^\mu + \underbrace{p_2\cdot n}_{\sim\lambda^0}\,\bar{n}^\mu. \tag{2.46}$$

The denominator in eq. (2.45) is expanded as

$$\begin{aligned} &\frac{1}{\ell_1^2+i\eta}\frac{1}{(\ell_1-p_1)^2-m^2+i\eta}\frac{1}{(\ell_1+p_2)^2-m^2+i\eta} = \frac{1}{\ell_1^2+i\eta} \\ &\times\frac{1}{(\ell_1^2-2\,\ell_1\cdot\bar{n}\,p_1\cdot n-2\,\ell_1\cdot n\,p_1\cdot\bar{n})+i\eta}\frac{1}{2\,\ell_1\cdot\bar{n}\,p_2\cdot n+i\eta}\left[1-\frac{\ell_1^2}{2\,\ell_1\cdot\bar{n}\,p_2\cdot n+i\eta}+\mathscr{O}(\lambda^4)\right], \end{aligned} \tag{2.47}$$

where all propagator denominators have now a homogenous λ-scaling. The numerator in eq. (2.45) is suppressed by one power of λ, allowing us to drop every term but the leading

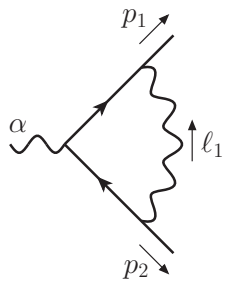

Figure 2.6: *One-loop diagram used for verification of the jet function results.*

one from the denominator expansion in eq. (2.47), including the explicitly shown $\mathcal{O}(\lambda^2)$ term. By discarding higher power corrections in the numerator too, we readily calculate the collinear region up to NLP from this expression using standard techniques: we perform the Dirac algebra using the `Mathematica` package `FeynCalc` [119, 120], Feynman parametrise the homogeneous denominators, shift the loop momentum and remove odd integrands, evaluate the momentum integrals through standard tensor integrals and finally integrate the Feynman parameters in a convenient order. We find

$$\begin{aligned}\mathscr{M}_{\mathrm{C}}^{(1)\alpha}(p_1,p_2) = \frac{i\,e^3}{16\,\pi^2}\frac{m}{p_2\cdot n}\left(\frac{m^2}{4\pi\mu^2}\right)^{-\epsilon}\frac{\Gamma(1+\epsilon)}{\epsilon} \\ \times\,\bar{u}(p_1)\left[n^\alpha - \frac{m}{2\,p_1\cdot\bar{n}}\frac{1-2\epsilon+4\epsilon^2}{(1-\epsilon)(1-2\epsilon)}\gamma^\alpha\right]v(p_2)\,.\end{aligned} \tag{2.48}$$

The subscript C indicates that this result is expanded in the collinear region. As expected, in axial gauge the diagram obeys the power counting, strictly contributing only at NLP. This expression has a single pole in ϵ, which receives both UV and IR contributions. The UV term regulates divergences that would be subtracted by one-loop renormalisation; the remainder has a collinear (rather than soft) origin.

The vector nature of the electromagnetic current and the Sudakov decomposition we employ in eq. (2.46) limit the possible Dirac structures that can appear in the result to γ^α, n^α, and $\bar{n}^\alpha$. In this specific case, the structure $\bar{n}^\alpha$ is absent due to a cancellation which, as our two-loop check will make clear, is accidental.

Turning to the factorisation approach, we note that the collinear photon in fig. 2.6 is emitted from an anti-collinear external line, such that the propagator before the emission carries a hard momentum. Consequently, this diagram should be described by the convolution of the one-loop $f\gamma$- and $f\partial\gamma$-jets with the respective (tree-level) hard functions, as claimed above. We expect the following factorisation structure up to $\mathcal{O}(\lambda^2)$

$$\begin{aligned}\mathscr{M}_{\text{fact.}}^{(1)\alpha}(p_1,p_2) = \int_0^1 dx\Big[J_{(f\gamma)}^{(1)\nu}(x,p_1)\,H_{(f\gamma)\nu}^{(0)\alpha}(x,p_1,p_2) \\ + J_{(f\partial\gamma)}^{(1)\nu\rho}(x,p_1)\,H_{(f\partial\gamma)\nu\rho}^{(0)\alpha}(x,p_1,p_2)\Big]J_{(f)}^{(0)}(p_2)\,.\end{aligned} \tag{2.49}$$

The hard functions are extracted from fig. 2.7, and its $f\gamma$- and $f\partial\gamma$- parts separated accord-

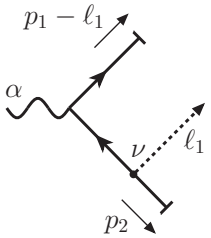

Figure 2.7: *Diagrammatic interpretation of the leading order hard function $\widetilde{H}^{(0)}_{(f\gamma)}$, from which $H^{(0)}_{(f\gamma)}$ and $H^{(0)}_{(f\partial\gamma)}$ are derived. The dashed line indicates where the collinear momentum ℓ is extracted. External lines are amputated.*

ing to the prescription of eq. (2.38), yielding

$$H^{(0)\alpha}_{(f\gamma)_\nu}(x,p_1,p_2) = -i\,e^2\,\frac{1}{2x\,p_1\cdot\bar{n}\,p_2\cdot n}\gamma^\alpha(x\,p_1\cdot\bar{n}\,\not{n}+p_2\cdot n\,\not{\bar{n}}-m)\gamma_\nu\,, \tag{2.50}$$

$$H^{(0)\alpha}_{(f\partial\gamma)_{\nu\rho}}(x,p_1,p_2) = +i\,e^2\,\frac{1}{2x\,p_1\cdot\bar{n}\,p_2\cdot n}\gamma^\alpha\gamma_{\perp\rho}\gamma_\nu\,. \tag{2.51}$$

We emphasise that since we are interested in the first two orders in λ, we cannot ignore $\mathcal{O}(\lambda)$ terms in the numerator of eq. (2.50), as they will combine with the leading term in the $f\gamma$-jet (eq. (2.43)). In particular, we cannot drop the mass term. However, we can do so in eq. (2.51), since the $f\partial\gamma$-jet is proportional to two powers of the mass (thus $\mathcal{O}(\lambda^2)$). After some Dirac algebra, we find

$$\begin{aligned} J^{(1)\nu}_{(f\gamma)}(x,p_1)H^{(0)\alpha}_{(f\gamma)_\nu}(x,p_1,p_2)J^{(0)}_{(f)}(p_2) &= \frac{i\,e^3}{8\,\pi^2}\frac{m}{p_2\cdot n}\left(\frac{m^2}{4\pi\mu^2}\right)^{-\epsilon}\Gamma(1+\epsilon)\,\bar{u}(p_1) \\ &\quad\times\left[\left(\frac{1}{\epsilon}-1\right)x^{1-2\epsilon}\,n^\alpha+\frac{m}{2\,p_1\cdot\bar{n}}\gamma^\alpha\frac{1}{1-\epsilon}\left(\delta(1-x)+x^{1-2\epsilon}\epsilon\right)\right]v(p_2)\,, \end{aligned} \tag{2.52}$$

$$\begin{aligned} J^{(1)\nu\rho}_{(f\partial\gamma)}(x,p_1)H^{(0)\alpha}_{(f\partial\gamma)_{\nu\rho}}(x,p_1,p_2)J^{(0)}_{(f)}(p_2) &= -\frac{i\,e^3}{32\,\pi^2}\frac{m^2}{p_1\cdot\bar{n}\,p_2\cdot n}\left(\frac{m^2}{4\pi\mu^2}\right)^{-\epsilon}x^{-2\epsilon}\,\bar{u}(p_1)\gamma^\alpha v(p_2) \\ &\quad\times\Gamma(1+\epsilon)\left[\frac{1}{\epsilon}-\frac{1}{1-\epsilon}\left(\frac{1}{\epsilon}-1-\epsilon\right)x\right]. \end{aligned} \tag{2.53}$$

The integral over the energy fraction x is easily performed, yielding indeed the result in eq. (2.48). This provides a first check of our jet functions. We observe that the singular structure of the collinear region is entirely reproduced by the jet functions of eq. (2.43), while the convolution with the respective hard functions does not generate any additional pole in ϵ. We stress that the endpoint contribution, described by the Dirac delta function in eq. (2.52), is essential to obtain the correct result.

Two-loop test

We now proceed with a more strenuous test, based on the same method. The goal is to validate the factorisation of a fermion-antifermion production amplitude into $f\gamma$- and $f\partial\gamma$-

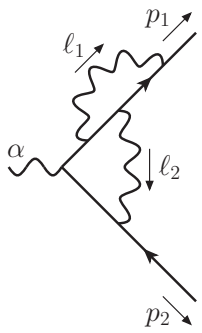

Figure 2.8: *A typical two-loop diagram that receives contributions from the $f\gamma$- and $f\partial\gamma$-jet functions.*

jet functions if the hard function is loop-induced. A minimal diagram suited for this task is given in fig. 2.8. It consists of an off-shell, one-loop vertex correction, described by the hard loop momentum ℓ_2, which gets probed by a collinear fermion-photon pair forming the ℓ_1-loop on the upper leg. We recall that focusing on one particular diagram is justified in axial gauge, where the power counting holds on a diagram-by-diagram basis and the factorisation picture is derived.[10] Naturally, a complete evaluation of such a process would require us to determine the full hard function, necessitating the calculation of additional diagrams.

We now proceed with the region expansion. The full two-loop amplitude reads

$$\mathscr{M}^{(2)\alpha}(p_1,p_2) = i\,e^5\mu^{4\epsilon}\int\frac{d^{4-2\epsilon}\ell_1}{(2\pi)^{4-2\epsilon}}\int\frac{d^{4-2\epsilon}\ell_2}{(2\pi)^{4-2\epsilon}}\,\frac{\bar{u}(p_1)N^{(2)\alpha}(p_i,\ell_i)\,v(p_2)}{\big[(\ell_1-p_1)^2-m^2\big]\big[(\ell_1-\ell_2-p_1)^2-m^2\big]} \times\frac{1}{\big[(\ell_2+p_1)^2-m^2\big]\big[(\ell_2-p_2)^2-m^2\big]\big[\ell_1^2\big]\big[\ell_2^2\big]}\,, \tag{2.54}$$

where for brevity we omitted the Feynman prescription $i\eta$ in each of the square brackets in the denominators. The numerator structure is given by

$$N^{(2)\alpha}(p_i,\ell_i) = \gamma^\mu(\not{p}_1-\not{\ell}_1+m)\gamma^\rho(\not{p}_1-\not{\ell}_1+\not{\ell}_2+m)\gamma^\nu(\not{p}_1+\not{\ell}_2+m)\gamma^\alpha(-\not{p}_2+\not{\ell}_2+m)\gamma^\sigma \times\left(\eta_{\mu\nu}-\frac{\ell_{1\mu}\bar{n}_\nu+\ell_{1\nu}\bar{n}_\mu}{\ell_1\cdot\bar{n}}\right)\left(\eta_{\rho\sigma}-\frac{\ell_{2\rho}\bar{n}_\sigma+\ell_{2\sigma}\bar{n}_\rho}{\ell_2\cdot\bar{n}}\right). \tag{2.55}$$

To carry out the integrals in eq. (2.54) we use the same techniques as the one-loop example. The main difference is the presence of two-loop integrals, but due to the regions expansion the added complexity is limited. In the presence of masses and axial-gauge propagators, numerator structures proliferate, which makes the calculation computationally more intensive. However, as in the one-loop case, the numerator (2.55) scales as λ, which allows us to neglect $\mathcal{O}(\lambda^2)$ terms from the denominator expansion. In fact, only the denominator in

[10] For covariant gauge choices, one is forced to sum over a gauge invariant set of diagrams, as we will see in section 2.3. An extensive analysis of relevant momentum configurations is given in section 2.3.3.

eq. (2.54) mixing the two loop momenta generates $\mathcal{O}(\lambda)$ terms, through the expansion

$$\frac{1}{(\ell_1-\ell_2-p_1)^2-m^2} = \frac{1}{\ell_2^2+2\,\ell_2\cdot n\,(p_1-\ell_1)\cdot\bar{n}} + \frac{2\,\ell_{1\perp}\cdot\ell_{2\perp}}{\left[\ell_2^2+2\,\ell_2\cdot n\,(p_1-\ell_1)\cdot\bar{n}\right]^2} + \mathcal{O}(\lambda^2), \quad (2.56)$$

which is a consequence of our frame choice, $p_{1\perp}=p_{2\perp}=0$. For the 1-loop-hard 1-loop-collinear (HC) region we thus obtain

$$\begin{aligned}\mathscr{M}^{(2)\alpha}_{\mathrm{HC}}(p_1,p_2) = \frac{i\,e^5}{128\,\pi^4}\left(\frac{-2\,p_1\cdot\bar{n}\,p_2\cdot n}{4\pi\mu^2}\right)^{-\epsilon}\left(\frac{m^2}{4\pi\mu^2}\right)^{-\epsilon}\frac{1}{1-2\epsilon}\,\bar{u}(p_1)\Bigg\{m\,\Gamma_1\left(\frac{1}{\epsilon^3}+\frac{2}{\epsilon^2}-\frac{3}{\epsilon}\right)\\ \times\left(\frac{\bar{n}^\alpha}{p_1\cdot\bar{n}}-\frac{n^\alpha}{p_2\cdot n}\right)+m\,\Gamma_2\Bigg[\left(\frac{2}{\epsilon^3}-\frac{1}{\epsilon^2}-\frac{8}{\epsilon}+11-4\epsilon\right)\frac{n^\alpha}{p_2\cdot n}\\ -\left(\frac{4}{\epsilon^3}-\frac{8}{\epsilon^2}+\frac{1}{\epsilon}+3\right)\frac{\bar{n}^\alpha}{p_1\cdot\bar{n}}\Bigg]+\frac{m^2}{2p_1\cdot\bar{n}\,p_2\cdot n}\,\gamma^\alpha\Bigg[\frac{\Gamma_1}{(1-\epsilon^2)}\left(\frac{3}{\epsilon^2}-\frac{8}{\epsilon}-11+14\epsilon+8\epsilon^2\right)\\ +\frac{\Gamma_2}{(1+\epsilon)}\left(\frac{2}{\epsilon^3}+\frac{1}{\epsilon^2}-\frac{13}{\epsilon}+44-28\epsilon-24\epsilon^2\right)\Bigg]\Bigg\}\,v(p_2), \end{aligned} \quad (2.57)$$

where $\Gamma_{1,2}$ denote the following combinations of Euler gamma functions

$$\Gamma_1=\frac{\Gamma^2(1-\epsilon)\,\Gamma^2(1+\epsilon)}{\Gamma^2(2-2\epsilon)}, \qquad \Gamma_2=\frac{\Gamma^3(1-\epsilon)\,\Gamma^2(1+\epsilon)}{\Gamma(3-3\epsilon)}. \quad (2.58)$$

It is instructive to compare this result with its one-loop equivalent in eq. (2.48). We observe a similar Dirac structure, but now all three different terms γ^α, n^α and $\bar{n}^\alpha$ contribute. Naturally the coefficients are more involved than at the one-loop level. An important difference is that the result features the two independent Γ-combinations in eq. (2.58), due to the more involved dynamical structure. Moreover, since now a hard and a collinear loop are present at the same time, both scale ratios $(m^2/\mu^2)^{-\epsilon}$ and $(-2\,p_1^+p_2^-/\mu^2)^{-\epsilon}$ show up in the prefactor. However, setting for convenience the renormalisation scale equal to the hard scale will remove the second factor. Upon expansion in ϵ this will result in logarithms of $m^2/(2p_1^+p_2^-)$ at NLP, as for the one-loop case. These are small-mass logarithms that ideally could be resummed by a complete factorisation framework.

We now continue with the calculation of the corresponding hard functions, and check that the convolution with the jet functions in eq. (2.43) reproduces our region calculation. Similar to the one-loop example, we can extract the hard functions by Taylor expanding the hard matrix element represented in fig. 2.9, according to the prescription of eq. (2.38). The unexpanded amplitude reads

$$\begin{aligned}\widetilde{H}^{(1)\alpha\nu}_{(f\gamma)}(p_1,p_2,\ell_1) = \int\frac{d^{4-2\epsilon}\ell_2}{(2\pi)^{4-2\epsilon}}\,\frac{e^4\mu^{2\epsilon}\,\bar{u}(p_1)\,\gamma^\sigma(\not{p}_1-\not{\ell}_1+\not{\ell}_2+m)\gamma^\nu(\not{p}_1+\not{\ell}_2+m)\gamma^\alpha(-\not{p}_2+\not{\ell}_2+m)}{\left[(\ell_2+p_1-\ell_1)^2-m^2\right]\left[(\ell_2+p_1)^2-m^2\right]\left[(\ell_2-p_2)^2-m^2\right]}\\ \times\frac{1}{\ell_2^2}\left(-\gamma_\sigma+\frac{\ell_2\,\bar{n}_\sigma+\not{n}\,\ell_{2\sigma}}{\ell_2\cdot\bar{n}}\right), \end{aligned} \quad (2.59)$$

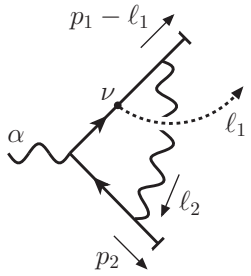

Figure 2.9: *Diagrammatic representation of the one-loop matrix element $\widetilde{H}^{(1)}_{(f\gamma)}$, from which we extract $H^{(1)}_{(f\gamma)}$ and $H^{(1)}_{(f\partial\gamma)}$.*

from which we separate the $f\gamma$- and $f\partial\gamma$-term,

$$H^{(1)\alpha\nu}_{(f\gamma)}(x,p_1,p_2) = e^4\mu^{2\epsilon}\int\frac{d^{4-2\epsilon}\ell_2}{(2\pi)^{4-2\epsilon}}\,\frac{N^{\alpha\nu}_{(f\gamma)}(x,p_i,\ell_2)}{D(x,p_i,\ell_2)}\,, \tag{2.60}$$

$$H^{(1)\alpha\nu\rho}_{(f\partial\gamma)}(x,p_1,p_2) = e^4\mu^{2\epsilon}\int\frac{d^{4-2\epsilon}\ell_2}{(2\pi)^{4-2\epsilon}}\,\frac{N^{\alpha\nu\rho}_{(f\partial\gamma)}(x,p_i,\ell_2)}{D(x,p_i,\ell_2)}\,. \tag{2.61}$$

Here the common denominator and the numerator structures are

$$\begin{aligned}
D(x,p_i,\ell_2) &= \big[\ell_2^2\big]\big[\ell_2^2+2\ell_2\cdot n\,p_1\cdot\bar n(1-x)\big]\big[\ell_2^2+2\ell_2\cdot n\,p_1\cdot\bar n\big]\big[\ell_2^2-2\ell_2\cdot\bar n\,p_2\cdot n\big],\\
N^{\alpha\nu}_{(f\gamma)}(x,p_i,\ell_2) &= \gamma^\mu\big[(1-x)p_1\cdot\bar n\,\not n+\not\ell_2+m\big]\gamma^\nu\big[p_1\cdot\bar n\,\not n+\not\ell_2+m\big]\gamma^\alpha\big[-\not p_2+\not\ell_2+m\big]\\
&\quad\times\big[-\gamma_\mu+\big(\ell_2\,\bar n_\mu+\not n\,\ell_{2\mu}\big)/\ell_2\cdot\bar n\big],\\
N^{\alpha\nu\rho}_{(f\partial\gamma)}(x,p_i,\ell_2) &= \left\{-\gamma^\mu\gamma_\perp^\rho\gamma^\nu(p_1\cdot\bar n+\ell_2)+\frac{2\,\ell_2^\rho\,\gamma^\mu\big[p_1\cdot\bar n(1-x)+\ell_2\big]\gamma^\nu(p_1\cdot\bar n+\ell_2)}{\big[\ell_2^2+2\ell_2\cdot n\,p_1\cdot\bar n(1-x)\big]}\right\}\\
&\quad\times\gamma^\alpha(-p_2\cdot n\,\not n+\not\ell_2)\big[-\gamma_\mu+\big(\ell_2\,\bar n_\mu+\not n\,\ell_{2\mu}\big)/\ell_2\cdot\bar n\big].
\end{aligned} \tag{2.62}$$

Note that the derivative in the transverse component defining the $f\partial\gamma$-term as in eq. (2.38) can act either on the spin structure in the numerator, or on the $\ell_{1\perp}$-dependent denominator of eq. (2.59), generating the two structures displayed in curly brackets. In the $f\partial\gamma$-numerator structure we already dropped $\mathcal{O}(\lambda)$ terms, since we know that this structure enters the factorisation formula in a convolution with a jet function that is already $\mathcal{O}(\lambda^2)$. We can now solve the integral with standard techniques. The presence of many different spin structures at this stage renders the intermediate expressions for the hard functions rather cumbersome, therefore we will not show them here. Taking the convolutions with the jet functions in eq. (2.43) yields the partial results shown in eqs. (2.96) and (2.97) in appendix 2.B. As one can readily verify, their sum correctly reproduces the hard-collinear region result obtained in eq. (2.57).

We will now examine the pole structure of eq. (2.57) in light of the equivalent factorisation result. Interestingly, we note the presence of triple poles. One overall inverse power of ϵ is due to the single pole in the jet functions in eq. (2.43), while the remaining factor of $1/\epsilon^2$ has two distinct origins. First, the hard functions contain explicit double poles since they

describe both hard and soft physics. In section 2.3.3 we will extensively comment on this effect when examining the hard function in eq. (2.81). Second, the hard functions contain $\frac{1}{\epsilon}\frac{1}{x}$ terms that produce an additional pole upon convolution with the respective jet functions. These endpoint singularities arise in the limit where the dominant momentum component of the collinear photon vanishes. Their origin is thus different from that of the (finite) endpoint contributions captured by $\delta(1-x)$ in eq. (2.43), which describe the soft quark limit. Endpoint singularities also appear in factorisation studies using SCET [88, 89, 103, 121], and seem inevitable at NLP. Since the expressions involved are unrenormalised quantities expressed in $d = 4-2\epsilon$ dimensions, the endpoint singularities are easily regulated.

2.3 Hard-collinear factorisation for massless fermions

In this section, we focus on the scenario of negligible fermion masses, $m = 0$, which is the standard approximation in high-energy collisions for light quarks. In the previous section we have seen that the fermion mass entered the non-radiative $f\gamma$-jet function through the overall scale factor $\left(m^2/\mu^2\right)^{-\epsilon}$ and a second-order polynomial in m. Removing this scale from the problem will thus have a serious impact on the ingredients in the factorisation framework. Virtual loop corrections to the f-jet, as well as all loop-induced, genuine NLP jet functions (like the $f\gamma$-jet), are rendered scaleless and do not contribute. However as we are ultimately interested in threshold effects associated to soft final-state radiation, we are required to compute *radiative* jet functions. For such functions a new scale arises, set by the dot product of the (external) momenta of the emitting fermion and the soft photon. In massless radiative jet functions this small scale takes the place of the mass as the collinear scale.

As in the previous section, we will focus on the $f\gamma$- and $f\partial\gamma$-jet functions. The radiative functions will be obtained from the non-radiative counterparts by inserting a soft photon on any of the collinear fermion lines. Checking the factorisation properties of gauge-invariant sets of diagrams will allow us to make a convenient choice of gauge. While axial gauge proved to be practical for power counting the pinch surfaces that underlie the factorisation ingredients, Feynman gauge is more suited for complex calculations. Therefore, we will extract the radiative jet functions here using the latter, and apply this gauge choice consistently in the calculation of the hard functions. The presence of longitudinally polarised photons in Feynman gauge will modify the power counting for individual diagrams. As a consequence, each diagram calculated in this section may contain spurious LP terms, which must cancel upon summing over a gauge-invariant set of diagrams.

The radiative jet functions we extract are process-independent quantities, which describe collinear physics regardless of the underlying hard scattering event. Similar to the massive case, we validate the expressions obtained by convolving these jets with appropriate hard functions by means of a one- and two-loop method of regions calculation. These non-trivial

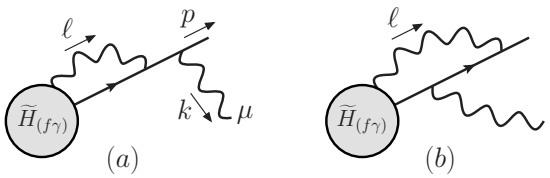

Figure 2.10: *Contributions to the radiative $f\gamma$- and $f\partial\gamma$-jet.*

checks show that the all-order factorisation formula for elastic amplitudes in eq. (2.31) provides a good starting point for the factorisation (and potentially resummation) of threshold effects due to soft final state radiation.

In particular, our current approach captures an intricate hard-collinear interplay effect that occurs in matrix elements beyond one-loop, while the simpler NLP factorisation formula presented in refs. [78, 79] is not equipped to describe such effects. In fact, our calculations show that this formula does also not suffice for one-loop accuracy at the matrix element level, although it works at the cross section level for the cases studied there. This has also been noted in a SCET context recently [88].

2.3.1 The radiative, massless $f\gamma$-jet

At the lowest order in perturbation theory the radiative $f\gamma$- and $f\partial\gamma$-jet receive contributions from the two diagrams in fig. 2.10. Both functions are defined in the same manner as in the massive fermion case and their evaluation relies on similar techniques. As before, we drop terms beyond NLP. In this case, we apply this constraint to the more involved denominator structure too, expanding denominators whose scaling is inhomogeneous in λ, as we did in the method of regions calculation of the amplitude. For example, after rescaling the momentum components by the appropriate powers of λ, the denominator of the innermost propagator is expanded as

$$\frac{1}{(\ell-p-k)^2+i\eta} = \frac{1}{D(\ell,p,k)}\left[1+\overbrace{\frac{2\ell_\perp\cdot k_\perp}{D(\ell,p,k)}}^{\sim\lambda}+\overbrace{\left(\frac{2\ell^- k^+}{D(\ell,p,k)}+\frac{(2\ell_\perp\cdot k_\perp)^2}{D(\ell,p,k)^2}\right)}^{\sim\lambda^2}\right], \tag{2.63}$$

assuming collinear and soft scaling for ℓ and k respectively and abbreviating the homogeneous denominator by

$$D(\ell,p,k) = 2\ell^+\ell^- + \ell_\perp^2 - 2p^+\ell^- - 2\ell^+k^- + 2p^+k^- + i\eta\,. \tag{2.64}$$

Note that, having set $m=0$, the external momentum can be chosen to be strictly in the $+$-direction $p=(p^+,0,0)$.

Using this approach, we require six one-loop integrals to evaluate the contributions to the $f\gamma$- and $f\partial\gamma$-jet, which are listed in appendix 2.C.1. We find the following result for these

jet functions

$$J^{(1)\mu\nu}_{(f\gamma)}(x,p,k) = -\frac{e^2}{16\pi^2}\left(\frac{-2p^+k^-}{4\pi\mu^2}\right)^{-\epsilon}\Gamma(\epsilon)\,[x(1-x)]^{-\epsilon}\,\bar{u}(p)\Big\{2(1-x)\,\eta^{\mu\nu} - \frac{\epsilon}{1-\epsilon}\,x\,\gamma^\nu\gamma^\mu + 2(1-2x)\frac{k^+}{k^-}n^\mu n^\nu - 2(1-2x)\,\bar{n}^\mu n^\nu + \frac{1}{k^-}\Big[x\,\gamma^\mu \not{k}\, n^\nu + 2\,\frac{\epsilon}{1-\epsilon}\,x\,k^\mu n^\nu + \frac{\epsilon}{1-\epsilon}\,x\,\gamma^\nu \not{k}\, n^\mu - 2(1-x)\,n^\mu k^\nu\Big]\Big\}, \tag{2.65}$$

$$J^{(1)\mu\nu\rho}_{(f\partial\gamma)}(x,p,k) = -\frac{e^2\,p^+}{8\pi^2}\left(\frac{-2p^+k^-}{4\pi\mu^2}\right)^{-\epsilon}\frac{\Gamma(\epsilon)}{1-\epsilon}\,[x(1-x)]^{1-\epsilon}\,\bar{u}(p)\,n^\nu\left(\eta^{\mu\rho}_\perp - \frac{n^\mu k^\rho_\perp}{k^-}\right). \tag{2.66}$$

We point out that eq. (2.65) is strictly $\mathcal{O}(\lambda^0)$, while the individual contributions from fig. 2.10a and fig. 2.10b have indeed a LP component $\mathcal{O}(\lambda^{-2})$. Note that eq. (2.65) does not contain the $\delta(1-x)$ term which appeared in the non-radiative jet function for the massive fermion case (see eq. (2.43)) which was associated to the soft quark limit. In principle, one might expect a similar contribution here, but the numerator supplements the standard integrals of eqs. (2.98c) and (2.100c) with sufficient powers of $(1-x)$ to suppress such a term.

The radiative f-jet is known to have a Ward identity [78] relating it to its non-radiative counterpart (order by order in perturbation theory) via

$$k_\mu J^{(n)\mu}_{(f)}(p,k) = -q\,e\,J^{(n)}_{(f)}(p), \tag{2.67}$$

where $q = \pm 1$ for an initial/final state fermion jet.[11] Similarly, we expect

$$k_\mu J^{(n)\mu\nu}_{(f\gamma)}(x,p,k) = -q\,e\,J^{(n)\nu}_{(f\gamma)}(x,p), \tag{2.68a}$$

$$k_\mu J^{(n)\mu\nu\rho}_{(f\partial\gamma)}(x,p,k) = -q\,e\,J^{(n)\nu\rho}_{(f\partial\gamma)}(x,p). \tag{2.68b}$$

In particular, since $J^{(f\gamma)\nu}$ and $J^{(f\partial\gamma)\nu\rho}$ consist solely of scaleless integrals (for $m = 0$) and thus vanish in dimensional regularisation, we should find

$$k_\mu J^{(n)\mu\nu}_{(f\gamma)}(x,k) = 0 \qquad \text{and} \qquad k_\mu J^{(n)\mu\nu\rho}_{(f\partial\gamma)}(x,k) = 0. \tag{2.69}$$

By contracting eq. (2.65) and eq. (2.66) with k_μ, one finds that eq. (2.69) is indeed satisfied, which serves as a first check on these jet functions.

2.3.2 NLP factorisation of the collinear sector at the one-loop level

Following the same approach as in 2.2.2, we wish to test the factorisation structure of *radiative* amplitudes in the collinear sector, by means of a comparison to a method-of-regions computation of the single-real single-virtual (1R1V) correction to a dijet production process.

[11] The explicit minus sign follows from the adopted convention for jet's charge $Q = -1$.

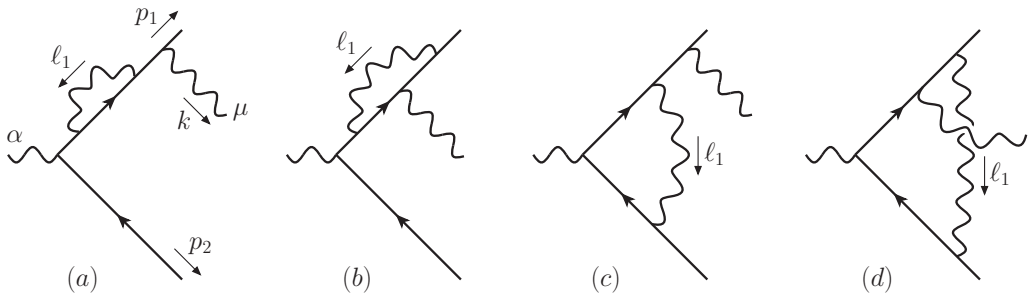

Figure 2.11: *Diagrams contributing to the collinear region of the 1R1V dijet production amplitude.*

A similar factorisation/regions analysis has been carried out in refs. [79, 122] for DY production, at the same loop order but at the cross-section level instead. In ref. [79], following ref. [78], a NLP factorisation formula for radiative amplitudes was derived from the standard LP factorisation picture for virtual amplitudes, while here we start from the generalised NLP factorisation formula of eq. (2.31). The difference between these two NLP approaches at the one- and two-loop level will be highlighted in the remainder of section 2.3.

The diagrams that contribute to the collinear sector at the one-loop order are shown in fig. 2.11. In diagrams (a) and (b) the collinear loop attaches solely to the upper leg, meaning that there is one fermion connection between the hard interaction and the part of the diagram containing the collinear dynamics. Therefore, these diagrams are predicted to factorise in terms of the one-loop radiative f-jet (see fig. 2.12), the Born-level hard scattering amplitude (with amputated legs) and a trivial jet function for the opposite leg:

$$\mathscr{M}^{(1)\alpha\mu}_{\text{a+b}\,|\,\text{fact.}}(p_1,p_2,k) = J^{(1)\mu}_{(f)}(p_1,k)\,H^{(0)\alpha}_{(f)}(p_1,p_2)\,J^{(0)}_{(f)}(p_2)\,, \tag{2.70}$$

with

$$J^{(0)}_{(f)}(p_2) = v(p_2) \qquad \text{and} \qquad H^{(0)\alpha}_{(f)} = -ie\gamma^\alpha.$$

The one-loop radiative f-jet is readily computed by standard techniques and the result reads

$$\begin{aligned} J^{(1)\mu}_{(f)}(p,k) = &-\frac{e^3}{16\pi^2}\frac{1}{p^+k^-}\left(\frac{-2\,p^+k^-}{4\pi\mu^2}\right)^{-\epsilon}\frac{\Gamma(1+\epsilon)\,\Gamma^2(1-\epsilon)}{\Gamma(2-2\epsilon)}\,\bar{u}(p) \\ &\times\left[\left(\frac{1}{\epsilon}+\frac{1}{2}\right)\gamma^\mu \not{k} + \left(\frac{1}{\epsilon}-1\right)k^\mu\right]. \end{aligned} \tag{2.71}$$

Note that this is strictly a NLP quantity, while from the non-radiative power counting formula (eq. (2.25)) one may have expected a contribution at LP. This power suppression is a radiative effect that only starts at one-loop order and is therefore not captured by the general power counting formula (the tree-level result does have a LP contribution). It is however fully consistent with ref. [78], in which the radiative f-jet is defined to account for the NLP effects induced by soft emissions from collinear loops.

As before, we may evaluate the contributions to the collinear sector of diagrams (a) and (b) in fig. 2.11, using again the method of regions. Keeping terms up to NLP, this approach

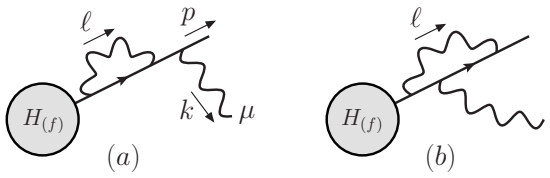

Figure 2.12: *One-loop contributions to the radiative f-jet.*

yields

$$\mathscr{M}^{(1)\alpha\mu}_{\text{a+b}\,|\,\text{C}}(p_1,p_2,k) = -\frac{ie^4}{8\pi^2}\frac{1}{t}\left(\frac{t}{4\pi\mu^2}\right)^{-\epsilon}\frac{\Gamma(1+\epsilon)\,\Gamma^2(1-\epsilon)}{\Gamma(2-2\epsilon)} \times \bar{u}(p_1)\left[\left(\frac{1}{\epsilon}+\frac{1}{2}\right)\gamma^\mu \not{k} + \left(\frac{1}{\epsilon}-1\right)k^\mu\right]\gamma^\alpha v(p_2)\,. \tag{2.72}$$

For massless fermions we may choose $p_1^\mu = (p_1^+,0,0)$ and $p_2^\mu = (0,0,p_2^-)$, such that the standard (massless) Mandelstam variable $t = (p_1-k)^2 = -2p_1^+k^-$. From eqs. (2.70) and (2.71) on the one hand and eq. (2.72) on the other, we see immediately that the regions result coincides with the factorisation result which, given the trivial factorisation structure of these diagrams, is perhaps not surprising.

For diagrams (c) and (d) in fig. 2.11 we expect a factorisation analogous to eq. (2.49)

$$\mathscr{M}^{(1)\alpha\mu}_{\text{c+d}\,|\,\text{fact.}}(p_1,p_2,k) = \int_0^1 dx\Big[J^{(1)\mu\nu}_{(f\gamma)}(x,p_1,k)\,H^{(0)\alpha}_{(f\gamma)\nu}(x,p_1,p_2) + J^{(1)\mu\nu\rho}_{(f\partial\gamma)}(x,p_1,k)\,H^{(0)\alpha}_{(f\partial\gamma)\nu\rho}(x,p_1,p_2)\Big]J^{(0)}_{(f)}(p_2)\,. \tag{2.73}$$

The hard functions are extracted from fig. 2.7 (now with $m=0$) according to the definition of eq. (2.38) and read

$$H^{(0)\alpha}_{(f\gamma)\nu}(x,p_1,p_2) = i\,e^2\,\frac{1}{x\,s}\gamma^\alpha\big(x\not{p}_1+\not{p}_2\big)\gamma_\nu\,, \tag{2.74}$$

$$H^{(0)\alpha}_{(f\partial\gamma)\nu\rho}(x,p_1,p_2) = i\,e^2\,\frac{1}{x\,s}\gamma^\alpha\gamma_{\perp\rho}\gamma_\nu\,, \tag{2.75}$$

where $s=(p_1+p_2)^2 = 2p_1^+p_2^-$. Since the $f\gamma$- and $f\partial\gamma$-jet function are strictly NLP quantities, we have discarded NLP corrections to both hard functions, as they would affect the full amplitude only at NNLP. Substituting eqs. (2.74) and (2.75) together with eqs. (2.65) and (2.66) into eq. (2.73) and simplifying the Dirac structure, we find

$$\mathscr{M}^{(1)\alpha\mu}_{\text{c+d}\,|\,\text{fact.}}(p_1,p_2,k) = \frac{i\,e^4}{8\pi^2}\left(\frac{t}{4\pi\mu^2}\right)^{-\epsilon}\Gamma(1+\epsilon)\,\frac{1}{\epsilon\,(1-\epsilon)}\int_0^1 dx\,[x\,(1-x)]^{-\epsilon}\,\bar{u}(p_1) \times\Bigg\{(1-\epsilon)\,\frac{1}{t}\,\gamma^\mu\not{k}\gamma^\alpha + 2\Bigg[\epsilon\,\frac{k^\mu}{t} - (1-2\epsilon)\,\frac{1}{s}\left(p_2^\mu - \frac{u}{t}\,p_1^\mu\right)\Bigg]\gamma^\alpha - 2\,\epsilon\,\frac{1}{s}\big[p_2^\alpha - (1-(1-\epsilon)\,x)\,p_1^\alpha\big]\Bigg[2\,\frac{p_1^\mu\not{k}}{t}+\gamma^\mu\Bigg]\Bigg\}\,v(p_2)\,, \tag{2.76}$$

with $u = (p_2 - k)^2 = -2p_2^- k^+$. Upon integration over the convolution parameter x, we conclude that this indeed reproduces the regions result

$$\begin{aligned}\mathscr{M}^{(1)\alpha\mu}_{\text{c+d}\,|\,\text{C}}(p_1,p_2,k) = \frac{i\,e^4}{8\pi^2}\left(\frac{t}{4\pi\mu^2}\right)^{-\epsilon}\frac{\Gamma(1+\epsilon)\,\Gamma^2(1-\epsilon)}{\Gamma(2-2\epsilon)}\\ \times\bar{u}(p_1)\bigg\{\frac{1}{\epsilon}\,\frac{1}{t}\,\gamma^\mu \not{k}\gamma^\alpha + 2\bigg[\frac{1}{1-\epsilon}\,\frac{k^\mu}{t} - \left(\frac{1}{\epsilon}-\frac{1}{1-\epsilon}\right)\frac{1}{s}\left(p_2^\mu - \frac{u}{t}\,p_1^\mu\right)\bigg]\gamma^\alpha\\ - \frac{1}{s}\bigg[\frac{2}{1-\epsilon}\,p_2^\alpha - \frac{1+\epsilon}{1-\epsilon}\,p_1^\alpha\bigg]\bigg[2\,\frac{p_1^\mu \not{k}}{t} + \gamma^\mu\bigg]\bigg\}\,v(p_2)\,. \end{aligned} \tag{2.77}$$

The collinear sector of the radiative amplitudes in fig. 2.11 is thus, up to NLP, correctly described by dressing the jet functions appearing in eq. (2.31) with a single soft emission. This is another indication that this factorisation formula organises NLP contributions correctly, even in presence of soft final state radiation. Moreover, this comparison serves as an explicit verification of the process-independent jet functions in eqs. (2.65) and (2.66).

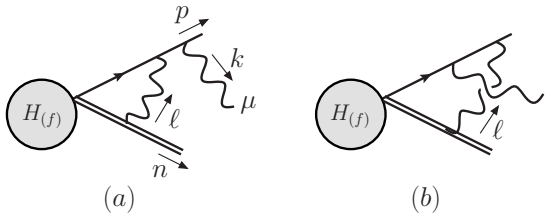

Figure 2.13: *Additional contributions to the radiative f-jet, denoted by $J^{(1)\mu}_{(f')}$, in a simplified NLP factorisation framework. Longitudinally polarised collinear photons that probe the hard scattering are described by the Wilson line interaction.*

We emphasise that the simplified radiative factorisation formula of refs. [78, 79] does not suffice to reproduce the 1R1V amplitude, as noted recently in ref. [88] (see in particular section 4.2.4 there). This approach relies on a direct product of the hard and (radiative) jet functions, as we do for the f-jet in eq. (2.70). We will illustrate this issue by supplementing our f-jet function with the additional contributions (denoted by f') shown in fig. 2.13, to recover the radiative-jet that has been calculated to one-loop order in ref. [79]. These diagrams have a Wilson line in the $\bar{n}$ direction and are the radiative equivalents of the traditional, LP jet functions.[12] This simplified factorisation approach would give the following result for diagrams (c) and (d) in fig. 2.11

$$\begin{aligned}\mathscr{M}^{(1)\alpha\mu}_{\text{c+d}\,|\,\text{simp. fact.}}(p_1,p_2,k) &= J^{(1)\mu}_{(f')}(p_1,k,\bar{n})\,H^{(0)\alpha}_{(f)}(p_1,p_2)\,J^{(0)}_{(f)}(p_2)\\ &= \frac{i\,e^4}{8\pi^2}\left(\frac{t}{4\pi\mu^2}\right)^{-\epsilon}\frac{\Gamma(1+\epsilon)\,\Gamma^2(1-\epsilon)}{\Gamma(2-2\epsilon)}\,\bar{u}(p_1)\bigg\{\frac{1}{\epsilon}\,\frac{1}{t}\,\gamma^\mu \not{k}\gamma^\alpha\\ &\quad + 2\bigg[\frac{1}{1-\epsilon}\,\frac{k^\mu}{t} - \left(\frac{1}{\epsilon}-\frac{1}{1-\epsilon}\right)\frac{1}{s}\left(p_2^\mu - \frac{u}{t}\,p_1^\mu\right)\bigg]\gamma^\alpha\end{aligned}$$

[12] Recall that in the derivation of factorisation at LP, in a general covariant gauge, only longitudinally polarised collinear photons probe the hard function [123]. By means of Ward identities these can be shown to decouple entirely and are cast into connections to a Wilson line.

$$-\frac{1}{s}\frac{2}{1-\epsilon}\,p_2^\alpha\left[2\,\frac{p_1^\mu \not{k}}{t}+\gamma^\mu\right]\Bigg\}\,v(p_2)\,, \tag{2.78}$$

where we have set $\bar{n}^\mu = p_2^\mu/p_2^-$. Comparison with the collinear result of eq. (2.77) shows

$$\begin{aligned}\mathscr{M}^{(1)\alpha\mu}_{\text{c+d}\,|\,\text{C}}(p_1,p_2,k)-\mathscr{M}^{(1)\alpha\mu}_{\text{c+d}\,|\,\text{simp. fact.}}(p_1,p_2,k) = \frac{i\,e^4}{8\pi^2}\left(\frac{t}{4\pi\mu^2}\right)^{-\epsilon}\frac{\Gamma(1+\epsilon)\,\Gamma^2(1-\epsilon)}{\Gamma(2-2\epsilon)}\,\frac{1+\epsilon}{1-\epsilon}\\ \times\,\bar{u}(p_1)\,p_1^\alpha\left[2\,\frac{p_1^\mu \not{k}}{t}+\gamma^\mu\right]v(p_2)\,.\end{aligned} \tag{2.79}$$

Since these missing terms vanish upon contraction with the conjugate amplitude, the simplified factorisation approach did suffice in the 1R1V cross-section calculation presented in ref. [79].

2.3.3 Hard-collinear interplay at the two-loop level

We now move to (single) radiative amplitudes at two-loop order (denoted as 1R2V) and carry out a similar test. At this loop order there is a more involved interplay between the hard and collinear sector, as the dominant component of the collinear momentum of the virtual photon may interfere with the hard loop. This effect is not power suppressed, and has to be properly accounted for in the factorisation picture in order to reproduce the exact NLP amplitude.

Our main effort here will be to explore this subtle interplay and therefore we (again) compare to a hard-collinear region with a method of regions calculation. The relevant diagrams for that purpose are shown in fig. 2.14, where the collinear momentum is denoted by ℓ_1 and the hard momentum by ℓ_2. We identify these diagrams through the following considerations.

First, the soft photon must originate from the collinearly enhanced region, rather than from the hard loop. Otherwise this would be described by a different term in the factorisation formula, as stated by the LBK theorem [76,77]: a soft final-state emission from the hard scattering is described by a derivative with respect to either one of the external hard momenta, acting on the non-radiative hard scattering amplitude, see the second term of eq. (1.25).[13]

Second, the ordering of the virtual photon attachments is crucial. This is best seen from a Coleman-Norton analysis, in which hard, off-shell lines are shrunk to a point. In fact, it is strictly the attachment on the upper leg that matters, since the fermion propagators on the lower leg are shrunk to a point irrespective of the ordering: a propagator that is not part of the hard loop but which carries both an anti-collinear external momentum as well as a collinear loop momentum, obeys a hard scaling too. This implies that we can treat the planar-topology diagrams (c) and (d) in fig. 2.14 as well as the crossed-topology diagrams (g) and (h) on equal footing. To see what happens if one inverts the order of attachments

[13] Note that even if formally needed these diagrams would not contribute, since the collinear loop integral in those configurations would be insensitive to the soft emission and therefore be scaleless.

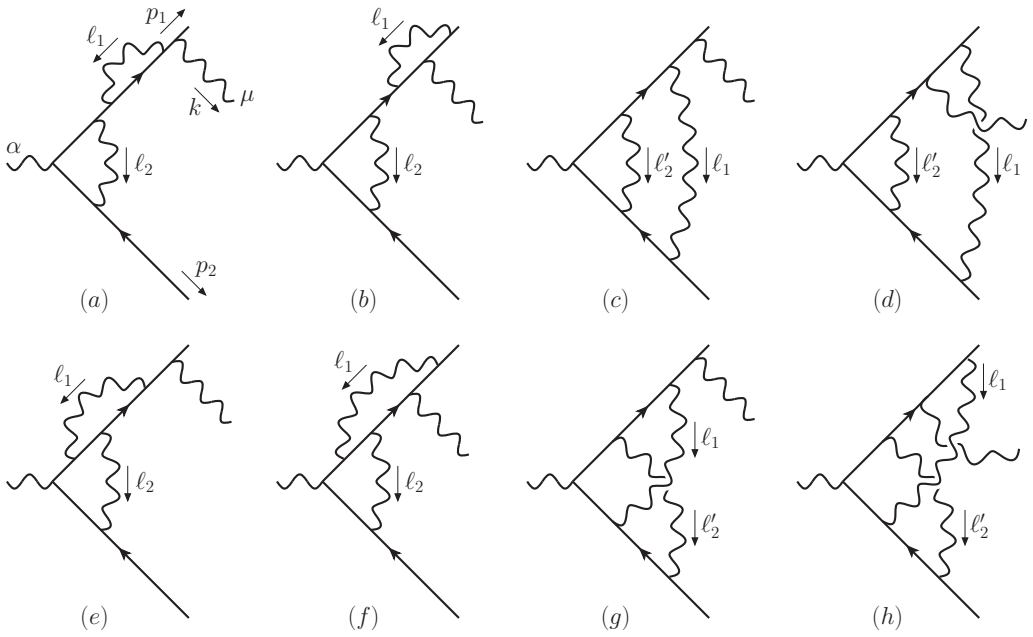

Figure 2.14: *Diagrams contributing to the hard-collinear region of the 1R2V dijet production amplitude, with ℓ_1 (ℓ_2) denoting the collinear (hard) loop momentum. We use the shorthand notation $\ell_2' = \ell_2 - \ell_1$.*

on the upper leg, let us consider diagram (c) as an example. In that case the outer loop would be hard and therefore shrunk to the tree-level hard scattering vertex, as shown in fig. 2.15. The supposedly collinear photon line would now form a tadpole-like attachment to the hard scattering vertex. However, this configuration cannot describe an on-shell line since it does not coincide with any classical trajectory [107], and does not contribute to the scattering amplitude. The collinear photon must thus attach to the upper leg outside of the hard loop, in order for the diagram to develop a hard-collinear region.

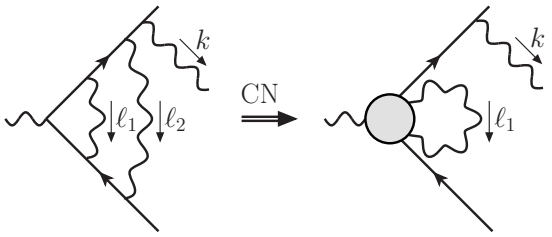

Figure 2.15: *Coleman-Norton picture that arises from attaching the hard photon to the right of the collinear photon on the upper leg. Diagrams with this inverted order of attachments do not contribute.*

Lastly, we note that these diagrams naturally contain a doubly collinear region too, which would be described by a higher-order radiative $f\gamma$- and corresponding $f\partial\gamma$-jet, as well as the radiative $f\gamma\gamma$-jet, all contracted with a tree-level hard function. In a complete description of the doubly collinear region at this loop order, one would even expect contributions from the radiative fff-jet, which would be an interesting analysis by itself. This region does not overlap with the hard-collinear region we explore here, and thus we leave it to future work.

Analogously to the one-loop order, we foresee a pair-wise factorisation of the diagrams in fig. 2.14, by collecting those graphs differing only by the position of the radiated photon. For diagrams (a) and (b), we have

$$\mathscr{M}^{(2)\alpha\mu}_{\text{a+b}\,|\,\text{fact.}}(p_1,p_2,k) = J^{(1)\mu}_{(f)}(p_1,k)\,H^{(1)\alpha}_{(f)}(p_1,p_2)\,J^{(0)}_{(f)}(p_2)\,, \tag{2.80}$$

with $H^{(1)\alpha}_{(f)}(p_1,p_2)$ the one-loop form factor. The hard function combined with the trivial jet function on the anti-collinear leg reads

$$\begin{aligned} H^{(1)\alpha}_{(f)}(p_1,p_2)\,J^{(0)}_{(f)}(p_2) = \frac{i\,e^3}{8\pi^2}\left(\frac{-s}{4\pi\mu^2}\right)^{-\epsilon}\frac{\Gamma(1+\epsilon)\,\Gamma^2(1-\epsilon)}{\Gamma(2-2\epsilon)}\Bigg\{\left(\frac{1}{\epsilon^2}-\frac{1}{2\epsilon}+1\right)\gamma^\alpha \\ +\frac{1}{s}\left[\left(\frac{1}{\epsilon}-1\right)p_1^\alpha-\left(\frac{2}{\epsilon^2}+1\right)p_2^\alpha\right]\Bigg\}\,v(p_2)\,. \end{aligned} \tag{2.81}$$

Equation (2.81) contains explicit double poles, while the unrenormalised hard function may only contain single poles of a UV nature; this double pole is thus of IR origin. In the method of regions, the appearance of IR poles in the hard region is a common phenomenon if the soft region is scaleless. (For the diagrams defined in fig. 2.14 this is indeed the case, as is easily verified by assigning ℓ_2 a soft scaling according to eq. (2.44) and expanding denominators in λ.) Scaleless integrals are set to zero, which typically follows from a cancellation of IR and UV poles. Isolating this UV pole in the soft region and absorbing it in the hard region would cancel the double pole there, thus moving the double pole associated to soft physics from the hard to the soft region. We do not address this mixing of the hard and soft physics, as it affects the method-of-regions calculation and the hard function in the exact same way, while the collinear sectors, which are the focus of this study, *do* factorise entirely from the rest.

Turning to the remaining diagrams in fig. 2.14, (c) to (h), we expect these to factorise according to

$$\begin{aligned} \mathscr{M}^{(2)\alpha\mu}_{\{\text{c+d, e+f, g+h}\}\,|\,\text{fact.}}(p_1,p_2,k) = \int_0^1 dx\Big[J^{(1)\mu\nu}_{(f\gamma)}(x,p_1,k)\,H^{(1)\alpha}_{(f\gamma\,|\,\{\text{I, II, III}\})\,\nu}(x,p_1,p_2) \\ +J^{(1)\mu\nu\rho}_{(f\partial\gamma)}(x,p_1,k)\,H^{(1)\alpha}_{(f\partial\gamma\,|\,\{\text{I, II, III}\})\,\nu\rho}(x,p_1,p_2)\Big]J^{(0)}_{(f)}(p_2)\,, \end{aligned} \tag{2.82}$$

with the one-loop $f\gamma$- and $f\partial\gamma$-hard functions extracted from fig. 2.16. The calculation of these functions is deferred to appendix 2.C.2 for conciseness. Upon evaluation of eqs. (2.80) and (2.82) we find

$$\begin{aligned} \mathscr{M}^{(2)\alpha\mu}_{\text{a+b}\,|\,\text{fact.}}(p_1,p_2,k) = -\frac{ie^6}{(4\pi)^4}\left(\frac{-s}{4\pi\mu^2}\right)^{-\epsilon}\left(\frac{t}{4\pi\mu^2}\right)^{-\epsilon}\Gamma_3\,\bar{u}(p_1)\Bigg\{2\Bigg[\left(\frac{2}{\epsilon^2}-\frac{1}{\epsilon}-1\right)p_1^\alpha \\ -\left(\frac{4}{\epsilon^3}+\frac{2}{\epsilon^2}+\frac{2}{\epsilon}+1\right)p_2^\alpha\Bigg]\frac{\gamma^\mu}{s}+2\left[-\frac{2}{\epsilon^3}+\frac{3}{\epsilon^2}-\frac{3}{\epsilon}+2\right]\frac{k^\mu\gamma^\alpha}{t}-\left[\frac{4}{\epsilon^3}+\frac{3}{\epsilon}+2\right]\frac{\gamma^\mu\not{k}\gamma^\alpha}{t} \\ +4\left[\left(\frac{2}{\epsilon^2}-\frac{1}{\epsilon}-1\right)p_1^\alpha-\left(\frac{4}{\epsilon^3}+\frac{2}{\epsilon^2}+\frac{2}{\epsilon}+1\right)p_2^\alpha\right]\frac{p_1^\mu\not{k}}{s\,t}\Bigg\}\,v(p_2)\,, \end{aligned} \tag{2.83}$$

$$\begin{aligned}\mathscr{M}^{(2)\alpha\mu}_{\text{c+...+h}\,|\,\text{fact.}}(p_1,p_2,k) = \frac{ie^6}{(4\pi)^4}\left(\frac{-s}{4\pi\mu^2}\right)^{-\epsilon}\left(\frac{t}{4\pi\mu^2}\right)^{-\epsilon}\bar{u}(p_1)\Bigg\{\frac{4\Gamma_3}{1-\epsilon}\Bigg[\left(\frac{2}{\epsilon^2}-\frac{1}{\epsilon}+2\right)\frac{k^\mu}{t}\\ +\left(\frac{2}{\epsilon^3}-\frac{5}{\epsilon^2}+\frac{4}{\epsilon}-4\right)\frac{1}{s}\left(\frac{u}{t}p_1^\mu-p_2^\mu\right)\Bigg]\gamma^\alpha+2\Gamma_3\left[\frac{2}{\epsilon^3}-\frac{1}{\epsilon^2}+\frac{2}{\epsilon}\right]\frac{\gamma^\mu\not{k}\gamma^\alpha}{t}\\ +\frac{2}{(1-\epsilon)^2}\frac{1}{s}\Bigg[\Bigg(\Gamma_3\left(-\frac{4}{\epsilon^3}+\frac{8}{\epsilon^2}+\frac{2}{\epsilon}-4-8\epsilon-2\epsilon^2\right)-\frac{2\Gamma_2}{1-2\epsilon}\left(-\frac{4}{\epsilon^3}+\frac{18}{\epsilon^2}\right.\\ \left.-\frac{20}{\epsilon}-11+15\epsilon+6\epsilon^2+4\epsilon^3\right)\Bigg)p_1^\alpha+\left(\Gamma_3\left(\frac{2}{\epsilon^2}-\frac{14}{\epsilon}+14+4\epsilon+2\epsilon^2\right)\right.\\ \left.+\frac{4\Gamma_2}{1-2\epsilon}\left(-\frac{2}{\epsilon^3}+\frac{9}{\epsilon^2}-\frac{9}{\epsilon}-6+5\epsilon+4\epsilon^2+3\epsilon^3\right)\right)p_2^\alpha\Bigg]\Bigg[2\frac{p_1^\mu\not{k}}{t}+\gamma^\mu\Bigg]\Bigg\}v(p_2)\,. \qquad (2.84)\end{aligned}$$

We have combined the diagrams (c) to (h) rather than giving results per diagram pair, and have denoted combinations of gamma functions by

$$\Gamma_2=\frac{\Gamma^3(1-\epsilon)\,\Gamma^2(1+\epsilon)}{\Gamma(3-3\epsilon)} \qquad \text{and} \qquad \Gamma_3=\frac{\Gamma^4(1-\epsilon)\,\Gamma^2(1+\epsilon)}{\Gamma^2(2-2\epsilon)}\,, \qquad (2.85)$$

the former coinciding with the second combination in eq. (2.58).

The results of eq. (2.83) and eq. (2.84) are verified by calculating the hard-collinear region of the diagrams in fig. 2.14. Given that the calculation is set up in a similar way as for the massive case, we will not provide further details for the sake of brevity. In particular, we find agreement between the factorisation and regions results per diagram pair $(a)+(b)$, $(c)+(d)$, $(e)+(f)$ and $(g)+(h)$. For the first three pairs we verified the exact agreement to all orders in ϵ, while for the last pair we compared series expansions in ϵ instead. This is due to the crossed topology of diagrams (g) and (h), which complicates the regions calculation by entangling Feynman parameters, yielding hypergeometric functions of the form ${}_3F_2(a_1,a_2,a_3;b_1,b_2;1)$ upon integration. These multiply the second gamma function combination Γ_2 and are expanded up to and including finite terms ($\mathcal{O}\left(\epsilon^0\right)$) using `HypExp` [124, 125]. By expanding the (exact) coefficients of the Γ_2 combination in the factorisation result up to the same order, we verified their consistency.

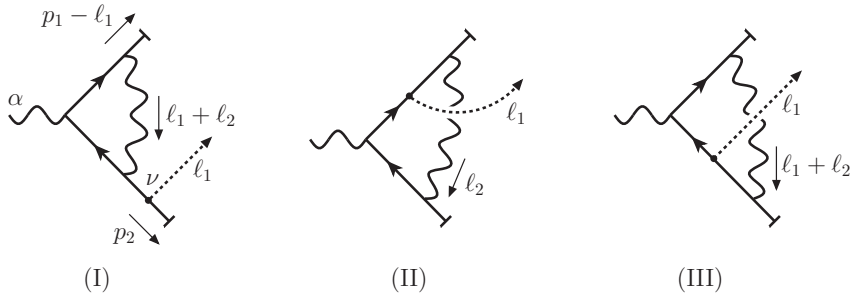

Figure 2.16: *Contributions to the one-loop matrix element $\widetilde{H}^{(1)}_{(f\gamma)}$, from which we extract $H^{(1)}_{(f\gamma)}$ and $H^{(1)}_{(f\partial\gamma)}$.*

The Γ_2 combination is in fact the signature of the mixing between hard and collinear loop momenta: starting at two loops, it originates from terms in the $f\gamma$- and $f\partial\gamma$-hard functions that carry an additional factor of $x^{-\epsilon}$, as seen in eq. (2.105). The appearance of those terms is, in turn, tied to an effective shift in the scale of the hard function; while the loop integration in $H_{(f)}$ knows only the single scale $2p_1^+p_2^- = s$, the $H_{(f\gamma)}$ and $H_{(f\partial\gamma)}$ functions are sensitive to the dominant component of the collinear photon through $2\ell_1^+p_2^- = xs$, giving additional x dependence.[14] Indeed, no Γ_2 combination is present for the f-jet factorisation of diagrams $(a)+(b)$ in eq. (2.83). As we see here, this effect is naturally captured by the NLP factorisation formula of eq. (2.31). A simplified NLP factorisation as in eq. (2.78), strictly in terms of f-jets, cannot do so: the complete factorisation of the collinear and hard sector is an over-simplification of the intricate dynamics at play here.

Lastly, we point out that eqs. (2.83) and (2.84) contain at most $1/\epsilon^3$ poles, while at two-loop order a maximal soft-collinear overlap would generate $1/\epsilon^4$ poles. These leading singularities are captured by the soft function.[15] This suggests that for NLP threshold resummation purposes the collinear sector is needed starting at NLL accuracy. This has been noted before in the calculation of the collinear region of the 1R1V correction to DY production in ref. [122], while in chapter 3 we will make a similar observation for the 2R1V correction. Indeed, in chapter 4 we will show that NLP threshold logarithms in DY production can be resummed at LL accuracy through an exponential next-to-soft function.

2.4 Conclusions

In this chapter we have formulated a next-to-leading power factorisation formula for n-jet production processes in QED, based on a power counting analysis for both zero and parametrically small fermion masses. We have thus begun the generalisation of the original Yukawa theory analysis of ref. [85] to gauge theories. A factorisation of degrees of freedom at NLP, following arguments such as in ref. [52], could be an important step towards resummation of NLP (threshold) logarithms beyond leading-logarithmic accuracy.

We focused on the interaction that contributes at the first sub-leading power in λ, and computed the $f\gamma$- and $f\partial\gamma$-jets, which are universal quantities, up to order λ^2. We first considered massive fermions, for which we calculated the non-radiative jet functions. To have a direct correspondence between the (next-to-)leading regions and their power counting we used axial gauge. We were able to test the factorisation formula by comparing the convolution of jet functions and hard parts with a regions calculation of the two-jet amplitude to one loop. Subsequently we successfully tested these parts of the predicted factorisation formula at the two-loop level by comparing the combined result against the hard-collinear region of

[14] The exact form of this x-dependence varies by diagram, as it is dictated by the denominators in the loop, and thus made explicit upon integration over the Feynman parameters that combine them.

[15] Upon a correct assignment of poles; in a regions analysis they would appear in the hard-hard region instead, by the same mechanism discussed before.

a two-loop diagram. In particular, we pointed out the existence of two classes of endpoint contributions, one of which singular, that we deal with within dimensional regularisation.

For massless fermions we ensured the presence of a small scale, following ref. [85], by adding an extra soft photon emission, so that the invariant of this photon momentum with a jet direction provides an analogue to the squared small fermion mass. We thus presented results for the radiative $f\gamma$- and $f\partial\gamma$-jet instead and tested the factorisation of a radiative amplitude in a similar way as before. Here we found that the present approach reproduces all collinear contributions in the one-loop matrix element, contrary to the simplified NLP factorisation of refs. [78, 79]. In addition, we noted a subtle interplay between hard and collinear modes, which is correctly accounted for in our factorisation formula. We conjecture that our factorisation formula is sufficiently general to factorise QED amplitudes up to NLP at arbitrary loop orders, and may thereby pave the way for the development of a similar factorisation for QCD amplitudes.

We focused in our analysis on testing a specific part of the factorisation framework. That is, the one that accounts for non-trivial hard-collinear interplay at the two-loop level, via novel jet functions which describe double hard-collinear interactions. In addition, similar tests should be carried out for the other ingredients (such as the triple hard-collinear interactions and the soft sector). Moreover, the jet functions used in this analysis are extracted from a generic jet-like scattering amplitude, rather than being derived from an operator definition. Such definitions would make the gauge invariance of the separate factorisation ingredients manifest, thereby formalising the NLP factorisation framework for QED. These further steps, together with the extension to QCD, are part of ongoing work.

2.A Momentum regions for a parametrically small fermion mass

The power-counting analysis in section 2.1 assumes the scaling $k^\mu \sim Q\left(\lambda^2, \lambda^2, \lambda^2\right)$, $k^\mu \sim Q\left(1, \lambda, \lambda^2\right)$ for soft and collinear momenta respectively. This follows from an analysis of the infrared structure of the scattering amplitude, which allows one to associate the pinch surfaces to momenta configurations that are soft and collinear. Here we complement this analysis by performing an expansion of the amplitude in momentum regions. This method provides an alternative approach for singling out the momentum configurations which are relevant for a given amplitude, in the presence of parametrically different scales, constituting a useful check for our assumptions in section 2.1.

To illustrate this second method, we focus on the scalar integral associated to the 1-loop diagram in figure 2.6. For fermions with mass $m > 0$ the integral reads

$$\begin{aligned} T(\hat{s}, m) &= \int \frac{d^{4-2\epsilon}\ell}{(2\pi)^{4-2\epsilon}} \frac{\mu^{2\epsilon}}{\left[\ell^2 + i\eta\right]\left[(p_1-\ell)^2 - m^2 + i\eta\right]\left[(p_2+\ell)^2 - m^2 + i\eta\right]} \\ &= \frac{i}{(4\pi)^2} \frac{\mathrm{e}^{\epsilon\gamma_E}\Gamma(1+\epsilon)}{2\epsilon\, m^2} \left(\frac{\bar{\mu}^2}{m^2}\right)^{\epsilon} {}_2F_1\left(1, 1+\epsilon, \frac{3}{2}; \frac{(\hat{s}+m^2)^2}{4m^2\hat{s}}\right) \\ &= -\frac{i}{(4\pi)^2} \frac{\hat{s}}{2(\hat{s}^2 - m^4)} \left\{ \left[\frac{2}{\epsilon} + 2\log\left(\frac{\bar{\mu}^2}{2m^2}\right)\right] \log\left(-\frac{\hat{s}}{m^2}\right) + \log^2\left(\frac{2\hat{s}}{\hat{s}-m^2}\right) \right. \\ &\qquad \left. - \log^2\left(\frac{2m^2}{m^2-\hat{s}}\right) + 2\mathrm{Li}_2\left(\frac{\hat{s}}{\hat{s}-m^2}\right) - 2\mathrm{Li}_2\left(\frac{m^2}{m^2-\hat{s}}\right) \right\}, \end{aligned} \tag{2.86}$$

with $\bar{\mu}$ the $\overline{\text{MS}}$ renormalisation scale, $\bar{\mu}^2 = 4\pi\, \mathrm{e}^{-\gamma_E}\mu^2$. In the last line we expand the result in powers of ϵ, showing that the integral has a single soft pole. In the second and third line we write the result in terms of the dominant component of the Mandelstam variable s, denoted by $\hat{s}$ and defined through

$$s = (p_1+p_2)^2 = 2m^2 + 2\,p_1^+ p_2^- + 2\,p_1^- p_2^+ \equiv 2m^2 + \hat{s} + \frac{m^4}{\hat{s}}, \tag{2.87}$$

where the momentum components $p_i^\pm$ are given by the decomposition in eq. (2.2). For small mass $m \ll \hat{s} \sim Q^2$ we can expand eq. (2.86), obtaining

$$\begin{aligned} T(\hat{s}, m) \;=\; & \frac{i}{(4\pi)^2} \frac{\mathrm{e}^{\epsilon\gamma_E}\Gamma(1+\epsilon)}{\epsilon^2\,\hat{s}} \left\{ -\left(\frac{\bar{\mu}^2}{m^2}\right)^{\epsilon} \left[1 + \frac{2}{1-\epsilon}\frac{m^2}{\hat{s}} + \frac{2-\epsilon+3\epsilon^2}{(1-\epsilon)(2-\epsilon)}\frac{m^4}{\hat{s}^2} + \mathcal{O}\left(\frac{m^6}{\hat{s}^3}\right)\right] \right. \\ & \left. + \left(\frac{\bar{\mu}^2}{-\hat{s}}\right)^{\epsilon} \frac{\Gamma^2(1-\epsilon)}{\Gamma(1-2\epsilon)} \left[1 + 2\epsilon\frac{m^2}{\hat{s}} + (1+\epsilon+2\epsilon^2)\frac{m^4}{\hat{s}^2} + \mathcal{O}\left(\frac{m^6}{\hat{s}^3}\right)\right] \right\}. \end{aligned} \tag{2.88}$$

Note that result in eq. (2.86) for finite, non-zero mass is free of collinear singularities, but exhibits mass thresholds when $\hat{s} = m^2$. When moving to the case of parametrically small masses by performing the mass expansion in eq. (2.88), the branch cuts responsible for mass thresholds collapse to a point, which is manifest in the presence of a double pole at

order $m^2/\hat{s}$. This indicates that the theory with parametrically small masses has collinear singularities analogous to the massless theory.[16]

We will now investigate which momentum regions reproduce the result in eq. (2.88), given that the external momenta are $p_1^+ \sim p_2^- \sim Q$, $p_1^- \sim p_2^+ \sim \lambda^2 Q$, with the parameter λ fixed by the condition $\lambda \sim m/Q$. In principle several regions can be considered:

$$\begin{aligned}
\text{Hard:} &\quad \ell^\mu \sim Q(1,1,1), & \text{Semi-hard:} &\quad \ell^\mu \sim Q(\lambda,\lambda,\lambda),\\
\text{Soft:} &\quad \ell^\mu \sim Q\big(\lambda^2,\lambda^2,\lambda^2\big), & \text{Ultra-soft:} &\quad \ell^\mu \sim Q\big(\lambda^4,\lambda^4,\lambda^4\big),\\
\text{Collinear:} &\quad \ell^\mu \sim Q\big(1,\lambda,\lambda^2\big), & \text{Ultra-collinear:} &\quad \ell^\mu \sim Q\big(1,\lambda^2,\lambda^4\big),
\end{aligned} \tag{2.89}$$

where similarly defined *anti*-collinear regions are obtained upon interchanging the scaling for plus- and minus-components. In general one can also have n-ultra-collinear regions with scaling $\ell^\mu \sim Q\big(1,\lambda^n,\lambda^{2n}\big)$ as well as n-ultra-soft regions. It is easy to check that only the hard, collinear and anti-collinear region are not scaleless, each contributing as follows:

$$\begin{aligned}
T_{\text{H}}(\hat{s},m) &= \int \frac{d^{4-2\epsilon}\ell}{(2\pi)^{4-2\epsilon}} \frac{\mu^{2\epsilon}}{\ell^2\big[\ell^2+2\ell^- p_1^+\big]\big[\ell^2-2\ell^+ p_2^-\big]}\bigg[1-\frac{2\ell^+ p_1^-}{\ell^2+2\ell^- p_1^+}+\frac{2\ell^- p_2^+}{\ell^2-2\ell^+ p_2^-}\\
&\quad+\frac{(2\ell^+ p_1^-)^2}{\big[\ell^2+2\ell^- p_1^+\big]^2}+\frac{(2\ell^+ p_1^-)(2\ell^- p_2^+)}{\big[\ell^2+2\ell^- p_1^+\big]\big[\ell^2-2\ell^+ p_2^-\big]}+\frac{(2\ell^- p_2^+)^2}{\big[\ell^2-2\ell^+ p_2^-\big]^2}+\mathcal{O}\bigg(\frac{m^6}{\hat{s}^3}\bigg)\bigg]\\
&=\frac{i}{(4\pi)^2}\bigg(\frac{\bar{\mu}^2}{-\hat{s}}\bigg)^{\epsilon}\frac{1}{\hat{s}}\frac{\mathrm{e}^{\epsilon\gamma_E}\Gamma(1+\epsilon)\Gamma^2(1-\epsilon)}{\epsilon^2\Gamma(1-2\epsilon)}\bigg[1+2\epsilon\frac{m^2}{\hat{s}}+(1+\epsilon+2\epsilon^2)\frac{m^4}{\hat{s}^2}+\mathcal{O}\bigg(\frac{m^6}{\hat{s}^3}\bigg)\bigg]\\
&=\frac{i}{(4\pi)^2}\frac{1}{\hat{s}}\bigg\{\frac{1}{\epsilon^2}+\frac{1}{\epsilon}\log\bigg(-\frac{\bar{\mu}^2}{\hat{s}}\bigg)-\frac{\pi^2}{12}+\frac{1}{2}\log^2\bigg(-\frac{\bar{\mu}^2}{\hat{s}}\bigg)+\frac{m^2}{\hat{s}}\bigg[\frac{2}{\epsilon}+2\log\bigg(-\frac{\bar{\mu}^2}{\hat{s}}\bigg)\bigg]\\
&\quad+\frac{m^4}{\hat{s}^2}\bigg[\frac{1}{\epsilon^2}+\frac{1}{\epsilon}\bigg[1+\log\bigg(-\frac{\bar{\mu}^2}{\hat{s}}\bigg)\bigg]+2-\frac{\pi^2}{12}+\log\bigg(-\frac{\bar{\mu}^2}{\hat{s}}\bigg)+\frac{1}{2}\log^2\bigg(-\frac{\bar{\mu}^2}{\hat{s}}\bigg)\bigg]\\
&\quad+\mathcal{O}\bigg(\frac{m^6}{\hat{s}^3},\epsilon\bigg)\bigg\},
\end{aligned} \tag{2.90}$$

for the hard region, and

$$\begin{aligned}
T_{\text{C}}(\hat{s},m) &= \int \frac{d^{4-2\epsilon}\ell}{(2\pi)^{4-2\epsilon}} \frac{\mu^{2\epsilon}}{\ell^2\big[\ell^2+2\ell^- p_1^+ + 2\ell^+ p_1^-\big]\big[-2\ell^+ p_2^-\big]}\\
&\quad\times\bigg[1-\frac{\ell^2}{-2\ell^+ p_2^-}+\frac{2\ell^- p_2^+}{-2\ell^+ p_2^-}+\frac{\ell^4}{\big[-2\ell^+ p_2^-\big]^2}+\mathcal{O}\bigg(\frac{m^6}{\hat{s}^3}\bigg)\bigg]\\
&=-\frac{i}{(4\pi)^2}\frac{\mathrm{e}^{\epsilon\gamma_E}\Gamma(1+\epsilon)}{2\epsilon^2\hat{s}}\bigg(\frac{\bar{\mu}^2}{m^2}\bigg)^{\epsilon}\bigg[1+\frac{2}{1-\epsilon}\frac{m^2}{\hat{s}}+\frac{2-\epsilon+3\epsilon^2}{(1-\epsilon)(2-\epsilon)}\frac{m^4}{\hat{s}^2}+\mathcal{O}\bigg(\frac{m^6}{\hat{s}^3}\bigg)\bigg]
\end{aligned}$$

[16] Alternatively, we may argue that a collinear singularity requires both $\ell^\mu \propto p_1^\mu$ and $\ell^2 = 0$, as dictated by the Landau equations. A large fermion mass violates these conditions as $p_1^2 = m^2$, but consistency is retrieved in the small mass limit. Again, this suggests that the singular structure for parametrically small fermion masses is comparable to that for massless fermions.

$$= \frac{i}{(4\pi)^2}\frac{1}{\hat{s}}\Bigg\{-\frac{1}{\epsilon^2}-\frac{1}{\epsilon}\log\left(\frac{\bar{\mu}^2}{m^2}\right)-\frac{\pi^2}{12}-\frac{1}{2}\log^2\left(\frac{\bar{\mu}^2}{m^2}\right)$$
$$+\frac{m^2}{\hat{s}}\left[-\frac{2}{\epsilon}-2-2\log\left(\frac{\bar{\mu}^2}{m^2}\right)\right]+\frac{m^4}{\hat{s}^2}\left[-\frac{1}{\epsilon^2}-\frac{1}{\epsilon}\left[1+\log\left(\frac{\bar{\mu}^2}{m^2}\right)\right]\right.$$
$$\left.-\frac{5}{2}-\frac{\pi^2}{12}-\log\left(\frac{\bar{\mu}^2}{m^2}\right)-\frac{1}{2}\log^2\left(\frac{\bar{\mu}^2}{m^2}\right)\right]+\mathcal{O}\left(\frac{m^6}{\hat{s}^3},\epsilon\right)\Bigg\}, \tag{2.91}$$

for the collinear region. The anti-collinear region is identical, $T_{\bar{\mathrm{C}}} = T_{\mathrm{C}}$. None of the other regions give a contribution, because they are of the form

$$T_{\mathrm{UC},\overline{\mathrm{UC}}}(\hat{s},m) = \int \frac{d^{4-2\epsilon}\ell}{(2\pi)^{4-2\epsilon}}\frac{\mu^{2\epsilon}\{1,\ell^\mu,\ell^\mu\ell^\nu,\ldots\}}{\ell^2\left[2\ell^\mp p_1^\pm\right]\left[-2\ell^\mp p_2^\pm\right]}, \tag{2.92}$$

$$T_{\mathrm{SH,S,US}}(\hat{s},m) = \int \frac{d^{4-2\epsilon}\ell}{(2\pi)^{4-2\epsilon}}\frac{\mu^{2\epsilon}\{1,\ell^\mu,\ell^\mu\ell^\nu,\ldots\}}{\ell^2\left[2\ell^- p_1^+\right]\left[-2\ell^+ p_2^-\right]}, \tag{2.93}$$

which are scaleless integrals. This analysis allows us to conclude that the relevant collinear region (third line in eq. (2.89)) has indeed the same scaling as the collinear momentum in eq. (2.4), whose scaling has been determined by investigating the pinch surfaces of the amplitude.

2.B Intermediate expressions for elastic amplitudes with $m \sim \lambda Q$

In this appendix we collect intermediate expressions needed for the calculations performed in section 2.2. Specifically, in section 2.B.1 we list results for the integrals needed in the computation of the $f\gamma$- and $f\partial\gamma$-jet, in the massive theory, while in section 2.B.2, we show the partial results for the two-loop check of factorisation performed there.

2.B.1 Integrals for jet functions

For the calculation of the jet functions in the massive fermion case, we require

$$\int \frac{d\ell^- d^{2-2\epsilon}\ell_\perp}{(2\pi)^{4-2\epsilon}}\frac{(i\mu^{2\epsilon}p^+)}{[2xp^+\ell^- + \ell_\perp^2 + i\eta][2(1-x)\ell^- p^+ - \ell_\perp^2 + xm^2 - i\eta]} = I_0\,, \tag{2.94a}$$

$$\int \frac{d\ell^- d^{2-2\epsilon}\ell_\perp}{(2\pi)^{4-2\epsilon}}\frac{(i\mu^{2\epsilon}p^+)\,\ell_\perp^\alpha\ell_\perp^\beta}{[2xp^+\ell^- + \ell_\perp^2 + i\eta][2(1-x)\ell^- p^+ - \ell_\perp^2 + xm^2 - i\eta]} = \frac{x^2m^2\eta_\perp^{\alpha\beta}}{2-2\epsilon}I_0\,, \tag{2.94b}$$

$$\int \frac{d\ell^- d^{2-2\epsilon}\ell_\perp}{(2\pi)^{4-2\epsilon}}\frac{(i\mu^{2\epsilon}p^+)\,\ell^-}{[2xp^+\ell^- + \ell_\perp^2 + i\eta][2(1-x)\ell^- p^+ - \ell_\perp^2 + xm^2 - i\eta]} = \frac{m^2}{2p^+}\left[\frac{\delta(1-x)}{1-\epsilon} - x\right]I_0\,, \tag{2.94c}$$

with a common factor

$$I_0 = \frac{\Gamma(\epsilon)}{16\pi^2}\left(\frac{4\pi\mu^2}{x^2 m^2}\right)^{\epsilon}. \tag{2.95}$$

Note the different signs for the $i\eta$ prescriptions in the denominators. As a consequence, the poles lie on opposite sides of the ℓ^- integration contour if and only if $0<x<1$, which restricts the convolution domain in x to that range.

2.B.2 Partial two-loop results

In the following we show expressions for the convolution of the one-loop massive jet and hard functions, as presented section 2.2.2. Here we list the $f\gamma$- and $f\partial\gamma$-terms separately:

$$\begin{aligned}
&\int_0^1 dx\, J^{(1)}_{(f\gamma)\nu}(x,p_1) H^{(1)\alpha\nu}_{(f\gamma)}(x,p_1,p_2) J^{(0)}_{(f)}(p_2) \\
&\quad = \frac{i e^5}{128\pi^4}\left(\frac{-2p_1\cdot\bar n\, p_2\cdot n}{4\pi\mu^2}\right)^{-\epsilon}\left(\frac{m^2}{4\pi\mu^2}\right)^{-\epsilon}\frac{1}{1-2\epsilon}\,\bar u(p_1) \\
&\qquad \times\Bigg\{\left(\frac{m}{p_1\cdot\bar n}\bar n^\alpha - \frac{m}{p_2\cdot n}n^\alpha\right)\Gamma_1\left(\frac{1}{\epsilon^3}+\frac{2}{\epsilon^2}-\frac{3}{\epsilon}\right) - \frac{m}{p_1\cdot\bar n}\Gamma_2\left(\frac{4}{\epsilon^3}-\frac{8}{\epsilon^2}+\frac{1}{\epsilon}+3\right)\bar n^\alpha \\
&\qquad + \frac{m}{p_2\cdot n}\Gamma_2\left(\frac{2}{\epsilon^3}-\frac{1}{\epsilon^2}-\frac{8}{\epsilon}+11-4\epsilon\right)n^\alpha \\
&\qquad + \frac{m^2}{2p_1\cdot\bar n\, p_2\cdot n}\gamma^\alpha\Bigg[\frac{\Gamma_1}{(1-\epsilon^2)(1-\epsilon)}\left(\frac{6}{\epsilon^4}-\frac{9}{\epsilon^3}+\frac{2}{\epsilon^2}-16+33\epsilon-8\epsilon^2-4\epsilon^3\right) \\
&\qquad - \frac{\Gamma_2}{1-\epsilon^2}\left(\frac{8}{\epsilon^4}-\frac{12}{\epsilon^3}-\frac{30}{\epsilon^2}+\frac{112}{\epsilon}-158+92\epsilon+4\epsilon^2-8\epsilon^3\right)\Bigg]\Bigg\}\nu(p_2),
\end{aligned} \tag{2.96}$$

$$\begin{aligned}
&\int_0^1 dx\, J^{(1)}_{(f\partial\gamma)\nu\rho}(x,p_1) H^{(1)\alpha\nu\rho}_{(f\partial\gamma)}(x,p_1,p_2) J^{(0)}_{(f)}(p_2) \\
&\quad = -\frac{i e^5}{128\pi^4}\left(\frac{-2p_1\cdot\bar n\, p_2\cdot n}{4\pi\mu^2}\right)^{-\epsilon}\left(\frac{m^2}{4\pi\mu^2}\right)^{-\epsilon}\frac{1}{1-2\epsilon}\,\bar u(p_1)\gamma^\alpha\nu(p_2) \\
&\qquad \times\frac{m^2}{2p_1\cdot\bar n\, p_2\cdot n}\Bigg\{\frac{\Gamma_1}{(1-\epsilon^2)(1-\epsilon)}\left(\frac{6}{\epsilon^4}-\frac{9}{\epsilon^3}-\frac{1}{\epsilon^2}+\frac{11}{\epsilon}-13+8\epsilon-2\epsilon^2+4\epsilon^3\right) \\
&\qquad - \frac{\Gamma_2}{(1-\epsilon^2)(1+\epsilon)}\left(\frac{8}{\epsilon^4}-\frac{2}{\epsilon^3}-\frac{41}{\epsilon^2}+\frac{67}{\epsilon}-3-81\epsilon+28\epsilon^2+24\epsilon^3+16\epsilon^4\right)\Bigg\}.
\end{aligned} \tag{2.97}$$

The sum of these contributions coincides with the HC region result in eq. (2.57).

2.C Intermediate expressions for radiative amplitudes with $m = 0$

In this appendix we collect intermediate expressions needed for the calculations performed in section 2.3. Section 2.C.1 lists integrals that enter the calculation of the one-loop radiative

$f\gamma$- and $f\partial\gamma$-jet functions, for massless fermions. In section 2.C.2, we present one-loop expressions for the corresponding hard functions.

2.C.1 Integrals for the radiative jet functions

In the calculation of the radiative, massless $f\gamma$- and $f\partial\gamma$-jet we expand denominators in λ. To keep expressions compact, we define the following notation for the homogeneous propagator denominators appearing in the diagrams of fig. 2.10

$$\begin{aligned}
D_1 &= 2\,x\,p^+\ell^- + \ell_\perp^2 + i\eta\,,\\
D_2 &= 2(1-x)p^+\ell^- - \ell_\perp^2 - i\eta\,,\\
D_3 &= 2(1-x)p^+\ell^- - \ell_\perp^2 - 2(1-x)p^+k^- - i\eta\,.
\end{aligned}$$

For diagram (a) in fig. 2.10 we need

$$(i\mu^{2\epsilon}p^+)\int\frac{d\ell^-d^{2-2\epsilon}\ell_\perp}{(2\pi)^{4-2\epsilon}}\frac{1}{D_1\,D_3^a} = x^{-\epsilon}\,(1-x)^{1-a-\epsilon}\,I_1(a)\,, \tag{2.98a}$$

$$(i\mu^{2\epsilon}p^+)\int\frac{d\ell^-d^{2-2\epsilon}\ell_\perp}{(2\pi)^{4-2\epsilon}}\frac{\ell_\perp^\alpha\ell_\perp^\beta}{D_1\,D_3^a} = -\frac{p^+k^-}{2-a-\epsilon}\eta_\perp^{\alpha\beta}x^{1-\epsilon}\,(1-x)^{2-a-\epsilon}\,I_1(a)\,, \tag{2.98b}$$

$$\begin{aligned}(i\mu^{2\epsilon}p^+)\int\frac{d\ell^-d^{2-2\epsilon}\ell_\perp}{(2\pi)^{4-2\epsilon}}\frac{\ell^-}{D_1\,D_3^a} =& -\frac{k^-}{2-a-\epsilon}\,(1-x)^{2-a-\epsilon}\\ &\times\left(\frac{1}{x}\,\delta(1-x)-(1-\epsilon)\,x^{-\epsilon}\right)I_1(a)\,,\end{aligned} \tag{2.98c}$$

with

$$I_1(a) = \frac{1}{16\pi^2}\left(\frac{-2p^+k^-}{4\pi\mu^2}\right)^{-\epsilon}\frac{\Gamma(a-1+\epsilon)}{\Gamma(a)}\left(-2p^+k^-\right)^{1-a}\,. \tag{2.99}$$

For diagram (b) in fig. 2.10 a set of slightly more involved integrals is needed:

$$(i\mu^{2\epsilon}p^+)\int\frac{d\ell^-d^{2-2\epsilon}\ell_\perp}{(2\pi)^{4-2\epsilon}}\frac{1}{D_1\,D_2\,D_3^a} = -\frac{1}{\epsilon}(1-x)^{-a-\epsilon}x^{-\epsilon}I_2(a)\,, \tag{2.100a}$$

$$(i\mu^{2\epsilon}p^+)\int\frac{d\ell^-d^{2-2\epsilon}\ell_\perp}{(2\pi)^{4-2\epsilon}}\frac{\ell_\perp^\alpha\ell_\perp^\beta}{D_1\,D_2\,D_3^a} = -\frac{p^+k^-}{1-a-\epsilon}\frac{\eta_\perp^{\alpha\beta}}{1-\epsilon}x^{1-\epsilon}(1-x)^{1-a-\epsilon}\,I_2(a)\,, \tag{2.100b}$$

$$\begin{aligned}(i\mu^{2\epsilon}p^+)\int\frac{d\ell^-d^{2-2\epsilon}\ell_\perp}{(2\pi)^{4-2\epsilon}}\frac{\ell^-}{D_1\,D_2\,D_3^a} =& -\frac{k^-}{1-a-\epsilon}\frac{1}{1-\epsilon}\,(1-x)^{1-a-\epsilon}\\ &\times\left(\frac{1}{x}\,\delta(1-x)-(1-\epsilon)\,x^{-\epsilon}\right)I_2(a)\,,\end{aligned} \tag{2.100c}$$

with

$$I_2(a) = \frac{1}{16\pi^2}\left(\frac{-2p^+k^-}{4\pi\mu^2}\right)^{-\epsilon}\frac{\Gamma(a+\epsilon)}{\Gamma(a)}\left(-2p^+k^-\right)^{-a}\,. \tag{2.101}$$

2.C.2 One-loop hard functions

Below we collect expressions for the one-loop $f\gamma$- and $f\partial\gamma$-hard functions used in the main text. We extract these functions from the diagrams shown in fig. 2.16, according to eq. (2.38). For the $f\gamma$-hard function defined by diagram (I), the simplest topology, we will quote an explicit result to give an impression of the form of these functions. For the remaining contributions to the $f\gamma$- and $f\partial\gamma$-hard functions we give expressions prior to any processing for brevity. The evaluation itself is a simple one-loop calculation that relies on standard techniques, but the resulting expressions are rather lengthy due to the numerous open indices. We obtain

$$H^{(1)\alpha}_{(f\gamma|\mathrm{I})\,\nu}(x,p_1,p_2) = -\frac{e^4}{x\,s}\int\frac{d^{4-2\epsilon}\ell_2}{(2\pi)^{4-2\epsilon}}\frac{N^\alpha_{\mathrm{I}}(\ell_1,\ell_2,p_1,p_2)(x\not{p}_1+\not{p}_2)\gamma_\nu}{\big[\ell_2^2+2\ell_2\cdot p_1\big]\big[\ell_2^2+2x\,\ell_2\cdot p_1\big]\big[\ell_2^2-2\ell_2\cdot p_2\big]}, \tag{2.102}$$

$$H^{(1)\alpha}_{(f\partial\gamma|\mathrm{I})\,\nu\rho}(x,p_1,p_2) = -\frac{e^4}{x\,s}\int\frac{d^{4-2\epsilon}\ell_2}{(2\pi)^{4-2\epsilon}}\frac{N^\alpha_{\mathrm{I}}(\ell_1,\ell_2,p_1,p_2)\Big[\gamma_{\perp\rho}-2\,\ell_{2\perp\rho}\,\frac{x\not{p}_1+\not{p}_2}{\ell_2^2+2x\,\ell_2\cdot p_1}\Big]\gamma_\nu}{\big[\ell_2^2+2\ell_2\cdot p_1\big]\big[\ell_2^2+2x\,\ell_2\cdot p_1\big]\big[\ell_2^2-2\ell_2\cdot p_2\big]}, \tag{2.103}$$

$$N^\alpha_{\mathrm{I}}(\ell_1,\ell_2,p_1,p_2) = (d-4)(\not{\ell}_2-\not{p}_2)\gamma^\alpha(\not{\ell}_2+\not{p}_1)+2(\not{\ell}_2+\not{p}_1)\gamma^\alpha(\not{\ell}_2-\not{p}_2),$$

after some Dirac algebra. Any perpendicular quantity $a^\rho_\perp$ can be rewritten as

$$\begin{aligned} a^\rho_\perp &= a^\rho - a\cdot\bar{n}\,n^\rho - a\cdot n\,\bar{n}^\rho \\ &= a^\rho - 2\frac{a\cdot p_2}{s}p_1^\rho - 2\frac{a\cdot p_1}{s}p_2^\rho, \end{aligned} \tag{2.104}$$

such that the loop integral can be carried out using standard integrals. Anticipating the contraction with the lowest order f-jet on the lower leg, we obtain a reasonably compact expression for the combination

$$\begin{aligned} &H^{(1)\alpha}_{(f\gamma|\mathrm{I})\,\nu}(x,p_1,p_2)J^{(0)}_{(f)}(p_2) \\ &\quad= \frac{i\,e^4}{8\pi^2}\frac{1}{s}\left(\frac{-s}{4\pi\mu^2}\right)^{-\epsilon}\frac{\Gamma^2(1-\epsilon)\Gamma(1+\epsilon)}{\Gamma(2-2\epsilon)}\frac{1}{1-x}\bigg\{\bigg(\frac{1}{\epsilon}-1\bigg)\bigg[\big(x^{-\epsilon}-1\big)p_2^\alpha \\ &\qquad+\big(1-x^{1-\epsilon}\big)p_1^\alpha\bigg]\gamma_\nu+2\bigg[\bigg(\frac{1}{x}\bigg(-\frac{1}{\epsilon}+1\bigg)+\frac{2}{\epsilon}-1-\frac{x^{1-\epsilon}}{\epsilon}\bigg)p_1^\alpha+\bigg(\bigg(-\frac{2}{\epsilon^2}+\frac{2}{\epsilon}\bigg)x^{-1-\epsilon} \\ &\qquad+\frac{1}{x}\bigg(\frac{2}{\epsilon^2}+1\bigg)-\frac{3}{\epsilon}x^{-\epsilon}+\frac{1}{\epsilon}-1\bigg)p_2^\alpha\bigg]\frac{\not{p}_1 p_{2\nu}}{s}+\bigg[\bigg(\frac{2}{\epsilon^2}-\frac{2}{\epsilon}\bigg)x^{-1-\epsilon}+\bigg(-\frac{2}{\epsilon^2}+\frac{1}{\epsilon}-2\bigg)\frac{1}{x} \\ &\qquad+\bigg(\frac{1}{\epsilon}+2\bigg)x^{-\epsilon}\bigg]p_{2\nu}\gamma^\alpha+\bigg[\bigg(\frac{1}{\epsilon}-1\bigg)x^{-\epsilon}-\frac{3}{2\epsilon}+1+\frac{x^{1-\epsilon}}{2\epsilon}\bigg]\not{p}_1\gamma^\alpha\gamma_\nu\bigg\}v(p_2). \end{aligned} \tag{2.105}$$

We stress that the inverse powers of $1-x$ and x present here, are associated to soft-collinear singularities caused by either the fermion or photon becoming soft in addition to being collinear. These endpoint singularities in the convolution variable are regulated by the $f\gamma$-jet through the overall factor $[x\,(1-x)]^{-\epsilon}$ in eq. (2.65).

The second diagram in fig. 2.16 provides us with

$$H^{(1)\alpha}_{(f\gamma|\mathrm{II})\,\nu}(x,p_1,p_2) = -e^4\int\frac{d^{4-2\epsilon}\ell_2}{(2\pi)^{4-2\epsilon}}\frac{\gamma^\sigma(\not\ell_2+(1-x)\not p_1)\gamma_\nu(\not\ell_2+\not p_1)\gamma^\alpha(\not\ell_2-\not p_2)\gamma_\sigma}{\left[\ell_2^2+2\ell_2\cdot p_1\right]\left[\ell_2^2+2(1-x)\ell_2\cdot p_1\right]} \times\frac{1}{\left[\ell_2^2\right]\left[\ell_2^2-2\ell_2\cdot p_2\right]}, \tag{2.106}$$

$$H^{(1)\alpha}_{(f\partial\gamma|\mathrm{II})\,\nu\rho}(x,p_1,p_2) = -e^4\int\frac{d^{4-2\epsilon}\ell_2}{(2\pi)^{4-2\epsilon}}\frac{\gamma^\sigma\left[2\ell_{2\perp\rho}\,\frac{\not\ell_2+(1-x)\not p_1}{\ell_2^2+2(1-x)\ell_2\cdot p_1}-\gamma_{\perp\rho}\right]}{\left[\ell_2^2+2\ell_2\cdot p_1\right]\left[\ell_2^2+2(1-x)\ell_2\cdot p_1\right]} \times\frac{\gamma_\nu(\not\ell_2+\not p_1)\gamma^\alpha(\not\ell_2-\not p_2)\gamma_\sigma}{\left[\ell_2^2\right]\left[\ell_2^2-2\ell_2\cdot p_2\right]}, \tag{2.107}$$

while the third diagram gives

$$H^{(1)\alpha}_{(f\gamma|\mathrm{III})\,\nu}(x,p_1,p_2) = -e^4\int\frac{d^{4-2\epsilon}\ell_2}{(2\pi)^{4-2\epsilon}}\frac{\gamma^\sigma(\not\ell_2+\not p_1)\gamma^\alpha(\not\ell_2-\not p_2)\gamma_\nu(\not\ell_2+x\not p_1-\not p_2)\gamma_\sigma}{\left[\ell_2^2+2\ell_2\cdot p_1\right]\left[\ell_2^2-2\ell_2\cdot p_2\right]} \times\frac{1}{\left[\ell_2^2+2x\ell_2\cdot p_1\right]\left[\ell_2^2+2x\ell_2\cdot p_1-2\ell_2\cdot p_2-xs\right]}, \tag{2.108}$$

$$H^{(1)\alpha}_{(f\partial\gamma|\mathrm{III})\,\nu\rho}(x,p_1,p_2) = -e^4\int\frac{d^{4-2\epsilon}\ell_2}{(2\pi)^{4-2\epsilon}}\frac{\gamma^\sigma(\not\ell_2+\not p_1)\gamma^\alpha(\not\ell_2-\not p_2)\gamma_\nu}{\left[\ell_2^2+2\ell_2\cdot p_1\right]\left[\ell_2^2-2\ell_2\cdot p_2\right]} \times\frac{\left[\gamma_{\perp\rho}-2\ell_{2\perp\rho}(\not\ell_2+x\not p_1-\not p_2)\left(\frac{1}{\ell_2^2+2x\ell_2\cdot p_1}+\frac{1}{\ell_2^2+2x\ell_2\cdot p_1-2\ell_2\cdot p_2-xs}\right)\right]\gamma_\sigma}{\left[\ell_2^2+2x\ell_2\cdot p_1\right]\left[\ell_2^2+2x\ell_2\cdot p_1-2\ell_2\cdot p_2-xs\right]}. \tag{2.109}$$

2.D Results for Yukawa theory

As a byproduct of our studies, we obtained results for Yukawa theory in presence of parametrically small fermion masses, analogous to the case of massive QED considered in section 2.2. Although this is not our main focus, the jet functions that we computed are a nontrivial generalisation of some of the results presented in ref. [85], so we briefly report our findings.

The vertex content of Yukawa theory is the same as QED, with photons replaced by scalars. In fact, following ref. [85], we will consider pseudoscalars (rather than scalars). The power counting procedure, extensively described in section 2.1.1, also applies step-by-step to Yukawa theory. In fact, at the level of Feynman rules, only the scaling of the fermion-scalar vertex is altered: the emission of a scalar with momentum k from a collinear fermion line with momentum p contributes with

$$\left(\not p-\not k\right)\gamma_5\not p = (-p^2+\not k\not p)\gamma_5\,. \tag{2.110}$$

The first term then scales as λ^2, while the second one is $\mathcal{O}(\lambda)$ when k is collinear and $\mathcal{O}(\lambda^2)$

when this is soft. This causes an enhancement of at least one power of λ with respect to the naive scaling, which is predicted to be $\mathcal{O}(\lambda^0)$ when only propagators are accounted for. As in QED (eq. (2.11)), this effective enhancement follows from $(\gamma^-)^2 = 0$. However, different from massless QED, the suppression occurs for both soft and collinear emissions. The consequent collinear power counting is unaltered, while the scaling in eq. (2.110) affects the connections between soft and collinear subgraphs. Following the QED analysis, we obtain

$$\gamma_{\mathcal{G}} = 2m_s + 3m_f + \sum_{i=1}^{n}(N_s^{(i)} + N_f^{(i)} + n_s^{(i)} + 3n_f^{(i)} - 1)\,, \qquad (m=0) \tag{2.111a}$$

$$\gamma_{\mathcal{G}} = I_f + 2m_s + 4m_f + \sum_{i=1}^{n}(N_s^{(i)} + N_f^{(i)} + n_s^{(i)} + 3n_f^{(i)} - 1)\,, \qquad (m\neq 0) \tag{2.111b}$$

where the subscript s identifies scalar particles. This reproduces the results derived in ref. [113] and ref. [85] for respectively the massless and massive case.

The NLP factorisation formula for the collinear sector of Yukawa theory has the same structure as eq. (2.31), and simply requires relabelling $\gamma \to s$. In particular, we focused on the fermion-scalar term

$$M_{(fs)} = \sum_{i=1}^{n}\Big(\prod_{j\neq i} J^j_{(f)}\Big)\Big[J^i_{(fs)}\otimes H^i_{(fs)} + J^i_{(f\partial s)}\otimes H^i_{(f\partial s)}\Big]S \tag{2.112}$$

and extracted the jet functions $J^i_{(fs)}$ and $J^i_{(f\partial s)}$ from the convolution with a generic hard function. The calculation follows step-by-step the one presented in section 2.2.1. In particular, the integrals in eq. (2.94) suffice to obtain the result, and one needs to carefully include endpoint contributions. We obtain

$$J_{(fs)}(x) = -\frac{g\,m}{16\pi^2}\Big(\frac{m^2}{4\pi\mu^2}\Big)^{-\epsilon}\Gamma(\epsilon)\,\bar{u}(p)\Big\{x^{1-2\epsilon} - \frac{m}{p^+}\bar{n}\Big[x^{1-2\epsilon} - \frac{\delta(1-x)}{2-2\epsilon}\Big]\Big\}\gamma_5\,, \tag{2.113}$$

$$J^\rho_{(f\partial s)}(x) = +\frac{g\,m^2}{16\pi^2}\Big(\frac{m^2}{4\pi\mu^2}\Big)^{-\epsilon}\Gamma(\epsilon)\,\bar{u}(p)\,\frac{x^{2-2\epsilon}}{2-2\epsilon}\,\gamma_\perp^\rho\gamma_5\,, \tag{2.114}$$

where g is the coupling constant of the theory, and the notation is otherwise the same as for the QED massive jet functions in eq. (2.43). The $\mathcal{O}(\lambda)$ result in the fs-function agrees with ref. [85], where the λ^2 correction we computed is needed to appreciate the interplay with the $f\partial s$-function we derived. As for QED, we remark that a full treatment of the collinear sector at this order in λ would require including fss- and fff-jets, which however start contributing at two-loop order. Similar to section 2.2.2, we validated the factorisation formula (2.112) using the method of regions. To this end, we expanded the two-loop diagram analogous to fig. 2.8 in the hard-collinear region, where now photons are replaced by scalars, and verified that such a region is reproduced by the convolution between the jet presented in eq. (2.112) and the hard functions. We thus provided a check of the formalism of ref. [85] beyond one loop and beyond $\mathcal{O}(\lambda)$.

Chapter 3

NLP threshold corrections in Drell-Yan production at N3LO

In chapter 2 we focused on the factorisation properties of all-order virtual amplitudes, and subsequently applied this approach to amplitudes with a single real emission. Here we shall explore the direction of multiple real emissions in presence of a single virtual correction instead, thus continuing our study of the structure of scattering processes at NLP, albeit from a slightly different perspective. We consider the production of colourless, heavy final states, where threshold logarithms are known to play an important role. Examples include the DY production of a vector boson, which has been calculated up to an impressive $\mathrm{N^3LO}$ [33, 44, 45, 126–130] and the closely related process of Higgs boson production via gluon-gluon fusion, in the large top mass limit known up to the same perturbative order [31, 32, 131–137].

The primary goal of the study presented in this chapter is to gather detailed theoretical data for a future comparison with a factorisation approach. DY production offers a particularly clean testing ground in this regard, given that all threshold logarithms associated with purely real radiation are manifestly (next-to-)soft in origin (see e.g. ref. [58]). Virtual gluons, however, can indeed be collinear with one of the incoming parton legs, as well as hard or soft, thus leading to a nontrivial structure of threshold logarithms. To dissect the cross section we employ the method of regions [108–111], allowing us to pin-point the various sources of threshold logarithms. This method was heavily used in the calculation of the total cross section for Higgs boson production at $\mathrm{N^3LO}$ [136, 137], and was also used in ref. [122] to reanalyse the 1R1V contribution to the NNLO DY cross section, first calculated in refs. [126–130], to obtain the contribution associated with each separate virtual region. This data proved to be essential in the derivation of the next-to-soft factorisation formula of ref. [122], highlighted in eq. (1.25), and the QCD generalisation thereof in ref. [81].

Reference [122] focused specifically on abelian-like contributions to the $q\bar{q}$ initial state, which in QCD are associated with the colour structure C_F^n at $\mathcal{O}(\alpha_s^n)$. At any given order, such terms are amongst the most complicated in terms of the number of different NLP effects that underly their structure. Furthermore, the development of factorisation formulae

and/or resummation prescriptions for threshold corrections can be made systematically simpler by beginning with the abelian-like theory (as in refs. [78, 79, 81, 122], and indeed in chapter 2), before generalising to the non-abelian case. In this chapter we will also restrict ourselves to abelian-like contributions, but extend the classification of threshold contributions, up to NLP in the threshold variable, to diagrams involving one virtual gluon and two real emissions (2R1V). The results will have a direct bearing on how to generalise NLP factorisation formulae to include the effects of more than one gluon emission, which is clearly a necessary component for resummation.

We emphasise that the work on which this chapter is based, ref. [1], appeared before the full N^{3}LO calculation of the DY cross section was carried out in ref. [33]. Given that previous calculations of N^{3}LO corrections were performed at threshold only [138–140], the results of this study constituted a yet unknown part of the N^{3}LO DY cross section at the time of publication.

In section 3.1, we first review some necessary facts about DY production and explain how the calculation is set up. The non-trivial steps in this procedure, to wit the regions analysis of the master integrals and the phase-space integration over the three-body final state, are discussed in sections 3.2 and 3.3 respectively. Our main results are presented in section 3.4, before concluding in section 3.5.

3.1 Outline of the calculation

Throughout this chapter we focus on DY production of a vector boson, and restrict our study to the $q\bar{q}$-channel. That is, we only consider higher order corrections that are induced by a quark-antiquark pair. As mentioned in section 1.3, at LO the process corresponds to $q(p_1) + \bar{q}(p_2) \to V(Q)$, where we take $V = \gamma^*$ to be an off-shell photon. At LO the cross section is given by

$$\frac{d\sigma^{(0)}(z)}{dz} = \sigma_0\, \delta(1-z) \qquad \text{where} \qquad \sigma_0 = 4\pi\, \alpha_{\text{EM}}\, \frac{e_q^2\, \pi}{N_c}\, \frac{1-\epsilon}{s}\,. \tag{3.1}$$

We let e_q denote the fractional charge of the incoming quark, normalised to the electromagnetic charge e, and N_c is the number of colours. The delta function imposes that at LO, in absence of radiation, the variable $z = Q^2/s$, defined as the fraction of the invariant mass of the photon Q^2 and the initial state $s = (p_1 + p_2)^2$, is unity. In presence of radiation $0 \leq z \leq 1$, such that the upper limit corresponds to threshold production. We may then define the K-factor

$$\left(\frac{\alpha_s}{4\pi}\right)^n K^{(n)}(z) = \frac{1}{\sigma_0}\frac{d\sigma^{(n)}(z)}{dz}\,, \tag{3.2}$$

where the right-hand side contains the differential cross section at $\mathcal{O}(\alpha_s^n)$. The complete K-factor for DY production, including all partonic channels and full z dependence, has been previously calculated up to NNLO ($n = 2$) [45, 126–130], and LP threshold contributions

at N^{3}LO have been evaluated in refs. [138–140].[1] At any given order, one must include the effects of additional radiation, which may be real or virtual. We shall analyse the 2R1V contribution to $K^{(3)}$ (for the $q\bar{q}$-channel), up to the first subleading power in a threshold expansion about $z = 1$. In this limit, the K-factor assumes a form similar to eq. (1.22), containing plus distributions and logarithms of the threshold variable $(1-z)$.

As mentioned in the introduction, we will focus on all NLP contributions that are proportional to the colour factor C_F^3, where C_F is the quadratic Casimir in the fundamental representation. Such contributions are similar to those one would obtain in an abelian theory, upon replacing $g_s^2 C_F$ with the squared electromagnetic charge of the emitting quark. We shall classify the precise origin of these contributions, according to whether the virtual gluon is hard, soft or collinear with one of the incoming (anti-)quarks. In addition, our analysis will reveal a novel NLP contribution in case an internal *quark* line is soft, reminiscent of the configuration in fig. 2.4e. The observation underlines the complexity of the factorisation structure of amplitudes at higher orders in perturbation theory.

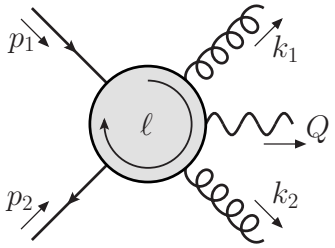

Figure 3.1: *Contribution to the Drell-Yan process at N^{3}LO, consisting of two real gluon emissions dressing the one-loop amplitude, which involves a loop momentum ℓ.*

The amplitude we consider is shown schematically in fig. 3.1, and corresponds to the process

$$q(p_1) + \bar{q}(p_2) \to \gamma^*(Q) + g(k_1) + g(k_2) \tag{3.3}$$

at one-loop order. Labelling this by $\mathscr{M}_{\text{2R1V}}$, its contribution to the differential cross section occurs through interference with the pure double-real emission amplitude $\mathscr{M}_{\text{2R}}$:[2]

$$\left.\frac{d\sigma^{(3)}_{q\bar{q}}(z)}{dz}\right|_{\text{2R1V},\,C_F^3} = \frac{1}{4N_c^2}\frac{1}{2s}2\,\text{Re}\left[\int\frac{d^d\ell}{(2\pi)^d}\int d\Phi^{(3)}\delta\left(z-\frac{Q^2}{s}\right)\right.$$
$$\left.\times\,\mathscr{M}_{\text{2R1V}}(p_1,p_2,k_1,k_2,\ell)\,\mathscr{M}^{\dagger}_{\text{2R}}(p_1,p_2,k_1,k_2)\right], \tag{3.4}$$

where the prefactors originate from colour and spin averaging as well as flux factor, and we integrate over the phase space for the three-body final state, denoted by $d\Phi^{(3)}$. Note that we kept the integral over the loop momentum ℓ explicit, rather than including it in $\mathscr{M}_{\text{2R1V}}$.

[1] That is, at the time of publication of this study. Recently the full K-factor at N^{3}LO was calculated in ref. [33].

[2] We emphasise that the contribution from complex conjugate diagrams is included by applying the $2\,\text{Re}[\dots]$ prescription to the interference term considered here.

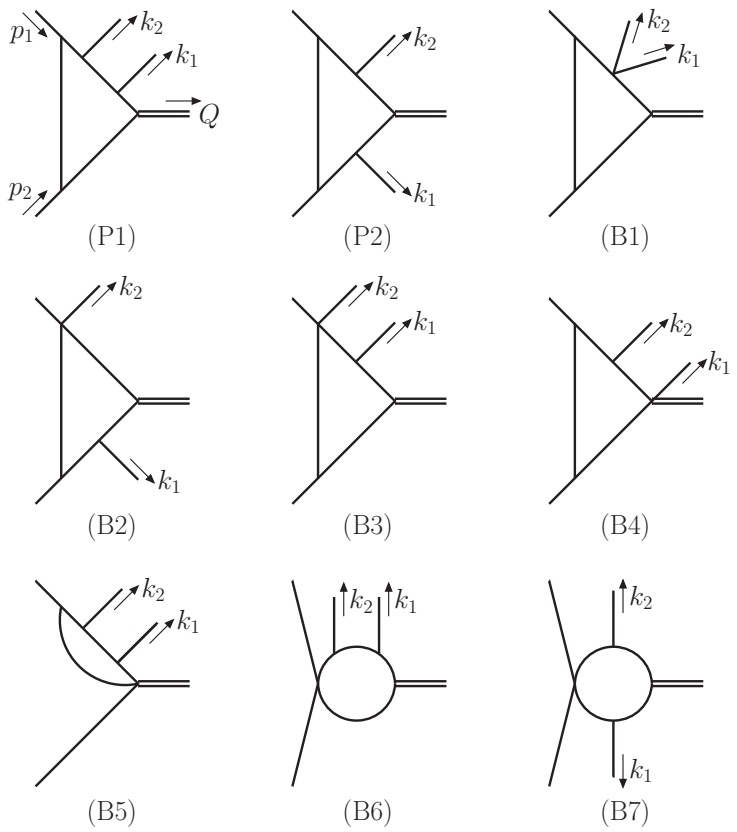

Figure 3.2: *Pentagon* (P_i) *and box* (B_i) *scalar master diagrams that contribute to eq. (3.4).*

There are 48 distinct Feynman diagrams that contribute to the abelian-like one-loop amplitude (where we define abelian-like diagrams to be those that contribute to the C_F^3 colour structure in the cross section, thereby also excluding diagrams with a fermion loop). We have generated all such diagrams using `QGRAF` [141], and subsequently used `Reduze` [142, 143] (version 2) to construct the interference term appearing in eq. (3.4). At this stage, one must carry out the integration over the loop momentum ℓ appearing in eq. (3.4), in $d = 4-2\epsilon$ dimensions. To this end, we also use `Reduze` to reduce the one-loop integration to a set of scalar master integrals, using integration by parts identities. These integrals may themselves be represented as scalar Feynman diagrams with topologies of increasing complexity. The box and pentagon master diagrams are shown in fig. 3.2, where the simpler bubbles and triangles are omitted for brevity.

As stated above, the aim of our study is to classify the structure of the *K*-factor up to NLP in the threshold expansion. We must then consider each master integral, and elucidate its corresponding contribution to threshold behaviour, according to whether the loop momentum is hard, soft or (anti-)collinear to one of the incoming partons. Here we follow the standard approach of the method of regions [108–111], which we describe in detail in the following section.

3.2 Method of regions analysis of master integrals

In the method of regions, singular parts of integrals in perturbative amplitudes are partitioned according to physical criteria on the loop momenta. In the case of the threshold expansion considered in this chapter, it is possible to separate the singular behaviour into *non-overlapping* regions, whose individual contributions reconstruct the full integral (itself expanded about the threshold limit) when summed. As an example, consider the diagram (B_1) of figure 3.2, where we have associated the loop momentum ℓ with a particular internal line. This momentum can be decomposed according to the prescription of eq. (2.2)

$$\ell^\mu = (\bar{n}\cdot\ell)\, n^\mu + (n\cdot\ell)\,\bar{n}^\mu + \ell_\perp^\mu \equiv \ell^+ n^\mu + \ell^- \bar{n}^\mu + \ell_\perp^\mu\,, \tag{3.5}$$

where the coefficients of this Sudakov decomposition define ℓ^μ in lightcone coordinates: $\ell^\mu = (\ell^+, \ell_\perp, \ell^-)$. We note that the notation used here coincides with that in chapter 2, but restate the necessary definitions for convenience of the reader. The dimensionless lightlike vectors n and $\bar{n}$ denote the directions of the incoming particles

$$p_1^\mu = \sqrt{\frac{s}{2}}\, n^\mu \qquad \text{and} \qquad p_2^\mu = \sqrt{\frac{s}{2}}\, \bar{n}^\mu\,, \tag{3.6}$$

with

$$n^\mu = (1,0,0)\,, \qquad \bar{n}^\mu = (0,0,1)\,, \qquad n\cdot\bar{n} = 1\,. \tag{3.7}$$

The four-vector $\ell_\perp$ is transverse to the beam direction such that

$$\ell_\perp \cdot n = \ell_\perp \cdot \bar{n} = 0\,. \tag{3.8}$$

Using this notation, we may define the various regions by the different scaling behaviour of the components of the loop momentum. That is, one may introduce a book-keeping parameter $\lambda \sim \sqrt{1-z}$, such that the regions we need to consider are given by momenta of the form

$$\begin{aligned} \text{Hard}: \quad & \ell^\mu \sim Q(1,1,1)\,, & \text{Soft}: \quad & \ell^\mu \sim Q\left(\lambda^2,\lambda^2,\lambda^2\right), \\ \text{Collinear}: \quad & \ell^\mu \sim Q\left(1,\lambda,\lambda^2\right), & \text{Anti-collinear}: \quad & \ell^\mu \sim Q\left(\lambda^2,\lambda,1\right), \end{aligned} \tag{3.9}$$

where the terms collinear and anti-collinear denote collinearity with respect to p_1 and p_2 respectively. Note that these are not the only possible scalings: in principle, one may also consider modes such as

$$\text{Semi-hard}: \quad \ell^\mu \sim Q(\lambda,\lambda,\lambda), \qquad \text{Ultra-collinear}: \quad \ell^\mu \sim Q(1,\lambda^2,\lambda^4)\,. \tag{3.10}$$

It is possible, however, to show that the only regions relevant for the threshold expansion are the hard, (anti-)collinear and soft regions defined by the scalings of eq. (3.9). All other regions give scaleless integrals, which vanish in dimensional regularisation, such that we may discard them in the following. By construction, the momenta of the initial state partons

are (anti-)collinear while final state gluons are soft, i.e. $k_1^\mu \sim k_2^\mu \sim Q(\lambda^2, \lambda^2, \lambda^2)$.

For any master integral, the denominators can be systematically expanded in λ in each region of eq. (3.9), keeping the first subleading power where necessary to achieve NLP accuracy in the final expression for the *K*-factor. Carrying out the integral in each region and subsequently adding the results together reproduces, in principle, the threshold expansion of the full integral.

There is an interesting subtlety in the above procedure, if one wants to be sure of having characterised *all* possible regions of a given master integral. Before the region expansion, a given master integral possesses a symmetry under shifts of the loop momentum, such that one may associate the loop momentum ℓ with an arbitrary internal line of the master diagram. However, the expansion of ℓ into regions breaks Lorentz invariance, leading to a violation of the shift symmetry. It may then be the case that particular choices of ℓ are such that one cannot unambiguously identify all possible regions.

To illustrate this point, let us consider diagram (B1) of fig. 3.2, which we redraw in fig. 3.3 with the purpose of labelling the internal lines. In this particular case, certain choices of the loop momentum may indeed lead to an important region being missed, if not interpreted carefully. Furthermore, this is a problem that arises for the first time at N^{3}LO, as the region in question requires the presence of a virtual gluon and two real emissions. In principle all regions are unambiguously identified by poles in propagators, as discussed in ref. [108]. However, some choices of loop momentum ℓ can be more convenient than others, in that they allow all regions to be characterised in terms of softness or collinearity of ℓ alone. Given that this can be a point of confusion, we believe it is instructive to spell out the fine details here.

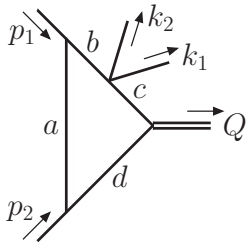

Figure 3.3: *Master diagram* B_1*, which is one of the topologies that requires a careful application of the method of regions. Internal lines are labelled for convenient referencing.*

We consider the expansion in regions of the box integral represented in fig. 3.3. The integral is defined as

$$I = \int [d\ell] \frac{1}{D_a D_b D_c D_d}, \tag{3.11}$$

where D_i represents the propagator associated with line i in fig. 3.3, and we have introduced the convenient notation

$$\int [d\ell] \equiv \frac{e^{\epsilon \gamma_E}}{(4\pi)^\epsilon} \bar{\mu}^{2\epsilon} \int \frac{d^d \ell}{(2\pi)^d}, \tag{3.12}$$

D_b	ℓ^2	$2p_1^+\ell^-$
H	1	1
C	λ^2	λ^2
$\overline{\text{C}}$	λ^2	1
S	λ^4	λ^2

D_d	ℓ^2	$-2\ell^+p_2^-$
H	1	1
C	λ^2	1
$\overline{\text{C}}$	λ^2	λ^2
S	λ^4	λ^2

Table 3.1: *Scaling associated with the terms in the propagators D_b and D_d, as defined in eq. (3.14). Leading terms in each region are highlighted in grey.*

D_c	ℓ^2	$2p_1^+\ell^-$	$-2\ell^+(k_1+k_2)^-$	$-2\ell^-(k_1+k_2)^+$	$-2\ell_\perp\cdot(k_1+k_2)_\perp$	$-2p_1^+(k_1+k_2)^-$	$2k_1\cdot k_2$
H	1	1	λ^2	λ^2	λ^2	λ^2	λ^4
C	λ^2	λ^2	λ^2	λ^4	λ^3	λ^2	λ^4
$\overline{\text{C}}$	λ^2	1	λ^4	λ^2	λ^3	λ^2	λ^4
S	λ^4	λ^2	λ^4	λ^4	λ^4	λ^2	λ^4

Table 3.2: *Scaling associated with the terms in the propagators D_c, as defined in eq. (3.14). Leading terms in each region are highlighted in grey.*

where $\bar{\mu}$ is the $\overline{\text{MS}}$ renormalisation scale, $\bar{\mu}^2 = 4\pi\,\mathrm{e}^{-\gamma_E}\mu^2$. Choosing the loop momentum ℓ to correspond to line a seems natural, because in this way the regions are directly associated with having a hard, collinear or soft gluon exchange in the loop, which should be easily interpreted in the context of an effective field theory containing soft and collinear gluons. We can then define the denominators

$$\begin{aligned}
D_a &= \ell^2\,,\\
D_b &= (\ell+p_1)^2 = \ell^2 + 2\ell\cdot p_1\,,\\
D_c &= (\ell+p_1-k_1-k_2)^2 = \ell^2 + 2\ell\cdot p_1 - 2\ell\cdot(k_1+k_2) - 2p_1\cdot(k_1+k_2) + 2k_1\cdot k_2\,,\\
D_d &= (\ell-p_2)^2 = \ell^2 - 2\ell\cdot p_2\,,
\end{aligned} \tag{3.13}$$

and decompose the loop momentum ℓ according to eq. (3.5). One obtains

$$\begin{aligned}
D_a &= \ell^2\,,\\
D_b &= \ell^2 + 2p_1^+\ell^-\,,\\
D_c &= \ell^2 + 2p_1^+\ell^- - 2\ell^+(k_1+k_2)^- - 2\ell^-(k_1+k_2)^+ - 2\ell_\perp\cdot(k_1+k_2)_\perp\\
&\quad - 2p_1^+(k_1+k_2)^- + 2k_1\cdot k_2\,,\\
D_d &= \ell^2 - 2\ell^+p_2^-\,.
\end{aligned} \tag{3.14}$$

The scaling in λ of the various terms in the different regions is provided in tables 3.1 and 3.2. In the following we keep only the leading terms in λ for each propagator, thus getting the LP contribution to this box integral. The hard region turns out to give

$$I_{\text{H}} = \int [d\ell\,]\,\frac{1}{\left[\ell^2\right]\left[\ell^2+2p_1^+\ell^-\right]^2\left[\ell^2-2\,\ell^+p_2^-\right]}$$

$$= \frac{i}{(4\pi)^2}\left(\frac{\bar{\mu}^2}{-s}\right)^{\epsilon}\frac{1}{s^2}\left(\frac{2}{\epsilon}-\epsilon\zeta_2-\frac{14\zeta_3}{3}\epsilon^2+\mathcal{O}(\epsilon^3)\right), \tag{3.15}$$

Following the same criterion, a naive expansion in the collinear region, assuming the scaling assigned in table 3.1 and 3.2 gives, to LP

$$\begin{aligned} I_{\mathrm{C}} &= \int[d\ell]\,\frac{1}{\left[\ell^2\right]\left[\ell^2+2p_1^+\ell^-\right]\left[\ell^2+2p_1^+\ell^--2\ell^+(k_1+k_2)^--2p_1^+(k_1+k_2)^-\right]\left[-2\ell^+p_2^-\right]} \\ &= -\frac{i}{4\pi^2}\left(\frac{\bar{\mu}^2}{2p_1^+(k_1+k_2)^-}\right)^{\epsilon}\frac{1}{s}\frac{1}{2p_1^+(k_1+k_2)^-}\left(\frac{2}{\epsilon^2}-\zeta_2-\frac{14\zeta_3}{3}\epsilon-\frac{47\zeta_4}{8}\epsilon^2+\mathcal{O}(\epsilon^3)\right). \end{aligned} \tag{3.16}$$

Note that the hard region gives a subleading power contribution compared to the collinear region, which scales as $\mathcal{O}\left(\lambda^{-2}\right)$. Within a consistent expansion to LP the hard region is thus zero, even if it is not scaleless. Furthermore, is it possible to show that integration in the anti-collinear and soft regions give scaleless results

$$\begin{aligned} I_{\overline{\mathrm{C}}} &= \int[d\ell]\,\frac{1}{\left[\ell^2\right]\left[2p_1^+\ell^-\right]^2\left[\ell^2-2\ell^+p_2^-\right]} = 0\,, \\ I_{\mathrm{S}} &= \int[d\ell]\,\frac{1}{\left[\ell^2\right]\left[2p_1^+\ell^-\right]\left[2p_1^+\ell^--2p_1^+(k_1+k_2)^-\right]\left[2\ell^+p_2^-\right]} = 0\,. \end{aligned} \tag{3.17}$$

Thus, the LP contribution to the integral in eq. (3.11) seems to be given by the collinear region in eq. (3.16). This conclusion is erroneous, however, as an important contribution has been missed. Shifting the loop momentum to $\ell' = \ell + p_1$ will reveal this contribution. As discussed above, shift symmetry is broken by the region expansion, such that shifting the loop momentum can lead to inequivalent regions in general. With the new choice of loop momentum, the propagators read

$$\begin{aligned} D_a &= (\ell'-p_1)^2 = \ell'^2-2\ell'\cdot p_1\,, \\ D_b &= \ell'^2\,, \\ D_c &= (\ell'-k_1-k_2)^2 = \ell'^2-2\ell'\cdot(k_1+k_2)+2k_1\cdot k_2\,, \\ D_d &= (\ell'-p_1-p_2)^2 = \ell'^2-2\ell'\cdot(p_1+p_2)+2p_1\cdot p_2\,, \end{aligned} \tag{3.18}$$

so that applying the Sudakov decomposition of eq. (3.5) gives

$$\begin{aligned} D_a &= \ell'^2-2p_1^+\ell'^-\,, \\ D_b &= \ell'^2\,, \\ D_c &= \ell'^2-2\ell'^+(k_1+k_2)^--2\ell'^-(k_1+k_2)^+-2\ell'_\perp\cdot(k_1+k_2)_\perp+2k_1\cdot k_2\,, \\ D_d &= \ell'^2-2(p_1^+\ell'^-+\ell'^+p_2^-)+s\,. \end{aligned} \tag{3.19}$$

The scaling of the various terms in the different regions is provided in tables 3.3 and 3.4. Notice that the new regions are labelled with a prime, to distinguish them from the regions

D_a	ℓ'^2	$-2p_1^+\ell'^-$
H′	1	1
C′	λ^2	λ^2
$\overline{\text{C}}'$	λ^2	1
S′	λ^4	λ^2

D_d	ℓ'^2	$-2p_1^+\ell'^-$	$-2\ell'^+p_2^-$	s
H′	1	1	1	1
C′	λ^2	λ^2	1	1
$\overline{\text{C}}'$	λ^2	1	λ^2	1
S′	λ^4	λ^2	λ^2	1

Table 3.3: *Scaling associated with the terms in the propagators D_a and D_d, as defined in eq. (3.19).*

D_c	ℓ'^2	$-2\ell'^+(k_1+k_2)^-$	$-2\ell'^-(k_1+k_2)^+$	$-2\ell'_\perp\cdot(k_1+k_2)_\perp$	$2k_1\cdot k_2$
H′	1	λ^2	λ^2	λ^2	λ^4
C′	λ^2	λ^2	λ^4	λ^3	λ^4
$\overline{\text{C}}'$	λ^2	λ^4	λ^2	λ^3	λ^4
S′	λ^4	λ^4	λ^4	λ^4	λ^4

Table 3.4: *Scaling associated with the terms in the propagators D_c, as defined in eq. (3.19).*

considered with the previous parametrisation. It is easy to check that the new hard, collinear and anti-collinear regions still give the same result as the old corresponding regions

$$I_{\text{H}'} = \int [d\ell'] \frac{1}{\left[\ell^2 - 2p_1^+\ell'^-\right]\left[\ell'^2\right]^2\left[\ell^2 - 2(p_1^+\ell'^- + \ell'^+p_2^-) + s\right]} = I_{\text{H}}\,, \tag{3.20}$$

$$I_{\text{C}'} = \int [d\ell] \frac{1}{\left[\ell^2 - 2p_1^+\ell'^-\right]\left[\ell'^2\right]\left[\ell'^2 - 2\ell'^+(k_1+k_2)^-\right]\left[-2\ell'^+p_2^- + s\right]} = I_{\text{C}}\,, \tag{3.21}$$

$$I_{\overline{\text{C}}'} = \int [d\ell] \frac{1}{\left[-2p_1^+\ell'^-\right]\left[\ell'^2\right]\left[\ell'^2 - 2\ell'^-(k_1+k_2)^+\right]\left[-2p_1^+\ell'^- + s\right]} = I_{\overline{\text{C}}} = 0\,. \tag{3.22}$$

The new soft region, however, is not scaleless, and gives an additional contribution equal to

$$\begin{aligned} I_{\text{S}'} &= \int [d\ell] \frac{1}{\left[-2p_1^+\ell'^-\right]\left[\ell'^2\right]\left[\ell'^2 - 2\ell'\cdot(k_1+k_2) + 2k_1\cdot k_2\right]\left[s\right]} \\ &= -\frac{i}{4\pi^2}\left(\frac{\bar{\mu}^2}{-2k_1\cdot k_2}\right)^\epsilon \frac{1}{s}\frac{1}{2p_1^+(k_1+k_2)^-}\left[-\frac{1}{\epsilon^2} + \frac{\zeta_2}{2} + \frac{7\zeta_3}{3}\epsilon + \frac{47\zeta_4}{16}\epsilon^2 + \mathcal{O}(\epsilon^3)\right], \end{aligned} \tag{3.23}$$

which was not present in the old parameterisation. To reconcile these results, we point out that the problem with the original choice of loop momentum is that the external scales are not well separated: both the collinear scale $-2p_1^+(k_1+k_2)^- \sim \lambda^2$ and the soft scale $2k_1\cdot k_2 \sim \lambda^4$ appear in the same propagator D_c. This causes problems in the collinear region as the loop integration is still over the full domain. There is therefore a part of the integration domain in which $\ell^\mu \sim -p_1^\mu$, such that

$$D_c\big|_{\text{C,LP}} \;=\; \ell^2 + 2p_1^+\ell^- - 2\ell^+(k_1+k_2)^- - 2p_1^+(k_1+k_2)^-$$

$$\overset{\ell\sim -p_1}{\to} 2p_1^+(k_1+k_2)^- - 2p_1^+(k_1+k_2)^- \to 0\,, \tag{3.24}$$

i.e. the LP terms at $\mathcal{O}\left(\lambda^2\right)$ cancel, causing the subleading power term $2k_1\cdot k_2 \sim \lambda^4$ to become leading. Considering this term small in the expansion of the propagator thus leads to the wrong analytic structure of the integral in this limit. The consequence is that the propagator D_c cannot be expanded in the collinear region when parametrizing the loop momentum as in eq. (3.13). Rather, one needs to consider a more general collinear region "C-gen.", in which the propagator D_c is kept unexpanded

$$\begin{aligned} I_{\text{C-gen.}} = \int [d\ell]\Big(\big[\ell^2\big]\big[\ell^2+2p_1^+\ell^-\big]\big[\ell^2+2p_1^+\ell^- - 2\ell^+(k_1+k_2)^- - 2\ell^-(k_1+k_2)^+ \\ - 2\ell_\perp\cdot(k_1+k_2)_\perp - 2p_1^+(k_1+k_2)^- + 2k_1\cdot k_2\big]\big[-2\ell^+p_2^-\big]\Big)^{-1}. \end{aligned} \tag{3.25}$$

Evaluating $I_{\text{C-gen.}}$ exactly and expanding at threshold *after* integration, indeed one finds that it contains both the contribution from the collinear and the soft region associated with the alternative loop momentum choice of eq. (3.18):

$$\begin{aligned} I_{\text{C-gen.}} = &-\frac{i\,\mathrm{e}^{\epsilon\gamma_{\text{E}}}}{(4\pi)^2}\frac{1}{s}\frac{1}{2p_1^+(k_1+k_2)^-}\frac{\Gamma^2(-\epsilon)\,\Gamma(\epsilon)}{\Gamma(-2\epsilon)} \\ &\times\left[\frac{1}{2}\left(\frac{\bar{\mu}^2}{-2k_1\cdot k_2}\right)^{\epsilon} - \left(\frac{\bar{\mu}^2}{2p_1^+(k_1+k_2)^-}\right)^{\epsilon}\right] = I_{S'} + I_{C'}\,. \end{aligned} \tag{3.26}$$

An independent check can be performed with the program `Asy` [110, 144], which provides a geometrical method to reveal the regions contributing to a given integral. For the integral in eq. (3.11) the program reveals the existence of three non-scaleless regions, which correspond to the hard, collinear and soft regions found within the second parametrisation of the loop momentum in eq. (3.18). The same program can be used to verify that we have captured all regions in every other diagram.

The appearance of IR singularities in the hard region of the B_1 master integral may be surprising. As discussed in chapter 2, this is however a common phenomenon in the method of regions. The approach we have taken above is to set to zero any integrals which remain scaleless in dimensional regularisation. In the soft region, expansion of the propagators changes the ultraviolet scaling behaviour of the integral, and thus introduces (spurious) ultraviolet divergences, whose effect is to cancel infrared divergences associated with exchange of gluons between the incoming (anti)-quark legs, i.e. associated with the scale s. One can instead choose to isolate these UV divergences and absorb them into the hard function, and the effect of this procedure is to transfer poles in ϵ from the hard to the soft region. Given that this has no effect on the final result for the K-factor (which is a sum of all regions), we do not do this here. However, it should be remembered that ϵ poles appearing in the hard region are indeed of soft origin.

Despite the cancellation between UV and IR divergences, there remains the above-mentioned non-zero contribution to the soft region from eq. (3.23). This is particularly interesting in

that it is new at N^{3}LO in perturbation theory, which is understood by the need for a virtual gluon in order to discuss decomposition of the loop momentum, while at least two soft gluons are needed in the final state to create the associated scale $k_1 \cdot k_2$. Detailed scrutiny of the region expansion applied to each of our Feynman diagrams reveals that the sole contribution to the soft region stems from physical configurations similar to those of fig. 3.4. In the example shown, the incoming collinear quark turns into a soft quark by emitting a collinear gluon, where the soft quark then emits two soft gluons. As is well-known, soft quarks are subleading (in the momentum expansion) relative to soft gluons. Thus, we expect the soft region to contribute at NLP level only. This expectation is confirmed by applying the power counting formula for massless QED, i.e. eq. (2.25a), to the diagram in question. Indeed, the diagram in fig. 3.4 is the simplest example of the class of diagrams collectively depicted in fig. 2.4e, upon dressing the soft blob with two emissions. Furthermore, the somewhat complicated structure of soft and collinear emissions, together with the fact that this region occurs for the first time at N^{3}LO, suggests that it will be suppressed by a number of powers of ϵ, which would result in subleading logs in the final result for the K-factor. In section 3.4 we will confirm this expectation. It is also worth mentioning that a similar soft region was seen in the N^{3}LO Higgs boson computation of ref. [137], where it was found to indeed be non-zero. We expect an essentially identical contribution to appear within SCET.

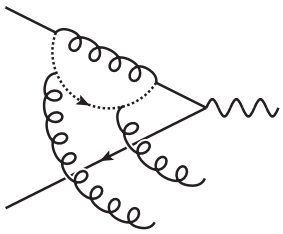

Figure 3.4: *Physical intepretation of the soft region occuring for the first time at N^{3}LO: an incoming collinear quark (or antiquark) turns into a soft quark (dotted line) by emitting a collinear gluon. The soft quark then emits two soft gluons.*

In summary, application of the method of regions to the process of figure 3.1 reveals the presence of hard, (anti-)collinear and soft regions. After expanding the propagators in each region, all integrals over the loop momentum ℓ can be carried out analytically. Given that such integrals at one-loop order are quite standard in the literature, we do not report intermediate results here. Results for the squared matrix element in each region can be found in the following section. In order to cross-check our results, all steps of this calculation (e.g. diagram calculation, reduction to master integrals, expansion in regions, loop integration) have been carried out twice, in independent implementations, and led to full agreement.

3.3 Phase space integration

Applying the methods of the previous section, one obtains the interference between one-loop double-real contribution contracted with the conjugate tree-level result appearing in

eq. (3.4), expanded in regions and integrated over the loop momentum. We denote these intermediate results by

$$|\mathscr{M}|^2 \equiv \int \frac{d^d\ell}{(2\pi)^d}\, \mathscr{M}_{\text{2R1V}}(p_1,p_2,k_1,k_2,\ell)\, \mathscr{M}^{\dagger}_{\text{2R}}(p_1,p_2,k_1,k_2)\,, \tag{3.27}$$

which forms the integrand of the three-body phase space integration that is still to be carried out. We define the kinematic invariants

$$\begin{aligned} t_1 &= (p_1-k_1)^2 = -2p_1\cdot k_1\,, & t_2 &= (p_1-k_2)^2 = -2p_1\cdot k_2\,,\\ u_1 &= (p_2-k_1)^2 = -2p_2\cdot k_1\,, & u_2 &= (p_2-k_2)^2 = -2p_2\cdot k_2\,,\\ s_{12} &= (k_1+k_2)^2 = 2k_1\cdot k_2\,. \end{aligned} \tag{3.28}$$

The squared matrix element for the hard region at (next-to-)leading power is then as follows

$$|\mathscr{M}|^2_{\text{H, LP}} = \mathscr{N}\left(\frac{\bar\mu^2}{-s}\right)^{\epsilon} f_1^{\text{H}}\, \frac{s^3}{t_1\,t_2\,u_1\,u_2}\,, \tag{3.29a}$$

$$|\mathscr{M}|^2_{\text{H, NLP}} = \mathscr{N}\left(\frac{\bar\mu^2}{-s}\right)^{\epsilon} f_1^{\text{H}}\, \frac{s^2(t_1+t_2+u_1+u_2)}{t_1\,t_2\,u_1\,u_2}\left[(1-\epsilon)+\frac{1}{2}\frac{t_1\,u_2+t_2\,u_1-s_{12}\,s}{(t_1+t_2)(u_1+u_2)}\right], \tag{3.29b}$$

where

$$\mathscr{N} = 128\pi\,\alpha_s^3(1-\epsilon)\,C_F^3\,e_q^2\,N_c\,(\mu^2)^{2\epsilon}\,, \tag{3.30}$$

and the various coefficient functions $\{f_i^X\}$ are defined in appendix 3.A. Likewise, for the collinear region we find

$$|\mathscr{M}|^2_{\text{C, LP}} = 0\,, \tag{3.31a}$$

$$\begin{aligned} |\mathscr{M}|^2_{\text{C, NLP}} = \mathscr{N}\,(\bar\mu^2)^{\epsilon}\frac{s^2}{t_1t_2u_1u_2}\Bigg\{&\left[u_1\,(-t_1)^{-\epsilon}+u_2\,(-t_2)^{-\epsilon}\right]f_1^{\text{C}}\\ &+\frac{t_2u_1+t_1u_2-s_{12}\,s}{t_1+t_2}\left[\left((-t_1)^{-\epsilon}-2\,(-t_1-t_2)^{-\epsilon}+(-t_2)^{-\epsilon}\right)f_2^{\text{C}}\right.\\ &\left.-\left(\frac{t_1}{t_2}(-t_1)^{-\epsilon}-\frac{t_1^2+t_2^2}{t_1t_2}(-t_1-t_2)^{-\epsilon}+\frac{t_2}{t_1}(-t_2)^{-\epsilon}\right)f_3^{\text{C}}\right]\Bigg\}. \end{aligned} \tag{3.31b}$$

The anti-collinear region can be straightforwardly obtained through the exchange $p_1 \leftrightarrow p_2$. Finally, there is the soft region, which yields

$$|\mathscr{M}|^2_{\text{S, LP}} = 0\,, \tag{3.32a}$$

$$\begin{aligned} |\mathscr{M}|^2_{\text{S, NLP}} = \mathscr{N}&\left(\frac{\bar\mu^2}{-s_{12}}\right)^{\epsilon}\frac{s^2}{t_1t_2u_1u_2}\\ &\times\left\{\frac{t_2\,f_1^{\text{S}}}{t_1(t_1+t_2)^2}\left[(s_{12}\,s-t_1u_2-t_2u_1)\left(t_1+t_2-t_2\,{}_2F_1\Big(1,1,1-\epsilon,\tfrac{t_1}{t_1+t_2}\Big)\right)\right]\right.\\ &\left.+\frac{f_2^{\text{S}}}{s\,s_{12}\,(t_1+t_2)}\left[(t_1u_2-t_2u_1)^2-s_{12}\,s\,(t_1u_2+t_2u_1)\right]\right. \end{aligned}$$

$$
\begin{aligned}
&+\frac{f_3^S}{s\,s_{12}\,t_1(t_1+t_2)^2}\Big[s_{12}^2 s^2\,t_2(t_1-t_2)+t_2(t_1+t_2)(t_1u_2-t_2u_1)^2\\
&+s_{12}\,s\,t_1(t_1+t_2)(t_1u_2-3t_2u_1)-t_2\Big(s_{12}^2 s^2(t_1-t_2)+(t_1+t_2)(t_1u_2-t_2u_1)^2\\
&-2s_{12}\,s t_1(t_1u_2+t_2u_1)\Big)\,{}_2F_1\Big(1,1,1-\epsilon,\tfrac{t_1}{t_1+t_2}\Big)\Big]\\
&+\{t_1,t_2\leftrightarrow u_1,u_2\}+\{t_1,t_2\leftrightarrow u_2,u_1\}+\{t_1,u_1\leftrightarrow t_2,u_2\}\Big\}. \qquad (3.32b)
\end{aligned}
$$

To compute the contribution of eqs. (3.29)–(3.32) to the differential cross section or K-factor, we must integrate over the Lorentz-invariant three-body phase space associated with the final state, as stated in eq. (3.4). One is free to choose a particular momentum frame for the phase space integration. Furthermore, given that each separate term in the squared matrix element is Lorentz invariant, we may even choose different frames for different types of contributions, which proves to be convenient in practice.

For the hard and (anti-)collinear regions, expanding eqs. (3.29) and (3.31) before substituting into eq. (3.4) reveals a series of terms, all described by the master integral

$$
I_1(\alpha_1,\alpha_2,\beta_1,\beta_2,\gamma_1,\gamma_2,\delta)=\int d\Phi^{(3)}\,s_{12}^{\delta}\,t_1^{-\alpha_1}\,t_2^{-\alpha_2}\,u_1^{-\beta_1}\,u_2^{-\beta_2}(t_1+t_2)^{-\gamma_1}(u_1+u_2)^{-\gamma_2}, \qquad (3.33)
$$

where $\delta\in\{0,1\}$. For these values of δ, it is possible to obtain a result for this integral as an expansion in the threshold variable $(1-z)$ in $d=4-2\epsilon$ dimensions, by decomposing each real gluon momentum k_i in the Sudakov decomposition of eq. (3.5). We spell out this derivation in appendix 3.B and present the results here. To integrate eqs. (3.29) and (3.31) over the phase-space, up to NLP in $(1-z)$, we require the integrals:

$$
\begin{aligned}
I_1(\alpha_1,\alpha_2,\beta_1,\beta_2,0,0,0)&=(-1)^{-C}\,2^{-1-2d}\,\pi^{3-2d}\,\Omega_{d-2}^2\,s^{d-3-C}\,\frac{(1-z)^{2d-5-C}}{\Gamma(2d-4-C)} \qquad (3.34a)\\
&\times\left[\prod_{i=1}^{2}\Gamma\Big(\frac{d-2}{2}-\alpha_i\Big)\Gamma\Big(\frac{d-2}{2}-\beta_i\Big)\right]\\
&\times\left\{1+(1-z)\left[\frac{\big(\frac{d-2}{2}-\alpha_1\big)\big(\frac{d-2}{2}-\beta_2\big)+\big(\frac{d-2}{2}-\alpha_2\big)\big(\frac{d-2}{2}-\beta_1\big)}{2d-4-C}\right]+\mathcal{O}\big((1-z)^2\big)\right\},
\end{aligned}
$$

$$
\begin{aligned}
I_1(\alpha_1,\alpha_2,\beta_1,\beta_2,\gamma_1,\gamma_2,0)&=(-1)^{-C-\gamma_1-\gamma_2}\,2^{-1-2d}\,\pi^{3-2d}\,\Omega_{d-2}^2\,s^{d-3-C-\gamma_1-\gamma_2} \qquad (3.34b)\\
&\times\frac{(1-z)^{2d-5-C-\gamma_1-\gamma_2}}{\Gamma(2d-4-C-\gamma_1-\gamma_2)}\left[\prod_{i=1}^{2}\Gamma\Big(\frac{d-2}{2}-\alpha_i\Big)\Gamma\Big(\frac{d-2}{2}-\beta_i\Big)\right]\\
&\times\frac{\Gamma(d-2-\alpha_1-\alpha_2-\gamma_1)\,\Gamma(d-2-\beta_1-\beta_2-\gamma_2)}{\Gamma(d-2-\alpha_1-\alpha_2)\,\Gamma(d-2-\beta_1-\beta_2)}\big[1+\mathcal{O}(1-z)\big],
\end{aligned}
$$

$$
I_1(\alpha_1,\alpha_2,\beta_1,\beta_2,\gamma_1,\gamma_2,1)=(-1)^{-C-\gamma_1-\gamma_2}\,2^{-1-2d}\,\pi^{3-2d}\,\Omega_{d-2}^2\,s^{d-2-C-\gamma_1-\gamma_2} \qquad (3.34c)
$$

$$\times \frac{(1-z)^{2d-3-C-\gamma_1-\gamma_2}}{\Gamma(2d-2-C-\gamma_1-\gamma_2)} \left[\prod_{i=1}^{2} \Gamma\left(\frac{d-2}{2}-\alpha_i\right)\Gamma\left(\frac{d-2}{2}-\beta_i\right)\right]$$
$$\times \frac{\Gamma(d-1-\alpha_1-\alpha_2-\gamma_1)\,\Gamma(d-1-\beta_1-\beta_2-\gamma_2)}{\Gamma(d-1-\alpha_1-\alpha_2)\,\Gamma(d-1-\beta_1-\beta_2)}$$
$$\times \left[\left(\frac{d-2}{2}-\alpha_1\right)\left(\frac{d-2}{2}-\beta_2\right)+\left(\frac{d-2}{2}-\alpha_2\right)\left(\frac{d-2}{2}-\beta_1\right)\right]\left[1+\mathcal{O}(1-z)\right].$$

Here we have defined $C=\sum_{i=1}^{2}(\alpha_i+\beta_i)$, as well as the total solid angle in $(d-2)$ spatial dimensions

$$\Omega_{d-2}=\frac{2\pi^{\frac{d-2}{2}}}{\Gamma\left(\frac{d-2}{2}\right)}. \tag{3.35}$$

For the soft region, we rely on the symmetry of eq. (3.32) under the (combined) exchange of $p_1 \leftrightarrow p_2$ and $k_1 \leftrightarrow k_2$ to reduce the number of distinct terms that need to be integrated. There remain two types of terms: (i) those involving the hypergeometric function ${}_2F_1(1,1;1-\epsilon;t_1/(t_1+t_2))$; (ii) those without the hypergeometric.

Terms of type (ii) are similar to those that occur in the double-real emission contribution to the NNLO Drell-Yan cross section [129]. To integrate them, one may apply straightforward algebraic identities such as

$$\frac{1}{t_1(t_1+t_2)}+\frac{1}{t_2(t_1+t_2)}=\frac{1}{t_1\,t_2} \qquad \text{and} \qquad \frac{t_1}{t_2}=\frac{(t_1+t_2)}{t_2}-1 \tag{3.36}$$

(and similarly for $\{u_i\}$) to create a series of terms of the form of eq. (3.33), with at most one α_i and at most one β_i non-zero. Furthermore, δ will have a fractional power that depends on ϵ, due to the presence of the factor $s_{12}^{-\epsilon}$ in eq. (3.32). As described in ref. [129], this integral can be carried out exactly in the centre of mass frame of the two final state gluons. We review this derivation in appendix 3.C.1.

The most difficult phase space integrals occur for terms of type (i) above, namely those in the soft region involving a hypergeometric function. All such terms involve the master integral

$$I_2(\alpha_1,\alpha_2,\beta_1,\beta_2,\gamma_1,\gamma_2,\delta)=\int d\Phi^{(3)}\, s_{12}^{\delta}\, t_1^{-\alpha_1}\, t_2^{-\alpha_2}\, u_1^{-\beta_1}\, u_2^{-\beta_2}(t_1+t_2)^{-\gamma_1}(u_1+u_2)^{-\gamma_2}$$
$$\times {}_2F_1\left(1,1;1-\epsilon;\frac{t_1}{t_1+t_2}\right), \tag{3.37}$$

and we note that similar integrals have been carried out for Higgs boson production in refs. [134, 145], whose methods proved very useful for the present study. We proceed as follows. We first apply identities similar to eq. (3.36) to put all terms in the form where at most one α_i and at most one β_i is non-zero, finding in all cases that $\alpha_2=0$. As we explain in appendix 3.C.2, for integrals with only (α_1,β_1) potentially non-zero, one may use the

centre of mass frame of the outgoing gluons to derive the analytic result

$$
\begin{aligned}
I_2(\alpha_1,0,\beta_1,0,\gamma_1,\gamma_2,\delta) &= 2^{1-2d}\,(-1)^{-\alpha_1-\beta_1-\gamma_1-\gamma_2}\,\pi^{1-d}\,s^{d-3+\delta-\alpha_1-\beta_1-\gamma_1-\gamma_2} \\
&\times \frac{\Gamma(d-2+\delta-\alpha_1-\gamma_1)\,\Gamma(d-2+\delta-\alpha_1-\beta_1)\,\Gamma(d/2-1+\delta)}{\Gamma(2d-4+2\delta-\alpha_1-\beta_1-\gamma_1-\gamma_2)\,\Gamma(d-2+\delta-\beta_1)\,\Gamma(d-2+\delta-\alpha_1)\,\Gamma(d-2-\alpha_1-\beta_1)} \\
&\times \frac{\Gamma(d/2-1-\beta_1)\,\Gamma(d/2-1-\alpha_1)\,\Gamma(d-2+\delta-\beta_1-\gamma_2)}{\Gamma(d/2-1)}\,(1-z)^{2d-5+2\delta-\alpha_1-\beta_1-\gamma_1-\gamma_2} \\
&\times {}_4F_3(1,1,d-2+\delta-\alpha_1-\beta_1,d/2-1-\alpha_1;d-2+\delta-\alpha_1,a+1,d-2-\alpha_1-\beta_1;1)+\ldots,
\end{aligned}
\tag{3.38}
$$

where the ellipsis denotes subleading powers of $(1-z)$. This exact expression is valid for arbitrary d, but can be easily expanded in ϵ using the HypExp package for the hypergeometric function [124, 125]. All necessary values of the parameters $\{\alpha_i,\beta_i,\gamma_i,\delta\}$ are collected in appendix 3.C.3, together with results for each integral, where for convenience we define

$$
\begin{aligned}
I_2(\alpha_1,\beta_1,\alpha_2,\beta_2,\gamma_1,\gamma_2,\delta) &= (4\pi)^{-3+2\epsilon}\,\mathrm{e}^{-2\epsilon\gamma_E}\,s^{d-3+\delta-C-\gamma_1-\gamma_2}\,(1-z)^{2d-5+2\delta-C-\gamma_1-\gamma_2} \\
&\times \hat{I}_2(\alpha_1,\beta_1,\alpha_2,\beta_2,\gamma_1,\gamma_2,\delta)+\ldots.
\end{aligned}
\tag{3.39}
$$

For integrals involving (α_1,β_2) non-zero, we were not able to find any comparable closed form expression. However, they can be evaluated using Mellin-Barnes techniques, and the *energies and angles* phase space parametrisation described in refs. [134, 145]. In this procedure one expands around $d=4$ at an intermediate stage, thus restricting the result to a Laurent series in ϵ, which still suffices for our purpose of calculating the K-factor. We describe this method in appendix 3.C.2, but note here that in order to apply it to integrals involving negative powers of γ_1 and/or γ_2, one must reexpress them in terms of other integrals, some involving more than two non-zero values of $(\alpha_1,\alpha_2,\beta_1,\beta_2)$. Results are collected in appendix 3.C.3, again using the notation of eq. (3.39). Also all aspects of the phase space integration have been carried out twice and completely independently, with full agreement.

3.4 Results

We now have all the necessary ingredients for assembling the abelian-like terms ($\sim C_F^3$) in the 2R1V contribution to the K-factor of eq. (3.2), in the $q\bar{q}$-channel up to NLP.[3] We will present separate results for the hard, (anti-)collinear and soft regions. In the normalisation of eq. (3.2), one finds for the hard region

$$
\begin{aligned}
K^{(3)}_{q\bar{q},\mathrm{H}}\Big|_{\mathrm{2R1V},\,C_F^3} &= 128 \\
&\times\left\{\frac{1}{\epsilon^5}(\mathscr{D}_0-1)+\frac{1}{\epsilon^4}\left(-4\mathscr{D}_1+\frac{3\mathscr{D}_0}{2}+4L-4\right)+\frac{1}{\epsilon^3}\left(8\mathscr{D}_2-6\mathscr{D}_1+\frac{(8-21\zeta_2)}{2}\mathscr{D}_0\right.\right.
\end{aligned}
$$

[3] We will present the unrenormalised K-factor, as in ref. [122].

$$-8L^2+16L-\frac{31}{4}+\frac{21}{2}\zeta_2\Big)+\frac{1}{\epsilon^2}\Big[-\frac{32\mathscr{D}_3}{3}+12\mathscr{D}_2+(-16+42\zeta_2)\mathscr{D}_1+\Big(8-\frac{63}{4}\zeta_2$$
$$-23\zeta_3\Big)\mathscr{D}_0+\frac{32}{3}L^3-32L^2+(31-42\zeta_2)L-18+42\zeta_2+23\zeta_3\Big]+\frac{1}{\epsilon}\Big[\frac{32}{3}\mathscr{D}_4-16\mathscr{D}_3$$
$$+(32-84\zeta_2)\mathscr{D}_2+(-32+63\zeta_2+92\zeta_3)\mathscr{D}_1+\Big(16-42\zeta_2-\frac{69}{2}\zeta_3+\frac{1017}{16}\zeta_4\Big)\mathscr{D}_0-\frac{32}{3}L^4$$
$$+\frac{128}{3}L^3+(-62+84\zeta_2)L^2+(72-168\zeta_2-92\zeta_3)L-36+\frac{651}{8}\zeta_2+92\zeta_3-\frac{1017}{16}\zeta_4\Big]$$
$$-\frac{128}{15}\mathscr{D}_5+16\mathscr{D}_4+\Big(-\frac{128}{3}+112\zeta_2\Big)\mathscr{D}_3+(64-126\zeta_2-184\zeta_3)\mathscr{D}_2+\Big(-64+168\zeta_2$$
$$+138\zeta_3-\frac{1017}{4}\zeta_4\Big)\mathscr{D}_1+\Big(32-84\zeta_2-92\zeta_3+\frac{3051}{32}\zeta_4-\frac{1053}{5}\zeta_5+\frac{483}{2}\zeta_3\zeta_2\Big)\mathscr{D}_0$$
$$+\frac{128}{15}L^5-\frac{128}{3}L^4+\Big(\frac{248}{3}-112\zeta_2\Big)L^3+(-144+336\zeta_2+184\zeta_3)L^2+\Big(144-\frac{651}{2}\zeta_2$$
$$-368\zeta_3+\frac{1017}{4}\zeta_4\Big)L\Big\}\,, \tag{3.40}$$

where, given the focus of our study, we report only logarithmically enhanced (non-constant) terms in the finite part. To keep the expressions compact, we abbreviate powers of the logarithm by $L^m\equiv\log^m(1-z)$, and denote plus distributions by $\mathscr{D}_m\equiv[\log^m(1-z)/(1-z)]_+$. In these expressions, we have neglected the delta function contributions that arise upon regulating the singular behaviour of the LP terms at $z=1$ using the identity

$$\frac{1}{(1-z)^{1+a\epsilon}}=-\frac{1}{a\epsilon}\delta(1-z)+\Big[\frac{1}{1-z}\Big]_+ +\sum_{n=1}^{\infty}\frac{(-a\epsilon)^n}{n!}\Big[\frac{\log^n(1-z)}{1-z}\Big]_+\,, \tag{3.41}$$

where the plus distribution $[g(z)]_+$ is defined through its effect on a smooth test function $f(z)$:

$$\int_0^1 dz\, f(z)\big[g(z)\big]_+ = \int_0^1 dz\big[f(z)-f(1)\big]g(z)\,. \tag{3.42}$$

The delta function terms mix with virtual corrections at the same perturbative order, which are not calculated here, and are thus not worth reporting. We have made the conventional choice $\bar{\mu}^2=4\pi e^{-\gamma_E}\mu^2=Q^2$ for the dimensional regularisation scale in the $\overline{\text{MS}}$ scheme. NLP terms are sensitive to this choice, given that the K-factor contains the dimensional combination

$$\left(\frac{\bar{\mu}^2}{s}\right)^{\epsilon}\to\left(\frac{Q^2}{s}\right)^{\epsilon}=z^{\epsilon}\,. \tag{3.43}$$

For the collinear region we find

$$K^{(3)}_{q\bar{q},\mathrm{C}}\Big|_{\mathrm{2R1V},C_F^3}=32\Big\{-\frac{1}{\epsilon^4}+\frac{1}{\epsilon^3}\Big(5L-\frac{5}{4}\Big)+\frac{1}{\epsilon^2}\Big(-\frac{3}{2}-\frac{25}{2}L^2+\frac{25}{4}L+\frac{21}{2}\zeta_2\Big)$$
$$+\frac{1}{\epsilon}\Big[\frac{125L^3}{6}-\frac{125L^2}{8}+\Big(\frac{15}{2}-\frac{105\zeta_2}{2}\Big)L-2+\frac{105}{8}\zeta_2+41\zeta_3\Big]-\frac{625}{24}L^4+\frac{625}{24}L^3$$
$$+\Big(-\frac{75}{4}+\frac{525\zeta_2}{4}\Big)L^2+\Big(10-\frac{525}{8}\zeta_2-205\zeta_3\Big)L\Big\}\,. \tag{3.44}$$

The anti-collinear region gives an identical contribution, reflecting the $p_1 \leftrightarrow p_2$ symmetry of the set of diagrams considered. Finally, we have the soft region, whose contribution is

$$K^{(3)}_{q\bar{q},\mathrm{S}}\Big|_{\mathrm{2R1V},C_F^3} = 32\left\{\frac{1}{\epsilon}\left(\frac{2}{3}\zeta_2+\frac{1}{3}\zeta_3\right)-(4\zeta_2+2\zeta_3)\,L\right\}. \tag{3.45}$$

The total result for the (unrenormalised) K-factor up to NLP in the threshold expansion can be obtained from the above results through the combination

$$K^{(3)}_{q\bar{q}}\Big|_{\mathrm{2R1V},C_F^3} = K^{(3)}_{q\bar{q},\mathrm{H}}\Big|_{\mathrm{2R1V},C_F^3} + 2K^{(3)}_{q\bar{q},\mathrm{C}}\Big|_{\mathrm{2R1V},C_F^3} + K^{(3)}_{q\bar{q},\mathrm{S}}\Big|_{\mathrm{2R1V},C_F^3}. \tag{3.46}$$

Equations (3.40), (3.44) and (3.45) constitute the main results of this chapter. As discussed above, our main motivation for deriving them is as a prerequisite for formulating and testing general prescriptions for classifying and potentially resumming NLP threshold corrections. We are not yet in the position to provide a full analysis in this regard, but we will make a few remarks on the implications of our results.

For the emission of a single soft gluon at the one-loop level, a factorisation formula that allowed for such a classification was proposed in refs. [79,81], as discussed in section 1.4. This study followed the detailed analysis of the DY 1R1V K-factor in the $q\bar{q}$-channel of ref. [122], and we hope that the data collected here on double-emission amplitudes may lead to new insights in a similar fashion. In this particular factorisation formula, a central role was played by the radiative jet function proposed in ref. [78], as its introduction was essential to accommodate NLP effects caused by the emission of a soft photon from a collinearly enhanced region. In chapter 2 we discussed at length that in the presence of multiple loop corrections, yet additional functions are needed to describe the amplitude at NLP accuracy from a factorisation point of view. In fact, we showed that the factorisation in terms of a standard radiative jet function as considered in eq. (1.25) is not quite sufficient to capture all NLP terms in the amplitude, even at the one-loop level. However, as the missed contribution vanishes upon contraction with the conjugate amplitude, this imperfection does not affect the factorisation of the K-factor and may be neglected for now.

Likewise, one might wonder if novel, more involved functions are needed for processes containing two or more additional gluons in the final state, or whether the functions appearing in the one-emission case are sufficient to capture all physics up to NLP in the threshold expansion. For example, one may consider generalising the radiative jet function to a family of quantities representing the dressing of a non-radiative jet with arbitrary numbers of additional gluons. For resummation of NLP effects to be possible, it should ideally be the case that these higher multiplicity radiative jet functions are related by an iterative property to those with lower numbers of emissions, or at least up to a particular logarithmic accuracy.

Insights into the iterative structure of our results can be obtained by examining the squared matrix elements in eqs. (3.29)–(3.32), before integration over the final state phase space, but after the integration over the loop momentum of the virtual gluon. In the case of the hard region (eq. (3.29)), we find that the coefficient f_1^{H} matches the similar function found

in the one-loop quark form factor. The LP term thus agrees with what one obtains from applying the well-known eikonal Feynman rules to the non-radiative one-loop DY process. Also at NLP the structure is clear: the first term in eq. (3.29b) receives contributions from the standard next-to-eikonal single emission vertex, as well as from the derivative term appearing in eq. (1.25), which describes a soft emission from within the hard loop. A similiar contribution appears, unsurprisingly, already in the 1R1V contributions at NNLO. The difference is in the presence of additional eikonal factors due to the second soft emission. The structure of the second term in eq. (3.29b) is understood in terms of an effective next-to-eikonal vertex

$$R^{\mu\nu}(p_i,k_1,k_2) = -\frac{p_i\cdot k_1\, p_i^\nu k_2^\mu + p_i\cdot k_2\, p_i^\mu k_1^\nu - p_i\cdot k_1\, p_i\cdot k_2\, \eta^{\mu\nu} - k_1\cdot k_2\, p_i^\mu p_i^\nu}{p_i\cdot(k_1+k_2)}\,, \tag{3.47}$$

describing the joint emission of two gluons, as discussed in refs. [41, 83]. Hence, there is strong evidence that the hard region can indeed be understood using existing tools.

At NNLO in DY production, it was noticed that the (anti-)collinear region in the method of regions calculation maps straightforwardly to the contribution of the radiative jet functions associated with the incoming (anti-)quark legs in the factorisation approach [79, 122]. At N^{3}LO we expect a similar mapping between these regions and radiative jet functions, but it is certainly less transparent. We find that the function f_1^{C} in the first line of eq. (3.31b) occurs already at NNLO, such that this contribution factorises into a one-loop radiative jet on the quark leg, dressed by a tree-level emission from the anti-quark (and vice versa for the anti-collinear region). The remaining collinear contributions, involving the additional coefficients $f_{2,3}^{\mathrm{C}}$, lack such a straightforward interpretation, leaving open the possibility that one must consider a separate radiative jet function for pairs of gluons.

Finally, there is the soft region tied to emissions from a soft quark, in line with our power counting analysis presented in chapter 2. As discussed above, its contribution starts at N^{3}LO, given the need for a virtual loop as well as two emission to set the associated scale. Hence, the region is not expected to be iteratively obtainable from lower order information.

The complex structure of the squared matrix elements poses a challenge for the eventual resummation of threshold logarithms at NLP in general, as increasingly more factorisation ingredients seem to contribute at higher orders in perturbation theory. The integrated results, however, offer a more optimistic perspective. Similar to what was observed at NNLO [79, 122], we note that contribution from the (anti-)collinear region does not contain the maximal number of poles in ϵ: the Laurent series starts only at $\mathcal{O}(\epsilon^{-4})$ rather than $\mathcal{O}(\epsilon^{-5})$. In addition to the fact that collinear effects are strictly NLP, they thus seem to give only subleading (NLL) threshold logarithms in the finite part. The soft (quark) region is even further suppressed in the ϵ expansion, such that it only contributes logarithmic terms at N^{4}LL level. If this behaviour persists at higher orders, such a region is unlikely to trouble realistic efforts to resum NLP effects.

Indeed, the only source of leading logarithmic effects, at both LP or NLP in the threshold expansion, is the hard region, as can be clearly seen in eq. (3.40). This observation will

certainly be a useful guide when examining the extent to which (multiple) jet emission functions are relevant at higher orders in perturbation theory. Furthermore, there is existing evidence (most notably in ref. [146]) that the highest power of the NLP logarithm exponentiates in DY. The observation that collinear effects do not affect this logarithm at $\mathrm{N^3LO}$ provides a significant hint regarding how to formally prove this property.

3.5 Conclusions

In this chapter, we examined abelian-like contributions to Drell-Yan production in the $q\bar{q}$-channel at $\mathrm{N^3LO}$, namely those with the colour structure $\sim C_F^3$. We have classified all logarithmically enhanced contributions near threshold when one gluon is virtual, and the other two real, up to NLP in the threshold variable $(1-z)$. Our motivation is to work towards a systematic classification of NLP threshold effects, for which detailed analytical data are indispensable. To this end, we presented results for the unrenormalised K-factor, using the method of regions [108–111] to separate contributions according to whether the virtual gluon is hard, soft or collinear with one of the incoming particles. Our hope is that this will aid in elucidating the general structure of NLP effects, similar to how previous methods of region analyses at NNLO [122] directly informed the construction of factorisation formulae beyond LP.

There are a number of noteworthy features in our result. Firstly, there is a non-zero soft region describing gluon emissions from a soft quark that appears for the first time at $\mathrm{N^3LO}$, and which we find persists upon integration over the final state phase space. The presence of such a contribution requires at least one virtual gluon and two real gluons, and thus does not appear to be iteratively relatable to lower order information. A similar region was found to be non-zero in the recent (and closely related) calculation of Higgs boson production via gluon-gluon fusion [145], whose methods prove very useful for the present analysis. The overall contribution of this region to the DY K-factor is highly subleading, in that it contributes with a single pole in the dimensional regularisation parameter ϵ at $\mathcal{O}(\alpha_s^3)$, corresponding to a $\mathrm{N^4LL}$ NLP logarithm in the finite part of the K-factor. It would be interesting to see what effect such a region has at higher orders in perturbation theory.

Both the hard and collinear regions in our analysis show signs of an iterative structure, whereby (parts of) the results can be obtained from lower order information. These observations will prove highly useful in generalising factorisation formulae for NLP effects to higher orders in perturbation theory. Unlike the hard region, the collinear region does not contribute to the leading NLP logarithm, suggesting that collinear effects are not relevant to the potential resummation of the highest power of NLP logs to all orders in perturbation theory. In the next chapter we shall follow up on this lead and find indeed that we can achieve resummation of the leading logarithmic contributions at NLP by considering the exponentiation of a next-to-soft function alone.

3.A Coefficients entering the matrix element

In this appendix, we collect results for the coefficients appearing in eqs. (3.29)–(3.32). Starting with the hard region, we have

$$\begin{aligned}
f_1^{\mathrm{H}} =& -\frac{2}{\epsilon^2}-\frac{3}{\epsilon}-8+\zeta_2+\epsilon\left(-16+\frac{3\zeta_2}{2}+\frac{14\zeta_3}{3}\right)+\epsilon^2\left(-32+4\zeta_2+7\zeta_3+\frac{47\zeta_4}{8}\right)\\
&+\epsilon^3\left(-64+8\zeta_2+\frac{56\zeta_3}{3}+\frac{141\zeta_4}{16}+\frac{62\zeta_5}{5}-\frac{7}{3}\zeta_3\zeta_2\right)+\epsilon^4\left(-128+16\zeta_2+\frac{112\zeta_3}{3}\right.\\
&\left.+\frac{47\zeta_4}{2}+\frac{93\zeta_5}{5}-\frac{7\zeta_2\zeta_3}{2}+\frac{949\zeta_6}{64}-\frac{49\zeta_3^2}{9}\right)+\mathcal{O}(\epsilon^5).
\end{aligned} \tag{3.48}$$

The coefficients for the (anti-)collinear regions are

$$\begin{aligned}
f_1^{\mathrm{C}} =& -\frac{2}{\epsilon}-\frac{5}{2}+\epsilon\left(-3+\zeta_2\right)+\epsilon^2\left(-4+\frac{5\zeta_2}{4}+\frac{14\zeta_3}{3}\right)+\epsilon^3\left(-6+\frac{3\zeta_2}{2}+\frac{35\zeta_3}{6}+\frac{47\zeta_4}{8}\right)\\
&+\epsilon^4\left(-10+2\zeta_2+7\zeta_3+\frac{235\zeta_4}{32}+\frac{62\zeta_5}{5}-\frac{7\zeta_2\zeta_3}{3}\right)+\mathcal{O}(\epsilon^5),\\
f_2^{\mathrm{C}} =& -\frac{1}{4\epsilon}+\frac{1}{8}+\epsilon\left(\frac{3}{4}+\frac{\zeta_2}{8}\right)+\epsilon^2\left(2-\frac{\zeta_2}{16}+\frac{7\zeta_3}{12}\right)+\epsilon^3\left(\frac{9}{2}-\frac{3\zeta_2}{8}-\frac{7\zeta_3}{24}+\frac{47\zeta_4}{64}\right)\\
&+\epsilon^4\left(\frac{19}{2}-\zeta_2-\frac{7\zeta_3}{4}-\frac{47\zeta_4}{128}+\frac{31\zeta_5}{20}-\frac{7\zeta_2\zeta_3}{24}\right)+\mathcal{O}(\epsilon^5),\\
f_3^{\mathrm{C}} =& \frac{1}{4\epsilon^2}-\frac{1}{8\epsilon}-\frac{3}{4}-\frac{\zeta_2}{8}+\epsilon\left(-2+\frac{\zeta_2}{16}-\frac{7\zeta_3}{12}\right)+\epsilon^2\left(-\frac{9}{2}+\frac{3\zeta_2}{8}+\frac{7\zeta_3}{24}-\frac{47\zeta_4}{64}\right)\\
&+\epsilon^3\left(-\frac{19}{2}+\zeta_2+\frac{7\zeta_3}{4}+\frac{47\zeta_4}{128}-\frac{31\zeta_5}{20}+\frac{7}{24}\zeta_2\zeta_3\right)+\epsilon^4\left(-\frac{39}{2}+\frac{9\zeta_2}{4}+\frac{14\zeta_3}{3}+\frac{141\zeta_4}{64}\right.\\
&\left.+\frac{31\zeta_5}{40}-\frac{7\zeta_2\zeta_3}{48}-\frac{949\zeta_6}{512}+\frac{49\zeta_3^2}{72}\right)+\mathcal{O}(\epsilon^5).
\end{aligned} \tag{3.49}$$

For the soft region, we have

$$\begin{aligned}
f_1^{\mathrm{S}} =& \frac{1}{4\epsilon^2}+\frac{1}{4\epsilon}+\frac{1}{2}-\frac{\zeta_2}{8}+\epsilon\left(1-\frac{\zeta_2}{8}-\frac{7\zeta_3}{12}\right)+\epsilon^2\left(2-\frac{\zeta_2}{4}-\frac{7\zeta_3}{12}-\frac{47\zeta_4}{64}\right)\\
&+\epsilon^3\left(4-\frac{\zeta_2}{2}-\frac{7\zeta_3}{6}-\frac{47\zeta_4}{64}-\frac{31\zeta_5}{20}+\frac{7\zeta_2\zeta_3}{24}\right)\\
&+\epsilon^4\left(8-\zeta_2-\frac{7\zeta_3}{3}-\frac{47\zeta_4}{32}-\frac{31\zeta_5}{20}+\frac{7\zeta_2\zeta_3}{24}-\frac{949\zeta_6}{512}+\frac{49\zeta_3^2}{72}\right)+\mathcal{O}(\epsilon^5),\\
f_2^{\mathrm{S}} =& \frac{1}{4\epsilon}+\frac{1}{2}+\epsilon\left(1-\frac{\zeta_2}{8}\right)+\epsilon^2\left(2-\frac{\zeta_2}{4}-\frac{7\zeta_3}{12}\right)+\epsilon^3\left(4-\frac{\zeta_2}{2}-\frac{7\zeta_3}{6}-\frac{47\zeta_4}{64}\right)\\
&+\epsilon^4\left(8-\zeta_2-\frac{7\zeta_3}{3}-\frac{47\zeta_4}{32}-\frac{31\zeta_5}{20}+\frac{7\zeta_2\zeta_3}{24}\right)+\mathcal{O}(\epsilon^5),\\
f_3^{\mathrm{S}} =& \frac{1}{4\epsilon}+\frac{1}{4}+\epsilon\left(\frac{1}{2}-\frac{\zeta_2}{8}\right)+\epsilon^2\left(1-\frac{\zeta_2}{8}-\frac{7\zeta_3}{12}\right)+\epsilon^3\left(2-\frac{\zeta_2}{4}-\frac{7\zeta_3}{12}-\frac{47\zeta_4}{64}\right)\\
&+\epsilon^4\left(4-\frac{\zeta_2}{2}-\frac{7\zeta_3}{6}-\frac{47\zeta_4}{64}-\frac{31\zeta_5}{20}+\frac{7\zeta_2\zeta_3}{24}\right)+\mathcal{O}(\epsilon^5).
\end{aligned} \tag{3.50}$$

3.B Phase space integrals in the hard and (anti-)collinear regions

In this appendix, we spell out the derivation of eq. (3.34), using the Sudakov decomposition of eq. (3.5). The three-body phase space in d dimensions is given by

$$\int d\Phi^{(3)} = \int \frac{d^d q}{(2\pi)^{d-1}}\,\delta_+(q^2-Q^2)\left[\prod_{i=1}^{2}\int \frac{d^d k_i}{(2\pi)^{d-1}}\,\delta_+(k_i^2)\right](2\pi)^d\,\delta^{(d)}\left(q+\sum_{j=1}^{2}k_j-p_1-p_2\right), \tag{3.51}$$

where

$$\delta_+(k^2) = \theta(k^0)\,\delta(k^2) \tag{3.52}$$

and θ is the Heaviside function

$$\theta(k^0) = \begin{cases} k^0 & \text{for } k^0 > 0 \\ 0 & \text{for } k^0 \leq 0 \end{cases}. \tag{3.53}$$

We may carry out the integral over the photon momentum q using the delta function in eq. (3.51), obtaining

$$\begin{aligned}\int d\Phi^{(3)} &= (2\pi)^{3-2d}\left[\prod_{i=1}^{2}\int d^d k_i\,\delta_+(k_i^2)\right]\delta\left((p_1+p_2-k_1-k_2)^2-Q^2\right)\\ &= (2\pi)^{3-2d}\left[\prod_{i=1}^{2}\int dk_i^+\,dk_i^-\,d^{d-2}\boldsymbol{k}_{i\perp}\,\delta_+(k_i^2)\right]\\ &\quad\times\delta\left((1-z)s-2(k_1+k_2)\cdot(p_1+p_2)+2k_1\cdot k_2\right),\end{aligned} \tag{3.54}$$

where in the second line we have used $z = Q^2/s$. The delta function in the last line can be expressed as a Fourier transform

$$\begin{aligned}&\delta\left((1-z)s-2(k_1+k_2)\cdot(p_1+p_2)+2k_1\cdot k_2\right)\\ &\qquad=\frac{1}{s}\int_{-\infty}^{\infty}\frac{d\omega}{2\pi}\,\mathrm{e}^{i\omega(1-z)}\,\mathrm{e}^{\frac{-2i\omega}{s}(k_1\cdot p_1+k_2\cdot p_1+k_1\cdot p_2+k_2\cdot p_2)}\,\mathrm{e}^{\frac{2i\omega}{s}k_1\cdot k_2},\end{aligned} \tag{3.55}$$

where we can Taylor expand the exponential in $k_1\cdot k_2$, given that higher order terms will be suppressed by further powers of $(1-z)$

$$\mathrm{e}^{\frac{2i\omega}{s}k_1\cdot k_2} = 1+\frac{2i\omega}{s}k_1\cdot k_2+\mathcal{O}(k_i^4). \tag{3.56}$$

Putting things together, the phase space becomes

$$\int d\Phi^{(3)} = \frac{(2\pi)^{3-2d}}{s}\left[\prod_{i=1}^{2}\frac{1}{2}\int_0^\infty dk_i^+\int_0^\infty dk_i^-\int d\Omega_{d-2}\int_0^\infty d\boldsymbol{k}_{i\perp}^2\left(\boldsymbol{k}_{i\perp}^2\right)^{\frac{d-4}{2}}\,\delta(2k_i^+k_i^--\boldsymbol{k}_{i\perp}^2)\right]$$

$$\times \int_{-i\infty}^{i\infty} \frac{d\tilde{\omega}}{2\pi i} \mathrm{e}^{\tilde{\omega}(1-z)} \mathrm{e}^{-\tilde{\omega}\sqrt{2/s}\sum_{j=1}^{2}(k_j^+ + k_j^-)} \left[1 + \frac{2\tilde{\omega}}{s}\left(k_1^+ k_2^- + k_1^- k_2^+ - \boldsymbol{k}_{1\perp}\cdot\boldsymbol{k}_{2\perp}\right)\right]. \tag{3.57}$$

Here we have absorbed the θ functions from the factors $\delta_+(k_i^2)$ into the integration limits for $k_i^\pm$, and used polar coordinates for the $d-2$ dimensional $\boldsymbol{k}_{i\perp}$ integrals. In addition, we have transformed $\tilde{\omega} = i\omega$. We can now use this result to carry out the integral of eq. (3.33) for the two special cases of $\delta \in \{0, 1\}$.

For $\delta = 0$, we may note that the integrand of eq. (3.33) has no transverse momentum dependence, such that the linear term $\boldsymbol{k}_{1\perp}\cdot\boldsymbol{k}_{2\perp}$ in eq. (3.57) leads to an odd integrand, and can be neglected. The on-shell delta functions can then be used eliminate the integral over $\boldsymbol{k}_{i\perp}^2$, such that eq. (3.33) becomes

$$\begin{aligned} I_1(\alpha_1,\alpha_2,\beta_1,\beta_2,\gamma_1,\gamma_2,0) = {} & \frac{(-1)^{C+\gamma_1+\gamma_2}\, 2^{-d-3-\frac{1}{2}(C+\gamma_1+\gamma_2)}\, \pi^{3-2d}}{s^{1+\frac{1}{2}(C+\gamma_1+\gamma_2)}}\, \Omega_{d-2}^2 \int_{-i\infty}^{i\infty} \frac{d\tilde{\omega}}{2\pi i}\, \mathrm{e}^{\tilde{\omega}(1-z)} \\ & \times \int_0^\infty dk_1^+\, \mathrm{e}^{-\tilde{\omega}\sqrt{\frac{2}{s}}k_1^+} \left(k_1^+\right)^{\frac{d-4}{2}-\beta_1} \int_0^\infty dk_2^+\, \mathrm{e}^{-\tilde{\omega}\sqrt{\frac{2}{s}}k_2^+} \left(k_2^+\right)^{\frac{d-4}{2}-\beta_2} \left(\frac{1}{k_1^+ + k_2^+}\right)^{\gamma_2} \\ & \times \int_0^\infty dk_1^-\, \mathrm{e}^{-\tilde{\omega}\sqrt{\frac{2}{s}}k_1^-} \left(k_1^-\right)^{\frac{d-4}{2}-\alpha_1} \int_0^\infty dk_2^-\, \mathrm{e}^{-\tilde{\omega}\sqrt{\frac{2}{s}}k_2^-} \left(k_2^-\right)^{\frac{d-4}{2}-\alpha_2} \left(\frac{1}{k_1^- + k_2^-}\right)^{\gamma_1} \\ & \times \left(1 + \frac{2\tilde{\omega}}{s}\left(k_1^+ k_2^- + k_1^- k_2^+\right)\right). \end{aligned} \tag{3.58}$$

After a variable change $\tilde{k}_i^\pm = \tilde{\omega}\sqrt{\frac{2}{s}}\, k_i^\pm$, we may recognise the inverse Laplace transform

$$\int_{-i\infty}^{i\infty} \frac{d\tilde{\omega}}{2\pi i}\, \mathrm{e}^{\tilde{\omega}(1-z)} \left(\frac{1}{\tilde{\omega}}\right)^m = \frac{(1-z)^{m-1}}{\Gamma(m)}. \tag{3.59}$$

The integrals over $\tilde{k}_i^\pm$ will be of the form:

$$\int_0^\infty d\tilde{k}_1^\pm\, \mathrm{e}^{-\tilde{k}_1^\pm} \left(\tilde{k}_1^\pm\right)^m \int_0^\infty d\tilde{k}_2^\pm\, \mathrm{e}^{-\tilde{k}_2^\pm} \left(\tilde{k}_2^\pm\right)^n \left(\frac{1}{\tilde{k}_1^\pm + \tilde{k}_2^\pm}\right)^l, \tag{3.60}$$

for which the variable transformation $\tilde{k}_1^\pm = v\, w$ and $\tilde{k}_2^\pm = v\,(1-w)$ yields

$$\int_0^1 dw\, w^m\, (1-w)^n \int_0^\infty dv\; e^{-v}\, v^{m+n+1-l} = \frac{\Gamma(m+1)\,\Gamma(n+1)}{\Gamma(m+n+2)}\, \Gamma(m+n-l+2). \tag{3.61}$$

Substituting these results, we obtain eqs. (3.34a) and (3.34b) as required.

The integral of eq. (3.33) with $\delta = 1$ appears only at NLP level, such that we may entirely neglect the term $k_1 \cdot k_2$ in eq. (3.56), as it will lead to terms suppressed by further powers of $(1-z)$. Carrying out similar steps to the $\delta = 0$ case, one finds eq. (3.34c).

3.C Phase space integrals in the soft region

In this appendix, we describe various integrals (of increasing complexity) that occur when integrating the squared matrix element in the soft region, eq. (3.32), over the final state phase space.

3.C.1 Integrands with no hypergeometric function

First, we need integrals of the form of eq. (3.33), in which at most one parameter α_i and at most one parameter β_i is non-zero. The Sudakov decomposition of appendix 3.B is, unfortunately, not helpful here, due to the fractional power of δ. Instead, one may simplify the calculation by working in the centre of mass frame of the two outgoing gluons [129]. In this frame, one writes in $d = 4-2\epsilon$ space-time dimensions

$$\begin{aligned}
k_1 &= \frac{\sqrt{s_{12}}}{2}(1,0,\ldots,\sin\theta_2\sin\theta_1,\cos\theta_2\sin\theta_1,\cos\theta_1)\,,\\
k_2 &= \frac{\sqrt{s_{12}}}{2}(1,0,\ldots,-\sin\theta_2\sin\theta_1,-\cos\theta_2\sin\theta_1,-\cos\theta_1)\,,\\
p_1 &= \frac{(s-\tilde{t})}{2\sqrt{s_{12}}}(1,0,\ldots,0,1)\,,\\
p_2 &= \left(\frac{\tilde{t}+s_{12}-Q^2}{2\sqrt{s_{12}}},0,\ldots,0,|\boldsymbol{q}|\sin\psi\,,|\boldsymbol{q}|\cos\psi-\frac{(s-\tilde{t})}{2\sqrt{s_{12}}}\right),\\
Q &= \left(\frac{s-Q^2-s_{12}}{2\sqrt{s_{12}}},0,\ldots,0,|\boldsymbol{q}|\sin\psi,|\boldsymbol{q}|\cos\psi\right),
\end{aligned}$$

where θ_1 denotes the angle between the parton (spatial) momenta $\boldsymbol{p}_1$ and $\boldsymbol{k}_1$, while θ_2 rotates $\boldsymbol{k}_1$ in the plane orthogonal to $\boldsymbol{p}_1$. Furthermore, ψ can be identified as the angle between $\boldsymbol{p}_1$ and the off-shell photon momentum $\boldsymbol{q}$, which is fixed by momentum conservation, as is the length of the latter vector:

$$\begin{aligned}
\cos\psi &= \frac{(s-Q^2)(\tilde{u}-Q^2)-s_{12}(\tilde{t}+Q^2)}{(s-\tilde{t})\sqrt{\lambda(s,Q^2,s_{12})}}\,,\\
|\boldsymbol{q}| &= \frac{\sqrt{\lambda(s,Q^2,s_{12})}}{2\sqrt{s_{12}}}\,,
\end{aligned}\tag{3.62}$$

where λ is the Källen function $\lambda(a,b,c) = a^2+b^2+c^2-2ab-2ac-2bc$. In addition, we have defined the Mandelstam variables

$$\begin{aligned}
\tilde{t} \equiv 2p_1\cdot Q &= (p_1+Q)^2-Q^2\,,\\
\tilde{u} \equiv 2p_2\cdot Q &= (p_2+Q)^2-Q^2\,,\\
s_{12} \equiv 2k_1\cdot k_2 &= s-\tilde{t}-\tilde{u}+Q^2\,.
\end{aligned}\tag{3.63}$$

The invariants $\tilde{t}$ and $\tilde{u}$ can in turn be expressed as functions of the photon energy fraction $z = Q^2/s$ and of two further variables $0 \le x \le 1$ and $0 \le y \le 1$, such that

$$\begin{aligned}\tilde{u} &= s\,[1-y\,(1-z)]\,,\\ \tilde{t} &= s\left[z + y(1-z) - \frac{y\,(1-y)\,x\,(1-z)^2}{1-y\,(1-z)}\right],\end{aligned} \tag{3.64}$$

where $(1-z)$ is the threshold variable. The three-body phase space in d dimensions eventually takes the form

$$\begin{aligned}\int d\Phi^{(3)} = \frac{1}{(4\pi)^d}\frac{s^{d-3}}{\Gamma(d-3)}(1-z)^{2d-5}\int_0^\pi d\theta_1 \int_0^\pi d\theta_2\,(\sin\theta_1)^{d-3}\,(\sin\theta_2)^{d-4}\\ \times \int_0^1 dy \int_0^1 dx\,[x(1-x)]^{d/2-2}\,[y(1-y)]^{d-3}\,[1-y(1-z)]^{1-d/2}\,.\end{aligned} \tag{3.65}$$

In terms of the above definitions, one finds

$$\begin{aligned} p_1\cdot k_1 &= \frac{s-\tilde{t}}{4}(1-\cos\theta_1)\,, & p_2\cdot k_1 &= A - B\cos\theta_1 - C\sin\theta_1\cos\theta_2\,,\\ p_1\cdot k_2 &= \frac{s-\tilde{t}}{4}(1+\cos\theta_1)\,, & p_2\cdot k_2 &= A + B\cos\theta_1 + C\sin\theta_1\cos\theta_2\,, \end{aligned} \tag{3.66}$$

where

$$A = \frac{\tilde{t}+s_{12}-Q^2}{4}\,, \qquad B = \frac{\sqrt{s_{12}}}{2}|\boldsymbol{q}|\cos\psi - \frac{(s-\tilde{t})}{4}\,, \qquad C = \frac{\sqrt{s_{12}}}{2}|\boldsymbol{q}|\sin\psi\,. \tag{3.67}$$

These quantities satisfy the relation $A^2 = B^2 + C^2$, allowing us to introduce the following notation

$$\cos\chi = \frac{B}{A} \qquad \text{and} \qquad \sin\chi = \frac{C}{A}\,. \tag{3.68}$$

We are now in the position to carry out the angular part of the phase space integral. For an integrand proportional to $(p_1\cdot k_1)^{-\alpha_1}\,(p_2\cdot k_1)^{-\beta_1}$, one finds [129] (first derived in ref. [147])

$$\begin{aligned}&\int_0^\pi d\theta_1 \int_0^\pi d\theta_2\,\frac{\sin^{d-3}\theta_1\,\sin^{d-4}\theta_2}{(1-\cos\theta_1)^{\alpha_1}(1-\cos\chi\cos\theta_1-\sin\chi\sin\theta_1\cos\theta_2)^{\beta_1}}\\ &= 2^{1-\alpha_1-\beta_1}\pi\,\frac{\Gamma(\frac{d}{2}-1-\alpha_1)\,\Gamma(\frac{d}{2}-1-\beta_1)}{\Gamma(d-2-\alpha_1-\beta_1)}\,\frac{\Gamma(d-3)}{\Gamma^2(\frac{d}{2}-1)}\,{}_2F_1\!\left(\alpha_1,\beta_1;\frac{d}{2}-1;\frac{1+\cos\chi}{2}\right).\end{aligned} \tag{3.69}$$

Results for other combinations of one non-zero α_i and β_i, are easily obtained from the above result by changing variables $\theta_{1,2} \to \pi-\theta_{1,2}$ and/or $\{\cos\chi, \sin\chi\} \to \{-\cos\chi, -\sin\chi\}$. Subsequently, one must carry out the integrals over the variables x and y appearing in eq. (3.65). These can all be carried out in terms of beta functions, or using the identity

$$\int_0^1 dx\,x^{\alpha-1}(1-x)^{\beta-1}\,{}_2F_1(a,b;c;zx) = \frac{\Gamma(\alpha)\,\Gamma(\beta)}{\Gamma(\alpha+\beta)}\,{}_3F_2(a,b,\alpha;c,\alpha+\beta;z)\,. \tag{3.70}$$

We stress that these results suffice for any value of δ in eq. (3.33). In terms of x and y, one has

$$s_{12}^{\delta} = s^{\delta}\,(1-z)^{2\delta}\,x^{\delta}\,[y(1-y)]^{\delta}\,[1-y(1-z)]^{-\delta}\,, \tag{3.71}$$

such that s_{12}^{δ} will merely alter the powers of those factors already present in the second line of eq. (3.65), without introducing new terms that might complicate the analytical structure.

3.C.2 Integrands with a hypergeometric function

Next, we must consider phase space integrals such as those of eq. (3.37), where the integrand contains a hypergeometric function. As is the case for the similar integrals in refs. [134, 145], we have not found it possible to obtain a useful closed form analytic result for arbitrary values of the parameters. However, for a certain subclass of the parameters, we can indeed find such a result, valid for any d. We shall present this case first.

The case $\alpha_2 = \beta_2 = 0$

If α_2 and β_2 are both zero, eq. (3.37) reduces to

$$I_2(\alpha_1, 0, \beta_1, 0, \gamma_1, \gamma_2, \delta) = (-2)^{-\alpha_1-\beta_1-\gamma_1-\gamma_2}\, I(\alpha_1, \beta_1, \gamma_1, \gamma_2, -\epsilon, 4-2\epsilon)\,, \tag{3.72}$$

where

$$\begin{aligned} I(\alpha_1, \beta_1, \gamma_1, \gamma_2, \delta, a, d) = \int d\Phi^{(3)} (p_1\cdot k_1)^{-\alpha_1} (p_2\cdot k_1)^{-\beta_1} (p_1\cdot k_1 + p_1\cdot k_2)^{-\gamma_1} (p_2\cdot k_1 + p_2\cdot k_2)^{-\gamma_2} \\ \times (2k_1\cdot k_2)^{\delta}\, {}_2F_1\left(1, 1; a+1; \frac{p_1\cdot k_1}{p_1\cdot k_1 + p_1\cdot k_2}\right). \end{aligned} \tag{3.73}$$

In the centre of mass frame of the two final state gluons (see section 3.C.1), this becomes

$$\begin{aligned} I(\alpha_1, \beta_1, \gamma_1, \gamma_2, \delta, a, d) = 2^{2\alpha_1+\gamma_1-\gamma_2} \int d\Phi^{(3)}\, s_{12}^{\delta}\, (s-\tilde{t})^{-\alpha_1-\gamma_1} A^{-\beta_1-\gamma_2} (1-\cos\theta_1)^{-\alpha_1} \\ \times (1-\cos\chi\cos\theta_1 - \sin\chi\sin\theta_1\cos\theta_2)^{-\beta_1}\, {}_2F_1\left(1, 1; a+1; \frac{1-\cos\theta_1}{2}\right). \end{aligned} \tag{3.74}$$

Next, one can use the Mellin-Barnes representation for the hypergeometric function

$$\begin{aligned} {}_pF_Q(a_1, \ldots, a_P; b_1, \ldots, b_Q; x) = \int_{-i\infty}^{i\infty} \frac{dw}{2\pi i}\, (-x)^w\, \Gamma(-w) \\ \times \left[\prod_{i=1}^{P} \frac{\Gamma(a_i + w)}{\Gamma(a_i)}\right] \left[\prod_{j=1}^{Q} \frac{\Gamma(b_i)}{\Gamma(b_i + w)}\right], \end{aligned} \tag{3.75}$$

such that eq. (3.74) becomes

$$I(\alpha_1,\beta_1,\gamma_1,\gamma_2,\delta,a,d) = 2^{2\alpha_1+\gamma_1-\gamma_2}\int d\Phi^{(3)} s_{12}^{\delta}(s-\tilde{t})^{-\alpha_1-\gamma_1}A^{-\beta_1-\gamma_2}\,\Gamma(1+a)$$
$$\times\int_{-i\infty}^{i\infty}\frac{dw_1}{2\pi i}(-1)^{w_1}2^{-w_1}\frac{\Gamma^2(1+w_1)\,\Gamma(-w_1)}{\Gamma(1+a+w_1)}(1-\cos\theta_1)^{-(\alpha_1-w_1)}$$
$$\times(1-\cos\chi\cos\theta_1-\sin\chi\sin\theta_1\cos\theta_2)^{-\beta_1}\,. \tag{3.76}$$

The angular integrals can be carried out using eq. (3.69), to get

$$I(\alpha_1,\beta_1,\gamma_1,\gamma_2,\delta,a,d) = 2^{1-2d+\alpha_1-\beta_1+\gamma_1-\gamma_2}\,\pi^{1-d}\,s^{d-3}(1-z)^{2d-5}\,\frac{\Gamma(1+a)\,\Gamma(d/2-1-\beta_1)}{\Gamma^2(d/2-1)}$$
$$\times\int_0^1 dy\int_0^1 dx\,[x(1-x)]^{d/2-2}\,[y(1-y)]^{d-3}\,[1-y(1-z)]^{1-d/2}\,s_{12}^{\delta}(s-\tilde{t})^{-\alpha_1-\gamma_1}A^{-\beta_1-\gamma_2}$$
$$\times\int_{-i\infty}^{i\infty}\frac{dw_1}{2\pi i}(-1)^{w_1}\frac{\Gamma^2(1+w_1)\,\Gamma(d/2-1-\alpha_1+w_1)\,\Gamma(-w_1)}{\Gamma(1+a+w_1)\,\Gamma(d-2-\alpha_1-\beta_1+w_1)}$$
$$\times\,{}_2F_1\left(\alpha_1-w_1,\,\beta_1;\,\frac{d}{2}-1;\,\frac{1+\cos\chi}{2}\right). \tag{3.77}$$

At this point, we may expand the integrand in $(1-z)$, taking the leading power only.[4] After some work, we end up with

$$I(\alpha_1,\beta_1,\gamma_1,\gamma_2,\delta,a,d) = 2^{1-2d+\alpha_1+\beta_1+\gamma_1+\gamma_2}\,\pi^{1-d}\,s^{d-3+\delta-\alpha_1-\beta_1-\gamma_1-\gamma_2}(1-z)^{2d-5+2\delta-\alpha_1-\beta_1-\gamma_1-\gamma_2}$$
$$\times\frac{\Gamma(1+a)\,\Gamma(d/2-1-\beta_1)}{\Gamma^2(d/2-1)}\int_0^1 dy\,y^{d-3+\delta-\beta_1-\gamma_2}(1-y)^{d-3+\delta+\alpha_1-\gamma_1}$$
$$\times\int_{-i\infty}^{i\infty}\frac{dw_1}{2\pi i}(-1)^{w_1}\,\frac{\Gamma^2(1+w_1)\,\Gamma(d/2-1-\alpha_1+w_1)\,\Gamma(-w_1)}{\Gamma(1+a+w_1)\,\Gamma(d-2-\alpha_1-\beta_1+w_1)}$$
$$\times\int_0^1 dx\,x^{d/2-2+\delta}(1-x)^{d/2-2}\,{}_2F_1\left(\alpha_1-w_1,\,\beta_1;\,\frac{d}{2}-1;\,1-x\right). \tag{3.78}$$

The y integral can be carried out immediately in terms of Gamma functions. The x integral would give a ${}_3F_2$, but then the remaining Mellin-Barnes integral could be cumbersome. Instead, we can introduce a second Mellin-Barnes representation, after which the x integral can be carried out in terms of Gamma functions, yielding

$$I(\alpha_1,\beta_1,\gamma_1,\gamma_2,\delta,a,d) = 2^{1-2d+\alpha_1+\beta_1+\gamma_1+\gamma_2}\,\pi^{1-d}\,s^{d-3+\delta-\alpha_1-\beta_1-\gamma_1-\gamma_2}(1-z)^{2d-5+2\delta-\alpha_1-\beta_1-\gamma_1-\gamma_2}$$
$$\times\frac{\Gamma(d/2-1-\beta_1)\,\Gamma(d-2+\delta-\beta_1-\gamma_2)\,\Gamma(d-2+\delta-\alpha_1-\gamma_1)\,\Gamma(d/2-1+\delta)}{\Gamma(d/2-1)\,\Gamma(2d-4+2\delta-\alpha_1-\beta_1-\gamma_1-\gamma_2)\,\Gamma(\beta_1)}$$
$$\times\,\Gamma(1+a)\int_{-i\infty}^{i\infty}\frac{dw_1}{2\pi i}\int_{-i\infty}^{i\infty}\frac{dw_2}{2\pi i}(-1)^{w_1+w_2}$$

[4] Note that the hypergeometric function depends on z through $\cos\chi$, such that it needs to be expanded in $(1-z)$ as well.

$$\times \frac{\Gamma^2(1+w_1)\,\Gamma(d/2-1-\alpha_1+w_1)\,\Gamma(-w_1)\,\Gamma(\alpha_1-w_1+w_2)\,\Gamma(\beta_1+w_2)\,\Gamma(-w_2)}{\Gamma(\alpha_1-w_1)\,\Gamma(1+a+w_1)\,\Gamma(d-2-\alpha_1-\beta_1+w_1)\,\Gamma(d-2+\delta+w_2)}\,. \tag{3.79}$$

We must now carry out the double Mellin-Barnes integral. This can be done straightforwardly, by recognising the w_2 integral as

$$\begin{aligned}\int_{-i\infty}^{i\infty}\frac{dw_2}{2\pi i}(-1)^{w_2}\,&\frac{\Gamma(\alpha_1-w_1+w_2)\,\Gamma(\beta_1+w_2)\,\Gamma(-w_2)}{\Gamma(d-2+\delta-w_2)}\\ &=\frac{\Gamma(\alpha_1-w_1)\,\Gamma(\beta_1)}{\Gamma(d-2+\delta)}\,{}_2F_1(\alpha_1-w_1,\,\beta_1;\,d-2+\delta;\,1)\\ &=\frac{\Gamma(d-2+\delta)\,\Gamma(d-2+\delta-\alpha_1-\beta_1+w_1)}{\Gamma(d-2+\delta-\alpha_1+w_1)\,\Gamma(d-2+\delta-\beta_1)}\,,\end{aligned} \tag{3.80}$$

where we have used Gauss' identity

$${}_2F_1(a,b;c;1)=\frac{\Gamma(c)\,\Gamma(c-a-b)}{\Gamma(c-a)\,\Gamma(c-b)}\,. \tag{3.81}$$

At this stage we are left with

$$\begin{aligned}I(\alpha_1,\beta_1,\gamma_1,\gamma_2,\delta,a,d)&=2^{1-2d+\alpha_1+\beta_1+\gamma_1+\gamma_2}\,\pi^{1-d}s^{d-3+\delta-\alpha_1-\beta_1-\gamma_1-\gamma_2}(1-z)^{2d-5+2\delta-\alpha_1-\beta_1-\gamma_1-\gamma_2}\\ &\times\frac{\Gamma(d/2-1-\beta-1)\,\Gamma(d-2+\delta-\beta_1-\gamma_2)\,\Gamma(d-2+\delta-\alpha_1-\gamma_1)\,\Gamma(d/2-1+\delta)}{\Gamma(d/2-1)\,\Gamma(2d-4+2\delta-\alpha_1-\beta_1-\gamma_1-\gamma_2)\,\Gamma(d-2+\delta-\beta_1)}\\ &\times\int_{-i\infty}^{i\infty}\frac{dw_1}{2\pi i}(-1)^{w_1}\frac{\Gamma^2(1+w_1)\,\Gamma(d-2+\delta-\alpha_1-\beta_1+w_1)\,\Gamma(d/2-1-\alpha_1+w_1)\,\Gamma(-w_1)}{\Gamma(d-2+\delta-\alpha_1+w_1)\,\Gamma(1+a+w_1)\,\Gamma(d-2-\alpha_1-\beta_1+w_1)}\,.\end{aligned} \tag{3.82}$$

Using eq. (3.75) we can recognise the w_1 integral as

$$\begin{aligned}&\int_{-i\infty}^{i\infty}\frac{dw_1}{2\pi i}(-1)^{w_1}\frac{\Gamma^2(1+w_1)\,\Gamma(d-2+\delta-\alpha_1-\beta_1+w_1)\,\Gamma(d/2-1-\alpha_1+w_1)\,\Gamma(-w_1)}{\Gamma(d-2+\delta-\alpha_1+w_1)\,\Gamma(1+a+w_1)\,\Gamma(d-2-\alpha_1-\beta_1+w_1)}\\ &=\frac{\Gamma(d-2+\delta-\alpha_1-\beta_1)\,\Gamma(d/2-1-\alpha_1)}{\Gamma(d-2+\delta-\alpha_1)\,\Gamma(1+a)\,\Gamma(d-2-\alpha_1-\beta_1)}\\ &\quad\times{}_4F_3\left(1,\,1,\,d-2+\delta-\alpha_1-\beta_1,\,\frac{d}{2}-1-\alpha_1;\,d-2+\delta-\alpha_1,\,1+a,\,d-2-\alpha_1-\beta_1;\,1\right).\end{aligned} \tag{3.83}$$

Putting everything together, we obtain the result of eq. (3.38).

General parameter values

As stated above, for other necessary values of the parameters, we are not able to find a closed form solution for the integral of eq. (3.37), valid for any spacetime dimension d. Instead, we settle for an expansion in the dimensional regularisation parameter ϵ. To this end, it is useful to use an alternative phase space parametrisation, as discussed in refs. [134, 145].

We first write eq. (3.37) as

$$I_2(\alpha_1,\alpha_2,\beta_1,\beta_2,\gamma_1,\gamma_2,\delta) = (-2)^{-C} J(\alpha_1,\alpha_2,\beta_1,\beta_2,\gamma_1,\gamma_2,\delta,-\epsilon,d), \tag{3.84}$$

where we have redefined C to encompass the γ_i as well, i.e. $C = \sum_{i=1}^{2}(\alpha_i+\beta_i+\gamma_i)$, while

$$\begin{aligned} J(\alpha_1,\alpha_2,\beta_1,\beta_2,\gamma_1,\gamma_2,\delta,a,d) = \int d\Phi^{(3)} (2k_1\cdot k_2)^{\delta} (p_1\cdot k_1)^{-\alpha_1}(p_1\cdot k_2)^{-\alpha_2}(p_2\cdot k_1)^{-\beta_1}(p_2\cdot k_2)^{-\beta_2} \\ \times (p_1\cdot k_1+p_1\cdot k_2)^{-\gamma_1}(p_2\cdot k_1+p_2\cdot k_2)^{-\gamma_2}\, {}_2F_1\left(1,1;a+1;\frac{p_1\cdot k_1}{p_1\cdot k_1+p_1\cdot k_2}\right), \end{aligned} \tag{3.85}$$

which differs from eq. (3.73) in having arbitrary powers of all two-particle invariants. Following, ref. [134] we rescale momenta according to

$$p_1^{\mu}\to\sqrt{s}\,p_1^{\mu}, \quad p_2^{\mu}\to\sqrt{s}\,p_2^{\mu}, \quad k_1^{\mu}\to(1-z)\sqrt{s}\,p_3^{\mu}, \quad k_2^{\mu}\to(1-z)\sqrt{s}\,p_4^{\mu}, \tag{3.86}$$

and define (dimensionless) Mandelstam variables $s_{ij} = 2p_i\cdot p_j$. We emphasise that in the current notation s_{12} differs from the scale $s_{12} = 2k_1\cdot k_2$ used in the main text. We may express eq. (3.85) as

$$\begin{aligned} J(\alpha_1,\alpha_2,\beta_1,\beta_2,\gamma_1,\gamma_2,\delta,a,d) = 2^C s^{d-3+\delta-C}(1-z)^{2d-5+2\delta-C} \int d\Phi^{(3)} s_{34}^{\delta} s_{13}^{-\alpha_1} s_{14}^{-\alpha_2} s_{23}^{-\beta_1} s_{24}^{-\beta_2} \\ \times (s_{13}+s_{14})^{-\gamma_1}(s_{23}+s_{24})^{-\gamma_2}\, {}_2F_1\left(1,1;a+1;\frac{s_{13}}{s_{13}+s_{14}}\right), \end{aligned} \tag{3.87}$$

where the phase space integral is now dimensionless. At this point one may introduce the following Mellin-Barnes representation for the hypergeometric function (see e.g. ref. [148])

$$\begin{aligned} {}_2F_1(a,b;c;x) = \frac{\Gamma(c)}{\Gamma(a)\Gamma(b)\Gamma(c-a)\Gamma(c-b)} \\ \times \int_{-i\infty}^{i\infty}\frac{dz}{2\pi i}\Gamma(a+z)\Gamma(b+z)\Gamma(c-a-b-z)\Gamma(-z)(1-x)^z, \end{aligned} \tag{3.88}$$

as well as the identity

$$\frac{1}{(A+B)^{\lambda}} = \frac{1}{\Gamma(\lambda)}\int_{-i\infty}^{i\infty}\frac{dz}{2\pi i}\Gamma(-z)\Gamma(\lambda+z)\frac{A^z}{B^{z+\lambda}}, \tag{3.89}$$

for values of $\lambda>0$, to rewrite the combinations $(s_{13}+s_{14})$ and $(s_{23}+s_{24})$. Then, eq. (3.87) assumes the triple Mellin-Barnes form

$$\begin{aligned} J(\alpha_1,\alpha_2,\beta_1,\beta_2,\gamma_1,\gamma_2,\delta,a,d) = 2^C s^{d-3+\delta-C}(1-z)^{2d-5+2\delta-C}\frac{\Gamma(a+1)}{\Gamma^2(a)\Gamma(\gamma_2)}\int_{-i\infty}^{i\infty}\frac{dz_1}{2\pi i}\int_{-i\infty}^{i\infty}\frac{dz_2}{2\pi i} \\ \times\int_{-i\infty}^{i\infty}\frac{dz_3}{2\pi i}\frac{\Gamma^2(1+z_1)\Gamma(a-1-z_1)\Gamma(\gamma_1+z_1+z_2)\Gamma(\gamma_2+z_3)\Gamma(-z_1)\Gamma(-z_2)\Gamma(-z_3)}{\Gamma(\gamma_1+z_1)} \end{aligned}$$

$$\times \int d\Phi^{(3)} s_{34}^{\delta} s_{13}^{z_2-\alpha_1} s_{14}^{-z_2-\alpha_2-\gamma_1} s_{23}^{z_3-\beta_1} s_{24}^{-z_3-\beta_2-\gamma_2}. \tag{3.90}$$

The integrand of the phase space integral in eq. (3.90) now consists entirely of two-particle invariants, and is therefore homogenous in individual momentum rescalings. The so-called *energies and angles* parametrisation used in refs. [134, 145] will exploit this property.

We shall work in the lab frame where we may set

$$p_1^\mu = \frac{1}{2}(1,1,0,\ldots) \qquad \text{and} \qquad p_2^\mu = \frac{1}{2}(1,-1,0,\ldots)\,. \tag{3.91}$$

Furthermore, we choose to write p_3 and p_4 in terms of an energy E_i and a d-velocity β_i, and introduce similar notation for the initial state partons:[5]

$$p_i^\mu = \frac{E_i}{2}\beta_i^\mu \quad \text{for} \quad i \in \{3,4\}\,, \tag{3.92a}$$

$$p_i^\mu = \frac{1}{2}\beta_i^\mu \quad \text{for} \quad i \in \{1,2\}\,. \tag{3.92b}$$

Note that, despite appearances, E_i is dimensionless due to the rescaling in eq. (3.86). Using eq. (3.92) we rewrite the invariants as follows

$$s_{1i} = \frac{E_i}{2}\beta_1\cdot\beta_i\,, \quad s_{2i} = \frac{E_i}{2}\beta_2\cdot\beta_i\,, \quad s_{34} = \frac{E_3 E_4}{2}\beta_3\cdot\beta_4 \quad \text{for} \quad i\in\{3,4\}\,. \tag{3.93}$$

In the current parametrisation the phase space measure reads [134]

$$d\Phi^{(3)} \xrightarrow{z\to 1} (2\pi)^{3-2d}\, 2^{-2(d-1)}\, \delta(1-E_3-E_4) \prod_{i=3}^{4} dE_i\, d\Omega_i^{(d-1)}\, E_i^{d-3}\, \theta(E_i)\,, \tag{3.94}$$

where $d\Omega_i^{(d-1)}$ is the differential solid angle associated with particle i, and where the argument of the delta function is obtained by taking the LP limit. This suffices for our purposes, since the soft region contributes only at NLP in $(1-z)$. Using eqs. (3.93) and (3.94) in eq. (3.90), one may carry out the E_i integrals using

$$\int_0^1 dE_3 \int_0^1 dE_4\, \delta(1-E_3-E_4)\, E_3^{\lambda_3-1}\, E_4^{\lambda_4-1} = \frac{\Gamma(\lambda_3)\,\Gamma(\lambda_4)}{\Gamma(\lambda_3+\lambda_4)}\,. \tag{3.95}$$

We emphasise that the integration over the energies E_i can be evaluated separately from the angular integrations by virtue of the homogeneity of all terms in eq. (3.90) under eq. (3.92a). We obtain

$$J(\alpha_1,\alpha_2,\beta_1,\beta_2,\gamma_1,\gamma_2,\delta,a,d) = 2^{2C-\delta+5-4d}\,\pi^{3-2d}\,\frac{\Gamma(a+1)}{\Gamma^2(a)\,\Gamma(\gamma_2)\,\Gamma(2d-C+2\delta-4)} \int_{-i\infty}^{i\infty} \frac{dz_1}{2\pi i}$$

[5] The d-velocities β_1^μ and β_2^μ should not be confused with the powers of the invariants s_{23} and s_{24} in eq. (3.87), which are also denoted by β_1 and β_2.

$$\times \int_{-i\infty}^{i\infty} \frac{dz_2}{2\pi i} \int_{-i\infty}^{i\infty} \frac{dz_3}{2\pi i} \frac{\Gamma^2(1+z_1)\,\Gamma(a-1-z_1)\,\Gamma(\gamma_1+z_1+z_2)\,\Gamma(\gamma_2+z_3)\,\Gamma(-z_1)\,\Gamma(-z_2)\,\Gamma(-z_3)}{\Gamma(\gamma_1+z_1)}$$
$$\times \Gamma(z_2+z_3+d-\alpha_1-\beta_1+\delta-2)\,\Gamma(d-z_2-z_3-\alpha_2-\beta_2-\gamma_1-\gamma_2+\delta-2)$$
$$\times \int d\Omega_3^{(d-1)} \int d\Omega_4^{(d-1)} (\beta_3\cdot\beta_4)^{\delta} (\beta_1\cdot\beta_3)^{z_2-\alpha_1} (\beta_2\cdot\beta_3)^{z_3-\beta_1} (\beta_1\cdot\beta_4)^{-z_2-\alpha_2-\gamma_1} (\beta_2\cdot\beta_4)^{-z_3-\beta_2-\gamma_2}. \tag{3.96}$$

Next, we must carry out the angular integrals. Given that each d-velocity β_3 and β_4 occurs thrice rather than twice, we can no longer use eq. (3.69). Unfortunately, there is no known closed form for the angular integral involving three angular quantities. There is, however, a triple Mellin-Barnes form [149] (see also eq. (5.17) of ref. [134]) in $d = 4-2\epsilon$ dimensions

$$\int d\Omega_i^{(d-1)} (\beta_i\cdot\beta_{j_1})^{-\lambda_1} (\beta_i\cdot\beta_{j_2})^{-\lambda_2} (\beta_i\cdot\beta_{j_3})^{-\lambda_3} = \frac{2^{2-\lambda_1-\lambda_2-\lambda_3-2\epsilon}\,\pi^{1-\epsilon}}{\Gamma(\lambda_1)\,\Gamma(\lambda_2)\,\Gamma(\lambda_3)\,\Gamma(2-\lambda_1-\lambda_2-\lambda_3-2\epsilon)}$$
$$\times \int_{-i\infty}^{i\infty} \frac{dz_4}{2\pi i} \int_{-i\infty}^{i\infty} \frac{dz_5}{2\pi i} \int_{-i\infty}^{i\infty} \frac{dz_6}{2\pi i}\, \Gamma(-z_4)\,\Gamma(-z_5)\,\Gamma(-z_6)\,\Gamma(1-\lambda_1-\lambda_2-\lambda_3-\epsilon-z_4-z_5-z_6)$$
$$\times \Gamma(\lambda_1+z_4+z_5)\,\Gamma(\lambda_2+z_4+z_6)\,\Gamma(\lambda_3+z_5+z_6) \left(\frac{\beta_{j_1}\cdot\beta_{j_2}}{2}\right)^{z_4} \left(\frac{\beta_{j_1}\cdot\beta_{j_3}}{2}\right)^{z_5} \left(\frac{\beta_{j_2}\cdot\beta_{j_3}}{2}\right)^{z_6}. \tag{3.97}$$

Upon using this result, the remaining integral over the angular variables of the second soft gluon can be carried out using eq. (3.69). We express this in the current notation for convenience and find

$$\int d\Omega_i^{(d-1)} (\beta_i\cdot\beta_{j_1})^{-\lambda_1} (\beta_i\cdot\beta_{j_2})^{-\lambda_2} = 2^{2-\lambda_1-\lambda_2-2\epsilon}\,\pi^{1-\epsilon}\, \frac{\Gamma(1-\epsilon-\lambda_1)\,\Gamma(1-\epsilon-\lambda_2)}{\Gamma(1-\epsilon)\,\Gamma(2-2\epsilon-\lambda_1-\lambda_2)}$$
$$\times {}_2F_1\left(\lambda_1,\, \lambda_2;\, 1-\epsilon;\, 1-\frac{\beta_{j_1}\cdot\beta_{j_2}}{2}\right). \tag{3.98}$$

Our general phase space integral now has the form of a six-fold Mellin-Barnes integral, which applies if γ_1 and γ_2 are both non-zero. If either of them is zero, we do not need to apply eq. (3.89) for the relevant combination of invariants, and thus we will obtain a lower order Mellin-Barnes integral from the outset. Our strategy for carrying out an integral for general $(\alpha_1, \alpha_2, \beta_1, \beta_2, \gamma_1, \gamma_2, \delta, a)$ is as follows:

1. For specific parameter values, one may try to reduce the Mellin-Barnes integral using Barnes' lemmas. These state that integration over the Mellin variable, along a contour that keeps poles at $z = -a_i$ to its left and poles at $z = b_i$ to its right, results in a combination of gamma functions if the integrand has a particular form:

$$\int_{-i\infty}^{i\infty} \frac{dz}{2\pi i}\, \Gamma(a_1+z)\,\Gamma(a_2+z)\,\Gamma(b_1-z)\,\Gamma(b_2-z)$$
$$= \frac{\Gamma(a_1+b_1)\,\Gamma(a_1+b_2)\,\Gamma(a_2+b_1)\,\Gamma(a_2+b_2)}{\Gamma(a_1+a_2+b_1+b_2)}, \tag{3.99a}$$

$$\int_{-i\infty}^{i\infty} \frac{dz}{2\pi i} \frac{\Gamma(a_1+z)\,\Gamma(a_2+z)\,\Gamma(a_3+z)\,\Gamma(-z)\,\Gamma(b_1-z)}{\Gamma(b_2+z)} = \frac{\Gamma(a_1)\,\Gamma(a_2)\,\Gamma(a_3)\,\Gamma(a_1+b_1)\,\Gamma(a_2+b_1)\,\Gamma(a_3+b_1)}{\Gamma(b_2-a_1)\,\Gamma(b_2-a_2)\,\Gamma(b_2-a_3)}\,. \tag{3.99b}$$

We have found that many integrals can be simplified in this manner.

2. One must shift the contours of the Mellin-Barnes integrals, picking up residues of poles where appropriate, to extract all singularities in ϵ. The output of this procedure is a set of (possibly simpler) Mellin-Barnes integrals whose integrands can be safely expanded in ϵ. To shift the contours, we use the publicly available package `MBResolve` [150].

3. One can expand the integrands in ϵ, and apply Barnes' lemmas where possible to simplify the list of Mellin-Barnes integrals. This is done using a combination of the publicly available packages `MB` [151] and `barnesroutines`. At this stage, the output consists of a list of (simpler) Mellin-Barnes integrals, some of which will have been carried out completely.

4. Each remaining integral can be carried out in terms of infinite sums, for which we use `MBsums` [152]. The resulting sums must then be carried out explicitly, and added together. Here, we use the package `xSummer` [153], which itself relies on `FORM` [154].

All analytic results for the ϵ expansions of Mellin-Barnes integrals have been checked numerically using the package `MB`. A complication in the final step is that the individual sums may not converge, and even the sum of the sums may not converge. In such cases, we introduce a regulator x^z into the Mellin-Barnes integral (where z is the Mellin variable), and take the limit $x \to 1$ after having carried out all sums. An additional possible complication in the second step is that `MBResolve` may not be able to resolve the singularities in ϵ. Here one can apply extra regulators to deal with the problem, as documented in ref. [150].

Note that the above method will fail if either of the parameters (γ_1, γ_2) is negative, given that eq. (3.89) assumes that the left-hand side is a genuine denominator. Using the simple identities

$$\frac{p_2\cdot(k_1+k_2)}{p_2\cdot k_2} = \frac{p_2\cdot k_1}{p_2\cdot k_2} + 1 \quad \text{and} \quad \frac{p_1\cdot(k_1+k_2)}{p_1\cdot k_2} = \frac{p_1\cdot k_1}{p_1\cdot k_2} + 1\,, \tag{3.100}$$

we may derive the following relations for such integrals (all with $\delta = -1-\epsilon$):

$$\begin{aligned}
J(1,0,0,1,0,-1,\delta,a,d) &= J(1,0,-1,1,0,0,\delta,a,d) \quad + J(1,0,0,0,0,0,\delta,a,d)\,,\\
J(0,0,1,1,-1,0,\delta,a,d) &= J(0,0,-1,1,1,0,\delta,a,d) \quad + J(0,0,0,0,1,0,\delta,a,d)\,,\\
J(2,0,0,1,-1,-1,\delta,a,d) &= J(1,0,-1,1,0,0,\delta,a,d) \quad + J(1,0,0,0,0,0,\delta,a,d) + \\
&\qquad J(2,-1,-1,1,0,0,\delta,a,d) + J(2,-1,0,0,0,0,\delta,a,d)\,.
\end{aligned} \tag{3.101}$$

Integrals on the right-hand side that only involve powers of $p_1\cdot k_1$ and/or $p_2\cdot k_1$ can be carried out using the analytic result of eq. (3.38). Remaining integrals can be carried out using the Mellin-Barnes approach outlined in this section.

We conclude this section by pointing out that for the last term in the last line of eq. (3.101), there is in fact a straightforward way to derive a closed form, valid for any d. Starting with the definition

$$J(2,-1,0,0,0,0,\delta,a,d)=\int d\Phi^{(3)}\,\frac{(2k_1\cdot k_2)^\delta\,(p\cdot k_2)}{(p\cdot k_1)^2}\,{}_2F_1\left(1,1;a+1;\frac{p\cdot k_1}{p\cdot(k_1+k_2)}\right), \quad (3.102)$$

we use the centre of mass frame of the two outgoing gluons, as in section 3.C.1, to get

$$\begin{aligned}J(2,-1,0,0,0,0,\delta,a,d)&=\frac{2}{(4\pi)^d}\frac{s^{d-4+\delta}(1-z)^{2d-6+2\delta}}{\Gamma(d-3)}\frac{\Gamma(d/2-1+\delta)\,\Gamma(d/2-1)\,\Gamma(d-3+\delta)}{\Gamma(2d-5+2\delta)}\\&\times\int_0^\pi d\theta_1\int_0^\pi d\theta_2\,\sin^{d-3}\theta_1\,\sin^{d-4}\theta_2\left(\frac{1+\cos\theta_1}{2}\right)\left(\frac{1-\cos\theta_1}{2}\right)^{-2}{}_2F_1\left(1,\,1;\,a+1;\frac{1-\cos\theta_1}{2}\right),\end{aligned} \quad (3.103)$$

where we have already carried out the x and y integrals from eq. (3.65)). The angular integrals can be carried out by transforming to $u=(1-\cos\theta_1)/2$ and $v=(1-\cos\theta_2)/2$ from which one finds

$$\begin{aligned}&\int_0^\pi d\theta_1\int_0^\pi d\theta_2\,\sin^{d-3}\theta_1\,\sin^{d-4}\theta_2\left(\frac{1+\cos\theta_1}{2}\right)\left(\frac{1-\cos\theta_1}{2}\right)^{-2}{}_2F_1\left(1,\,1;\,a+1;\frac{1-\cos\theta_1}{2}\right)\\&\quad=2^{2d-7}\int_0^1 dv\,[v(1-v)]^{(d-5)/2}\int_0^1 du\,u^{d/2-4}(1-u)^{d/2-1}\,{}_2F_1(1,\,1;\,a+1;\,u)\\&\quad=2^{2d-7}\,\frac{\Gamma^2((d-3)/2)\,\Gamma(d/2-3)\,\Gamma(d/2)}{\Gamma^2(d-3)}\,{}_3F_2(1,\,1,\,d/2-3;\,a+1,\,d-3;\,1).\end{aligned} \quad (3.104)$$

Putting everything together, one obtains

$$\begin{aligned}J(2,-1,0,0,0,0,\delta,a,d)&=\frac{1}{64\pi^d}s^{d-4+\delta}(1-z)^{2d-6+2\delta}\frac{\Gamma(d/2-1+\delta)\,\Gamma(d-3+\delta)}{\Gamma(2d-5+2\delta)}\\&\times\frac{\Gamma^2(d/2)\,\Gamma^2((d-3)/2)\,\Gamma(d/2-3)}{(d/2-1)\,\Gamma^3(d-3)}\,{}_3F_2(1,\,1,\,d/2-3;\,a+1,\,d-3;\,1).\end{aligned} \quad (3.105)$$

3.C.3 Results

Here we collect all analytic results, as a Laurent expansion in ϵ, for the integrals $\hat{I}_2(\alpha_1,\beta_1,\alpha_2,\beta_2,\gamma_1,\gamma_2,\delta)$ defined in eq. (3.39). Given that we report only logarithmic terms in $(1-z)$, it is sufficient to expand up to $\mathcal{O}(\epsilon)$.

$$\begin{aligned}\hat{I}_2(0,0,1,0,2,0,-\epsilon)&=\frac{1}{12\epsilon^3}-\frac{5\pi^2}{24\epsilon}-\frac{115\zeta_3}{18}-\frac{337\pi^4\epsilon}{4320},\\\hat{I}_2(1,0,1,0,2,1,1-\epsilon)&=\frac{1}{12\epsilon^3}-\frac{1}{12\epsilon^2}-\frac{1}{\epsilon}\left(\frac{1}{4}+\frac{5\pi^2}{24}\right)-\frac{3}{4}+\frac{11\pi^2}{72}-\frac{115\zeta_3}{18}\\&\quad+\epsilon\left(-\frac{9}{4}+\frac{11\pi^2}{24}-\frac{337\pi^4}{4320}+\frac{67\zeta_3}{18}\right),\end{aligned}$$

$$\hat{I}_2(0,0,1,0,1,-1,-1-\epsilon) = \frac{5}{24\epsilon^3} - \frac{83\pi^2}{144\epsilon} - \frac{659\zeta_3}{36} - \frac{173\pi^4\epsilon}{960},$$

$$\hat{I}_2(1,0,1,0,1,0,-\epsilon) = \frac{7}{36\epsilon^3} - \frac{103\pi^2}{216\epsilon} - \frac{775\zeta_3}{54} - \frac{149\pi^4\epsilon}{864},$$

$$\hat{I}_2(2,0,1,0,1,1,1-\epsilon) = \frac{7}{36\epsilon^3} + \frac{5}{36\epsilon^2} - \frac{1}{\epsilon}\left(\frac{1}{12} + \frac{103\pi^2}{216}\right) + \frac{1}{12} - \frac{83\pi^2}{216} - \frac{775\zeta_3}{54} + \epsilon\left(-\frac{1}{12} - \frac{\pi^2}{72} - \frac{149\pi^4}{864} - \frac{659\zeta_3}{54}\right),$$

$$\hat{I}_2(0,0,0,1,2,0,-\epsilon) = \frac{1}{16\epsilon^3} - \frac{13\pi^2}{96\epsilon} - \frac{23\zeta_3}{6} - \frac{107\pi^4\epsilon}{1920},$$

$$\hat{I}_2(1,0,0,1,1,0,-\epsilon) = \frac{11}{48\epsilon^3} - \frac{53\pi^2}{96\epsilon} - \frac{148\zeta_3}{9} - \frac{727\pi^4\epsilon}{3456},$$

$$\hat{I}_2(1,0,0,1,2,1,1-\epsilon) = \frac{1}{6\epsilon^3} + \frac{1}{12\epsilon^2} + \frac{1}{\epsilon}\left(\frac{1}{4} - \frac{5\pi^2}{12}\right) + \frac{3}{4} - \frac{19\pi^2}{72} - \frac{227\zeta_3}{18} + \epsilon\left(\frac{9}{4} - \frac{19\pi^2}{24} - \frac{167\pi^4}{1080} - \frac{157\zeta_3}{18}\right),$$

$$\hat{I}_2(2,0,0,1,1,1,1-\epsilon) = \frac{5}{12\epsilon^2} - \frac{1}{4\epsilon} + \frac{1}{4} - \frac{77\pi^2}{72} + \epsilon\left(-\frac{1}{4} + \frac{17\pi^2}{72} - \frac{295\zeta_3}{9}\right),$$

$$\hat{I}_2(1,0,-1,1,0,0,-1-\epsilon) = \frac{3}{16\epsilon^3} + \frac{19}{48\epsilon^2} - \frac{1}{\epsilon}\left(\frac{19}{12} + \frac{149\pi^2}{288}\right) + \frac{19}{3} - \frac{247\pi^2}{288} - \frac{49\zeta_3}{3} + \epsilon\left(-\frac{76}{3} + \frac{247\pi^2}{72} - \frac{3137\pi^4}{17280} - \frac{433\zeta_3}{18}\right),$$

$$\hat{I}_2(1,0,0,0,0,0,-1-\epsilon) = \frac{1}{8\epsilon^3} - \frac{41\pi^2}{144\epsilon} - \frac{33\zeta_3}{4} - \frac{971\pi^4\epsilon}{8640},$$

$$\hat{I}_2(0,0,-1,1,1,0,-1-\epsilon) = -\frac{1}{24\epsilon^3} + \frac{19}{48\epsilon^2} + \frac{1}{\epsilon}\left(-\frac{19}{12} + \frac{13\pi^2}{144}\right) + \frac{19}{3} - \frac{247\pi^2}{288} + \frac{47\zeta_3}{18} + \epsilon\left(-\frac{76}{3} + \frac{247\pi^2}{72} + \frac{41\pi^4}{960} - \frac{433\zeta_3}{18}\right),$$

$$\hat{I}_2(2,0,0,1,0,0,-\epsilon) = \frac{11}{48\epsilon^3} + \frac{2}{3\epsilon^2} - \frac{1}{\epsilon}\left(\frac{1}{3} + \frac{53\pi^2}{96}\right) + \frac{1}{3} - \frac{59\pi^2}{36} - \frac{148\zeta_3}{9} + \epsilon\left(-\frac{1}{3} + \frac{2\pi^2}{3} - \frac{727\pi^4}{3456} - \frac{887\zeta_3}{18}\right),$$

$$\hat{I}_2(0,0,0,0,1,0,-1-\epsilon) = \frac{1}{24\epsilon^3} - \frac{13\pi^2}{144\epsilon} - \frac{47\zeta_3}{18} - \frac{41\pi^4\epsilon}{960},$$

$$\hat{I}_2(2,-1,-1,1,0,0,-1-\epsilon) = \frac{5}{16\epsilon^3} + \frac{1}{\epsilon^2} - \frac{1}{\epsilon}\left(\frac{1}{3} + \frac{77\pi^2}{96}\right) + \frac{1}{3} - \frac{95\pi^2}{36} - \frac{295\zeta_3}{12} + \epsilon\left(-\frac{1}{3} + \frac{5\pi^2}{9} - \frac{491\zeta_3}{6} - \frac{1693\pi^4}{5760}\right),$$

$$\hat{I}_2(2,-1,0,0,0,0,-1-\epsilon) = \frac{1}{4\epsilon^2} - \frac{1}{6\epsilon} + \frac{1}{6} - \frac{41\pi^2}{72} + \epsilon\left(-\frac{1}{6} + \frac{13\pi^2}{36} - \frac{33\zeta_3}{2}\right). \quad (3.106)$$

Chapter 4

Diagrammatic resummation of leading-logarithmic threshold effects at NLP

The vast amount of research dedicated to LP resummation (see section 1.3 for an impression), has had significant impact on phenomenology. Together with the increasing precision of measurements in contemporary collider experiments, it is only natural to ponder whether NLP terms in the threshold expansion can also be resummed, particularly since they seem to be numerically significant, for example in the case of Higgs production [155, 156], as we will confirm in chapter 5.

This topic has been investigated before using path-integral methods in ref. [41], which derived a set of effective Feynman rules for the emission of massless gauge bosons at next-to-soft level, and argued that a large class of NLP contributions exponentiates. The results were subsequently confirmed by an all-order analysis of Feynman diagrams [83]. In a different approach, using a *physical evolution kernel* [146, 157–160], NLP effects in certain processes were argued to be resummable as well (see also refs. [161–165] for other early work related to elucidating all-order properties). In recent years, the SCET framework has been used to demonstrate that the LL NLP contributions can be resummed, first for event shapes (thrust) [166], and subsequently for DY production [167], where the results agree with the predictions of the aforementioned physical evolution kernel approach.[1]

Threshold resummation at LP is known to be a consequence of the universal factorisation of soft and collinear divergences in scattering amplitudes of gauge theories (see e.g. ref. [52]). Over the years, this has motivated attempts to construct a factorisation formula for NLP effects using diagrammatic techniques, as outlined in section 1.4. In chapter 2 a more complete analysis was undertaken for QED, which revealed the importance of new functions or factorisation ingredients (both universal and non-universal) that appear beyond LP in the emitted gluon momentum. The aim of this study is to show how resummation of LL NLP effects can be achieved building on the diagrammatic approach developed in refs. [41, 83],

[1] Since the publication of the study on which this chapter is based (ref. [2]), other NLP LL resummation efforts have been undertaken using SCET, e.g. refs. [103, 121, 168–171].

and is in fact analogous to the original LP resummations of refs. [38–40, 48, 49]. We will see that many of the new functions that contribute in NLP factorisation formulae are in fact irrelevant for discussing the highest power of the NLP logarithm at any given order in perturbation theory, consistent with what was noted in the SCET approach of ref. [167] and in the diagrammatic studies of refs. [79, 81, 85] and chapters 2 and 3. This makes the resummation of LL NLP contributions remarkably straightforward. Importantly, our method is sufficiently simple and universal that it can be directly applied to any hadronic cross section with colour-singlet final states; we explicitly discuss applications to Higgs boson production in the gluon fusion channel, and the formalism can readily be generalised to multi-boson final states. It is valuable to obtain a resummation prescription independent of the SCET approach, as a comparison of different techniques to describe equivalent physics may lead to new insights. Furthermore, our result provides an alternative starting point for generalising the NLP resummation formalism beyond LL accuracy.

The structure of this chapter is as follows. In section 4.1, we review the resummation of LP threshold contributions, and relate our calculation to the path-integral methods of ref. [41], which provide a particularly elegant proof of exponentiation. In section 4.2, we show how the picture can be naturally extended to NLP level, using existing results. We will argue in detail that potential additional contributions to NLP behaviour, including hard collinear effects, non-universal behaviour and phase-space correlations between gluons, can be ignored at LL accuracy. Armed with this knowledge, we will then perform an explicit calculation that resums the LL NLP terms in DY and compare to results in the literature [146, 157–160]. We will then comment on the general applicability of our framework to the production of an arbitrary number of colour-singlet particles, before examining Higgs production in the large top mass limit as a further example. We conclude in section 4.6.

4.1 Threshold resummation at LP

In this section, we review the resummation of terms at LP in the threshold variable, using factorisation methods. Given that our aim is to sum only LL terms at NLP, here we will mostly work at the same logarithmic accuracy. Furthermore, we will phrase our discussion in terms of methods and notation that allow a straightforward generalisation to subleading power in the threshold expansion. While our discussion applies to general colour-singlet final states, we will first explicitly consider the DY production of a massive or off-shell vector boson. We will not consider here the quark-gluon production channel, which in fact also starts to contribute at NLP. The gluon-gluon channel for DY gives rise to terms that are further suppressed (NNLP), and is also left out of our analysis.

We write the invariant mass distribution in the $q\bar{q}$-channel as

$$\frac{d\sigma}{d\tau} = \sigma_0(Q^2, S) \int_0^1 dz\, dx_1\, dx_2\, \delta(\tau - x_1 x_2 z)\, q(x_1, \mu_F^2)\, \bar{q}(x_2, \mu_F^2)\, \Delta\left(z, \alpha_s(\mu_R^2), \frac{\mu_F^2}{Q^2}, \frac{\mu_R^2}{Q^2}\right), \quad (4.1)$$

where we assume a single quark flavour for simplicity (and thus restrict the vector boson to be an off-shell photon or a Z boson). Here $\sigma_0(Q^2)$ is the LO total partonic cross section, whose precise value will depend on the nature of the vector boson.[2] Furthermore, $\alpha_s(\mu_R^2)$ is the strong coupling at the renormalisation scale μ_R, $q(x,\mu_F^2)$ is a quark distribution function with longitudinal momentum fraction x and factorisation scale μ_F, while $\bar{q}$ is the equivalent for an antiquark. We choose to identify the factorisation and renormalisation scales, and denote these collectively by $\mu = \mu_F = \mu_R$. Given that scale choice effects contribute to only subleading logarithms (see e.g. ref. [49]), we will set $\mu = Q$ from now on, and simplify notation accordingly. In eq. (4.1) we defined $\tau = Q^2/S$, which is the hadronic equivalent of the by now familiar variable $z = Q^2/s$. At LO this must be unity, so that one has

$$\Delta^{(0)}(z) = \delta(1-z). \tag{4.2}$$

In certain instances we use the term *partonic cross section* for quantities such as that of eq. (4.2), which are strictly speaking partonic coefficient functions, given that they have a LO Q^2-dependent expression factored out.

The invariant mass distribution in eq. (4.1) is a convolution in z, and can be diagonalised by taking the Mellin moment with respect to τ

$$\int_0^1 d\tau\, \tau^{N-1} \frac{d\sigma}{d\tau} = \sigma_0(Q^2,S)\, q(N,Q^2)\, \bar{q}(N,Q^2)\, \Delta(N,Q^2), \tag{4.3}$$

as the right hand side is now factorised into direct product of Mellin transformed PDFs

$$q(N,Q^2) = \int_0^1 dx_1\, x_1^{N-1}\, q(x_1,Q^2) \qquad \text{and} \qquad \bar{q}(N,Q^2) = \int_0^1 dx_2\, x_2^{N-1}\, \bar{q}(x_2,Q^2), \tag{4.4}$$

and the Mellin moment of the partonic coefficient function

$$\Delta(N,Q^2) = \int_0^1 dz\, z^{N-1}\, \Delta(z,Q^2). \tag{4.5}$$

We note that functions and their Mellin transforms are distinguished only by their arguments. Beyond LO, the partonic coefficient function in eq. (4.5) receives potentially large threshold corrections. In momentum space, the LP threshold logarithms take the form of plus distributions $\mathscr{D}_m(z) = [\log^m(1-z)/(1-z)]_+$, defined in eq. (3.42), where the highest power of the logarithm is $m = 2n-1$ at $\mathcal{O}(\alpha_s^n)$, as seen in eq. (1.22). In Mellin space, these contributions take the form

$$\alpha_s^n \log^m N \qquad \text{for} \qquad m = 0,\ldots,2n. \tag{4.6}$$

In this chapter we shall mostly work with *bare* partonic quantities, before renormalisation

[2] We note that also for the production of an off-shell photon the definition of $\sigma_0(Q^2)$ differs from the LO cross section in eq. (3.1), due to absorption of a factor of $\frac{\tau}{z}$, which arises from expressing the convolution with the PDFs in the form of eq. (4.1). See eq. (5.66) in appendix 5.B for the fine details of this normalisation.

of the coupling α_s, and before the absorption of residual collinear divergences in the PDFs (know as mass factorisation). As usual, we will be regulating UV and IR divergences using dimensional regularisation in $d = 4 - 2\epsilon$. For clarity, we will denote this bare partonic coefficient function with $\widehat{\Delta}(z, Q^2, \epsilon)$ in momentum space, and with $\widehat{\Delta}(N, Q^2, \epsilon)$ in Mellin space. Mass factorisation is understood to be performed in the $\overline{\text{MS}}$ scheme.

For any QCD process where a colour-singlet final state is produced near threshold, the bare partonic cross section $\widehat{\Delta}$ admits a factorised form and can be written as [48, 54]

$$\widehat{\Delta}\left(N, Q^2, \epsilon\right) = \left|H\left(Q^2\right)\right|^2 S\left(N, Q^2, \epsilon\right) \prod_i \frac{\psi_i\left(N, Q^2, \epsilon\right)}{\psi_{\text{E},i}\left(N, Q^2, \epsilon\right)}, \tag{4.7}$$

where $H\left(Q^2\right)$ is an amplitude-level finite hard function containing off-shell virtual contributions, $S(N, Q^2, \epsilon)$ is a soft function collecting all soft enhancements associated with (real or virtual) soft radiation, and $\psi_i(N, Q^2, \epsilon)$ is a perturbative (anti-)quark distribution function, collecting collinear singularities associated with initial parton i. We stress that the latter two function are defined at the cross section level, contrary to the soft and collinear functions discussed so far in this thesis. Given that infrared enhancements of both soft and collinear origin are included twice (both in the soft and quark distribution functions), one may remove the double counting by dividing each quark distribution by its own eikonal approximation $\psi_{\text{E},i}(N, Q^2, \epsilon)$. Formal definitions of the (eikonal) quark distributions and of the soft function are given, for example, in ref. [54].

The eikonal quark distributions are sometimes absorbed into the soft function to build the so-called reduced soft function, which then describes strictly *wide-angle* soft radiation. Alternatively, one may consider the factor

$$\psi_{\text{hard col.},i}(N, Q^2, \epsilon) = \frac{\psi_i(N, Q^2, \epsilon)}{\psi_{\text{E},i}(N, Q^2, \epsilon)}, \tag{4.8}$$

for each initial parton line. This has the effect of removing the soft physics from each quark distribution, leaving hard collinear behaviour only. This arrangement is particularly convenient if one wishes to focus only on leading logarithms: at any fixed order in α_s, LLs at LP arise only when the maximum number of singular integrations is performed, yielding the highest inverse power of ϵ. Thus, the factor $\psi_{\text{hard col.},i}(N, Q^2, \epsilon)$ contributes only at subleading logarithmic accuracy, and can be put equal to unity at LL. We are then left with the simple result

$$\widehat{\Delta}_{\text{LL}}\left(N, Q^2, \epsilon\right) = \left|H\left(Q^2\right)\right|^2 S\left(N, Q^2, \epsilon\right), \tag{4.9}$$

implying that LLs at LP in the DY cross section, at any order in perturbation theory, are governed purely by the soft function [48, 49, 51]. We shall thus focus on this function in what follows.

For any QCD process with a colour-singlet final state, the soft function has a formal definition as a vacuum expectation value of Wilson line operators associated with the colliding partons. Defining the dimensionless four-vectors β_i via $p_i^\mu = \sqrt{s/2}\,\beta_i^\mu$, one may write the

soft function (in momentum space) as

$$S(z,Q^2,\epsilon) = \frac{1}{N_c}\sum_n \mathrm{Tr}\left[\left\langle 0\left|\Phi^\dagger_{\beta_1}\Phi_{\beta_2}\right|n\right\rangle\left\langle n\left|\Phi^\dagger_{\beta_2}\Phi_{\beta_1}\right|0\right\rangle\right]\delta\left(z-\frac{Q^2}{s}\right). \tag{4.10}$$

Here the trace is over colour indices and the Wilson line operators are defined as

$$\Phi_{\beta_i} = \mathscr{P}\exp\left[ig_s\mathbf{T}^a\int_{-\infty}^{0} d\lambda\,\beta_i\cdot A_a(\lambda\beta_i)\right], \tag{4.11}$$

where $\mathbf{T}^a$ is a colour generator in the fundamental representation. The path-ordering operator $\mathscr{P}$ would order these non-commutative matrices upon expansion of the Wilson line in a perturbative calculation, according to the point of emission of the gauge field along β_i. We note that eq. (4.10) includes a sum over final states containing n partons generated by the Wilson lines, including the appropriate phase space integration, and subject to the constraint that the total energy radiated in the final state equals $(1-z)s$. Finally, the division by the number of colours N_c corrects for the fact that this factor has already been included in the LO cross section σ_0 in eq. (4.9).

Introducing the momentum space gauge field $\tilde{A}_\mu(k)$, the Wilson line exponent reads

$$ig_s\mathbf{T}_a\int\frac{d^dk}{(2\pi)^d}\,\beta_i\cdot\tilde{A}^a(k)\int_{-\infty}^{0}d\lambda\,e^{i\lambda\beta_i\cdot k} = \int\frac{d^dk}{(2\pi)^d}\,\tilde{A}^a_\mu(k)\left[g_s\mathbf{T}_a\,\frac{\beta_i^\mu}{\beta_i\cdot k - i\varepsilon}\right], \tag{4.12}$$

where the square-bracketed factor on the right constitutes the momentum-space factor associated to the emission of a gluon from the Wilson line. We recognise this as the well-known eikonal Feynman rule for a soft gluon emission, so that finding the soft function amounts to calculating the cross section for the incoming partons in the eikonal approximation. This cross section is known to exponentiate, which relies on two properties. Firstly, vacuum expectation values of Wilson lines exponentiate before any phase space integrations are carried out, which may be shown diagrammatically [38–40], or using renormalisation group arguments, themselves relying on the multiplicative renormalisability of Wilson line operators [172–177]. Secondly, the phase space for the emission of n soft partons factorises into n decoupled one-parton phase space integrals, given that momentum conservation can be ignored at LP in the threshold expansion.

The cross section level soft function in eq. (4.9) thus has an exponential form, and the exponent can be directly computed in terms of a special class of Feynman diagrams known as *webs* [38–40]. These results have been reinterpreted more recently using a path integral approach [41], which incorporated statistical physics methods (the *replica trick*) to provide a particularly streamlined proof of diagrammatic exponentiation. These methods have in turn allowed the web language to be generalised to multiparton scattering [42, 43] (see refs. [178–186] for related work and ref. [187] for a pedagogical review on webs). We review the replica trick here in appendix 4.A, as it can also be used to demonstrate directly the exponentiation of a large class of contributions at NLP in the threshold expansion.

We point out that the pattern of exponentiation of soft and collinear singularities is non-trivial, in that the exponent is single-logarithmic (containing terms of the form $\alpha_s^n \log^m N$ with $m \leq n+1$), while the cross section is double-logarithmic, as noted in eq. (4.6). This implies that the LP LLs in the partonic coefficient function are completely determined by a one-loop evaluation of the soft function or, equivalently, a one-loop evaluation of the K-factor in the eikonal limit. We will review this calculation below.

The soft function in momentum space, up to NLO, can be written as[3]

$$S\big(z,Q^2,\epsilon\big) = \big(1+S_{\rm V}^{(1)}(Q^2,\epsilon)\big)\,\delta(1-z) + S_{\rm R}^{(1)}(z,Q^2,\epsilon) + \mathscr{O}\left(\alpha_s^2\right). \tag{4.13}$$

Note that the we have calculated the real emission contribution before in section 1.3 using a different regularisation method. The contribution is obtained from the graphs of fig. 1.4 using eikonal Feynman rules. One finds

$$S_{\rm R}^{(1)}(z,Q^2,\epsilon) = \mu^{2\epsilon} g_s^2\, C_F \int \frac{d^dk}{(2\pi)^{d-1}} \frac{2p_1\cdot p_2}{p_1\cdot k\, p_2\cdot k}\,\delta_+(k^2)\,\delta\!\left(1-z-\frac{2k\cdot(p_1+p_2)}{s}\right). \tag{4.14}$$

The phase space integral is easily evaluated using the familiar Sudakov decomposition

$$k^\mu = k\cdot\beta_2\,\beta_1^\mu + k\cdot\beta_1\,\beta_2^\mu + k_\perp^\mu \equiv k^+\beta_1^\mu + k^-\beta_2^\mu + k_\perp^\mu, \tag{4.15}$$

with $k_\perp\cdot\beta_1 = k_\perp\cdot\beta_2 = 0$ and $\beta_1\cdot\beta_2 = 1$, while the integration measure in eq. (4.14) becomes

$$\int d^dk = \frac{1}{2}\int dk^+\,dk^-\,d\boldsymbol{k}_\perp^2\,d\Omega_{d-2}\left(\boldsymbol{k}_\perp^2\right)^{(d-4)/2}. \tag{4.16}$$

Integration over the $d-2$ dimensional orthogonal momentum space, yields

$$S_{\rm R}^{(1)}(z,Q^2,\epsilon) = 2g_s^2\,C_F\,\frac{\mu^{2\epsilon}\,\Omega_{d-2}}{(2\pi)^{d-1}}\int_0^\infty dk^+\int_0^\infty dk^-\left(2k^+k^-\right)^{\frac{d-6}{2}}\,\delta\left(1-z-\frac{k^++k^-}{\sqrt{s/2}}\right), \tag{4.17}$$

where we used the on shell condition for the soft gluon, and with Ω_{d-2} as defined in eq. (3.35). We then introduce the reparameterisation

$$k^+ = \sqrt{s/2}\,x\,y \qquad \text{and} \qquad k^- = \sqrt{s/2}\,x\,(1-y), \tag{4.18}$$

to carry out the remaining integrals in eq. (4.17). We obtain

$$\begin{aligned} S_{\rm R}^{(1)}(z,Q^2,\epsilon) &= g_s^2\,C_F\,s^{\frac{d-4}{2}}\,\frac{\mu^{2\epsilon}\Omega_{d-2}}{(2\pi)^{d-1}}\int_0^1 dy\,\left[y\,(1-y)\right]^{\frac{d-6}{2}}\int_0^\infty dx\,x^{d-5}\,\delta\,(1-z-x) \\ &= \frac{\alpha_s C_F}{\pi}\left(\frac{\bar\mu^2}{Q^2}\right)^\epsilon \frac{e^{\epsilon\gamma_E}\,\Gamma^2(-\epsilon)}{\Gamma(1-\epsilon)\,\Gamma(-2\epsilon)}(1-z)^{-1-2\epsilon}\,\left[1-\epsilon\,(1-z)+\ldots\right], \end{aligned} \tag{4.19}$$

where we have restored the Q dependence via $s = Q^2/z$, since this is the external variable

[3] Our presentation is motivated by that of ref. [49].

of interest: the DY cross section is measured at a particular invariant mass Q^2, while s is an internal variable governed by the momentum fraction carried by the colliding partons. We subsequently expanded around threshold and we will drop the term proportional to ϵ in the square brackets in the following, given that we focus on LL corrections which originate from the highest inverse power of ϵ. This can be seen explicitly in eq. (3.41), used to regulate the $z \to 1$ divergence of eq. (4.19), where each power of $\log(1-z)$ in the plus-distributions is associated with a power of ϵ.

The virtual contribution at $\mathcal{O}(\alpha_s)$ can be obtained by direct calculation, or by imposing the soft gluon unitarity requirement [49]

$$\int_0^1 dz\, S\left(z, Q^2, \epsilon\right) = 1\,, \tag{4.20}$$

reflecting the requirement soft divergences from the virtual and real contributions must cancel, and the fact that Wilson line correlators are pure counterterms in dimensional regularisation. This requirement implies

$$S_{\rm V}^{(1)}(Q^2, \epsilon) = -\int_0^1 dz\, S_{\rm R}^{(1)}(z, Q^2, \epsilon)\,, \tag{4.21}$$

which applied to eq. (4.19) immediately gives

$$S_{\rm V}^{(1)}(Q^2, \epsilon) = \frac{\alpha_s C_F}{\pi}\left(\frac{\bar{\mu}^2}{Q^2}\right)^{\epsilon} \frac{e^{\epsilon\gamma_E}\,\Gamma^2(-\epsilon)}{\Gamma(1-\epsilon)\,\Gamma(-2\epsilon)}\left[\frac{1}{2\epsilon} + \dots\right]. \tag{4.22}$$

Summing the real and virtual correction as in eq. (4.13) we obtain the NLO soft function

$$S^{(1)}(z, Q^2, \epsilon) = \frac{\alpha_s C_F}{\pi}\left(\frac{\bar{\mu}^2}{Q^2}\right)^{\epsilon} \frac{e^{\epsilon\gamma_E}\,\Gamma^2(-\epsilon)}{\Gamma(1-\epsilon)\,\Gamma(-2\epsilon)}\left\{(1-z)^{-1-2\epsilon} + \frac{1}{2\epsilon}\delta(1-z)\right\}, \tag{4.23}$$

so that application of eq. (3.41) reveals indeed the cancellation of the non-integrable soft divergence at threshold between the real and virtual counterparts. At this point we can take the Mellin transform, which gives

$$\begin{aligned} S^{(1)}(N, Q^2, \epsilon) &= \int_0^1 dz\, z^{N-1}\, S^{(1)}(z, Q^2, \epsilon) \\ &= \frac{\alpha_s C_F}{\pi}\left(\frac{\bar{\mu}^2}{Q^2}\right)^{\epsilon} \frac{e^{\epsilon\gamma_E}\,\Gamma^2(-\epsilon)}{\Gamma(1-\epsilon)\,\Gamma(-2\epsilon)}\left[\frac{\Gamma(-2\epsilon)\,\Gamma(N)}{\Gamma(-2\epsilon+N)} + \frac{1}{2\epsilon}\right]. \end{aligned} \tag{4.24}$$

Expanding in ϵ one finds

$$\begin{aligned} S^{(1)}(N, Q^2, \epsilon) = \left(\frac{\bar{\mu}^2}{Q^2}\right)^{\epsilon} \frac{\alpha_s}{\pi}\, C_F \Bigg[&\frac{2}{\epsilon}\Big(\psi^{(0)}(N) + \gamma_E\Big) \\ &+ \frac{6\psi^{(0)}(N)\Big(\psi^{(0)}(N) + 2\gamma_E\Big) - 6\psi^{(1)}(N) + \pi^2 + 6\gamma_E^2}{3}\Bigg], \end{aligned} \tag{4.25}$$

where $\psi^{(n-1)}(z) = \frac{d^n}{dz^n}\log\Gamma(z)$, i.e. it denotes the n-th derivative of the logarithm of the Γ function. Keeping the dominant behaviour as $N \to \infty$ one finds the simple result

$$S^{(1)}(N,Q^2,\epsilon)\Big|_{\rm LL} = \left(\frac{\bar{\mu}^2}{Q^2}\right)^{\epsilon} \frac{2\alpha_s}{\pi} C_F \left[\frac{\log N}{\epsilon} + \log^2 N\right], \tag{4.26}$$

where we kept the leading power of the logarithm separately for the divergent and for the finite contributions. As discussed above, we may exponentiate this result to obtain the LL behaviour at all orders. Upon doing so, we may absorb the residual collinear poles into the parton distributions, using the $\overline{\rm MS}$ scheme. This amounts to defining renormalised and resummed PDFs for initial state partons via

$$q_{\rm LL}(N,Q^2) = q(N,Q^2)\exp\left[\frac{\alpha_s}{\pi} C_F \frac{\log N}{\epsilon}\right], \tag{4.27}$$

and similarly for the antiquark, so that eq. (4.3) becomes

$$\int_0^1 d\tau\, \tau^{N-1} \frac{d\sigma_{\rm DY}}{d\tau}\bigg|_{\rm LL} = \sigma_0(Q^2,S)\, q_{\rm LL}(N,Q^2)\,\bar{q}_{\rm LL}(N,Q^2)\exp\left[\frac{2\alpha_s}{\pi} C_F \log^2 N\right]. \tag{4.28}$$

This formula explicitly sums up to LP LL in N to all orders. It can easily be verified that eq. (4.28) reproduces the well-known results of earlier studies, see for example refs. [48, 49, 146], both in Mellin space and in momentum space.

We note that in our analysis that scale μ appears only through the factor $\bar{\mu}^{2\epsilon}$, as must be the case on dimensional grounds. Given that μ is identified with the renormalisation and factorisation scales, it follows that logarithms of these scales are suppressed by a single power of ϵ for general choices of μ, and thus do not contribute to leading-logarithmic behaviour in the threshold variable, as mentioned earlier. As a final remark, we note that we will have to keep track of subleading terms in eq. (4.25) once we go beyond LP. Also retaining LLs for the divergent and finite parts at NLP, one finds

$$S^{(1)}(N,Q^2,\epsilon) = \left(\frac{\bar{\mu}^2}{Q^2}\right)^{\epsilon} \frac{2\alpha_s C_F}{\pi}\left[\frac{1}{\epsilon}\left(\log N - \frac{1}{2N}\right) + \log^2 N - \frac{\log N}{N}\right]. \tag{4.29}$$

4.2 The origin of leading logarithms at NLP

In the previous section, we reviewed the exponentiation of LP LL contributions to the DY cross section. We now discuss how to extend this procedure to NLP, and we will keep our remarks general enough to apply to both quark and gluon-initiated processes, and for general colour-singlet final states. Recall that LP resummation at LL accuracy relied on two facts: the exponentiation of the soft function before integration over phase space (at squared matrix element level), and the factorisation of phase space for m parton emissions into m decoupled single-parton phase space integrals. This motivates the following schematic

decomposition of the partonic cross section up to NLP, as presented before in ref. [83]

$$\hat{\sigma} = \frac{1}{2s}\left[\int d\Phi_{\text{LP}}\,|\mathscr{M}|^2_{\text{LP}} + \int d\Phi_{\text{LP}}\,|\mathscr{M}|^2_{\text{NLP}} + \int d\Phi_{\text{NLP}}\,|\mathscr{M}|^2_{\text{LP}} + \dots\right]. \tag{4.30}$$

The first term on the right-hand side of eq. (4.30) gives the LP result of section 4.1, integrating the LP squared matrix element with LP phase space, i.e. neglecting correlations between radiated partons. The second term consists of the NLP contribution to the squared matrix element, integrated with LP phase space. The third term consists of the LP matrix element, but where the phase space includes the effect of parton correlations at NLP. Finally, the ellipsis denotes terms which are NNLP and beyond in the threshold expansion. Based on this classification, the task of determining whether LL NLP terms can be resummed amounts to elucidating the relevant structure of the NLP matrix element, as well as considering whether NLP corrections to the LP phase space are important. We consider each of these issues in turn.

4.2.1 Structure of the NLP squared matrix element

We first describe the structure of squared matrix elements at NLP when the hard emitters are *massive*, so that collinear loop effects play no role, following refs. [41, 83] (themselves building on refs. [76,77]). We discussed in section 1.4 that emissions are then considered to be external or internal to a hard interaction, as shown in fig. 1.5a and fig. 1.5b respectively.

As shown for the first time in ref. [41], external emissions can be described by *generalised Wilson lines*, which extend the definition given in eq. (4.11) to NLP in the soft expansion. Along the lines of eq. (4.12), we may write this operator in momentum space as [81]

$$F(p) = \mathscr{P}\exp\left[g_s\mathbf{T}^a\int\frac{d^dk}{(2\pi)^d}\tilde{A}^a_\mu(k)\left(\frac{p^\mu}{p\cdot k} - \frac{k^\mu}{2p\cdot k} + k^2\frac{p^\mu}{2(p\cdot k)^2} + ik_\nu\frac{S^{\nu\mu}}{p\cdot k}\right) + \dots\right] \tag{4.31}$$

for a generalised semi-infinite straight Wilson in the direction of four-momentum p. Here $\mathbf{T}^a$ is a colour generator in the appropriate representation, and $S^{\mu\nu}$ is the generator of Lorentz transformations for the parton under consideration, which vanishes for scalar fields and is given for spin one-half and spin one particles in eq. (1.11). The first term in eq. (4.31) corresponds to the eikonal Feynman rule of eq. (4.12), and the remaining terms (suppressed by one power of the gluon momentum k) correspond to effective next-to-eikonal Feynman rules, describing the emission of a next-to-soft gauge bosons [41], as discussed in section 1.2.

The ellipsis in eq. (4.31) refers to terms involving the emission of a pair of gluons through an effective vertex. These vertices start contributing to the cross section at NNLO, therefore they cannot contribute at leading-logarithmic accuracy at NLP, as was the case at LP. This follows from the fact that the proposed resummation rests upon an amplitude-level factorisation theorem [78, 79, 81], which implies the existence of evolution equations of operator matrix elements. The solution to such equations always leads to a particular pattern of exponentiation, with single logarithms in the exponent generating double logarithms in the

cross section. This implies that all LLs are generated by the one-loop exponent, also at NLP. A test of this argument is provided by ref. [162], where the exponentiation of LLs at NLP was explicitly tested at NNLO. As a further check, we verify in appendix 4.C that next-to-soft Feynman rules for double radiation in eq. (4.31) do no contribute to LLs in the case of DY production at two loops.

Let us now consider the contribution of internal emissions. When massive external particles are being considered, the hard interaction is analytic in the total momentum K of the emitted radiation, and can safely be expanded about the soft limit $K^\mu \to 0$. One may then show, using Ward identities, that the effect of a single internal emission is given by derivatives of the non-radiative amplitude with respect to its external momenta. As has been noted in the context of next-to-soft theorems for gravity amplitudes [188, 189], these derivatives can be organised in terms of the orbital angular momentum operator associated with each external leg, which has the form

$$L_{(i)}^{\nu\mu} = i\left(p_i^\nu \frac{\partial}{\partial p_{i\mu}} - p_i^\mu \frac{\partial}{\partial p_{i\nu}}\right). \tag{4.32}$$

These contributions are depicted in fig. 1.5b and appear as the second term in the factorisation formula of eq. (1.25). Using the definition of the G-polarisation in eq. (1.26), we can readily see that it takes indeed the form of eq. (4.32):

$$\begin{aligned} G_i^{\nu\mu}\frac{\partial}{\partial p_i^\nu} &= \left[\eta^{\nu\mu} - \frac{(2p_i - k)^\mu k^\nu}{2p_i\cdot k}\right]\frac{\partial}{\partial p_i^\nu} \\ &= \frac{k_\nu}{p_i\cdot k}\left[p_i^\nu\frac{\partial}{\partial p_{i\mu}} - p_i^\mu\frac{\partial}{\partial p_{i\nu}}\right] + \mathcal{O}(k) = -\frac{ik_\nu}{p_i\cdot k}L_{(i)}^{\nu\mu} + \mathcal{O}(k)\,, \end{aligned} \tag{4.33}$$

suppressing the NNLP term in the second identity. On each hard leg, this combines with the spin angular momentum contribution to construct the total angular momentum operator $S^{\nu\mu} + L^{\nu\mu} \equiv J^{\nu\mu}$. In ref. [41], the orbital angular momentum contribution was not included in the generalised Wilson line operator of eq. (4.31). Given that the *total* angular momentum is associated to rotational invariance, it might make sense to do so. For practical purposes, however, it remains convenient to keep the orbital angular momentum separate, given that it involves derivatives which have yet to act on the hard interaction.

Armed with the operator defined in eq. (4.31), we may construct the *next-to-soft function*

$$\widetilde{S}\left(z, Q^2, \epsilon\right) = \frac{1}{N_c}\sum_{n\,|\,\mathrm{LP}} \mathrm{Tr}\Big[\big\langle 0\big|F^\dagger(p_1)F(p_2)\big|n\big\rangle\big\langle n\big|F^\dagger(p_2)F(p_1)\big|0\big\rangle\Big]\,\delta\left(z - \frac{Q^2}{s}\right). \tag{4.34}$$

Here we have replaced the Wilson line operators in the LP soft function of eq. (4.10) by their NLP counterparts. The subscript in the sum over final states indicates that all phase space integrals are to be carried out with LP phase space only (i.e. with a measure of integration consisting of a product of single-gluon phase space integrals). Corrections to this will be considered in section 4.2.2. As was the case at LP, the next-to-soft function in eq. (4.34) can be shown to exponentiate using replica trick arguments (see appendix 4.A). However, we must carefully disentangle what this means, given that the generalised Wilson line of

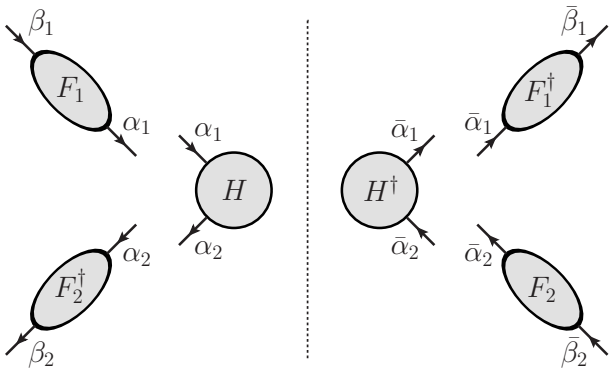

Figure 4.1: *Labelling of spin indices for the squared amplitude, where H is the hard function, and F_i a generalised Wilson line.*

eq. (4.31) is matrix-valued in the spin space of the external hard particles. As an example, consider the spin one-half case, and let us write the non-radiative amplitude for an incoming fermion and antifermion with explicit spin indices $\{\alpha, \beta\}$, as

$$\mathscr{M} = \bar{v}_\alpha(p_2)\, M^{\alpha\beta}\, u_\beta(p_1), \tag{4.35}$$

so that the spin matrix $M^{\alpha\beta}$ is defined by stripping off the initial state wave functions from the full amplitude. It factorises into a product of hard and next-to-soft factors, so that the integrated squared matrix element, dressed by arbitrary amounts of radiation from the next-to-soft function, can be written as

$$\int d\Phi^{(n+1)}\, |\mathscr{M}|^2 = \widetilde{S}^{\,\alpha_1\alpha_2\bar\alpha_1\bar\alpha_2}_{\beta_1\beta_2\bar\beta_1\bar\beta_2}(z, Q^2, \epsilon) \int d\Phi^{(1)} \Big[\bar{v}^{\beta_2}(p_2) H_{\alpha_2\alpha_1} u^{\beta_1}(p_1)\Big]\Big[\bar{u}^{\bar\beta_1}(p_1) H^\dagger_{\bar\alpha_1\bar\alpha_2} v^{\bar\beta_2}(p_2)\Big], \tag{4.36}$$

where the next-to-soft function of eq. (4.34) is now explicitly written as a spin operator

$$\widetilde{S}^{\,\alpha_1\alpha_2\bar\alpha_1\bar\alpha_2}_{\beta_1\beta_2\bar\beta_1\bar\beta_2}(z, Q^2, \epsilon) = \frac{1}{N_c} \sum_{n\,|\,\mathrm{LP}} \Big\langle 0 \Big| F^{\dagger\,\bar\alpha_1}_{\bar\beta_1}(p_1)\, F^{\bar\alpha_2}_{\bar\beta_2}(p_2) \Big| n \Big\rangle \Big\langle n \Big| F^{\dagger\,\alpha_2}_{\beta_2}(p_2)\, F^{\alpha_1}_{\beta_1}(p_1) \Big| 0 \Big\rangle\, \delta\!\left(z - \frac{Q^2}{s}\right). \tag{4.37}$$

The ordering of spinor indices is depicted in fig. 4.1. In eq. (4.36), $d\Phi^{(m)}$ denotes the m-particle Lorentz-invariant phase space measure. We have singled out the integration over the phase space of the heavy vector boson, relying upon the factorisation of the n-body phase space at LP. Note that eq. (4.36) also applies to the case of incoming particles of spin one, if the spinor wave functions are replaced with polarisation vectors, and spinor indices by vector indices.

The discussion so far applies strictly only to the case of massive external particles. When massless particles are involved, it is no longer true that the hard function H is analytic in the momentum carried by soft radiation: it develops logarithmic singularities due to the presence of collinear divergences, which are described by radiative jet functions as discussed in section 1.4 and chapter 2. However, ref. [122] and previous chapters in this thesis provide suggestive evidence that these functions contribute only at sub-leading-logarithmic accuracy, while all LL contributions can be traced to the (next-to-)soft function, if the results are

recast in the present framework. In addition, such hard collinear contributions have also been argued to be subleading in various SCET approaches [96, 98, 167, 190]. We will argue below that LLs at NLP can indeed only arise from momentum regions of integration that are already fully accounted for by the next-to-soft function introduced in eq. (4.31).

To illustrate this point, let us consider first the well-understood situation at LP for comparison. In that case, threshold singularities are directly related to IR singularities of the amplitude. These arise from integrations of the relevant momentum components, the so-called normal variables, near singular surfaces in momentum space, which can be completely characterised to all orders in perturbation theory by means of Landau equations and power-counting techniques [191]. For massless theories, it can be shown in general that IR singularities arise only from soft and collinear momentum configurations. At LP one finds that at n loops there are precisely $2n$ normal variables that must be integrated with a logarithmic measure. In a suitable frame, these can be taken to be n parton energies E_i, with a LP integration measure dE_i/E_i, and n transverse momenta with respect to the directions defined by external particles, $k_{i\perp}$, with a LP integration measure $dk_{i\perp}/k_{i\perp}$. Threshold logarithms in general arise when different combinations of normal variables become small at different rates, but LLs arise only with a very specific scaling, when all energies and transverse momenta are strongly ordered, say $E_1 \ll \ldots \ll E_n$ and $k_{1\perp} \ll \ldots \ll k_{n\perp}$.[4] In that limit, the $2n$ logarithmic integrations yield contributions of the form $\ln^{2n-1}(1-z)/(1-z)$, since the last logarithmic integration is not performed when computing $d\hat{\sigma}/dz$.

If either the phase-space measure or the squared matrix element provides a single power of one of the normal variables, only $2n-1$ momentum components are integrated with a logarithmic measure. Once again, the most divergent contributions will arise from the configuration where the remaining normal variables are strongly ordered. Now, two possibilities arise. On the one hand, the normal variable whose integration has become non-singular can be a transverse momentum, in which case the corresponding parton is soft, but not strictly collinear. This would lead to a subleading logarithmic contribution at LP, such as $\log^{2n-2}(1-z)/(1-z)$. This configuration is in fact accounted for by the LP soft function, which also describes *wide-angle* soft gluons. On the other hand, the suppressed variable can be an energy, while all transverse momenta are still strongly ordered. Such next-to-soft, collinear configurations are accounted for by the next-to-soft function defined in eq. (4.34) and give the NLP LL contribution $\log^{2n-1}(1-z)$, where the remaining integration over z will not introduce a further singularity.

Notice that radiative jet functions such as the one computed in ref. [79] also contain the next-to-soft, collinear configuration: this, however, contributes to a double counting that must be explicitly subtracted, either by introducing eikonal jets, as done in eq. (4.7), or by defining an appropriate counterterm, as done for example in ref. [81]. The subtracted

[4] This property is not special to threshold resummation, but underlies the understanding of leading-logarithmic singularities in variety of kinematical situations: classic applications involve the ladder-based derivation of the DDT formula for the resummed DY transverse momentum distribution [192], the resummation of leading collinear logarithms in ref. [193], the ladder resummation of Sudakov behaviour in [29] and the treatment of leading high-energy logarithms (see e.g. the pedagogical discussion in ref. [194]).

radiative jet function then contains only hard collinear configurations for all virtual partons as well as (next-to-)soft real emissions, and cannot contribute at leading-logarithmic accuracy. An explicit example and test of the above discussion is provided in ref. [81], where the non-abelian radiative jet function for quarks was computed at one-loop order, and the overlap between (next-to-)soft and collinear emissions was explicitly identified. Furthermore, a large class of (N)LP threshold effects has been calculated in DY production at NNLO in ref. [122] and N^{3}LO in chapter 3, where hard collinear effects are indeed found to be associated with NLL terms and beyond. Notice that, as discussed above, upon exponentiation LLs at NLP must be generated by one-loop contributions: the results of refs. [1, 81, 122] therefore provide a complete test of our argument for the DY process.

To summarise, NLP contributions to squared matrix elements can be categorised into two main types, as follows:

(i) *Next-to-soft emissions*. These are captured by the next-to-soft function, defined in terms of generalised Wilson lines in eq. (4.34), together with the orbital angular momentum contributions associated with internal emissions as depicted in fig. 1.5b. The next-to-soft function exponentiates (see appendix 4.A), as did the LP soft function.

(ii) *Collinear contributions*. These originate from collinearly enhanced regions, as shown in fig. 1.5c, and are described by radiative jet functions, which overlap with the next-to-soft function. Upon removing the double counting, the remaining collinear effects do not contribute at LL accuracy.

In this section, we have discussed the second term on the right-hand side of eq. (4.30), and argued that the next-to-soft emissions are the only contributions to the NLP matrix element that can result in LL terms in the cross section. We must also check whether or not LL terms can arise from the phase space integration of the LP matrix element, once correlations between radiated gluons are included. This is the subject of the following section.

4.2.2 NLP phase space correction

The third term in eq. (4.30) consists of the LP matrix element integrated over the NLP phase space. To see whether or not this term can give LL contributions at NLP, it is sufficient to take the LL contribution to the LP matrix element at each order, and then evaluate the phase space integral up to NLP. The LL contributions to the matrix element have already been discussed in section 4.1, and involve exponentiating the NLO eikonal squared matrix element. This generates terms with $n \geq 1$ gluon emissions, and, according to eq. (4.10), one must then integrate each such term over the n-gluon phase space. Considering all possible contributions to an n-gluon final state yields a squared matrix element of the form

$$|\mathscr{M}|^2_{\mathrm{LP,n}} = f\left(\alpha_s, \epsilon, \mu^2\right) \prod_{i=1}^{n} \frac{p_1 \cdot p_2}{p_1 \cdot k_i \, p_2 \cdot k_i}, \tag{4.38}$$

where the prefactor $f(\alpha_s,\epsilon,\mu^2)$ collects coupling dependence, possible poles in ϵ due to the integration over loop momenta, and final state combinatorial factors. The explicit form of this function is irrelevant for what follows. We must now integrate eq. (4.38) over the $(n+1)$-body phase space, consisting of n gluons, as well as the electroweak vector boson that defines the final state at LO. We note that a similar phase space integral is carried out in great detail in appendix 3.B, for a two-gluon final state. The integration measure reads

$$d\Phi^{(n+1)} = \left[\prod_{i=1}^{n}\int\frac{d^dk_i}{(2\pi)^{d-1}}\,\delta_+(k_i^2)\right](2\pi)\,\delta\left[s-Q^2+\sum_{i=1}^{n}\left(-2k_i\cdot(p_1+p_2)+\sum_{j=1}^{i-1}2k_i\cdot k_j\right)\right], \quad (4.39)$$

where the integration of the vector boson momentum has already been carried out, using the overall momentum conservation delta function. In order to compute the integral, it is particularly convenient to use the Sudakov decomposition of eq. (4.15) for each momentum k_i. One finds

$$\int d\Phi^{(n+1)}|\mathscr{M}|^2_{\text{LP,n}} = f(\alpha_s,\epsilon,\mu^2)\,\frac{2\pi}{s}\left[\prod_{i=1}^{n}\int_0^\infty\frac{dk_i^+}{k_i^+}\int_0^\infty\frac{dk_i^-}{k_i^-}\int\frac{d^{d-2}\boldsymbol{k}_{i\perp}}{(2\pi)^{d-1}}\,\delta\left(2k_i^+k_i^--\boldsymbol{k}_{i\perp}^2\right)\right]$$
$$\times\,\delta\left[1-z+\sum_{i=1}^{n}\left(-\frac{(k_i^++k_i^-)}{\sqrt{s/2}}+2\sum_{j=1}^{i-1}\frac{k_i^+k_j^-+k_i^-k_j^+-\boldsymbol{k}_{i\perp}\cdot\boldsymbol{k}_{j\perp}}{s}\right)\right]. \quad (4.40)$$

In order to proceed, we represent the delta function in the second line of eq. (4.40) using

$$\delta(x) = \int_{-i\infty}^{i\infty}\frac{d\omega}{2\pi i}\,\mathrm{e}^{\omega x}. \quad (4.41)$$

We may then rewrite eq. (4.40) as

$$\int d\Phi^{(n+1)}\,|\mathscr{M}|^2_{\text{LP,n}} = f(\alpha_s,\epsilon,\mu^2)\,\frac{2\pi}{s}\int_{-i\infty}^{i\infty}\frac{d\omega}{2\pi i}\,\mathrm{e}^{\omega(1-z)}\left[\prod_{i=1}^{n}\int_0^\infty\frac{dk_i^+}{k_i^+}\int_0^\infty\frac{dk_i^-}{k_i^-}\int\frac{d^{d-2}\boldsymbol{k}_{i\perp}}{(2\pi)^{d-1}}\right.$$
$$\left.\times\,\mathrm{e}^{-\frac{\omega}{\sqrt{s/2}}(k_i^++k_i^-)}\,\delta\left(2k_i^+k_i^--\boldsymbol{k}_{i\perp}^2\right)\right]\left(1+\frac{2\omega}{s}\sum_{i,j=1}^{n;\,i-1}k_i^+k_j^-+k_i^-k_j^+-\boldsymbol{k}_{i\perp}\cdot\boldsymbol{k}_{j\perp}+\mathscr{O}\left(k^4\right)\right), \quad (4.42)$$

where in the second line we Taylor-expanded the term in the exponent that is quadratic in soft momentum, anticipating that higher order contributions will correspond to subleading powers of $(1-z)$ in the final result. The term proportional to ω corresponds to a phase space correlation between pairs of gluons that is absent at LP. Thus, this term constitutes the "NLP phase space" correction referred to in eq. (4.30). The term involving the transverse momenta leads to an odd integrand in each $\boldsymbol{k}_{i\perp}$ in eq. (4.42), and will therefore give a vanishing contribution to the final result. We can then carry out the remaining transverse momentum integrals, and subsequently make the transformation $\tilde{k}_i^\pm = \frac{\omega}{\sqrt{s/2}}k_i^\pm$, to obtain

$$\int d\Phi^{(n+1)}\,|\mathscr{M}|^2_{\text{LP,n}} = f(\alpha_s,\epsilon,\mu^2)\,\frac{2\pi}{s}\int_{-i\infty}^{i\infty}\frac{d\omega}{2\pi i}\,\mathrm{e}^{\omega(1-z)}\left[\prod_{i=1}^{n}\frac{\Omega_{d-2}}{(2\pi)^{d-1}}\frac{s^{\frac{d-4}{2}}}{2}\frac{1}{\omega^{d-4}}\right.$$

$$\times \int_0^\infty dk_i^+ \, \mathrm{e}^{-\tilde{k}_i^+} (\tilde{k}_i^+)^{\frac{d-6}{2}} \int_0^\infty dk_i^- \, \mathrm{e}^{-\tilde{k}_i^-} (\tilde{k}_i^-)^{\frac{d-6}{2}} \Bigg] \Bigg(1 + \frac{1}{\omega} \sum_{i,j=1}^{n;\, i-1} \tilde{k}_i^+ \tilde{k}_j^- + \tilde{k}_i^- \tilde{k}_j^+ + \mathscr{O}\left(\omega^{-2}\right) \Bigg). \quad (4.43)$$

Next, the $k_{i\pm}$ integrals can be straightforwardly carried out to give

$$\int d\Phi^{(n+1)} |\mathscr{M}|^2_{\mathrm{LP,n}} = f(\alpha_s, \epsilon, \mu^2) \, \frac{\Omega_{d-2}^n \, s^{n\frac{(d-4)}{2}-1}}{2^{nd-1} \, \pi^{n(d-1)-1}} \int_{-i\infty}^{i\infty} \frac{d\omega}{2\pi i} \, \frac{1}{\omega^{n(d-4)}} \, \mathrm{e}^{\omega(1-z)} \Bigg[\Gamma^{2n}\Big(\frac{d-4}{2}\Big) + \frac{n(n-1)}{\omega} \, \Gamma^{2n-2}\Big(\frac{d-4}{2}\Big) \Gamma^2\Big(\frac{d-2}{2}\Big) + \mathscr{O}\Big(\frac{1}{\omega^{n(d-4)+2}}\Big) \Bigg]. \quad (4.44)$$

The integral in ω is recognisable as an inverse Laplace transform (see eq. (3.59)), which yields the result

$$\int d\Phi^{(n+1)} |\mathscr{M}|^2_{\mathrm{LP,n}} = f(\alpha_s, \epsilon, \mu^2) \, \frac{\Omega_{d-2}^n \, s^{n\frac{d-4}{2}-1}}{2^{nd-1} \, \pi^{n(d-1)-1}} \, \frac{\Gamma^{2n}[(d-4)/2]}{\Gamma[n(d-4)]} \, (1-z)^{n(d-4)-1} \times \Big(1 + \frac{(n-1)(d-4)(1-z)}{4} + \mathscr{O}\big[(1-z)^2\big] \Big). \quad (4.45)$$

Note that the terms $\mathscr{O}(k^4)$ we have neglected in expanding the exponential factor in eq. (4.42) give indeed subleading power corrections in $(1-z)$, justifying the approximation made above. Eq. (4.45) is the final result of integrating the LP contribution to the matrix element responsible for LL terms, with the multigluon phase-space measure expanded to NLP. The second term in the last line of eq. (4.45) is the desired NLP correction, as it is suppressed by a single power of $(1-z)$. Furthermore, it contains an explicit factor of $d-4 = -2\epsilon$, which directly implies that the phase space correction does not affect LL terms, which are associated with the most singular poles in ϵ.

In summary, we have shown that the third term in eq. (4.30), consisting of the LP matrix element dressed with NLP phase space corrections, does not contribute to LL terms at NLP. It can thus be neglected for the purposes of this chapter. Combining this observation with the results of the previous section, we now have everything we need to perform an explicit resummation of LL NLP threshold logarithms in DY production. We turn to this task in the next section.

4.3 Resummation of NLP LL terms in Drell-Yan production

In the previous sections, we have seen that LL contributions at NLP are governed by next-to-soft radiation. This in turn is captured by the next-to-soft function defined in eq. (4.34), possibly complemented by contributions involving the orbital angular momentum of each incoming parton. In this section, we apply these ideas to resum LL NLP terms in DY production. While very interesting in its own right, this example also serves as a useful warm-up

case for two reasons. Firstly, it will allow us to make contact with the LP treatment of section 4.1. Secondly, in this case the hard interaction is particularly simple at leading order, as there is no dependence on the external momenta. Thus, we do not have to worry about orbital angular momentum contributions at LL accuracy, and it is sufficient to calculate the next-to-soft function. Once this has been calculated for single radiation, it may be exponentiated (as at LP), yielding the resummation formula that we are seeking.

For the first steps of our derivation, we do not need to specify the final-state particle content of the process we are studying. Rather, we will consider a general hard interaction H connecting to an incoming $q\bar{q}$ pair, such that the LO amplitude is given by eq. (4.35). Representative diagrams contributing to the squared amplitude arising from the next-to-soft function at NLO, eq. (4.36), are shown in figure 4.2. We may directly evaluate them using the Feynman rules arising from eq. (4.31). First, we may note that contributions involving k^2 vanish, since the radiated gluon is on shell. Next, it is convenient to combine the scalar-like and spin-dependent emission vertices as

$$\frac{k^\mu}{2p_i\cdot k} - ik_\nu \frac{\Sigma^{\nu\mu}}{p_i\cdot k} = \frac{\not{k}\gamma^\mu}{2p_i\cdot k}\,. \tag{4.46}$$

Then, the diagrams of figure 4.2 yield a NLP contribution

$$\begin{aligned}|\mathscr{M}|^2_{\text{NLP, (a)+(b)}} &= 2g_s^2 C_F \left(\frac{p_1^\mu}{p_1\cdot k} - \frac{p_2^\mu}{p_2\cdot k}\right) \mathrm{Tr}\left[\not{p}_2 H \left(\frac{\not{k}\gamma_\mu}{2p_1\cdot k}\right)\not{p}_1 H^\dagger\right] \\ &= -\frac{g_s^2 C_F}{p_1\cdot k\, p_2\cdot k}\,\mathrm{Tr}\left[\not{p}_2 H\,\not{k}\,\not{p}_2\,\not{p}_1 H^\dagger\right], \end{aligned} \tag{4.47}$$

where a factor of two is included to account for the complex conjugate diagrams. Note that the contribution from fig. 4.2b is no longer present in the second line because of the resulting factor $\not{p}_1\not{p}_1 = 0$ in the trace. In order to extract the LO squared amplitude, we may use an argument similar to one presented recently in ref. [84]. In the spirit of eq. (4.15), we decompose $\not{k}$ in terms of $\not{p}_1$ and $\not{p}_2$ in the following way

$$\not{k} = \frac{p_2\cdot k}{p_1\cdot p_2}\,\not{p}_1 + \frac{p_1\cdot k}{p_1\cdot p_2}\,\not{p}_2 + \not{k}_\perp\,. \tag{4.48}$$

Substitution into eq. (4.47) reveals that the term involving transverse momentum occurs linearly in the squared matrix element, leading to an odd integrand which vanishes upon integrating over $k_\perp$. This contribution can thus be ignored, leading effectively to the expression

$$|\mathscr{M}|^2_{\text{NLP, (a)+(b)}} = -\frac{2g_s^2 C_F}{p_1\cdot k}\,\mathrm{Tr}\left[\not{p}_2 H\,\not{p}_1 H^\dagger\right]. \tag{4.49}$$

We now see that the LO squared matrix element is factored out in eq. (4.49). Combining this with diagrams obtained from those in figure 4.2 by interchanging p_1 with p_2, summing over spins and colours, and dividing out the LO partonic cross section one easily obtains an expression for the real emission contribution to the one-loop next-to-soft function. We emphasise that at NLP singularities as $z \to 1$ are integrable, such that there is no need to

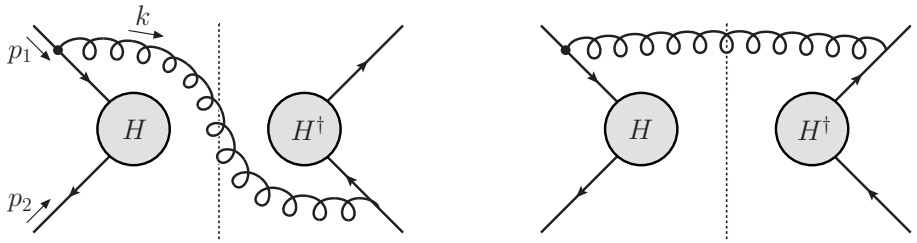

Figure 4.2: *Diagrams contributing to a squared amplitude with a $q\bar{q}$ initial state, arising from the next-to-soft function $\tilde{S}$ acting on the LO hard interaction H, as in eq. (4.36). NE vertices are indicated with a dot. Further diagrams are obtained by reflection about the final state cut, and/or by interchanging $p_1 \longleftrightarrow p_2$.*

include virtual corrections in order to generate LL contributions. The NLP soft function we require is thus given by

$$\begin{aligned} S^{(1)}_{\rm NLP}\left(z,Q^2,\epsilon\right) &= -2\mu^{2\epsilon} g_s^2 C_F \int \frac{d^d k}{(2\pi)^{d-1}}\,\delta_+(k^2)\,\delta\!\left(1-z-\frac{2k\cdot(p_1+p_2)}{s}\right)\!\left(\frac{1}{p_1\cdot k}+\frac{1}{p_2\cdot k}\right) \\ &= -\frac{2\alpha_s C_F}{\pi}\left(\frac{\bar{\mu}^2}{Q^2}\right)^{\epsilon} \frac{e^{\epsilon\gamma_E}\,\Gamma^2(-\epsilon)}{\Gamma(1-\epsilon)\,\Gamma(-2\epsilon)}\,(1-z)^{-2\epsilon}\,. \end{aligned} \tag{4.50}$$

where the phase space integral is carried out straightforwardly using the Sudakov decomposition of eq. (4.15), and the subsequent change of variables in eq. (4.18). Taking the Mellin transform we find

$$\begin{aligned} S^{(1)}_{\rm NLP}\left(N,Q^2,\epsilon\right) &= -\frac{2\alpha_s C_F}{\pi}\left(\frac{\bar{\mu}^2}{Q^2}\right)^{\epsilon} \frac{e^{\epsilon\gamma_E}\Gamma(-\epsilon)\Gamma(N)}{\Gamma(1-2\epsilon+N)} \\ &= \frac{2\alpha_s C_F}{\pi}\left(\frac{\bar{\mu}^2}{Q^2}\right)^{\epsilon} \frac{1}{N}\left[\frac{1}{\epsilon}+2\psi^{(0)}(N+1)+2\gamma_E\right]+\mathcal{O}(\epsilon)\,. \end{aligned} \tag{4.51}$$

The leading behaviour as $N\to\infty$ is

$$S^{(1)}_{\rm NLP}\left(N,Q^2,\epsilon\right) = \frac{2\alpha_s C_F}{\pi}\left(\frac{\bar{\mu}^2}{Q^2}\right)^{\epsilon}\left[\frac{1}{\epsilon}\frac{1}{N}+\frac{2\log N}{N}+\ldots\right], \tag{4.52}$$

where the ellipsis denotes terms which are non-singular in ϵ and non-logarithmic in N, as well as terms suppressed by further powers of N. We see that the NLP soft function generates contributions which are suppressed by (at least) a single power of N compared to LP, as expected. We must now combine eq. (4.52) with the LP soft function given in eq. (4.29), which itself includes subleading terms in N-space arising from the Mellin transformation from z-space. The result is

$$S_{\rm LP+NLP}\left(N,Q^2,\epsilon\right) = \frac{2\alpha_s C_F}{\pi}\left(\frac{\bar{\mu}^2}{Q^2}\right)^{\epsilon}\left[\frac{1}{\epsilon}\left(\log N+\frac{1}{2N}\right)+\log^2 N+\frac{\log N}{N}\right]. \tag{4.53}$$

As explained above, we may directly exponentiate eq. (4.53) and combine it with the LO cross section to resum the leading-logarithmic terms at LP and NLP. We subsequently absorb

the residual collinear pole in the PDFs, generalising eq. (4.27), by defining

$$q_{\text{LL, NLP}}\big(N,Q^2\big) = q(N,Q^2)\exp\left[\frac{\alpha_s C_F}{\pi}\frac{1}{\epsilon}\left(\log N + \frac{1}{2N}\right)\right], \tag{4.54}$$

and similarly for the antiquark. The resummed cross section up to NLP in the threshold expansion and at LL accuracy then becomes

$$\begin{aligned}\int_0^1 d\tau\,\tau^{N-1}\,\frac{d\sigma_{\text{DY}}}{d\tau}\bigg|_{\text{LL, NLP}} &= \sigma_0(Q^2)\,q_{\text{LL, NLP}}\big(N,Q^2\big)\,\bar{q}_{\text{LL, NLP}}\big(N,Q^2\big)\\ &\quad\times\exp\left[\frac{2\alpha_s C_F}{\pi}\left(\log^2 N + \frac{\log N}{N}\right)\right].\end{aligned} \tag{4.55}$$

Upon expanding the exponential factor in powers of α_s, we may perform the inverse Mellin transform of the partonic cross section order by order, using the results of appendix 4.B, to get

$$\Delta^{\text{LL}}_{\text{LP+NLP}}(z) = \sum_{m=1}^{\infty}\left(\frac{2\alpha_s C_F}{\pi}\right)^m \frac{1}{(m-1)!}\left[2\left(\frac{\log^{2m-1}(1-z)}{1-z}\right)_+ - 2\log^{2m-1}(1-z)\right]. \tag{4.56}$$

This is in complete agreement with the result of ref. [146], which argued (consistent with previous observations in refs. [155, 162]) that the LL NLP terms at any order have a coefficient which is always the negative of that of the corresponding leading-logarithmic plus distribution. Our result provides independent proof thereof. The origin of this phenomenon can be traced to the coefficient of the ϵ pole in eq. (4.52). Given that this pole represents a collinear singularity that must be absorbed in the parton distributions, it has to emerge from the NLP contribution to the LO DGLAP splitting kernel that governs such terms. More specifically, the collinear poles in the NLO DY cross section have the form $-2\,P^{(0)}_{qq}/\epsilon$ (see e.g. ref. [195]), where the factor of two arises from having collinear singularities associated with either of the incoming partons. The splitting function can be expanded near threshold as

$$P^{(0)}_{qq}(z) = \frac{\alpha_s}{2\pi}\,C_F\left[\frac{2}{(1-z)_+} - 2 + \dots\right]. \tag{4.57}$$

where the second term gives the NLP contribution in z-space, whose Mellin transform is

$$\int_0^1 dz z^{N-1}\;P^{(0)}_{qq}(z)\Big|_{\text{NLP}} = -\frac{\alpha_s C_F}{\pi}\frac{1}{N}. \tag{4.58}$$

We thus expect the collinear pole of the NLP contribution to the next-to-soft function in Mellin space to be given by

$$\frac{2\,\alpha_s\,C_F}{\pi}\,\frac{1}{N}\,\frac{1}{\epsilon}, \tag{4.59}$$

which is indeed observed in eq. (4.52), and in momentum space in eq. (4.50). We see that the next-to-soft function correctly generates the NLP correction to the splitting kernel. This in turn dictates the LL behaviour in the finite part: in z-space, this contribution arises

completely from an overall ϵ-dependent power of $(1-z)$, dressing the pole term. Thus, ensuring that the NLP behaviour of the pole term is correct is sufficient to describe the finite part as well.

Equation (4.55) resums the leading-logarithmic behaviour of the DY cross section at LP and NLP in the threshold expansion: it completely agrees with expectations from the literature [146, 162], as well as with the recent SCET analysis of ref. [167]. We emphasise that, of course, at LP there is no need to limit the resummation to LLs. This was done in eq. (4.55) only for simplicity, and to underline the close connection between LL terms at LP and NLP. Because of the link discussed above between NLP LLs and the DGLAP kernels, it is straightforward to incorporate our results in the standard LP resummation formalism: it is sufficient to include NLP terms in the quark splitting function. This was argued to be appropriate in refs. [146,155,162], and, with the mild assumptions discussed in section 4.2.1, it is now proven. For completeness, we include here the general resummation ansatz introduced in ref. [162], which implements this change in the classic threshold resummation formula of refs. [48,49,196], together with other proposed modifications that have effects on subleading NLP logarithms. In Mellin space, the result of ref. [162] for the DY process can be written as

$$\ln\Big[\Delta(N,Q^2)\Big] = F_{\rm DY}\Big[\alpha_s(Q^2)\Big] + \int_0^1 dz\, z^{N-1}\left\{\frac{1}{1-z}\,D\Big[\alpha_s\Big(\frac{(1-z)^2Q^2}{z}\Big)\Big] + 2\int_{Q^2}^{(1-z)^2Q^2/z}\frac{dq^2}{q^2}\,P_{qq}^{\rm LP+NLP}\Big[z,\alpha_s(q^2)\Big]\right\}_+ . \tag{4.60}$$

In eq. (4.60), $D(\alpha_s)$ is the well-known LP wide-angle soft function for DY, which has been computed up to three loops [59, 197–199], $F_{\rm DY}(\alpha_s)$ resums N-independent contributions following ref. [200], and $P_{qq}^{\rm LP+NLP}(z,\alpha_s)$ is the soft expansion of the DGLAP splitting function up to NLP, order by order in perturbation theory, which was derived in ref. [162] starting from the results of ref. [201]. Furthermore, the overall plus prescription is defined to apply only to LP contributions, that are singular as $z\to 1$. Leading NLP logarithms in eq. (4.60) are generated by the one-loop NLP contribution to $P_{qq}^{\rm LP+NLP}$, as discussed in this section. Higher order terms in the NLP splitting function will contribute to, but not exhaust, subleading NLP logarithms. For example, the phase space boundary and argument of the coupling in eq. (4.60), which correspond to an exact rather than a LP definition of the soft scale of the process, also contribute to subleading logarithms at NLP. Yet other subleading logarithmic contributions at NLP would come from the radiative jet functions.

In ref. [162], the accuracy of eq. (4.60) was tested by comparing its expansion to NNLO with existing exact results. As expected from our discussion, NLP LLs are exactly predicted. Furthermore, they observed that next-to-leading NLP logarithms are predicted quite accurately, and they mostly arise from the NLO contribution to the NLP splitting function. The small discrepancy arising at this level of accuracy (NLL at NLP) between the resummation and the finite order result shows the need to include radiative jet functions at NLP. Although accounting for such effects in a resummation formula would be the ultimate goal of our

NLP studies we will apply the current framework first, and shall use eq. (4.60) to study the numerical effects of LL resummation at NLP in chapter 5.

4.4 NLP LL resummation for general quark-initiated colour-singlet production

In section 4.3 we have seen how to resum the highest power of threshold logarithms at NLP, for the specific case of DY production. In fact, the result can be generalised to the production of N colour-singlet particles (of which the LO cross section may be loop-induced), with a $q\bar{q}$ initial state. Crucial to our arguments throughout this chapter is the exponentiation of the soft function (up to NLP) in terms of webs [41, 83], which implies that the next-to-soft function has the schematic form[5]

$$S_{\text{NLP}} = \exp\left[\sum_i W_{\text{LP}}^{(i)} + \sum_j W_{\text{NLP}}^{(j)}\right], \tag{4.61}$$

where the first sum is over LP webs, composed entirely with eikonal Feynman rules, and the second sum is over NLP webs with at most one NE vertex. However, one should realise that if we are only interested in NLP terms in the final result for the cross section, we do not have to exponentiate the NLP webs, as expanding eq. (4.61) in powers of the coupling will generate quadratic and higher powers of the NLP term, which contribute at NNLP and beyond. Thus up to NLP, we may replace eq. (4.61) with

$$S_{\text{NLP}} = \exp\left[\sum_i W_{\text{LP}}^{(i)}\right]\left(1 + \sum_j W_{\text{NLP}}^{(j)}\right). \tag{4.62}$$

This expression shows us that, in order to generate a contribution to the highest power of the NLP logarithm at any given order, we must take the leading-logarithmic behaviour from the NLP web term, namely the contribution proportional to $\alpha_s \log(N)/N$, and dress this with the LLs coming from the LP soft function. Note in particular that the webs $W_{\text{NLP}}^{(i)}$ do not contain terms of the type $\alpha_s^p \log^{2p-1}(N)/N$, such terms will arise in the cross section only through the expansion of the exponential in eq. (4.61), precisely through the interference between LP and NLP webs. We can see this directly in eq. (4.55) for DY production: upon Taylor-expanding in α_s, the leading logarithm at NLP comes from a single instance of the leading NLP log at $\mathcal{O}(\alpha_s)$, dressed by arbitrary powers of the LL at LP. The insight that we need the NLP contribution just once will be key in what follows.

For arbitrary processes, we must include an additional next-to-soft contribution, associated with the orbital angular momentum of incoming particles. To this end, let us consider

[5] In previous sections our phrasing has been somewhat inexact, in that we talked about the exponentiation of the NLO (N)LP soft function itself. Given that at LL accuracy the required webs coincide with the diagrams that contribute to the NLO (N)LP soft function, this is in fact equivalent. In general, however, webs are particular (next-to-)soft diagrams that enter the exponent with modified colour factors (see appendix 4.A).

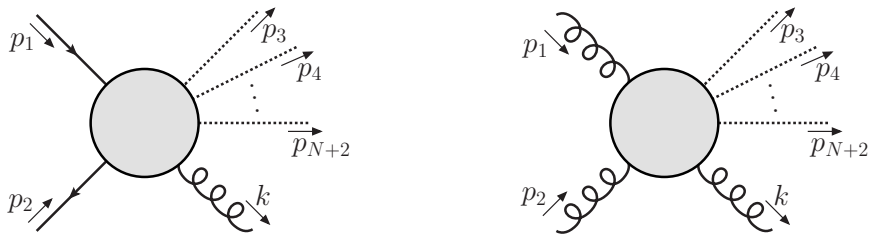

Figure 4.3: *Production of N colour-singlet particles with either a $q\bar{q}$ or gg initial state.*

the effect of a single emission from the non-radiative amplitude. This has been examined recently in ref. [84], and we will present a short summary of that discussion here, before commenting on the consequences for the present study. We label momenta as shown in fig. 4.3a, and we write the LO non-radiative amplitude for a $q\bar{q}$-initiated process as

$$\mathscr{M}_{\text{LO}}^{(q\bar{q})}\big(\{p_i\}\big) = \bar{v}(p_2)\, M_{\text{LO}}^{(q\bar{q})}\big(\{p_i\}\big) u(p_1) = \bar{v}(p_2)\, H_{\text{LO}}^{(q\bar{q})}\big(\{p_i\}\big) u(p_1)\,. \tag{4.63}$$

where $\{p_i\}$ are the incoming and outgoing momenta of, respectively, the initial state partons and the those particles that define the LO final state. We also point out that the LO hard function H_{LO} coincides with the LO stripped matrix element $M_{\text{LO}}^{(q\bar{q})}$. Let us now consider the *radiative* amplitude with external wave functions removed, which we denote by $M_{\sigma}^{(q\bar{q}g)}$. As shown in ref. [84], this amplitude can be decomposed (up to NLP) as

$$M_{\text{NLP}}^{(q\bar{q}g)\sigma} = M_{\text{scal.}}^{(q\bar{q}g)\sigma} + M_{\text{spin}}^{(q\bar{q}g)\sigma} + M_{\text{orb.}}^{(q\bar{q}g)\sigma}\,, \tag{4.64}$$

where the first (second) term on the right-hand side originates from the spin-independent (spin-dependent) part of the next-to-soft function, while the third term corresponds to the orbital angular momentum contribution discussed in section 4.2.1. The squared single emission amplitude, summed over colours and spins, is then given by

$$\Big|\mathscr{M}_{\text{NLP}}^{(q\bar{q}g)}\Big|^2\big(p_1,p_2,k\big) = -\sum_{\text{colours}} \text{Tr}\Big[\not{p}_2\, M_{\text{NLP}}^{(q\bar{q}g)\sigma}\not{p}_1\, M_{\text{NLP},\,\sigma}^{(q\bar{q}g)\dagger}\Big]\,, \tag{4.65}$$

where we conveniently summed over physical and non-physical polarisations alike, using

$$\sum_{\lambda} \varepsilon_{\sigma}^{(\lambda)}(k)\, \varepsilon_{\tau}^{(\lambda)*}(k) = -\eta_{\sigma\tau}\,, \tag{4.66}$$

requiring one to include diagrams with final state ghost to subtract the latter. Such diagrams contribute to the squared amplitude only at NNLP and beyond, as the ghost emission vertices are proportional to the soft momentum, and can be omitted in practice. Likewise, we neglect NNLP terms that arise from squaring NLP contributions in eq. (4.65).

The various contributions to eq. (4.64) have been calculated explicitly in ref. [84], and it was shown that one can express eq. (4.65), at NLP accuracy, as

$$\Big|\mathscr{M}_{\text{NLP}}^{(q\bar{q}g)}\Big|^2(p_1,p_2,k) = g_s^2 C_F \frac{s}{p_1\cdot k\, p_2\cdot k}\Big|\mathscr{M}_{\text{LO}}^{(q\bar{q})}\Big|^2\big(p_1+\delta p_1, p_2+\delta p_2\big)\,, \tag{4.67}$$

where initial state momenta in the LO matrix element have been shifted according to

$$\delta p_1 = -\frac{1}{2}\left(\frac{p_2\cdot k}{p_1\cdot p_2}p_1^\alpha - \frac{p_1\cdot k}{p_1\cdot p_2}p_2^\alpha + k^\alpha\right), \quad \delta p_2 = -\frac{1}{2}\left(\frac{p_1\cdot k}{p_1\cdot p_2}p_2^\alpha - \frac{p_2\cdot k}{p_1\cdot p_2}p_1^\alpha + k^\alpha\right). \tag{4.68}$$

The NLP squared amplitude for single real emission (summed over colours and spins) thus consists of an overall eikonal factor dressing the LO squared amplitude, whose incoming momenta are shifted according to eq. (4.68). Note that the shifts of eq. (4.68) include more physics than is captured solely by the next-to-soft function: they also contain the orbital angular momentum contributions of eq. (4.64). In fact, for a gg-induced process the derivation of this result is quite straightforward, given that no spin part is present (see ref. [84]). In that case the interference term between the $M^{(q\bar{q}g)}_{\text{orb.}}$ and $M^{(q\bar{q}g)}_{\text{scal.}}$ is the sole NLP contribution, and the orbital angular momentum operator is easily recognised as a first order term in the Taylor expansion of eq. (4.67) about $\mathscr{M}^{(q\bar{q})}_{\text{LO}}(p_1,p_2)$. As a result the partonic Mandelstam invariant s is rescaled according to

$$s = (p_1+p_2)^2 \quad\longrightarrow\quad (p_1+\delta p_1+p_2+\delta p_2)^2 = (p_1+p_2-k)^2 = zs\,, \tag{4.69}$$

where, in the case of an N particle final state, the threshold variable z is defined by

$$z = \frac{P^2}{s} \quad \text{for} \quad P^\mu = \sum_{i=3}^{N+2} p_i^\mu\,, \tag{4.70}$$

satisfying the momentum conservation condition $p_1^\mu + p_2^\mu = P^\mu + k^\mu$. Crucially for what follows, all NLP effects in the matrix element are absorbed in the momentum shift, so that the prefactor in eq. (4.67) simply dresses the shifted matrix element with a LP soft emission.

To illustrate the workings of eq. (4.67), we apply the procedure to DY production. In that case the shift in the LO matrix element amounts to

$$\begin{aligned} &|\mathscr{M}^{q\bar{q}}_{\text{DY;LO}}|^2(p_1,p_2) = (4\pi\alpha)\,e_q^2\,N_c\,(1-\epsilon)s \\ \longrightarrow\quad &|\mathscr{M}^{q\bar{q}}_{\text{DY;LO}}|^2(p_1+\delta_{p_1},p_2+\delta_{p_2}) = (4\pi\alpha)\,e_q^2\,N_c\,(1-\epsilon)(zs)\,, \end{aligned} \tag{4.71}$$

thus generating an overall factor of z, which we can express as $z = 1-(1-z)$. This shows immediately that the NLP coefficient in eq. (4.67) at $\mathscr{O}(\alpha_s)$ is equal but of opposite sign as the LP terms, consistent with the result in eq. (4.56).

We may obtain the partonic cross section for the single real emission contribution by integrating over the phase space and including flux and spin/colour averaging factors. The phase space for the $(N+1)$-body final state may be written in factorised form as

$$\int d\Phi_{N+1}(P+k;p_3,\ldots,p_{N+2},k) = \int\frac{dP^2}{2\pi}\int d\Phi_2(P+k;P,k)\int d\Phi_N(P;p_3,\ldots,p_{N+2})\,, \tag{4.72}$$

namely as the convolution of a two-body phase space for the gluon momentum k and the total momentum P carried by colour-singlet particles, with the subsequent decay of the latter

into the individual momenta $\{p_i\}$ for $i = \{1, N+2\}$. We may now recognise the integral of eq. (4.67) over the two-body phase space as the real part of the LP soft function calculated in section 4.1. Then, the NLP partonic cross section for the radiative $q\bar{q}$-initiated process be expressed as

$$\hat{\sigma}^{(q\bar{q})}_{\text{NLP}}(z,\epsilon) = z\, S^{(1)}_{\text{LP;R}}(z,\epsilon)\, \hat{\sigma}^{(q\bar{q})}_{\text{LO}}(zs)\,. \tag{4.73}$$

Note that we include an explicit factor z in eq. (4.73), so that we can introduce a shifted flux factor to express the LO partonic cross section with shifted kinematics entirely. It is given by

$$\hat{\sigma}^{(q\bar{q})}_{\text{LO}}(zs) = \frac{1}{2(zs)}\frac{1}{4N_c^2}\int d\Phi_N^{(z)} \left|M^{(q\bar{q})}_{\text{LO}}\right|^2(p_1+\delta p_1, p_2+\delta p_2)\,, \tag{4.74}$$

where $d\Phi_N^{(z)}$ denotes the phase space measure for the N colour-singlet particles, but with kinematics shifted according to eq. (4.69). If these integrals are evaluated in the center of mass frame of the LO final state particles, no explicit k dependence arises from the kinematic shift, and the effect of the shift is governed entirely by setting $P^2 = zs$. This allows one to carry out the soft gluon's phase space integral independently, as done in eq. (4.73).

The generalisation of eq. (4.73) to all orders is obtained by dressing the single-emission cross section with a further arbitrary number of LP soft gluon emissions: after all we argued that we needed to include the NLP effects just once. In eq. (4.67), this has the effect of replacing the real part of the NLO soft function with the all-order LP soft function. Furthermore, the $(N+m)$-body phase space for the emission of N colour-singlet particles and m additional gluons, with momenta $\{p_i\}$ and $\{k_j\}$ respectively, factorises as in eq. (4.72), and one may write

$$\int d\Phi_{N+m}\Big(P+\sum_{j=1}^{m}k_j;\{p_i\},\{k_j\}\Big) = \int\frac{dP^2}{2\pi}\int d\Phi_{m+1}\Big(P+\sum_{j=1}^{m}k_j;P,\{k_j\}\Big)\int d\Phi_N\big(P;\{p_i\}\big)\,, \tag{4.75}$$

so that eq. (4.73) can be straightforwardly replaced with

$$\hat{\sigma}^{(q\bar{q})}_{\text{NLP;res.}}(z,\epsilon) = z\, S_{\text{LP}}(z,\epsilon)\, \hat{\sigma}^{(q\bar{q})}_{\text{LO}}(zs) = z\, S_{\text{LP}}(z,\epsilon)\, \hat{\sigma}^{(q\bar{q})}_{\text{LO}}\big(Q^2\big)\,. \tag{4.76}$$

In the second equality we emphasise that the LO partonic cross section with shifted kinematics becomes a function of Q^2, which is the physically measured invariant mass that must be kept fixed. The factor $\hat{\Delta}^{(q\bar{q})}_{\text{LO}}$ can thus be treated as being independent of z. Taking the Mellin transform we find

$$\int_0^1 dz\, z^{N-1}\hat{\sigma}^{(q\bar{q})}_{\text{NLP;res.}}(z,\epsilon) = S_{\text{LP}}(N+1,\epsilon)\, \hat{\sigma}^{(q\bar{q})}_{\text{LO}}\big(Q^2\big)\,. \tag{4.77}$$

Since the LP soft function is insensitive to the details of the hard process, we can directly use eq. (4.29) for the soft factor, provided we exponentiate the expression to obtain the all-order result. Note that the soft function is evaluated at $N+1$ rather than N, so we re-expand in the large N limit to obtain the correct leading behaviour in N at $\mathcal{O}(1/N)$. We subsequently absorb the residual collinear poles in ϵ in the (anti)quark distribution functions, and finally

expand the $1/N$ corrections to first order, since our formula is accurate up to NLP. One finds

$$\int_0^1 dz\, z^{N-1} \hat{\sigma}^{(q\bar{q})}_{\text{NLP; res.}}(z) = \hat{\sigma}^{(q\bar{q})}_{\text{LO}}(Q^2) \exp\left[\frac{2\alpha_s C_F}{\pi} \log^2(N)\right]\left(1 + \frac{2\alpha_s C_F}{\pi}\frac{\log N}{N}\right). \tag{4.78}$$

This simple result resums LLs in Mellin space at both LP and NLP, in the partonic cross section, for a general quark-induced colour-singlet production process. A comparison with the DY result of eq. (4.55) shows that the expressions are equivalent up to NLP, thus providing an important cross-check of eq. (4.78). Recall that in eq. (4.55), we were able to exponentiate the NLP term due to the known exponentiation properties of the next-to-soft function. In the general case, the NLP term contains additional physics that is not captured by the next-to-soft function, but arises from orbital angular momentum effects of which the exponentiation is not manifest.

Given that eq. (4.78) is (up to NLP) equivalent to eq. (4.55), we find that even for $q\bar{q}$-initiated processes with a more involved final state, one may extend the result to include the complete resummation of subleading logarithms at LP. The orbital angular momentum contribution that was trivial for the DY cross section (due to its point like interaction at LO) will result in a shift of the center-of-mass energy s, which must be applied to the Born cross section, with consequences that will depend on the particular process and observable being considered. The Sudakov exponent, on the other hand, is still governed by the radiation from the initial state partons so that eq. (4.60) will still apply.

4.5 NLP LL resummation for general gluon-initiated colour-singlet production

In section 4.4 we considered the production of a generic colour-singlet final state in quark-antiquark scattering, and showed how LLs may be resummed at LP and NLP. For gluon-initiated processes as shown in fig. 4.3b a similar analysis can be made: one may obtain leading-logarithmic NLP contributions by combining the next-to-soft function with orbital angular momentum contributions. As for the quark case of section 4.4, we can then dress the effect of a single gluon emission at NLP with an arbitrary number of LP soft gluon emissions. The case of single emission has been studied alongside the quark case in ref. [84], leading to a result identical in form to eq. (4.67) for the squared amplitude. Indeed one finds

$$\left|\mathscr{M}^{(ggg)}_{\text{NLP}}\right|^2(p_1, p_2, k) = g_s^2 C_A \frac{s}{p_1\cdot k\, p_2\cdot k}\left|\mathscr{M}^{(gg)}_{\text{LO}}\right|^2(p_1 + \delta p_1, p_2 + \delta p_2)\,. \tag{4.79}$$

As in the quark case, this takes the form of the LO non-radiative transition probability, with kinematics shifted according to eq. (4.68), dressed by a single LP soft emission. The colour factor in this case reflects that the emitter is an initial-state gluon rather than an initial-state (anti)-quark. The factorisation of phase space will be identical to the previous section, given

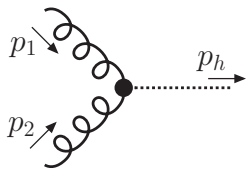

Figure 4.4: *Higgs boson production via gluon-fusion. The dot denotes the effective coupling that results from integrating out the top-quark in the infinite top-mass limit.*

that this is independent of the particle species. One then obtains the resummed result

$$\hat{\sigma}^{(gg)}_{\text{NLP; res.}}(z,\epsilon) = z\, S_{\text{LP}}(z,\epsilon)\, \hat{\sigma}^{(gg)}_{\text{LO}}(zs)\,, \tag{4.80}$$

where the soft function on the right-hand side is defined in terms of Wilson lines in the adjoint representation. One may then follow similar arguments to those leading to eq. (4.78), yielding

$$\int_0^1 dz\, z^{N-1} \hat{\sigma}^{(gg)}_{\text{NLP; res.}}(z) = \hat{\sigma}^{(gg)}_{\text{LO}}(Q^2) \exp\left[\frac{2\alpha_s C_A}{\pi}\log^2(N)\right]\left(1+\frac{2\alpha_s C_A}{\pi}\frac{\log N}{N}\right). \tag{4.81}$$

We will verify the results of this section by applying the outlined technique to the case of Higgs boson production, and compare to known LP and conjectured NLP results in the large top mass limit [159]. As is well-known, the LO process consists of an effective coupling between the Higgs boson and a pair of gluons, as shown in figure 4.4. The squared matrix element corresponds to

$$\left|\mathscr{M}^{(gg)}_{\text{LO}}\right|^2(p_1,p_2) = \frac{s^2}{8(N_c^2-1)}\frac{C^2(\mu^2)}{v^2}\,,\quad C(\mu^2) = -\frac{\alpha_s(\mu^2)}{3\pi}\left(1+11\frac{\alpha_s(\mu^2)}{4\pi}+\mathscr{O}\left(\alpha_s^2\right)\right), \tag{4.82}$$

where v denotes the vacuum expectation value of the Higgs field. Note that Wilson coefficient $C(\mu^2)$ contains higher order corrections to the effective vertex as well, which may be neglected for a LL result. Applying the kinematic shift to the LO matrix element thus generates two powers of z, such that we the resummed partonic cross section reads

$$\hat{\sigma}^{(gg)}_{\text{NLP; res.}}(z,\epsilon) = z^2\, S_{LP}(z,\epsilon)\,\frac{\alpha_s^2(\mu^2)}{72\pi\, v^2}\frac{1}{N_c^2-1}\,\delta\left(z-\frac{Q^2}{s}\right). \tag{4.83}$$

As mentioned before, this may be related to the resummed partonic coefficient function $\Delta^{(gg)}_{\text{NLP;res.}}(z)$ by the matching relation of eq. (5.66). We obtain

$$\begin{aligned}\widehat{\Delta}^{(gg)}_{\text{NLP; res.}}(z,\epsilon) &= z\, S_{LP}(z,\epsilon)\,\frac{1}{\sigma_0^{\text{h}}(S,m_h^2)}\frac{\alpha_s^2}{72\pi\, v^2}\frac{1}{N_c^2-1}\,\tau\,\delta\left(z-\frac{Q^2}{s}\right)\\ &= z\, S_{LP}(z,\epsilon)\,\delta\left(z-\frac{m_h^2}{s}\right),\end{aligned} \tag{4.84}$$

by using $\tau = m_h^2/S$, with the Higgs boson mass m_h, and dividing out the LO cross section, which is typically expressed as in eq. (5.2). Factorising the residual singularities into the gluon distributions, and re-expressing the factor of z results in

$$\Delta^{(gg)}_{\text{NLP; res.}}(z) = [1-(1-z)]\, S_{\text{LP; fin.}}(z)\, \delta\left(z - \frac{m_h^2}{s}\right). \tag{4.85}$$

Again, this implies that the coefficient of the LL NLP term in the partonic coefficient at any order in α_s is related to the LL LP term by a minus sign. Furthermore, both sets of terms are related to their counterparts in DY production by the simple replacement $C_F \to C_A$, given that the LP soft functions in both cases obey *Casimir scaling* to the relevant order.[6] We thus reproduce the results of ref. [159] for the resummation of LL NLP logarithms in single Higgs production in the large top mass limit. Note that eq. (4.85) is also valid away from the infinite top mass limit where $\widehat{\Delta}^{(gg)}_{\text{LO}}(zs) = F\left(m_H^2/(4m_t^2)\right)\delta\left(1-m_h^2/s\right)$, so where we not explicitly take $F\left(m_H^2/(4m_t^2)\right) \to 1$, while the main result of this section (eq. (4.81)) applies to other gluon-induced processes in a similar fashion.

Also for gluon-initiated processes, we note that subleading LP logarithms can be included, and the result will take the general form of eq. (4.60). In this case, the gluon DGLAP splitting functions will be involved, while the soft function for gluon annihilation can be obtained from the quark case by Casimir scaling, at least up to three loops.

4.6 Conclusions

In this study, we have developed a formalism for resumming leading-logarithmic threshold contributions to perturbative hadronic cross sections, at NLP in the threshold variable. This generalises previous approaches at LP, and applies to the production of an arbitrary colour-singlet final state at LO. Our method builds upon the previous work of refs. [41,83] (and subsequent studies [79,81]), which describes leading NLP effects in terms of a next-to-soft function, which can be shown to exponentiate at the diagram level, so that the logarithm of the next-to-soft function can be directly expressed in terms of Feynman diagrams dubbed next-to-soft webs. In general processes, the next-to-soft function must then be supplemented by terms involving derivatives acting on the non-radiative amplitude, which can be interpreted in terms of the orbital angular momentum of the colliding partons. Leading-logarithmic accuracy can then be achieved by dressing the effect of a single emission, computed up to NLP, with the LP soft function.

We have explicitly reproduced previously conjectured results for both DY production [146] and Higgs boson production in the large top mass limit [159]. In particular, we have verified the observation that the LL NLP contribution at a given order in perturbation theory is

[6] This universality between DY and Higgs production for the leading-logarithmic terms at LP and NLP provides an additional hint that the orbital angular momentum contributions, which are important for the latter process, may exponentiate as well. A recent SCET study of NLP LL resummation in Higgs production indeed found that *all* relevant NLP terms exponentiate [168].

generated by including a subleading term in the DGLAP kernels that accompany the leading pole in ϵ in the unsubtracted cross section. Our reasoning provides a proof of one of the ingredients building up the resummation ansatz proposed in ref. [162], which was partly based on the idea of exponentiating NLP contributions to DGLAP splitting functions. We note that it might be natural, in this context, to also exponentiate NLP contributions to the splitting functions beyond LO in perturbation theory: this step is strongly suggested by the arguments in ref. [201], which were based on the idea of reciprocity between time-like and space-like splitting kernels. Reference [162] verified that the inclusion in the Sudakov exponent of NLP terms in the NLO DGLAP kernel is responsible for the bulk of NLLs at NLP in the DY and DIS cross sections.

There are many directions for further work. First, of course, is the extension of the present results to subleading logarithmic accuracy at NLP. This will require a proper treatment of non-factorising phase-space effects for real emission contributions, and a thorough study of the radiative jet functions of chapter 2. The latter have yet to be fully classified in QCD, while considerable progress was recently achieved in SCET [87]. A second direction for further studies is the inclusion of processes with final state partons at LO: in these cases, additional threshold contributions associated with hard collinear real radiation are expected, as happens at LP in the threshold variable. An analysis of processes of this kind was performed recently in refs. [82, 202].

In order to move towards phenomenological applications of this formalism, a required step is the inclusion of threshold contributions from different partonic channels. For example, in DY production the quark-gluon channel enters at NLO, and generates Sudakov logarithms suppressed by an overall power of the threshold variable, because of the required radiation of a final state fermion. The inclusion of such contributions is necessary for consistent treatment of (resummed) NLP threshold effects. To further improve the phenomenological relevance of NLP resummation, also various effects *beyond* $\mathcal{O}(1/N)$ accuracy should studied carefully. The NLP terms in the Sudakov exponent will generate a large set of contributions at NNLP and beyond upon expanding the exponential to any finite order, while genuine NNLP effects for a single emission are not included. One might therefore be inclined to devise some method to limit the resummation strictly to NLP terms, for example by expanding the NLP part of the Sudakov exponent to fixed order. However, one should keep in mind that Mellin transformed expressions in the exponent are typically expanded in the large N limit and truncated, before the inverse Mellin transform is performed numerically. This procedure also limits the accuracy of the resummation procedure, as subleading terms in N originating from a (N)LP expression in z-space are discarded. For the NLP resummation proposed here, this truncation effect is also of $\mathcal{O}(1/N^2)$. Finally, the possible exponentiation of NLP terms originating from the orbital angular momentum affects the accuracy of the resummed cross section at the same order in N. Due the above mentioned inability to resum LLs at NLP in the off-diagonal channel, our study of NLP effects presented in chapter 5 is more of a exploratory than phenomenological nature. We shall therefore also take a less conservative approach regarding the exponentiation of NLP terms and leave a careful analysis of the various $\mathcal{O}(1/N^2)$ effects to future work.

4.A Exponentiation via the replica trick

In this appendix, we review the methods of ref. [41], that provide a convenient shortcut for proving that the soft function exponentiates at the diagrammatic level. For simplicity, let us first focus on QED rather than QCD, and consider a single vacuum expectation value of n Wilson line operators, as would be appropriate for contributions to the soft function involving virtual radiation. We take a number of semi-infinite Wilson lines emanating from a common vertex, and write

$$S_n = \langle 0 | \prod_{i=1}^{n} \Phi_i | 0 \rangle \,, \tag{4.86}$$

where

$$\Phi_i = \exp\left[ie \int dx_i^\mu A_\mu(x_i) \right]. \tag{4.87}$$

In path-integral language, this matrix element may be expressed as

$$\begin{aligned} S_n &= \int \mathscr{D}A_\mu \prod_{i=1}^{n} \Phi_i e^{iS\left(A_\mu, \bar{\psi}, \psi\right)} \\ &= \int \mathscr{D}A_\mu \exp\left[\sum_{i=1}^{n} ie \int dx_i^\mu A_\mu(x_i) + iS\left(A_\mu, \bar{\psi}, \psi\right) \right]. \end{aligned} \tag{4.88}$$

where $S\left(A^\mu, \bar{\psi}, \psi\right)$ is the QED action. Carrying out the path integral generates Feynman diagrams in which multiple Wilson lines are connected by *subdiagrams* consisting of photons and fermion loops, as shown for example in fig. 4.5a. Now let us generate N independent copies or *replicas* of the gauge and fermion fields, labelled by $\{A_\mu^{(j)}\}$ and $\{\psi^{(j)}\}$, such that particle species with different replica number j never interact. The soft function in such a theory is given by

$$S_{n,R} = \int \mathscr{D}A_\mu^{(1)} \ldots \int \mathscr{D}A_\mu^{(N)} \exp\left[ie \sum_{j=1}^{N} \sum_{i=1}^{n} \int dx_i^\mu A_\mu^{(j)} + \sum_{j=1}^{N} S\left(A_\mu^{(j)}, \bar{\psi}^{(j)}, \psi^{(j)}\right) \right]. \tag{4.89}$$

Note that the sum in the Wilson line term in eq. (4.89) is over both the replica numbers and the external lines, since all replicated gauge fields may interact with any given Wilson line. Furthermore, the fact that the action for the replicated theory is just the sum of the actions of individual replicas follows from the fact that replicas are non-interacting. Carrying out the path integral in the replicated theory amounts to generating Feynman diagrams such as that shown in fig. 4.5b. Any such diagram must be built of connected subdiagrams, such as G and H in the figure, and each individual connected subdiagram must contain only a *single* replica number, given that the replicated gauge fields only interact with their respective replicated fermions, and with the Wilson lines.

The replicated soft function in eq. (4.88) is therefore related to the original soft function simply by

$$S_{n,R} = S_n^N \,, \tag{4.90}$$

which can be expanded in powers of N to obtain

$$S_{n,R} = 1 + N \log(S_n) + \mathcal{O}(N^2)\,. \tag{4.91}$$

It follows that one may write

$$S_n = \exp\left[\sum_i W_i\right], \tag{4.92}$$

where the sum is over diagrams W_i that are precisely $\mathcal{O}(N)$ in the replicated theory. To find these, note that mutual independence of the replicated fields implies that a diagram containing m connected subdiagrams must be $\mathcal{O}(N^m)$, given that there is a choice of N possible replicas for each subdiagram. Thus, the logarithm of the soft function in QED must contain only *connected subdiagrams*. This result was originally derived using detailed combinatorial arguments [36], which are conveniently circumvented using the replica trick.

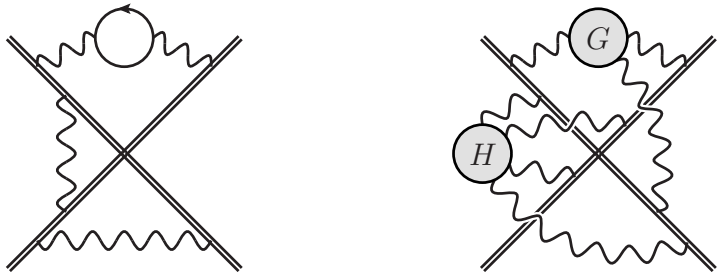

(a) **(b)**

Figure 4.5: *(a) Example diagram generated by the path integral in eq. (4.88), with four semi-infinite Wilson lines containing three subdiagrams. (b) Example diagram in the replicated theory, with subdiagrams G and H consisting of distinct replicas.*

In QCD, the exponentiation is complicated by the non-commuting nature of the emission vertices coupling gluons to the Wilson lines. In that case, a replica ordering operator $\mathscr{R}$ can be introduced which orders the sequence of colour matrices, so that a product of path ordered exponentials, each for a different replica, can be expressed as a single exponential factor containing the sum over the replicas. With this modification, the replica argument works just as well [41] and leads to the conclusion that the logarithm of the soft function, for processes involving only two partons, is built with subdiagrams that are *two-line irreducible*, which were dubbed *webs* in the pioneering work of refs. [38–40]. Due to the replica ordering, which explicitly interchanges colour matrices so as to make the replica number increase from left to right, the colour structure of webs involving multiple copies is changed. These webs contribute to the logarithm of the soft function with a so-called modified colour factor, which is calculable in a straightforward way (see e.g. ref. [187]). Similar methods apply to the case of three partons, but when more than three coloured particles are involved the nature of webs becomes more complicated, due to the multiple possible colour flows contributing to the amplitude. Again, however, the replica trick can be used to reconstruct the logarithm of the soft function [42]. In the multi-parton case, webs turn out to be sets of diagrams related to each other by permutations of gluon attachments

to the Wilson lines [42, 178]. Multi-parton webs are governed by interesting mathematical objects known as *web mixing matrices*, whose combinatorial properties are continuing to be explored [181, 182, 185].

The arguments just discussed apply directly only to the case of virtual contributions to the soft function, which arise from a single vacuum expectation value of Wilson lines. Including also real emissions, we must define the soft function according to eq. (4.10), which contains two expectation values involving non-trivial external states, as well as integrals over the multi-gluon phase space. This does not prevent us from using the replica trick: the arguments of this appendix can be used to straightforwardly show exponentiation at cross section level, provided real radiations associated with different replica numbers are mutually independent. The latter requirement is fulfilled if the phase space integral for n gluon emissions factorises into n decoupled single-gluon phase space integrals. This condition is satisfied at LL accuracy, as discussed in section 4.1.

In this brief summary, we have only explicitly discussed LP soft effects, where the soft function is defined in terms of vacuum expectation values of conventional Wilson lines, as in eq. (4.10). The argument, however, readily generalises to the next-to-soft function defined in eq. (4.34), which involves the generalised Wilson lines of eq. (4.31). Crucial in the definition of eq. (4.34) is that the sum over final states involves only LP (and therefore uncorrelated) phase space integrals for n gluon emissions. Thus, the replica trick is not invalidated, given that emissions of different gluon replicas remain independent, even at the next-to-soft level.

4.B Mellin transforms of NLP contributions

In this appendix, we collect results concerning the Mellin transforms of logarithmic threshold contributions to hadronic cross sections, both at LP and NLP. The relevant integrals that need to be performed in order to compute the Sudakov exponent at LP and NLP can be written as

$$\mathscr{D}_p(N) = \int_0^1 dz\, \frac{z^{N-1}-1}{1-z} \ln^p(1-z), \qquad \mathscr{J}_p(N) = \int_0^1 dz\, z^{N-1} \ln^p(1-z). \tag{4.93}$$

These integrals were computed to the required accuracy (that is, up to corrections suppressed by N^{-2} at large N) in ref. [162], which is a generalisation of the LP (N^0) calculation carried out in ref. [58]. For completeness, we review the calculation here, following a slightly different approach. We may introduce generating functions

$$G_{\mathscr{D}}(N,\eta) = \int_0^1 dz \left(z^{N-1}-1\right)(1-z)^{\eta-1} = \frac{\Gamma(N)\,\Gamma(\eta)}{\Gamma(N+\eta)} - \frac{1}{\eta}, \tag{4.94a}$$

$$G_{\mathscr{J}}(N,\eta) = \int_0^1 dz\, z^{N-1}(1-z)^{\eta} = \frac{\Gamma(N)\,\Gamma(\eta+1)}{\Gamma(N+\eta+1)}, \tag{4.94b}$$

such that the integrals of eq. (4.93) are derived from these functions via

$$\mathscr{D}_p(N) = \frac{d^p}{d\eta^p} G_{\mathscr{D}}(N,\eta)\bigg|_{\eta=0} \qquad \text{and} \qquad \mathscr{J}_p(N) = \frac{d^p}{d\eta^p} G_{\mathscr{J}}(N,\eta)\bigg|_{\eta=0}. \tag{4.95}$$

Expanding eq. (4.94) in the limit $N \to \infty$ gives up to $\mathscr{O}(1/N^2)$ corrections

$$G_{\mathscr{D}}(N,\eta) = -\frac{1}{\eta} + \frac{1}{\eta}\frac{\Gamma(\eta+1)}{N^\eta}\left(1 + \frac{\eta(1-\eta)}{2N}\right), \tag{4.96a}$$

$$G_{\mathscr{J}}(N,\eta) = \frac{\Gamma(\eta+1)}{N^{1+\eta}}, \tag{4.96b}$$

Focusing on the $\mathscr{D}$-terms, we subsequently perform a Taylor expansion around $\eta = 0$

$$G_{\mathscr{D}}(N,\eta) = -\frac{1}{\eta} + \sum_{n=0}^{\infty} \frac{1}{n!}\frac{d^n}{d\eta^n}\left[\Gamma(\eta+1)\left(1 + \frac{\eta(1-\eta)}{2N}\right)\exp(-\eta \ln N)\right]_{\eta=0} \eta^{n-1}, \tag{4.97}$$

where we have expressed $1/N^\eta = \exp(-\eta \ln N)$. Using the general Leibniz rule we find

$$\begin{aligned} G_{\mathscr{D}}(N,\eta) &= -\frac{1}{\eta} + \sum_{n=0}^{\infty} \frac{1}{n!} \sum_{k=0}^{n} \binom{n}{k} d^{(k)}(N) (-\ln N)^{n-k} \eta^{n-1} \\ &= \sum_{n=1}^{\infty} \sum_{k=0}^{n} \frac{1}{k!(n-k)!} d^{(k)}(N) (-\ln N)^{n-k} \eta^{n-1}, \end{aligned} \tag{4.98}$$

having cancelled the $n = 0$ term in the second line, and where

$$d^{(k)}(N) = \frac{d^k}{d\eta^k}\left[\Gamma(\eta+1)\left(1 + \frac{\eta(1-\eta)}{2N}\right)\right]_{\eta=0}. \tag{4.99}$$

The result for $\mathscr{D}_p(N)$ is now easily obtained from eq. (4.95), by noting that $n = p+1$ constitutes the only non-vanishing contribution to the sum over n. We obtain

$$\mathscr{D}_p(N) = \frac{1}{p+1} \sum_{k=0}^{p+1} \binom{p+1}{k} d^{(k)}(N) (-\ln N)^{p-k+1} + \mathscr{O}\left(\frac{\ln^m N}{N^2}\right). \tag{4.100}$$

Analogously we find for eq. (4.96b)

$$G_{\mathscr{J}}(N,\eta) = \frac{1}{N} \sum_{n=0}^{\infty} \sum_{k=0}^{n} \frac{1}{k!(n-k)!} \Gamma^{(k)}(1) (-\ln N)^{n-k} \eta^n, \tag{4.101}$$

where $\Gamma^{(k)}(z)$ is the k-th derivative of the $\Gamma(z)$ function. With eq. (4.95) now enforcing $n = p$, the result for the Mellin transform of the NLP threshold logarithms in z-space is

$$\mathscr{J}_p(N) = \frac{1}{N} \sum_{k=0}^{p} \binom{p}{k} \Gamma^{(k)}(1) (-\ln N)^{p-k} + \mathscr{O}\left(\frac{\ln^m N}{N^2}\right). \tag{4.102}$$

Keeping only LLs at both LP and NLP, one finds

$$\mathscr{D}_p(N) = (-1)^{p+1}\left[\frac{1}{p+1}\log^{p+1}N - \frac{\log^p N}{2N}\right] + \dots, \tag{4.103a}$$

$$\mathscr{J}_p(N) = \frac{(-\log N)^p}{N} + \dots. \tag{4.103b}$$

Considering now the application of these results to eq. (4.55), we note that the partonic coefficient function for the $q\bar{q}$-channel of the resummed DY cross section at LL accuracy, in Mellin space at $\mathscr{O}(\alpha_s^m)$, takes the form

$$\begin{aligned}\Delta_{\rm NLP}(N)\big|_{\mathscr{O}(\alpha_s^m)} &= \left(\frac{2\alpha_s C_F}{\pi}\right)^m \frac{1}{m!}\left(\log^2 N + \frac{\log N}{N}\right)^m \\ &= \left(\frac{2\alpha_s C_F}{\pi}\right)^m \frac{1}{(m-1)!}\left[2\left(\frac{\log^{2m}N}{2m} - \frac{\log^{2m-1}N}{2N}\right) + \frac{2\log^{2m-1}N}{N}\right],\end{aligned} \tag{4.104}$$

where we have rewritten the result in the second line to explicitly recognise the LL contributions to the integrals $\mathscr{D}_{2m-1}$ and $\mathscr{J}_{2m-1}$, given in eq. (4.103a) and in eq. (4.103b), respectively. One finds then

$$\Delta_{\rm NLP}(N)\big|_{\mathscr{O}(\alpha_s^m)} = \left(\frac{2\alpha_s C_F}{\pi}\right)^m \frac{2}{(m-1)!}\Big(\mathscr{D}_{2m-1}(N) - \mathscr{J}_{2m-1}(N)\Big), \tag{4.105}$$

which leads immediately to eq. (4.56).

4.C Two gluon emission from the generalised Wilson line

In section 4.2.1, we defined a next-to-soft function in terms of generalised Wilson lines, which have been introduced and discussed extensively in refs. [41, 83]. These operators generate effective Feynman rules for the emission of (next-to-)soft gluons from a given hard particle, and the one-gluon emission terms required for describing radiation at $\mathscr{O}(\alpha_s)$ are shown in eq. (4.31). However, the Feynman rules also involve effective vertices describing the emission of a gluon pair. These are neglected in the analysis of this chapter, for reasons discussed in section 4.2.1. Below, we check explicitly that such vertices cannot contribute to NLP LL terms at higher orders in perturbation theory, using a simple example.

The two-gluon emission vertex from ref. [41] is given in eq. (3.47), where p_i denotes the hard momentum of the emitting particle, and (k_1, k_2) are the soft momenta of the emitted gluons. The latter may also be sums of individual gluon momenta, which will not affect the following. We consider a process with two incoming massless partons carrying four-momenta p_1 and p_2. Without loss of generality, let us consider the two-gluon emission vertex as occurring on the leg with momentum p_1. Then, as we have argued in section 4.2.1, leading logarithmic effects can only come from radiation that is maximally (next-to) soft,

as well as collinear. This in turn means that k_1 and k_2 must be proportional to either p_1 or p_2. From eq. (3.47), it is straightforward to see that $R(p_1; k_1, k_2)$ vanishes if $k_1^\mu \sim p_1^\mu$ or if $k_2^\mu \sim p_1^\mu$. Thus, for a non-zero contribution, both k_1 and k_2 must be proportional to p_2. Introducing proportionality constants α_i such that $k_i^\mu = \alpha_i\, p_2^\mu$, we obtain

$$R^{\mu\nu}(p_1; \alpha_1 p_2, \alpha_2 p_2) = \frac{\alpha_1 \alpha_2}{2(\alpha_1 + \alpha_2)} \left[p_1 \cdot p_2\, \eta^{\mu\nu} - \left(p_1^\mu p_2^\nu + p_1^\nu p_2^\mu \right) \right] . \tag{4.106}$$

In a squared matrix element summed over final state gluon polarisations, the Lorentz indices μ and ν must ultimately be contracted with one of the external momenta p_1 or p_2, or with a further soft momentum k_3. However, the combination in the square brackets in eq. (4.106) acts as a projection tensor that removes the component of any four-momentum that is collinear with either p_1 or p_2, which k_3 must be given that leading logarithmic behaviour arises only from soft gluon emissions that are maximally (next-to) soft and collinear. We thus find that the two-gluon emission vertex is irrelevant at LL accuracy.

The above discussion applies to next-to-soft emissions from a scalar particle, as well as to emissions from a spin particle in an abelian gauge theory. For gluon emissions from a fermion, an extra contribution to the two-gluon emission vertex is present, that involves the spin generator of the emitting particle. This term, like the one but term last in eq. (3.47), is a local vertex (or *seagull* vertex) that describes the emission of two-gluons from a single point along the generalised Wilson line.[7] However, since such local vertices are obtained by the contraction of the propagator that would separate the two emissions in standard Feynman diagrams, they involve one fewer propagator than contributions involving *two* separate gluon emissions. This means that two fewer integrations are performed with a logarithmic measure, which results in (at most) NLLs at NLP, as argued in section 4.2.1. We therefore conclude that, also in the case of spinning hard particles, the two-gluon next-to-soft emission vertex can be neglected at LL accuracy.

[7] The remaining terms in eq. (3.47) are associated to correlated emissions from different positions along the generalised Wilson line.

Chapter 5

Numerical effects of NLP terms in finite- and all-order cross sections

Despite the long-standing interest in the formal aspects of NLP contributions (see references in previous chapters, as well as ref. [203]), their numerical/phenomenological consequences have received less attention in the literature. Notable contributions include the early numerical studies on the threshold approximation in the DY production process in refs. [204, 205], which already advocated the importance of subleading-power logarithms. Later, threshold expansions of the Higgs coefficient functions at NNLO and N^3LO were studied in refs. [31, 137, 206], showing that the convergence of this series is slow and subleading-power corrections are thus important. In a resummation context, NLP contributions were first taken into account and shown to contribute significantly in ref. [155], while refs. [207–211] studied the subtleties of how to handle NLP contributions and pointed out the phenomenological relevance for both DY and Higgs.[1] Lastly, refs. [202, 212] studied numerical effects of subleading powers corrections in prompt photon production. All these studies suggest that, although not as divergent as the LP contributions, NLP terms can have sizeable numerical effects.

In this chapter, we will perform a rather extensive study of the numerical effects of NLP threshold logarithms on partonic and hadronic cross sections, at both fixed order and at all-orders in perturbation theory. In section 5.1 we provide a detailed analysis of the convergence of the threshold expansion for DY and Higgs production. For the former process this has, to the best of our knowledge, not been shown earlier (neither for the diagonal nor off-diagonal production channels), while for the latter we confirm results that have appeared earlier in refs. [137, 156] (for the dominant production channel). In section 5.2 we review and slightly improve LP and NLP resummation for these processes, building upon the results of chapter 4, and derive the resummation exponent (eq. (5.44)) that is used to asses the numerical effects of resumming NLP threshold logarithms at LL accuracy. Results are presented in section 5.3, where we show the impact of the NLP LL resummation on top of the LP NNLL(′) resummed and matched DY and Higgs cross sections, and compare to the

[1] We will compare these results to our work in section 5.3.4.

effects of subleading logarithmic corrections at LP. In addition, we comment on the numerical importance for off-diagonal emissions, for which no resummation has been achieved yet.[2] Finally, we show the effect of NLP LL resummation in other colour-singlet production processes, to wit di-Higgs and di-vector boson (W^+W^- or ZZ) production. We conclude in section 5.4.

5.1 Threshold expansions at fixed order

In this section we study the convergence of the threshold expansion in fixed order calculations for the single Higgs and the DY processes, first at the parton level, and subsequently for the hadronic cross section. The partonic flux plays an important role in the threshold expansion of the latter. As mentioned above, partonic and/or hadronic threshold expansions for these processes have been performed before, but results are scattered. Here, we provide an extended analysis tailored to study NLP corrections. As such it also serves as an introduction to the numerical study of NLP effects in resummed cross sections in section 5.3.

5.1.1 The partonic coefficients for single Higgs production

We start with the study of the behaviour of the partonic coefficient functions for single Higgs production at NLO [131,213,214] and NNLO [132,133,215]. First we review some relevant quantities and variables. The hadronic cross section for this process is given by

$$\sigma_{pp\to h+X}(m_h^2,S) = \sigma_0^{\mathrm{h}} \sum_{i,j} \int_0^1 dx_1\, f_i(x_1,\mu) \int_0^1 dx_2\, f_j(x_2,\mu) \int_0^1 dz\, \Delta_{\mathrm{h},ij}(z, m_h^2/\mu^2)\, \delta\left(x_1 x_2 z - \tau\right) . \tag{5.1}$$

Recall that $\tau = m_h^2/S$, with m_h the Higgs boson mass and S the hadronic center-of-mass (CM) energy squared, while $f_i(x,\mu)$ denote the PDFs and $\Delta_{\mathrm{h},ij}(z, m_h^2/\mu^2)$ is the partonic coefficient function. Note that the LO partonic cross section σ_0^h is factored out. In the infinite top mass limit[3] it reads (see e.g. ref. [132])

$$\sigma_0^{\mathrm{h}} = \frac{\sqrt{2}\, G_F}{72(N_c^2-1)} \frac{\alpha_s^2}{\pi} \frac{m_h^2}{S} , \tag{5.2}$$

in units of GeV^{-2}. The strong coupling is denoted by $\alpha_s \equiv \alpha_s(\mu)$, N_c is the number of colours, and Fermi's constant G_F has the value 1.16639×10^{-5} GeV^{-2}. Throughout this chapter we employ the central member of the PDF4LHC15 NNLO 100 PDF set [216] for proton-proton collisions with $\sqrt{S} = 13$ TeV, corresponding to $\alpha_s(M_Z^2) = 0.118$ with the Z-boson mass $M_Z = 91.18$ GeV. In practice we use a polynomial fit of these PDFs (see appendix 5.A),

[2] Although important progress has been made, see e.g. [104, 121, 160].

[3] In this limit, the effect of the top quark mass is contained in a Wilson coefficient, whose lowest-order contribution is $-\alpha_s/(3\pi v)$ with $v^2 = 1/(\sqrt{2}G_F)$. We include this coefficient (squared) in eq. (5.2).

which is particularly convenient for obtaining the resummed results presented in section 5.3. We choose the renormalisation and factorisation scale equal and denote both as μ. The threshold variable is $1-z = 1-m_h^2/s$, with $\sqrt{s}$ the partonic CM energy. The hadronic cross section can also be expressed in terms of the parton flux as

$$\sigma_{pp\to h+X}(m_h^2, S) = \sigma_0^{\mathrm{h}} \sum_{i,j} \int_\tau^1 \frac{dz}{z}\, \mathscr{L}_{ij}\left(\frac{\tau}{z}\right) \Delta_{\mathrm{h},ij}(z), \qquad \text{with} \tag{5.3a}$$

$$\mathscr{L}_{ij}\left(\frac{\tau}{z}\right) = \int_{\tau/z}^1 \frac{dx}{x}\, f_i(x,\mu)\, f_j\left(\frac{\tau/z}{x},\mu\right). \tag{5.3b}$$

Here we have suppressed scale dependence in both the flux and coefficient functions. The perturbative expansion of the partonic coefficient functions $\Delta_{\mathrm{h},ij}(z)$ reads

$$\Delta_{\mathrm{h},ij}(z) = \Delta^{(0)}_{\mathrm{h},ij}(z) + \Delta^{(1)}_{\mathrm{h},ij}(z) + \Delta^{(2)}_{\mathrm{h},ij}(z) + \dots, \tag{5.4}$$

where $\Delta^{(n)}_{\mathrm{h},ij}(z)$ includes α_s^n. The definition in eq. (5.3a) implies that $\Delta^{(0)}_{\mathrm{h},ij}(z)$ is normalised as

$$\Delta^{(0)}_{\mathrm{h},ij}(z) = \delta_{ig}\delta_{jg}\delta(1-z), \tag{5.5}$$

since the Born-level process involves the gluon-gluon fusion channel.

Near $z=1$ the function $\Delta_{\mathrm{h},ij}(z)$ can be expanded as

$$\Delta_{\mathrm{h},ij}(z) = \sum_{n=0}^{\infty}\left(\frac{\alpha_s}{\pi}\right)^n \left\{ c^{(\delta)}_{ij,n}\delta(1-z) + \sum_{m=0}^{2n-1}\left[c^{(-1)}_{ij,nm}\left(\frac{\ln^m(1-z)}{1-z}\right)_+ + c^{(0)}_{ij,nm}\ln^m(1-z) + c^{(1)}_{ij,nm}(1-z)\ln^m(1-z) + \dots \right]\right\}. \tag{5.6}$$

The $c^{(-1)}_{ij,nm}$ are the coefficients of the LP contributions (as in eq. (1.22), but with a slightly different normalisation), which contain a factor of $(1-z)^{-1}$, while NLP contributions at $\mathscr{O}((1-z)^0)$ have coefficients $c^{(0)}_{ij,nm}$; in general N^{k}LP contributions contain a factor $(1-z)^{k-1}$. Explicit forms of the NLO and NNLO coefficients $\Delta^{(1)}_{\mathrm{h},ij}$ and $\Delta^{(2)}_{\mathrm{h},ij}$ are obtained from the functions $\eta^{(n)}_{ij}(z)$ in eq. (45)-(51) of ref. [132]. We note that the factor of $1/z$ appearing in eq. (15) of that reference is included in our partonic coefficient functions, i.e. we have[4]

$$\Delta^{(n)}_{\mathrm{h},ij}(z) = \left(\frac{\alpha_s}{\pi}\right)^n \eta^{(n)}_{ij}(z)/z\,. \tag{5.7}$$

In our threshold expansion the factor $1/z$ is expanded too, an approach also taken in ref. [133], following ref. [217]. One may choose to keep that factor unexpanded. This would lead to somewhat different results, a consequence of truncating the expansion in eq. (5.6). Let us comment here further on the role of the extra factor of $1/z$. In general, one

[4] We refer to appendix 5.B for the origin of the additional factor of $1/z$ with respect to the DY case discussed in section 5.1.2.

may define the partonic coefficient functions to contain additional powers of $1/z$, provided a compensating factor is introduced. For some power p we would find instead

$$\sigma_{pp\to h+X}(m_h^2,S) = \sigma_0^{\mathrm{h}} \sum_{i,j} \int_\tau^1 dz\, z^{p-1}\, \mathscr{L}_{ij}\left(\frac{\tau}{z}\right)\left[\frac{\Delta_{\mathrm{h},ij}(z)}{z^p}\right]. \tag{5.8}$$

If one expands the term in square brackets around threshold and truncate that series at some power in $(1-z)$, the above result is no longer equal to eq. (5.3a), and is thus sensitive to the p additional inverse powers of z that are expanded

$$\frac{1}{z^p}\left[\frac{\ln(1-z)}{1-z}\right]_+ = \left[\frac{\ln(1-z)}{1-z}\right]_+ + p\ln(1-z) + \frac{1}{2}p(1+p)(1-z)\ln(1-z) + \dots . \tag{5.9}$$

This makes results of threshold expansions somewhat ambiguous, an aspect also discussed at length in ref. [156] (see in particular the caption of fig. 2 in that reference). In our case we fix the power of $1/z$ by requiring the universality of LL NLP terms in the dominant channel of colour-singlet production processes, as shown in refs. [82, 84] at fixed order, as well as in chapter 4 in a resummation context. In both DY and Higgs production the coefficients of the highest power of $\ln(1-z)$ at LP and NLP are, at each order in α_s, identical but with opposite sign. This follows from both terms resulting from multiplying the same residual collinear singularity with an overall ϵ-dependent power of $(1-z)$. This singularity, which is absorbed in the PDF by mass factorisation, is associated to the lowest-order splitting kernel, such that the logarithms in the finite part are indirectly generated by the splitting kernel too. Expansion of the lowest order splitting function, $P_{qq}^{(1)}$ and $P_{gg}^{(1)}$ for DY and Higgs respectively, reveals that they indeed obey this relation between the LP and NLP terms

$$P_{qq}^{(1)} = C_F\left(2\left[\frac{1}{1-z}\right]_+ - 2 + \mathscr{O}(1-z)\right), \quad P_{gg}^{(1)} = C_A\left(2\left[\frac{1}{1-z}\right]_+ - 2 + \mathscr{O}(1-z)\right). \tag{5.10}$$

The definition of the (partonic) cross section in eq. (5.3a) satisfies the condition, as we show explicitly for the NLO coefficient function $\Delta_{\mathrm{h},ij}^{(1)}(z)$ below. The full one-loop coefficient reads [132]

$$\begin{aligned}\frac{\pi}{\alpha_s}\Delta_{\mathrm{h},gg}^{(1)}(z) &= \frac{1}{z}\left[\left(\frac{11}{2}+6\zeta_2\right)\delta(1-z) + 12\left[\frac{\ln(1-z)}{1-z}\right]_+ - 12z(2-z+z^2)\ln(1-z)\right.\\ &\qquad \left. - \frac{6(z^2-z+1)^2}{1-z}\ln(z) - \frac{11}{2}(1-z)^3\right]\\ &= 12\left[\frac{\ln(1-z)}{1-z}\right]_+ + \left(\frac{11}{2}+6\zeta_2\right)\delta(1-z) - 12\ln(1-z) + 6 + \mathscr{O}(1-z), \end{aligned} \tag{5.11}$$

where we have expanded around threshold in the last line, and where we observe the advertised relation between the coefficient of the LL at LP and NLP.

We now examine how well the partonic coefficient functions are approximated by the threshold expansion at NLO and NNLO, for each partonic channel. Our default scale choice is

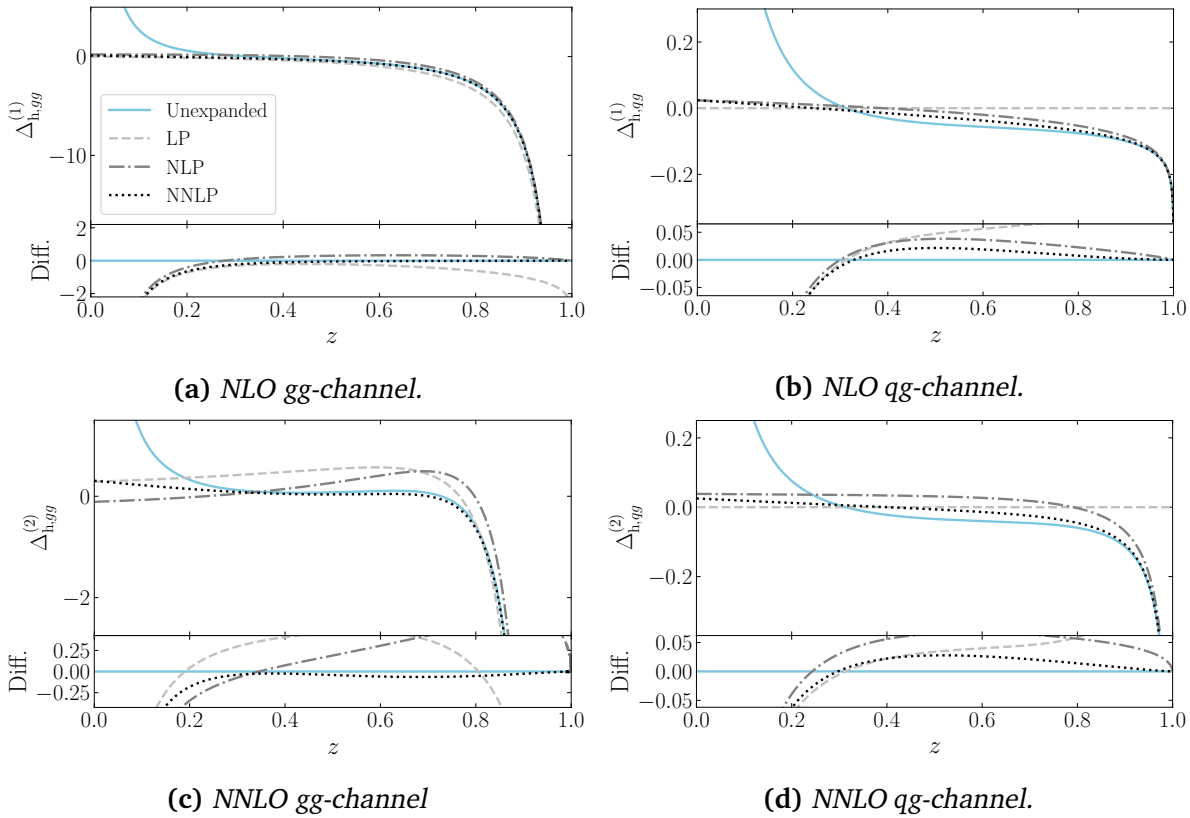

(a) *NLO gg-channel.*

(b) *NLO qg-channel.*

(c) *NNLO gg-channel*

(d) *NNLO qg-channel.*

Figure 5.1: *Threshold expansions of the NLO and NNLO coefficients for single Higgs production. The bottom panes show the difference between the truncated and unexpanded expressions. The vertical-axis range of these difference plots is fixed at one fifth of the range of* $\Delta_{\mathrm{h}}^{(1)}$ *shown in the upper panes, for a uniformised comparison. Note that we have included the (trivial) LP approximation of the qg-channels, which vanishes, as these channels start contributing at* NLP*.*

$\mu = m_h$. In figs. 5.1a and 5.1b we show the threshold expansion of the two NLO coefficients $\Delta_{\mathrm{h},gg}^{(1)}$ and $\Delta_{\mathrm{h},qg}^{(1)}$. The third partonic NLO channel ($q\bar{q}$) only contributes at N^{4}LP, hence we leave it out of our discussion.[5] We show the results without the $\delta(1-z)$ term, which is present in the gg-channel. In figs. 5.1c and 5.1d the corresponding NNLO results are shown. Considering the gg-initiated channel first (fig. 5.1a and fig. 5.1c), we observe that the LP threshold expansion of $\Delta_{\mathrm{h},gg}^{(1)}$ deviates considerably from the unexpanded result in the $z \to 1$ limit, which might be surprising at first sight. This is caused by the NLP terms: $\ln^i(1-z)$ terms do not vanish as $z \to 1$, and are not captured by the LP truncation of the matrix element. Although subdominant to the LP contribution, they are not altogether negligible as $z \to 1$. The unexpanded NLO result is, however, well-described by the NLP approximation for $z \gtrsim 0.2$. None of the truncations captures the behaviour below $z \lesssim 0.2$ well, due to the factor of $1/z$ in the partonic coefficient function. The threshold expansion of the NNLO coefficient function $\Delta_{\mathrm{h},gg}^{(2)}$ performs worse (fig. 5.1c) than that of the NLO coefficient function:

[5] The channel contributes via the process $q\bar{q} \to g \to gh$, which is proportional to $\frac{u^2+t^2}{s}$. Parametrising the Mandelstam variables $t = -s(1-z)v$ and $u = -s(1-z)(1-v)$, this leads to a factor $(1-z)^2$ from the matrix element. An extra factor of $(1-z)$ follows from the phase space measure.

the LP approximation underestimates the unexpanded result in the large-z domain, while the NLP approximation overestimates it. Convergence is seemingly only obtained at NNLP.

Turning to the qg-channel (fig. 5.1b), whose LP approximation vanishes, we see that the NLP approximation overestimates the unexpanded result in the large-z domain. Also here the small-z domain is poorly described by the $z \to 1$ expansion of the full partonic coefficient function due to a $1/z$ factor. The NNLO contribution in the qg-channel (fig. 5.1d) shows similar behaviour.

5.1.2 The partonic coefficients for DY

Next we perform the same studies for the DY process. The distribution in the squared invariant mass Q^2 is given by

$$\frac{d\sigma_{\text{DY}}}{dQ^2} = \sigma_0^{\text{DY}} \sum_{i,j} \int_\tau^1 \frac{dz}{z} \mathscr{L}_{ij}\left(\frac{\tau}{z}\right) \Delta_{\text{DY},ij}(z), \tag{5.12}$$

with $z = Q^2/s$. The α_s expansion of $\Delta_{\text{DY},ij}(z)$ is similar to eq. (5.4), and the threshold expansion of $\Delta_{\text{DY},ij}(z)$ is as in eq. (5.6). The LO coefficient $\Delta^{(0)}_{\text{DY},ij}(z) = \delta_{iq}\delta_{j\bar{q}}\delta(1-z)$ is obtained by extracting the prefactor[6]

$$\sigma_0^{\text{DY}} = \frac{4\pi\alpha_{\text{EM}}^2}{3Q^2S}\frac{1}{N_c}, \tag{5.13}$$

where $\alpha_{\text{EM}} = 1/127.94$ is the electromagnetic fine-structure constant at the scale M_Z. See appendix 5.B for a careful derivation of this normalisation. To compare directly with single Higgs production we set $\mu = Q = m_h$ for the discussion in this subsection.

In figs. 5.2a and 5.2c, we show the threshold expansions truncated up to NNLP of the NLO and NNLO $q\bar{q}$-channel, whose exact expressions are obtained from ref. [129]. Both perturbative orders are well described by the NLP approximation for a large range of z-values. The convergence of the threshold expansions of the qg-channel, shown in figs. 5.2b and 5.2d, is worse than for the dominant $q\bar{q}$-channel. In contrast to the Higgs case, the NLP approximation underestimates the $\Delta^{(1)}_{\text{DY},qg}$ and $\Delta^{(2)}_{\text{DY},qg}$ coefficients near $z = 1$. The NNLP expansion behaves slightly better, although convergence is again slow for this channel. As for the Higgs case, the partonic channels (qq and gg) that open up at NNLO do not contribute at NLP, as these channels require the emission of two soft quarks.

Recapitulating, for both single Higgs and DY production we have seen that the *partonic* threshold expansion works best for the dominant production channel. The NLP truncation

[6] The cross section in eq. (5.12) describes the entire DY process, including the production of a lepton pair through the intermediate off-shell photon. Since the leptonic interaction receives no QCD corrections, it is captured entirely by σ_0^{DY}. The partonic coefficient thus coincides with that for the production of an off-shell photon as LO final state.

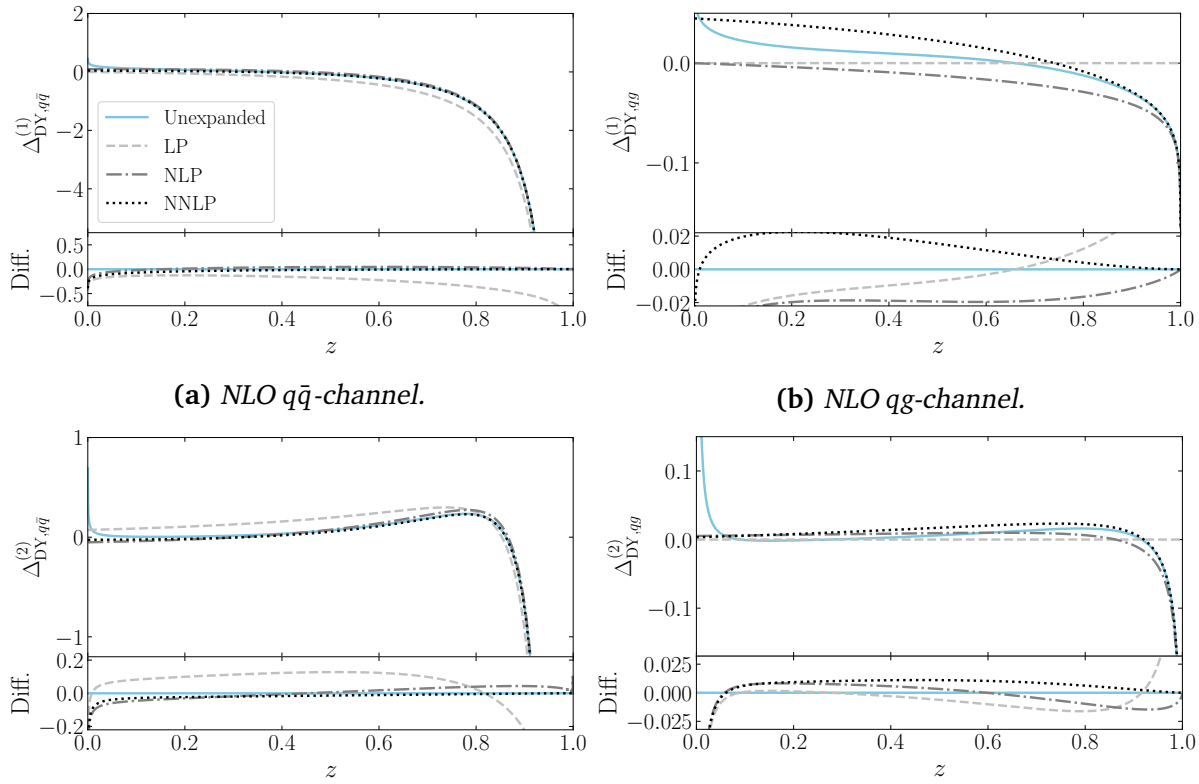

(a) *NLO $q\bar{q}$-channel.*

(b) *NLO qg-channel.*

(c) *NNLO $q\bar{q}$-channel.*

(d) *NNLO qg-channel.*

Figure 5.2: *Expansions of the NLO and NNLO partonic coefficients for the DY production of an off-shell photon. Presentation is the same as in fig. 5.1.*

overestimates the coefficient functions for intermediate and large values of z in these dominant channels, but convergence is reached at NNLP. In the qg-channels, the NLP expansion overestimates the exact result for Higgs production for $z \to 1$, while it underestimates it for DY. At NNLP no substantial improvement is obtained in this channel. The contribution in the $z \to 0$ region, corresponding to the high-energy limit, is for Higgs production more pronounced than for DY, for both production channels. This is due to the factor of $1/z$ that is part of the partonic coefficient function of the former process, which magnifies small-z contributions. To what extent the various differences manifest themselves in hadronic cross sections depends of course on the parton flux. This question is addressed in the next subsection.

5.1.3 Threshold behaviour in luminosity weighted cross sections

In the previous subsection it became clear that the Higgs partonic coefficient functions have a more pronounced small-z contribution than those of DY. In the hadronic cross sections, these coefficient functions are weighted by the parton flux as in eqs. (5.3a) and (5.12), which possibly affects the quality of the threshold expansion for the hadronic cross section.

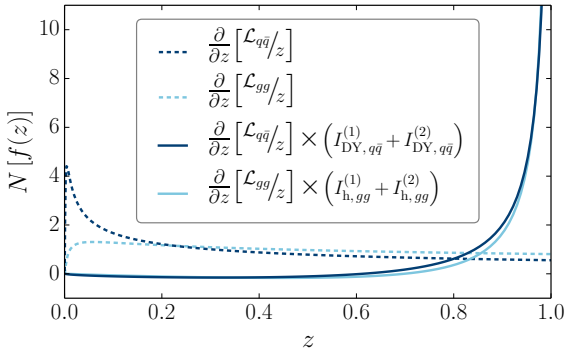

Figure 5.3: *The derivative of the parton luminosity (dashed) and its point-by-point multiplication with the integrated LP partonic coefficient function up to NNLO (solid), for both DY (dark blue) and single Higgs (light blue) production at* $Q = \mu = 125$ GeV*. All curves are normalised according to eq.* (5.15)*.*

For non-singular terms in the partonic coefficient functions (those that do not contain plus-distributions), the convolutions in eqs. (5.3a) and (5.12) correspond to a point-by-point multiplication with the parton luminosity function. The product, which is the integrand for the inclusive cross section at fixed τ, is a function of z only. This *weight distribution* shows which parts of the coefficient functions are enhanced or suppressed by the parton flux, and thus gives much information about how well the threshold expansion can approximate the exact result. We emphasise that for understanding the quality of the threshold expansion, only the shape of the weight distribution for the non-singular contributions matters: the plus-distributions cannot be expanded any further in the threshold limit. For completeness, we nevertheless review the weight distributions for these LP terms briefly, as these notably involve the *derivative* of the parton flux, as well as the separately integrated partonic coefficient function (see appendix 5.C). For brevity we denote the latter by

$$I^{(n)}_{\mathrm{DY/h},ij}(z) \equiv -\int_0^z dz'\ \Delta^{(n)}_{\mathrm{DY/h},ij}(z')\Big|_{\mathrm{LP}}\,. \tag{5.14}$$

In fig. 5.3 we plot the resulting weight distribution for DY and Higgs production, up to NNLO and for $Q = \mu = m_h$. To aid comparison we normalise the plotted functions, generically denoted by $f(z)$, as

$$N\,[f(z)] = \frac{f(z)}{\left|\int_\tau^1 dz\ f(z)\right|}\,, \tag{5.15}$$

such that the absolute area under each curve equals unity. The $q\bar{q}$ parton luminosity is defined as a charge weighted sum of symmetrised parton flux contributions from the five lightest quark flavours:

$$\mathscr{L}_{q\bar{q}}\left(\frac{\tau}{z}\right) = \sum_{q\in\{u,d,c,s,b\}} e_q^2 \int_{\tau/z}^1 \frac{dx}{x}\left[f_q(x,\mu)\,f_{\bar{q}}\left(\frac{\tau/z}{x},\mu\right) + f_{\bar{q}}(x,\mu)\,f_q\left(\frac{\tau/z}{x},\mu\right)\right], \tag{5.16}$$

with e_q the fractional charge of the quark, normalised to the electromagnetic charge e. The

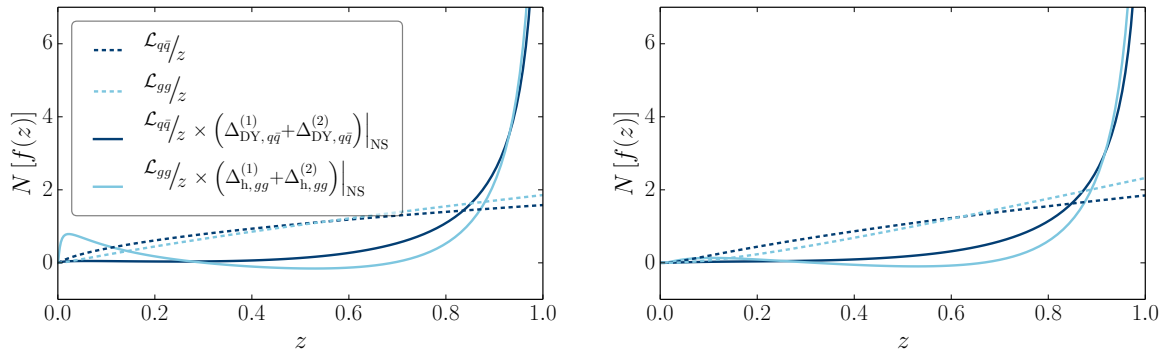

(a) $Q = \mu = 125$ *GeV* **(b)** $Q = \mu = 500$ *GeV*

Figure 5.4: *The luminosity function (dashed) and its point-by-point multiplication with the non-singular part of the coefficient functions up to NNLO (solid), for the dominant channel in both DY ($q\bar{q}$, dark blue) and single Higgs (gg, light blue) production. All curves are normalised according to eq.* (5.15).

differentiated $q\bar{q}$-flux highlights the small-z region more than the differentiated gg-flux, as shown by the dashed lines, but since the LP terms of the partonic coefficient functions for DY are small in that regime (see figs. 5.2a and 5.2c), this affects their product with the coefficient functions (solid lines) only little. The product diverges (integrably so) for both channels for $z \to 1$, as one would expect for the LP terms. Overall, the LP behaviour of both processes is very similar. Around $z \sim 0.8$ a small difference appears, caused by the stronger decrease of the derivative of the $q\bar{q}$-flux. This results in a slightly more spread-out (i.e. less threshold-centered) weight distribution for DY, but as we mentioned above, this cannot affect the quality of the threshold expansion. We point out that, somewhat counter-intuitively, the LP terms make up only a modest fraction of the total cross section, for both processes (we shall quantify this in figs. 5.8 and 5.9).

In fig. 5.4 we show the normalised non-singular part of the partonic coefficient functions up to NNLO, weighted by the respective parton luminosity (solid lines).[7] We focus on the dominant production channel for each process and show the z-dependence of the parton fluxes themselves as well (dashed lines). In addition to the natural comparison scale for on-shell Higgs production of $Q = \mu = 125$ GeV (fig. 5.4a), we also consider one off-shell Higgs-production scenario with $Q = \mu = 500$ GeV (fig. 5.4b). In both cases we see that the product of the parton luminosities and the coefficient functions are suppressed in the small-z regime, as a result of the small parton flux. This, in turn, is due to the momentum fractions x_1 and x_2 being large when $z \to \tau$ since $x_1 x_2 = \frac{\tau}{z}$. The individual sea quark and gluon PDFs are small in the large x domain, suppressing the luminosity.[8] Larger values of μ in the flux

[7] Some contributions to the DY NNLO partonic coefficient in the $q\bar{q}$-channel ought to be summed over the quark flavours without charge weighing (see appendix A of ref. [129]). We have explicitly verified that these terms contribute only from N^{6}LP onwards and that these contributions are numerically negligible. Therefore, the overall point-by-point multiplication with the parton luminosity function in eq. (5.16) is deemed to be valid approximation.

[8] The valence quark contributions to the parton luminosity defined in eq. (5.16) cause it to fall off less steeply with x than for sea-quarks (or gluons) alone. This is reflected in the stronger small-z suppression of the

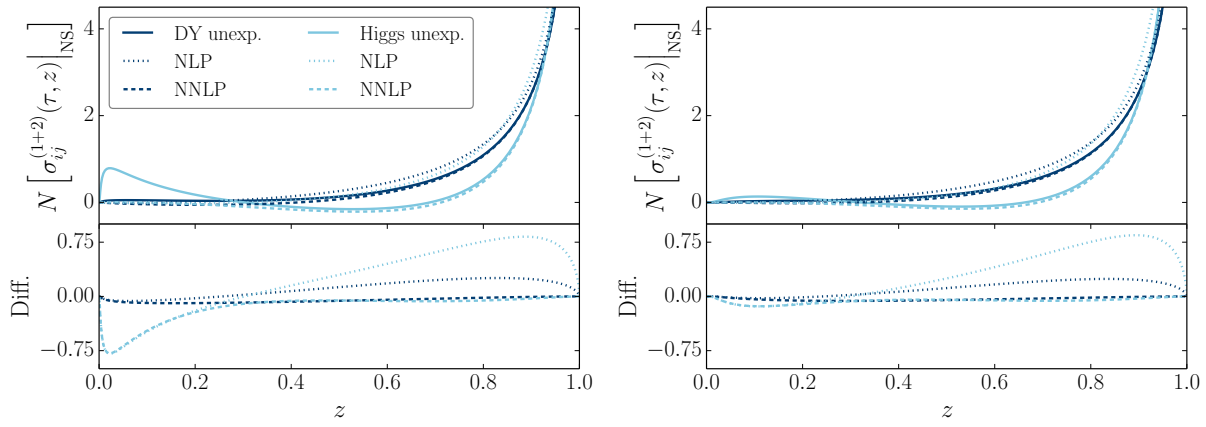

(a) $Q = \mu = 125$ *GeV* **(b)** $Q = \mu = 500$ *GeV*

Figure 5.5: *Exact (solid lines) as well as truncated expressions at NLP (dotted) and NNLP (dashed) for the non-singular part of the coefficient functions up to NNLO, weighted with the parton luminosity, for the dominant channel of DY ($q\bar{q}$, dark blue) and single Higgs (gg, light blue) production. All curves are normalised according to eq.* (5.15)*.*

strengthen this suppression. Therefore, the singular behaviour of the coefficient functions for single Higgs production near $z = 0$ is more suppressed by the parton luminosity as μ increases. Thus at $Q = \mu = 125$ GeV a notable peak is present in the small-z region (it is more pronounced at smaller μ values). It disappears due to the above-mentioned suppression for larger μ values, as seen in fig. 5.4b for $Q = 500$ GeV. However, at $Q = 125$ GeV this feature should still affect the quality of the threshold expansion for the hadronic Higgs cross section. As the DY partonic coefficient function does not show singular behaviour in the small-z regime, the μ-dependent suppression of the parton luminosity has less impact and we expect the quality of the threshold expansion to be mostly Q-independent. Based on these considerations we therefore expect that, especially for small Q values, the quality of the threshold expansion of the dominant channel for DY is better than that for Higgs production.

To test this expectation, we compare the parton-luminosity-weighted NLP and NNLP approximations of the partonic coefficient functions to the unexpanded NLO+NNLO result. This product, being the (approximated) integrand of the non-singular (NS) contribution to the hadronic cross section, is denoted by

$$\sigma_{ij}^{(1+2)}(\tau,z)\Big|_{\text{NS}}^{\text{unexp./NLP/NNLP}} = \frac{\mathscr{L}_{ij}(\tau/z)}{z}\left(\Delta_{ij}^{(1)}(z)+\Delta_{ij}^{(2)}(z)\right)\Big|_{\text{NS}}^{\text{unexp./NLP/NNLP}}. \tag{5.17}$$

Fig. 5.5 shows normalised plots of these quantities. We see that the weight distribution for DY production is approximated well, for both Q values, by the NLP truncation over the full range of z. At NNLP the agreement with the exact result is excellent. For Higgs production at $Q = 125$ GeV, we again observe that the expansion does not capture the

parton luminosity for gg compared to $q\bar{q}$.

small-z region well, neither at NLP nor at NNLP. The stronger parton luminosity suppression at $Q = 500$ GeV does aid the convergence, with a NNLP truncation that is almost as good as for DY. Therefore, these plots confirm the expectation that the threshold expansions works better for the dominant production channel of DY than for Higgs production.

In figs. 5.6 and 5.7 we show similar plots for the qg-channels of both processes. In particular, fig. 5.6 shows that the z-dependence of the qg-flux is not qualitatively different from the $q\bar{q}$- and gg-flux.[9] Just as for the gg-channel, the parton luminosity suppresses the small-z domain, such that the enhancement in that region from the factor of $1/z$ in the Higgs partonic coefficient function is tempered. From fig. 5.7 we see that the power expansions approximate the full result less well for this channel than for the dominant production channels. Moreover, while the NLP and NNLP approximations for the Higgs qg-channel get significantly better for higher Q values, those for the DY qg-channel do not, and the threshold expansion for Higgs outperforms the one for DY at $Q = 500$ GeV. Again this is due to the parton luminosity suppression in the small-z region. For Higgs production the truncated expression deviates most from the exact (N)NLO coefficient function in this region, as seen in fig. 5.1, while for DY (fig. 5.2) this deviation is more spread out and therefore benefits less from going to large Q values.

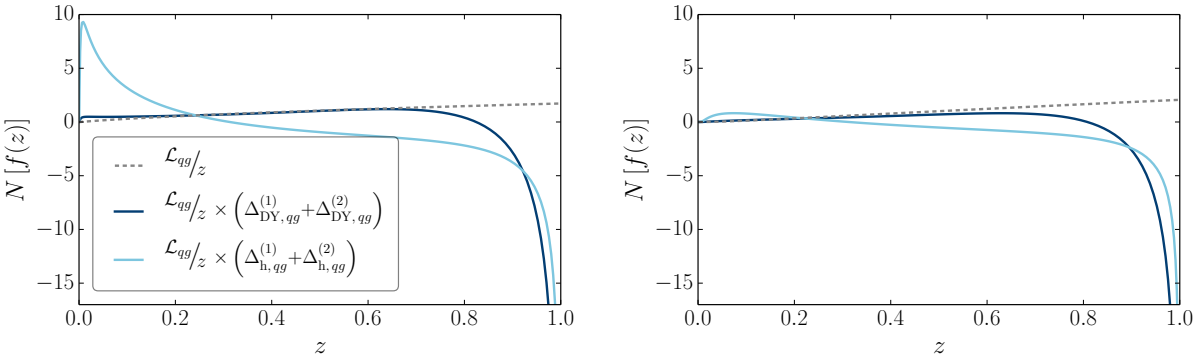

(a) $Q = 125$ *GeV* **(b)** $Q = 500$ *GeV*

Figure 5.6: *The luminosity function (grey dashed) and its point-by-point multiplication with the coefficient functions up to NNLO (solid), for the qg-channel of DY (dark blue) and single Higgs (light blue) production. All curves are normalised according to eq.* (5.15).

We note that the results presented in this subsection contain a level of detail that is of course lost upon integration over z. As such, the integration over z may lead to a seemingly contradictory result: cancellations between under- and overestimations of the exact result across the z domain may cause crude approximations to look more favourable than expected. This is what we observe in the next subsection, where we consider the quality of the threshold expansion of the integrated hadronic cross section. For example, for $Q = 125$ GeV the integrated NLP truncation approximates the exact NLO+NNLO result for the qg-channel in

[9] We note that the parton luminosity shown is summed over the five lightest (anti)quark flavours. For DY this luminosity function is weighted with the quark charge as well, but since this does not alter the line shape significantly, we do not show it separately to improve readability.

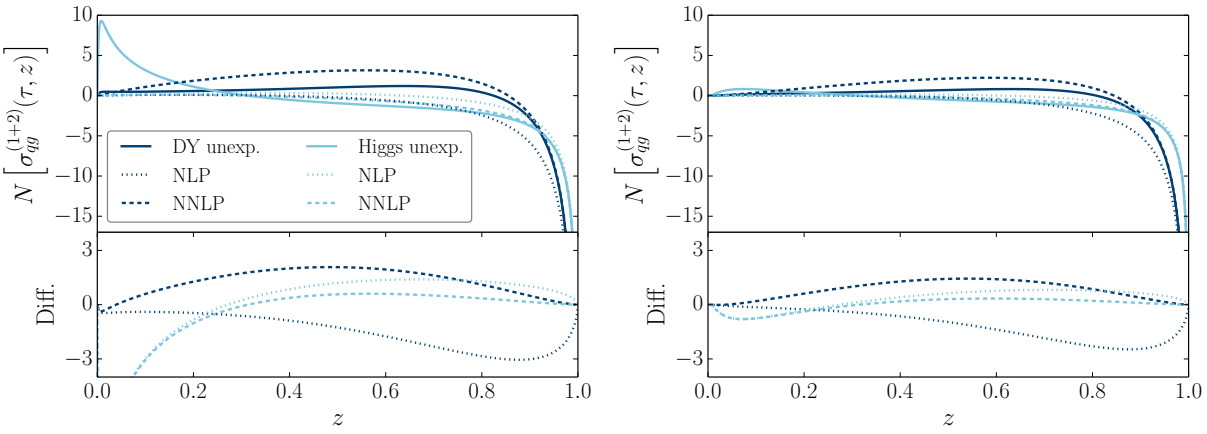

(a) $Q = 125$ *GeV* **(b)** $Q = 500$ *GeV*

Figure 5.7: *Exact and truncated expressions of the coefficient functions up to NNLO, weighted with the parton luminosity, for the qg-channel of DY and single Higgs production. Labelling is the same as for fig. 5.5. All curves are normalised according to eq.* (5.15)*.*

Higgs production better than the NNLP one, as will be seen in fig. 5.8, since the more severe overshoot for $z \gtrsim 0.3$ provides a better cancellation for the undershoot at small z.

5.1.4 Convergence of the threshold expansion in integrated hadronic cross sections

We now turn our attention to the behaviour of the threshold expansions of the total hadronic cross section, starting with single Higgs production. We show the expansions up to $\mathrm{N}^{p+1}\mathrm{LP}$, which follows from

$$\sigma^{(ij),p}_{pp\to h+X} = \sum_{n=1}^{2} \sigma_0^{\mathrm{h}} \left(\frac{\alpha_s}{\pi}\right)^n \int_\tau^1 \frac{dz}{z}\, \mathscr{L}_{ij}\left(\frac{\tau}{z}\right) \left[\sum_{m=0}^{2n-1} \sum_{k=-1}^{p} (1-z)^k\, c^{(k)}_{ij,nm}\, \ln^m(1-z)\right]. \quad (5.18)$$

As a possible δ-contribution cannot be expanded around $z = 1$, we show this term separately if its coefficient is non-zero. As in the previous subsection, we add the NLO and NNLO contributions in eq. (5.18), and we restrict our discussion to those partonic channels that contribute at NLP.

The truncated cross sections can be seen in fig. 5.8, where the power expansions are shown up to $\mathrm{N}^{20}\mathrm{LP}$. Results for the gg-channel for $Q = 125$ GeV are presented in fig. 5.8a. The LP expansion severely underestimates the unexpanded part of the hadronic cross section (without the δ-contribution), while the NLP expansion overestimates it by a much smaller amount. After including the NNLP term, the expansion stabilises.[10] Note that even at high orders in the expansion a small part of the cross section is still unaccounted for. This missing

[10] This is consistent with ref. [156], eq. (3) when we pick $g(z) = 1$.

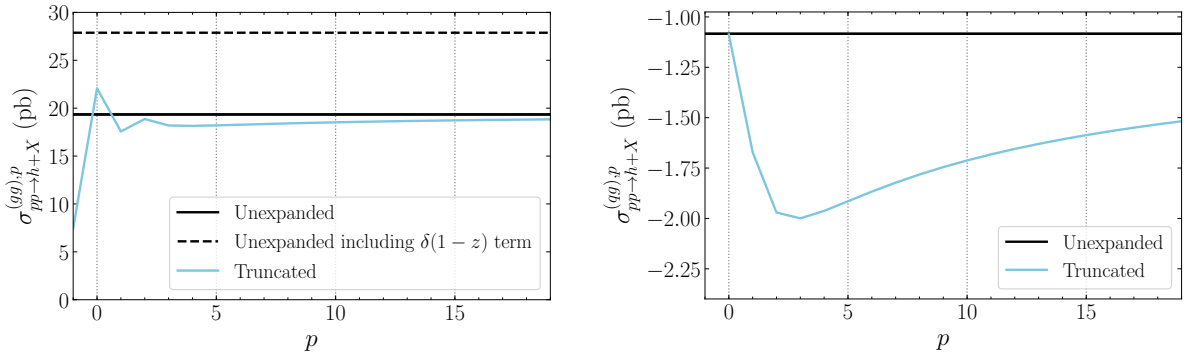

(a) *gg-channel* **(b)** *qg-channel*

Figure 5.8: *Power expansions of the NLO+NNLO hadronic cross sections for single Higgs production for $Q = 125$ GeV. The results are shown in a cumulative way: in the expansion up to power p, all $\mathcal{O}\big((1-z)^k\big)$ terms for $k \leq p$ are included. The $\delta(1-z)$ contribution in the dominant production channel is shown separately, and the LO contribution is not included.*

contribution can can be traced to the peak in the small-z regime in fig. 5.4a, which the threshold expansion fails to capture. We also observe a significant δ-contribution, as is well known for this process.

For the qg-channel in fig. 5.8b, we observe that the NLP truncation exactly produces the unexpanded cross section. This is however somewhat of a coincidence: the (N)NLO NLP truncation underestimates (overestimates) the magnitude of the negative unexpanded (N)NLO contribution by a similar amount. When added together, these under- and overestimates cancel. The NNLP truncation for the integrated cross section performs much worse, consistent with what we predicted based on fig. 5.7a. An overestimation of the negative contribution from this channel perseveres for higher-power truncations, and the expansion converges only very slowly to the full result. Again, this is due to the NLO and NNLO coefficients having a negative contribution at $z \to 1$, compensated by a large positive contribution for $z \to 0$, which is however only slowly reconstructed in a $1-z$ expansion.

Also for DY production at $Q = 125$ GeV, the LP expansion of dominant channel is not a good approximation of the exact cross section, as seen in fig. 5.9a. The NLP expansion shows moderate overestimation, consistent with what is reported in fig. 5.5a, but performs significantly better already. In general the power expansion converges quickly. For the qg-channel, shown in fig. 5.9b, we see that the NLP (NNLP) expansion overestimates (underestimates) the absolute value of the unexpanded NLO+NNLO coefficient, consistent with the deviations observed in fig. 5.7a. Contrary to the Higgs qg-channel, the threshold expansion does converge after including the N^4LP contribution.

Before we conclude this section, we comment on the behaviour of the threshold expansions for other values of Q. For the gg-channel in single Higgs production, the convergence of the threshold expansion happens faster for higher values of Q, which is a direct consequence of the stronger $1/z$ suppression of the gg-luminosity function. Also for the Higgs qg-channel

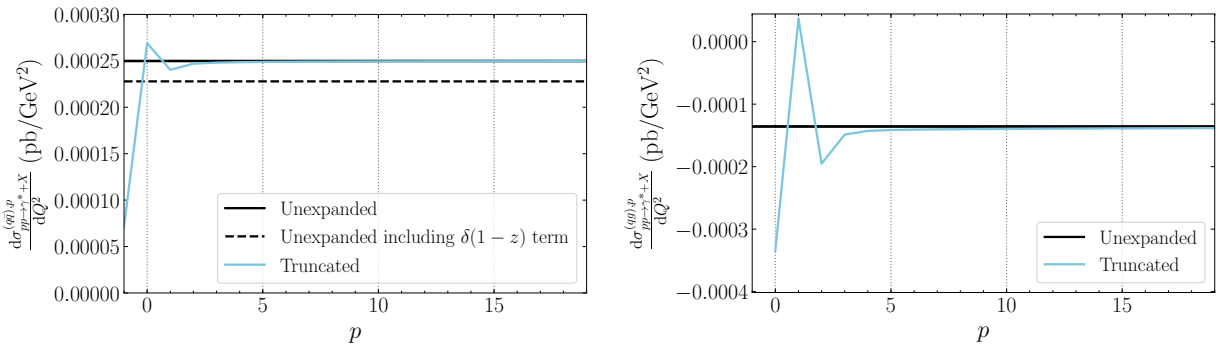

(a) *$q\bar{q}$-channel* **(b)** *qg-channel*

Figure 5.9: *Same as fig. 5.8, but for the total cross section of the DY production of an off-shell photon with $Q = 125$ GeV.*

the threshold expansion converges more slowly for small Q values than for larger ones, for the same reason. On the other hand, the behaviour of the threshold expansion of the $q\bar{q}$- and qg-channels in DY marginally improves at higher Q values. We conclude that the threshold expansion for NNLO cross sections is in general more reliable for DY than for single Higgs production for both the dominant ($q\bar{q}/gg$) and subleading qg production channels.

5.2 NLP resummation in QCD

Having exhibited the effect and quality of NLP approximations in fixed order cross sections, we now turn to consider NLP effects for resummed cross sections. This section discusses analytical aspects of NLP resummation, building on the results established in chapter 4, whereas numerical results are shown in section 5.3. We concentrate on the dominant channels, and address LP and NLP resummation at the same time.

5.2.1 From LP to NLP resummation

Resummation in QCD is customarily performed in Mellin-moment (N) space, where the cross section is a product of N-space functions. Thus, for the gluon-fusion contribution to Higgs production in eq. (5.1) one obtains

$$\sigma^{(gg)}_{pp\to h+X}(N) \equiv \int_0^1 d\tau\, \tau^{N-1} \sigma_{pp\to h+X}(\tau) = \sigma_0^{\mathrm{h}} f_g(N,\mu) f_g(N,\mu) \Delta_{gg}(N, Q^2/\mu^2)\,, \tag{5.19}$$

and similarly for the DY production (with $g \to q(\bar{q})$ and $\sigma_0^{\mathrm{h}} \to \sigma_0^{\mathrm{DY}}$). To perform the resummation in N-space, one uses the resummed perturbative coefficient $\Delta_{aa}(N)$. The resummed hadronic cross section in momentum space is obtained after taking the inverse Mellin transform

$$\sigma^{(gg)}_{pp\to h+X}(\tau) = \frac{1}{2\pi i} \int_{c-i\infty}^{c+i\infty} dN\, \tau^{-N} \sigma^{(gg)}_{pp\to h+X}(N)\,, \tag{5.20}$$

where we choose the Minimal Prescription [53] for the N integration contour. This corresponds to choosing $c = C_{\rm MP}$ to left of the large-N branch-cut (starting for us at the branch-point $\bar{N} = \exp[1/(2\alpha_s b_0)]$) originating from the Landau pole, but to the right of all other singularities. We note that this approach works for both LP and NLP terms, as the branch cut is identical for both terms. To minimise numerical instabilities, the integration contour is usually bent towards the negative real axis. We include analytic N-space PDFs in our inverse Mellin transform, for which we use a fitted form of the PDFs (see the discussion around eq. (5.61)).

In chapter 4 we derived a resummed partonic coefficient for colour-singlet production processes that incorporates the LL NLP contributions for the dominant channel (eq. (4.60)). Here we repeat the formula and express it in a slightly different form to connect to the standard notation for LP resummation. Subsequently, we will discuss the various components, highlighting to what perturbative order they are required for our purposes. The resummed NLP partonic coefficient is given by

$$\begin{aligned}\Delta_{aa}^{\rm LP+NLP}(N,Q^2/\mu^2) &= g_0(\alpha_s)\exp\Bigg[\int_0^1 dz\, z^{N-1}\Bigg\{\frac{1}{1-z}D_{aa}\left(\alpha_s\left(\frac{(1-z)^2Q^2}{z}\right)\right)\\ &\qquad + 2\int_{\mu^2}^{(1-z)^2Q^2/z}\frac{dk_T^2}{k_T^2}\,P_{aa}^{\rm LP+NLP}\left(z,\alpha_s(k_T^2)\right)\Bigg\}_+\Bigg]\\ &\equiv g_0(\alpha_s)\exp\left[D_{aa}^{\rm LP+NLP}(N)+2E_a^{\rm LP+NLP}(N)\right],\end{aligned} \tag{5.21}$$

where the overall +-subscript denotes that the plus-prescription needs to be applied to all LP contributions. The exponent $E_a^{\rm LP+NLP}$ contains the diagonal DGLAP splitting function P_{aa} expanded up to NLP in the threshold variable, which may be expressed as

$$\begin{aligned}P_{aa}^{\rm LP+NLP}\left(z,\alpha_s(k_T^2)\right) &= \sum_{n=1}^{\infty}P_{aa}^{(n)\,\rm LP+NLP}(z)\left(\frac{\alpha_s(k_T^2)}{\pi}\right)^n\\ &= A_a\left(\alpha_s(k_T^2)\right)\left[\left(\frac{1}{1-z}\right)_+-1\right],\end{aligned} \tag{5.22}$$

where

$$A_a\left(\alpha_s(k_T^2)\right)\equiv\sum_{n=1}^{\infty}A_a^{(n)}\left(\frac{\alpha_s(k_T^2)}{\pi}\right)^n. \tag{5.23}$$

The coefficients $A_a^{(n)}$ are known up to fourth order [218], but for NNLL accurary we need them only up to third order [219, 220]. We list these in appendix 5.D. Note that the factor of two associated to this term in eq. (5.21) reflects an initial state consisting of identical partons (either gg or $q\bar{q}$). The soft wide-angle contributions are collected in $D_{aa}(\alpha_s)$, which enjoys the perturbative expansion

$$D_{aa}(\alpha_s) = D_{aa}^{(1)}\frac{\alpha_s}{\pi}+D_{aa}^{(2)}\left(\frac{\alpha_s}{\pi}\right)^2+\dots. \tag{5.24}$$

In fact, this function starts at the two-loop level since $D_{aa}^{(1)}=0$. For a resummation at NNLL(′)

accuracy we then only need the coefficient $D_{aa}^{(2)}$ (see appendix 5.D). Both the $D_{aa}^{\text{LP+NLP}}$ and $E_a^{\text{LP+NLP}}$ terms are process-independent to the extent that they only depend on the colour structure of the underlying hard-scattering process. After the Mellin transform has been carried out, these terms contain *all* logarithmic N dependence at LP and *leading*-logarithmic N dependence at NLP. In fact, also some contributions that are beyond NLP LL accuracy are included here: both the argument of α_s in the function D_{aa} and the $1/z$-dependence of the upper limit of the k_T integral generate such terms, as we will see. Finally, there is the process-dependent function $g_0(\alpha_s)$ that collects the N-independent contributions. For an N^{k}LL resummation, we need this function only up to $\mathcal{O}(\alpha_s^{k-1})$, but if available we include the $\mathcal{O}(\alpha_s^k)$ terms as well, which upgrades N^{k}LL to N^{k}LL$'$ resummation.

If we substitute eq. (5.22) into eq. (5.21), we may compare the resummed NLP partonic coefficient with its LP counterpart [48, 49]

$$\Delta_{aa}^{\text{LP}}(N, Q^2/\mu^2) = g_0(\alpha_s)\exp\Bigg[\int_0^1 dz\,\frac{z^{N-1}-1}{1-z}\,D_{aa}\Big(\alpha_s\big((1-z)^2Q^2\big)\Big) + 2\int_0^1 dz\,\frac{z^{N-1}-1}{1-z}\int_{\mu^2}^{(1-z)^2Q^2}\frac{dk_T^2}{k_T^2}A_a\Big(\alpha_s(k_T^2)\Big)\Bigg], \tag{5.25}$$

where the plus-prescription is already applied. We highlight two changes with respect to (5.21). The first is that the splitting function is approximated to LP accuracy instead, removing the additional -1 term of eq. (5.22). The second is that the upper limit of the k_T integration on the second line, reflecting the exact phase-space constraint on the soft emission, has been replaced by its LP approximation. The same replacement has been made in the argument of α_s in D_{aa} on the first line. How to calculate the integrals in eq. (5.25) is outlined in refs. [49, 57, 58], and extended to accommodate NLP contributions to the splitting function in ref. [162]. However, the latter reference did not implement the exact phase-space constraint. If one does, a simpler formula can be derived that obtains the NLP contribution directly from the LP exponent using a derivative with respect to the Mellin moment N, which we show in the next subsection.

5.2.2 The NLP exponent as a differential operator

To this end, we calculate $E_a^{\text{LP+NLP}}$ explicitly at LL accuracy:

$$E_a^{\text{LP+NLP, LL}}(N) = \frac{A_a^{(1)}}{\pi}\int_0^1 dz\, z^{N-1}\left[\left(\frac{1}{1-z}-1\right)\int_{\mu^2}^{(1-z)^2Q^2/z}\frac{dk_T^2}{k_T^2}\alpha_s(k_T^2)\right]_+, \tag{5.26}$$

where we only need $A_a^{(1)}$. The integral over k_T may be evaluated using the QCD β-function, for which we only need the one-loop coefficient b_0 (see appendix 5.D), and write

$$\int_{\mu^2}^{(1-z)^2Q^2/z}\frac{dk_T^2}{k_T^2}\,\alpha_s(k_T^2) = -\frac{1}{b_0}\int_{\alpha_s}^{\alpha_s\left((1-z)^2Q^2/z\right)}\frac{d\alpha_s}{\alpha_s}$$

$$= \frac{1}{b_0} \ln\left(\frac{\alpha_s}{\alpha_s((1-z)^2Q^2/z)}\right), \tag{5.27}$$

where we use $\alpha_s \equiv \alpha_s(\mu^2)$. Using the running of α_s as described by the one-loop solution to the β-function

$$\alpha_s((1-z)^2Q^2/z) = \frac{\alpha_s}{1+\alpha_s b_0 \ln\left(\frac{(1-z)^2Q^2/z}{\mu^2}\right)}, \tag{5.28}$$

we find

$$\begin{aligned}\int_{\mu^2}^{(1-z)^2Q^2/z} \frac{dk_T^2}{k_T^2}\,\alpha_s(k_T^2) &= \frac{1}{b_0}\ln\left(1+\alpha_s b_0 \ln\left(\frac{(1-z)^2Q^2/z}{\mu^2}\right)\right) \\ &= -\frac{1}{b_0}\sum_{k=1}^{\infty}\frac{(-\alpha_s b_0)^k}{k}\left[\ln\left(\frac{(1-z)^2}{z}\right)+\ln\left(\frac{Q^2}{\mu^2}\right)\right]^k,\end{aligned} \tag{5.29}$$

where we have separated the scale-dependent logarithms from those with z-dependence. Since we wish to resum the highest power of the threshold logarithms at each order in α_s, we select the pure $\ln^k((1-z)^2/z)$ term from the above expression, discarding the explicit scale logarithms that only contribute at NLL accuracy and beyond.[11] Expanding this term up to NLP gives

$$\ln^k\left(\frac{(1-z)^2}{z}\right) = 2^k\ln^k(1-z) + k\,(1-z)\,2^{k-1}\ln^{k-1}(1-z) + \mathcal{O}\left((1-z)^2\right), \tag{5.30}$$

such that eq. (5.26) becomes

$$\begin{aligned}E_a^{\text{LP+NLP, LL}}(N) &= -\frac{A_a^{(1)}}{\pi b_0}\int_0^1 dz \sum_{k=1}^{\infty}\frac{(-2\alpha_s b_0)^k}{k}\left(\frac{z^{N-1}-1}{1-z}\ln^k(1-z) - z^{N-1}\ln^k(1-z)\right. \\ &\qquad\left. + \frac{k}{2}z^{N-1}\ln^{k-1}(1-z)\right) \\ &\equiv -\frac{A_a^{(1)}}{\pi b_0}\sum_{k=1}^{\infty}\frac{(-2\alpha_s b_0)^k}{k}\left(\mathscr{D}_k - \mathscr{J}_k + \frac{1}{2}\mathscr{J}'_k\right).\end{aligned} \tag{5.31}$$

In the second line we introduced shorthand notation for the Mellin integrals, which are evaluated through their generating functions $\mathscr{G}_{\mathscr{F}}$.[12] We define for $\mathscr{F} = \{\mathscr{D}, \mathscr{J}, \mathscr{J}'\}$

$$\mathscr{F}_k(N) = \left.\frac{d^k}{d\eta^k}G_{\mathscr{F}}(N,\eta)\right|_{\eta=0}, \tag{5.32}$$

with

$$G_{\mathscr{D}}(N,\eta) = \int_0^1 dz\left(z^{N-1}-1\right)(1-z)^{\eta-1} = \frac{\Gamma(N)\Gamma(\eta)}{\Gamma(N+\eta)} - \frac{1}{\eta}, \tag{5.33a}$$

[11] One obtains the same result by replacing $\mu^2 \to Q^2$ in the lower integration boundary of eq. (5.26).

[12] While $\mathscr{J}'$ constitutes a new contribution, results for $\mathscr{D}$ and $\mathscr{J}$ were already presented in appendix 4.B. We repeat the definitions for the latter two (eq. (4.94)) below for convenience.

$$G_{\mathscr{J}}(N,\eta) = \int_0^1 dz\, z^{N-1}(1-z)^{\eta} = \frac{\Gamma(N)\Gamma(1+\eta)}{\Gamma(1+N+\eta)}, \tag{5.33b}$$

$$G_{\mathscr{J}'}(N,\eta) = \eta\, G_{\mathscr{J}}(N,\eta). \tag{5.33c}$$

This method was proposed in ref. [58] for the LP contributions $\mathscr{D}_k$ and generalised to the NLP integrals $\mathscr{J}_k$ in ref. [162]. The terms labelled by $\mathscr{J}'_k$ were not included before. Although of sub-leading logarithmic accuracy, they are important for our final result. Expanding eq. (5.33) around the limit $N \to \infty$ yields, up to $\mathscr{O}(1/N^2)$ corrections

$$G_{\mathscr{D}}(N,\eta) = \frac{1}{\eta}\left[\frac{\Gamma(1+\eta)}{N^{\eta}}\left(1+\frac{\eta(1-\eta)}{2N}\right)-1\right], \tag{5.34a}$$

$$G_{\mathscr{J}}(N,\eta) = \frac{\Gamma(1+\eta)}{N^{1+\eta}}, \tag{5.34b}$$

$$G_{\mathscr{J}'}(N,\eta) = \frac{\eta\,\Gamma(1+\eta)}{N^{1+\eta}}. \tag{5.34c}$$

We see that pure LP contributions in z-space, as contained in $\mathscr{D}_k$, give NLP contributions in Mellin space (i.e. terms proportional to $1/N$). Given that the resummation is done in Mellin space, *NLP* refers to all terms proportional to $1/N$ in the remainder of this chapter. We now observe that all $\mathscr{O}(1/N)$ terms can be generated from the LP contributions in N-space by means of a derivative with respect to N

$$\begin{aligned} G_{\mathscr{D}}(N,\eta) - G_{\mathscr{J}}(N,\eta) + \frac{1}{2}G_{\mathscr{J}'}(N,\eta) &= \frac{1}{\eta}\left[\Gamma(1+\eta)\left(1-\frac{\eta}{2N}\right)N^{-\eta}-1\right] \\ &= \left(1+\frac{1}{2}\frac{\partial}{\partial N}\right)\frac{1}{\eta}\left[\Gamma(1+\eta)\exp\left[-\eta\,\ln N\right]-1\right]. \end{aligned} \tag{5.35}$$

Note that this only holds when including $\mathscr{J}'$, as it cancels the η^2 term in the square brackets of eq. (5.34a). Taylor expansion of the LP contribution (i.e. the term in eq. (5.35) without the derivative) around $\eta = 0$ yields

$$\begin{aligned} \frac{1}{\eta}\left[\Gamma(1+\eta)N^{-\eta}-1\right] &= \frac{1}{\eta}\Bigg(\sum_{m=0}^{\infty}\sum_{n=0}^{m}\frac{1}{n!\,(m-n)!} \\ &\qquad \times\left[\frac{\partial^n}{\partial\eta^n}\Gamma(1+\eta)\,\frac{\partial^{m-n}}{\partial\eta^{m-n}}\exp\left[-\eta\,\ln N\right]\right]_{\eta=0}\eta^m - 1\Bigg) \\ &= \sum_{m=1}^{\infty}\sum_{n=0}^{m}\frac{(-1)^{m-n}}{n!\,(m-n)!}\,\Gamma^{(n)}(1)\,\ln^{m-n}N\,\eta^{m-1}, \end{aligned} \tag{5.36}$$

with $\Gamma^{(n)}$ denoting the n-th derivative of the gamma function, i.e.

$$\Gamma^{(n)}(1) = \frac{d^n}{d\eta^n}\Gamma(1+\eta)\Big|_{\eta\to 0}. \tag{5.37}$$

In this way, we have isolated the η behaviour in one simple factor, such that the derivative of eq. (5.32) amounts to the relation $\frac{d^k\eta^{m-1}}{d\eta^k}\big|_{\eta=0} = k!\,\delta_{k,m-1}$. Rewriting eq. (5.35) using

eq. (5.36) we obtain, via eq. (5.32):

$$E_a^{\text{LP+NLP, LL}}(N) = \frac{A_a^{(1)}}{\pi b_0}\left(1+\frac{1}{2}\frac{\partial}{\partial N}\right)\sum_{k=1}^{\infty}\frac{(2\alpha_s b_0)^k}{k(k+1)}\sum_{n=0}^{k+1}\binom{k+1}{n}(-1)^n\,\Gamma^{(n)}(1)\,\ln^{k+1-n}N\,, \quad (5.38)$$

Terms in the sum with $n>0$ are sub-leading logarithmic terms in N, but some of those are easily included by redefining N to $\bar{N}=\exp[\gamma_E]N$. To illustrate this, we note that

$$(-1)^n\,\Gamma^{(n)}(1) = \gamma_E^n + \frac{\zeta(2)}{2}n(n-1)\gamma_E^{n-2}+\dots\,, \quad (5.39)$$

where the ellipsis denotes terms involving lower powers of γ_E as well as constants of higher transcendental weight ($\zeta(n)$ for $n\geq 3$). Using eq. (5.39) and shifting the summation index $n\to n'+2$ for the second term in eq. (5.39) (where $n=0$ and $n=1$ do not contribute) yields

$$\begin{aligned}E_a^{\text{LP+NLP, LL}}(N) &= \frac{A_a^{(1)}}{\pi b_0}\left(1+\frac{1}{2}\frac{\partial}{\partial N}\right)\sum_{k=1}^{\infty}(2\alpha_s b_0)^k \\ &\quad\times\left[\frac{1}{k(k+1)}\sum_{n=0}^{k+1}\binom{k+1}{n}\gamma_E^n\,\ln^{k+1-n}N+\frac{\zeta(2)}{2}\sum_{n'=0}^{k-1}\binom{k-1}{n'}\gamma_E^{n'}\,\ln^{k-1-n'}N\right] \\ &= \frac{A_a^{(1)}}{\pi b_0}\left(1+\frac{1}{2}\frac{\partial}{\partial N}\right)\sum_{k=1}^{\infty}(2\alpha_s b_0)^k\left[\frac{\ln^{k+1}(\bar{N})}{k(k+1)}+\frac{\zeta(2)}{2}\ln^{k-1}(\bar{N})\right], \end{aligned} \quad (5.40)$$

having recognised the binomial series for $(\ln N+\gamma_E)^{k\pm1}\equiv\ln^{k\pm1}\bar{N}$ in the last line. We see that the $\zeta(2)$ term in eq. (5.39) contributes only at NNLL accuracy. Defining $\lambda=b_0\alpha_s\ln\bar{N}$ and performing the summation over k, this NNLL term results in

$$\begin{aligned}E_a^{\text{LP+NLP, NNLL}}(N) &= \alpha_s\frac{A_a^{(1)}}{\pi}\left(1+\frac{1}{2}\frac{\partial}{\partial N}\right)\frac{\zeta(2)}{1-2\lambda} \\ &= \alpha_s\zeta(2)\frac{A_a^{(1)}}{\pi}\left(1+\frac{1}{2}\frac{\partial}{\partial N}\right)\left[\frac{2\lambda}{1-2\lambda}+1\right]. \end{aligned} \quad (5.41)$$

The $+1$ contribution in the last line is included in the $\mathcal{O}(\alpha_s)$ contribution of g_0. The first term in the square brackets is instead included in the NNLL contribution to the resummed exponent (see eq. (5.79c) of appendix 5.D). Finally, we find for the LL term

$$\begin{aligned}E_a^{\text{LP+NLP, LL}}(N) &= \frac{A_a^{(1)}}{2\pi b_0^2\,\alpha_s}\left(1+\frac{1}{2}\frac{\partial}{\partial N}\right)[2\lambda+(1-2\lambda)\ln(1-2\lambda)] \\ &= \frac{A_a^{(1)}}{2\pi b_0^2\,\alpha_s}[2\lambda+(1-2\lambda)\ln(1-2\lambda)]-\frac{A_a^{(1)}}{2\pi b_0}\frac{\ln(1-2\lambda)}{N} \\ &\equiv \frac{1}{\alpha_s}g_a^{(1)}(\lambda)+h_a^{(1)}(\lambda,N) = \frac{1}{\alpha_s}\left(1+\frac{1}{2}\frac{\partial}{\partial N}\right)g_a^{(1)}(\lambda), \end{aligned} \quad (5.42)$$

where the LL NLP resummation function $h_a^{(1)}$ is obtained from the LL LP function $g_a^{(1)}$ by taking the derivative towards N.

We stress that the logarithmic accuracy of the generated NLP terms is limited by that of the LP function on which it acts. By using the full $A(\alpha_s)$ function for $E_a^{\text{LP+NLP}}$ one can in principle extend the result to higher logarithmic accuracy, generating a *partial* N^{i}LL NLP exponent through the derivative of the relevant LP resummation functions with respect to N:

$$E_a^{\text{LP+NLP}}(N) = \left(1+\frac{1}{2}\frac{\partial}{\partial N}\right)\int_0^1 dz\,\frac{z^{N-1}-1}{1-z}\int_{\alpha_s}^{\alpha_s((1-z)^2Q^2)}\frac{d\alpha_s}{\beta(\alpha_s)}A_a(\alpha_s), \tag{5.43}$$

while a similar result can be obtained for the wide-angle contribution $D_{aa}^{\text{LP+NLP}}$ in eq. (5.21).

Given our focus on the resummation of NLP LL contributions, we shall only use the function $h_a^{(1)}$ in eq. (5.42) for the numerical studies in section 5.3. Our final form of the resummation exponent, at LP NNLL$'$ and NLP LL accuracy, thus reads

$$\begin{aligned}\Delta_{aa}^{\text{LP+NLP}}(N,Q^2/\mu^2) = g_0(\alpha_s)\exp\Bigg[&\frac{2}{\alpha_s}g_a^{(1)}(\lambda)+2g_a^{(2)}\left(\lambda,Q^2/\mu^2\right)\\&+2\alpha_s g_a^{(3)}\left(\lambda,Q^2/\mu^2\right)+2h_a^{(1)}(\lambda,N)\Bigg],\end{aligned} \tag{5.44}$$

where the wide-angle contribution is contained entirely in $g_a^{(3)}$. Explicit expressions for these resummation exponents are collected in appendix 5.D.

5.3 Numerical effects of NLP LL resummation

Having set-up the framework for threshold resummation at LP NNLL$'$ and NLP LL accuracy, we turn to the numerical study of its effects on various colour-singlet production processes, in the context of LHC collisions at $\sqrt{S} = 13$ TeV. We use fitted PDFs that allow for an analytical evaluation of the Mellin transform, as explained in appendix 5.A. For DY and single Higgs production we will show resummed observables that are matched to the fixed-order result at NNLO. The matching is defined by

$$\sigma^{(\text{matched})} = \sigma^{\text{LP+NLP}} - \sigma^{\text{LP+NLP}}\Big|_{(\text{fixed order})} + \sigma^{(\text{fixed order})}. \tag{5.45}$$

Note that $\sigma^{(\text{fixed order})}$ denotes the *full* fixed-order result, including contributions from the sub-dominant production channels. The second term on the right hand side is the expanded resummed observable. We calculate this term by Taylor-expanding the resummed coefficient function in N-space

$$\Delta_{aa}^{\text{LP+NLP}}(N,Q^2/\mu^2)\Big|_{(\text{fixed order})} = \sum_{j=0}^{n}\frac{\alpha_s^j}{j!}\left[\frac{\partial^j}{\partial\alpha_s^j}\Delta_{aa}^{\text{LP+NLP}}(N,Q^2/\mu^2)\right]_{\alpha_s=0}, \tag{5.46}$$

where we only need the terms up to $\mathcal{O}(\alpha_s^n)$ for matching with an N^{n}LO fixed-order calculation. The result is substituted into eq. (5.19), after which the Mellin-space inversion is

handled via eq. (5.20). The expansion of (5.46) will create terms that are further suppressed than $\mathcal{O}(1/N)$. They are kept in the matching and thus subtracted from the resummed result as they are also contained in the complete fixed-order expression. We perform the LP resummation at NNLL′ accuracy, where NNLL′ resummation offers an improvement over NNLL by the inclusion of the exact N-independent terms at NNLO (i.e. we include g_0 up to $\mathcal{O}(\alpha_s^2)$). This is not strictly necessary for NNLL resummation, but it is relevant in case of large virtual corrections at the two-loop level, such as for single Higgs production. We stress again that we only resum the channels that contribute at LP. To examine the impact of NLP resummation on colour-singlet processes other than DY or single Higgs production, we also show at the end of this section results for di-boson and di-Higgs production, which we include at LP NLL accuracy and do not match to fixed higher-order results.

5.3.1 Single Higgs production

To obtain the total resummed Higgs cross section in N-space, we start from eq. (5.19)

$$\sigma_{pp\to h+X}(N) = \sigma_0^{\rm h} f_g(N,\mu) f_g(N,\mu) \Delta_{gg}^{\rm LP+NLP}(N, Q^2/\mu^2), \tag{5.47}$$

with $\sigma_0^{\rm h}$ as given in eq. (5.2), and the resummed coefficient function of eq. (5.44) for $a = g$ and g_0 up to $\mathcal{O}(\alpha_s^2)$. We vary $Q(= m_h)$ with the aim of exploring the resummation effects more widely than only for the physical scale $Q = 125$ GeV.

The results are shown in fig. 5.10, where all lines have been normalised either to LO (a) or NNLO (b). All resummed results are matched to the NNLO fixed-order result. The large enhancement due to the NNLL′ matched resummation with respect to the LO result is caused by the sizable $\delta(1-z)$ contribution to both the NLO and NNLO fixed-order cross sections, which enter the resummed distribution via $g_0(\alpha_s)$. The enhancement of the LP NNLL′+ NLP LL resummed result, with respect to the LO distribution (using $\mu = Q$), is roughly 300−360% in the considered Q range, the strongest increase occurring for smaller Q values.

When compared to the matched LP NNLL′ resummed cross section, we find an NLP enhancement between 4.3−6.3%, with larger effects for smaller Q values, as shown in fig. 5.11a. We contrast this increase with the effect of upgrading the LP accuracy to N3LL. To obtain this we need to include only the $g_a^{(4)}(\lambda, Q^2/\mu^2)$ function in the resummation exponent, which we extract from the publicly available TROLL code [209], given that $g_0(\alpha_s)$ is already included up to $\mathcal{O}(\alpha_s^2)$ for NNLL′ accuracy. Only a modest (negative) N^{3}LL correction to the NNLL′ resummed cross section is found: between $-(0.3-0.5)$%. We have verified that the NLP corrections are competitive with the numerical increase from NLL to NNLL, and we show explicitly in figs. 5.10b and 5.11a that they dominate over the increase from NNLL′ to N^{3}LL.[13]

[13] One could also compare to the N^{3}LL′ results, where the $\mathcal{O}(\alpha_s^3)$ contribution to $g_0(\alpha_s)$ is included. Here we choose not to do so, in order to directly compare the numerical contribution of terms that are of $\mathcal{O}(\alpha_s^k \ln^{k-2}(\bar{N}))$ with those that are of $\mathcal{O}(\alpha_s^k \ln(\bar{N})^k/N)$ (where k runs from 1 to ∞). If we would compare at LP N^{3}LL′ instead, the $\mathcal{O}(\alpha_s^k \ln^{k-2}(\bar{N}))$ terms in the exponent would be multiplied by a different hard

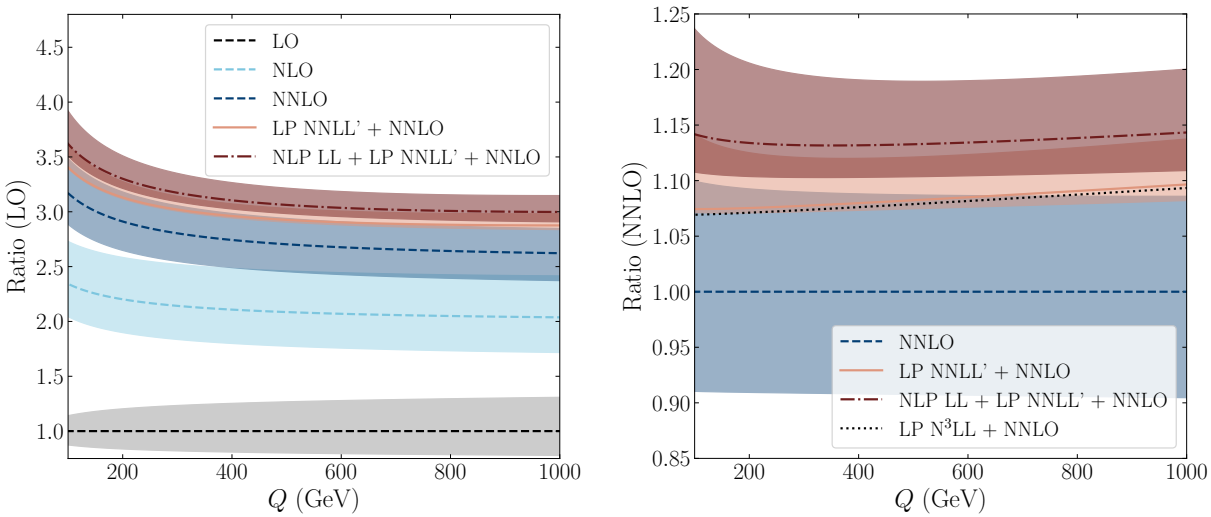

(a) *Ratio with respect to LO* **(b)** *Ratio with respect to NNLO*

Figure 5.10: *Cross section for the production of a single Higgs boson in the infinite top mass limit as a function of its mass Q (with $Q = 125$ GeV corresponding to the physical Higgs mass), normalised to fixed-order results. The scale uncertainty, obtained by varying μ between $\mu = Q/2$ and $\mu = 2Q$, is indicated by the coloured bands.* ***(a)*** *The LO, NLO and NNLO results are shown in black, light-blue and dark-blue dashed lines respectively. The LP NNLL$'$ (+NLP LL) resummed result matched to NNLO is indicated by the orange solid (red dash-dotted) line.* ***(b)*** *Here we also show the LP N^3LL resummed result, indicated by the black dotted line. The scale-uncertainty band for the N^3LL distribution is not shown, as it coincides with the one obtained for the NNLL$'$ distribution.*

Furthermore, we note that scale uncertainty increases somewhat after including the NLP resummation. For the LP NNLL$'$ resummed result, the scale uncertainty is between -0.03% and $+6.2\%$, whereas the NLP resummed result shows a scale uncertainty between -2.9% and $+8.3\%$ (we expect that the inclusion NLP NLL terms would reduce this scale uncertainty). We also point out that the central value for the LP NNLL$'$ + NLP LL resummed result lies outside the uncertainty band of the LP NNLL$'$ resummed result, over the entire range of Q values considered here. Finally, we report below on the Higgs cross sections at $Q = 125$ GeV, corresponding to the physical Higgs mass:

$$\begin{aligned}
\sigma^{(\text{NNLO})}_{pp\to h+X}(m_\text{h}) &= 39.80^{+9.7\%}_{-9.0\%}\ \text{pb}\,,\\
\sigma^{(\text{LP NNLL}')}_{pp\to h+X}(m_\text{h}) &= 42.76^{+5.6\%}_{-0.3\%}\ \text{pb}\,,\\
\sigma^{(\text{LP N}^3\text{LL})}_{pp\to h+X}(m_\text{h}) &= 42.64^{+5.8\%}_{-0.1\%}\ \text{pb}\,,\\
\sigma^{(\text{LP NNLL}' + \text{NLP LL})}_{pp\to h+X}(m_\text{h}) &= 45.32^{+7.5\%}_{-2.8\%}\ \text{pb}\,.
\end{aligned} \tag{5.48}$$

We thus find a notable NLP LL contribution in the diagonal channel.

function than the LP NNLL$'$ + NLP LL result, which pollutes the comparison with a (possibly sizeable) constant contribution.

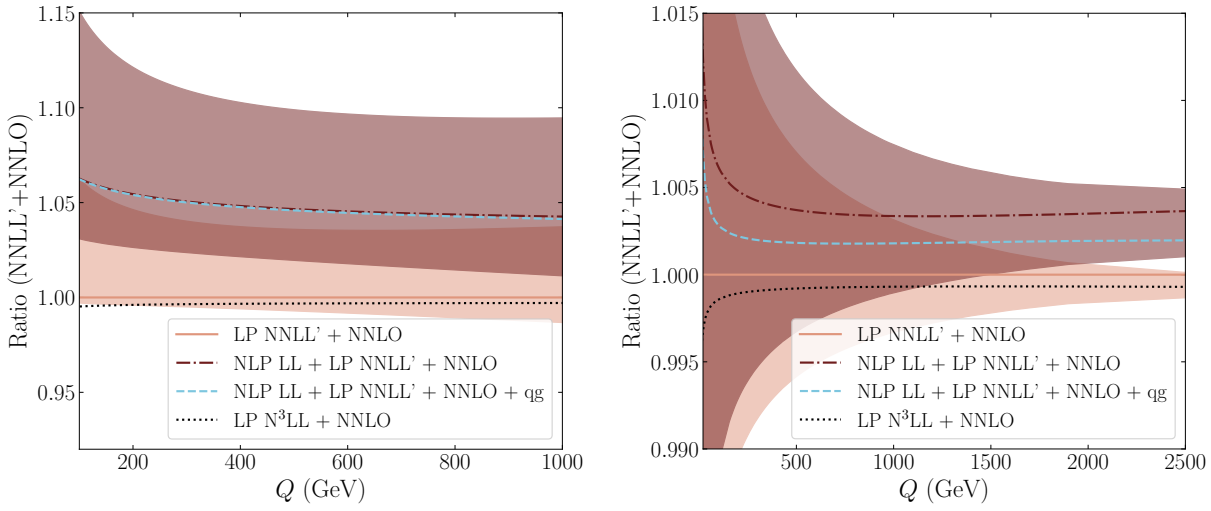

(a) **(b)**

Figure 5.11: *Ratio plots for the Higgs total cross section* ***(a)*** *and DY invariant mass distribution* ***(b)****, both normalised to the LP NNLL′ + NNLO result. The colour coding for the LP NNLL′ (+NLP LL) and LP N³LL results is the same as in fig. 5.10b. The result obtained by adding the N³LO NLP LL qg contribution is shown by the dotted light-blue line.*

Of course, the resummation of the qg-channel is missing, which would also result in NLP LL enhanced terms (see fig. 5.8), and may potentially alter the observed NLP effect. To estimate the size of such contributions we include the NLP LL contribution from the qg-channel at N^{3}LO, the order at which we expect the largest contribution from a potential resummation in that channel. The full N^{3}LO result for the Higgs total cross section is available in the infinite top mass limit [32], and can be inferred from the `iHixs2` code [221]. We find that the qg-induced NLP LL contribution reads

$$\Delta_{\mathrm{h},qg}\big|_{\alpha_s^3}(N) = -\left(\frac{\alpha_s}{\pi}\right)^3 \frac{C_F(115C_A^2 + 50C_AC_F + 27C_F^2)}{96}\frac{\ln^5 \bar{N}}{N}, \tag{5.49}$$

which coincides with the prediction of ref. [160]. This qg-contribution results in a correction of the NLP LL resummation effect of −0.5% (−3%) for small (large) Q values (see fig. 5.11a).

The $\mathcal{O}(\alpha_s^3)$ contribution of the qg-channel thus gives a negligible contribution to the NLP LLs. Adding the terms of eq. (5.49) does not lead to a noticeable reduction of the scale uncertainty (not shown in the figure). Note that the smallness of the qg-initiated result is not caused by the partonic flux: the qg-flux exceeds the gg-flux at $\mu = 125$ GeV. Instead, this contribution is relatively small because, in contrast to the NLP LL contribution from the gg-channel, the qg-contribution is not proportional to the sizable higher-order constant terms of the LP gg-channel contained in the $\mathcal{O}(\alpha_s)$ and $\mathcal{O}(\alpha_s^2)$ contributions to the hard function $g_0(\alpha_s)$. A similar hard function is not included for the qg-channel, as we cannot use an exponentiated form for the qg contribution, nor know what the hard function in that case would be. We expect that the qg-channel will play a larger role in the DY process, where the g_0^1 and g_0^2 coefficients are comparatively small.

5.3.2 The DY process

For the computation of the N-space resummed DY invariant mass distribution we use

$$\frac{d\sigma_{pp\to\gamma^*+X}(N)}{dQ^2} = \sigma_0^{\mathrm{DY}} \sum_q e_q^2 f_q(N,\mu) f_{\bar{q}}(N,\mu) \Delta_{q\bar{q}}^{\mathrm{LP+NLP}}(N, Q^2/\mu^2), \tag{5.50}$$

with σ_0^{DY} given in eq. (5.13) and $\Delta_{q\bar{q}}^{\mathrm{LP+NLP}}(N,Q^2/\mu^2)$ in eq. (5.44), and where the sum runs over the quarks $q \in \{u,d,c,s,b\}$ that are considered to be massless. We show the ratio plots with respect to the LO and NNLO result in fig. 5.12. The various resummed distributions are plotted in fig. 5.11b, normalised to the LP NNLL′ result. As in the Higgs case, all resummed results are matched to the NNLO result.

Figure 5.12a shows that the LP NNLL′ + NLP LL resummation enhances the LO distribution (using $\mu = Q$) by $15-34\%$, with increasing effect for larger Q values. The NLP contribution provides an increase with respect to the LP NNLL′+NNLO resummed (and matched) distribution of only $0.35-1.15\%$, as can be read off from fig. 5.11b. Larger NLP enhancements are found for very small values of Q, where one moves further away from threshold. Note that also the effect of LP resummation is smaller than for Higgs production, as can be seen in fig. 5.12b, as a result of the quicker (asymptotic) convergence of the perturbative series for DY. As for the Higgs production case, the NLP increase dominates over the N^{3}LL effect, which deviates by $-(0.1-0.3)\%$ from the LP NNLL′ distribution, where the larger deviation is only found for small values of Q (as best seen in fig. 5.11b). The larger size of the NLP LL with respect to the N3LL is not as pronounced as in the Higgs production case.

The scale uncertainty of the NNLL′ resummed result lies between -4.4% and $+5.4\%$ for the range of Q values shown in fig. 5.12, while that of the NLP resummed result is between -4.8% and $+5.8\%$. Therefore, by including the NLP LL contribution, we find a modest increase in the scale uncertainty of the resummed result, which would expect to decrease if NLL resummation at NLP were available. Note that for large Q values ($Q > 1$ TeV), the central value of the NLP result lies outside the uncertainty band of the LP distribution.

As in the Higgs production case, the NLP LL resummation is not complete, since the qg-channel is missing (see fig. 5.9). Using the results of ref. [160], we may obtain the N^{3}LO NLP LL contribution stemming from the qg-channel, resulting in

$$\Delta_{\mathrm{DY},qg}\big|_{\alpha_s^3}(N) = -\left(\frac{\alpha_s}{\pi}\right)^3 T_F \frac{27C_A^2 + 50C_AC_F + 115C_F^2}{96} \frac{\ln^5 \bar{N}}{N}. \tag{5.51}$$

As already anticipated, in contrast to what was observed for single Higgs production, we see that the addition of this result to the resummed $q\bar{q}$-channel significantly alters the NLP effect (fig. 5.11b). The qg-contribution gives a -54% correction to the NLP effect of the dominant channel for small Q values, while for larger Q values it gives a -44% correction. As for Higgs production, we find that the scale uncertainties do not decrease after adding the qg NLP LL contribution at $\mathcal{O}(\alpha_s^3)$. This is perhaps not surprising: for both the Higgs and

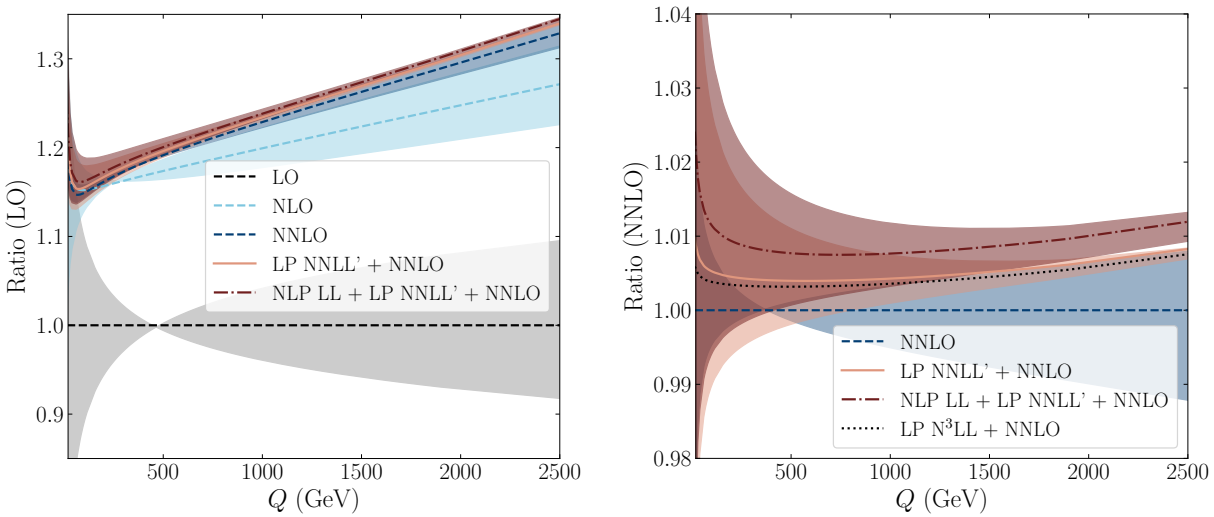

(a) *Ratio with respect to LO* **(b)** *Ratio with respect to NNLO*

Figure 5.12: *Ratio plots for the DY invariant mass distribution, normalised to fixed order results. The colour coding and scale variation is the same as in fig. 5.10.*

DY processes we introduce additional scale-dependence via α_s in either the NLP LL function $h_a^{(1)}$ for the leading channel, or via eq. (5.50)/(5.51) for the off-diagonal channel. This scale dependence is not balanced at LL, but could (for both channels) be balanced at NLP NLL via the introduction of a scale term proportional to $\ln(Q^2/\mu^2)$. However, since we have no control over any other contribution that might appear at NLP NLL, we refrain from adding such contributions.

5.3.3 Other colour-singlet production processes

Based on the considerations of chapter 4 we may apply our NLP resummation prescription also to gg- or $q\bar{q}$-induced processes with N colour-singlet particles in the LO final state. In this section we will therefore consider di-Higgs and di-boson production, as key examples of such processes. As it is not our aim to provide a precise phenomenological prediction, but rather analyse the numerical effects of NLP LL resummation, we consider the (unmatched) resummation of these processes up to LP NLL + NLP LL, and include only the LO contribution to $g_0(\alpha_s)$.

We start with the di-Higgs production process, which is also dominated by gluon fusion. Threshold resummation has been achieved first up to NLL in the SCET framework in the heavy top mass limit, including form factors dependent on the top-quark mass to partially correct for this approximation [222]. This study has been extended to NNLL in ref. [223], and the inclusion of the full top mass effects was studied up to NLL+NLO in ref. [224]. With full top mass dependence, the lowest-order expression for the hadronic differential

distribution is given by [225]

$$\frac{d\sigma_{pp\to hh}}{dQ} = \frac{2Q}{S}\int_\tau^1 \frac{dx}{x} f_g(x,\mu)\, f_g\left(\frac{\tau}{x},\mu\right) \sigma_{gg\to hh}(Q^2), \tag{5.52}$$

with $\tau = Q^2/S$ and

$$\sigma_{gg\to hh}(Q^2) = \frac{G_F^2\alpha_s^2}{256\,(2\pi)^3}\int_{t_-}^{t^+} dt\, \left(\left|C_\triangle F_\triangle + C_\square F_\square\right|^2 + \left|C_\square G_\square\right|^2\right). \tag{5.53}$$

where the integration variable $t = -\frac{1}{2}\left(Q^2 - 2m_h^2 - Q^2\sqrt{1-4m_h^2/Q^2}\cos\theta\right)$, while the integration limits are obtained by setting $\cos\theta = \pm 1$. The exact expressions of ref. [225] are used for $C_\triangle$, $C_\square, F_\triangle$, $F_\square$ and $G_\square$, where no approximation on the mass ratio between the top-quark and the Higgs boson has been applied.

For the resummation of this process, it suffices to follow the same procedure as before. That is, we Mellin transform eq. (5.52) with respect to the hadronic threshold variable τ. Then we replace the partonic LO coefficient by its resummed version

$$\sigma_{gg\to hh}(Q^2) \longrightarrow \sigma_{gg\to hh}(Q^2)\,\Delta_{gg}^{\text{LP+NLP}}\left(N, Q^2/\mu^2\right). \tag{5.54}$$

This replacement is valid at LP (see ref. [226]). We exploit the universal structure of NLP resummation for colour-singlet processes, as discussed in chapter 4, to justify the same substitution at NLP. The resummed expression then reads

$$\frac{d\sigma_{pp\to hh+X}}{dQ} = \sigma_{gg\to hh}(Q^2)\,\frac{2Q}{S}\int \frac{dN}{2\pi i}\,\tau^{-N} f_g(N,\mu)\, f_g(N,\mu)\,\Delta_{gg}^{\text{LP+NLP}}\left(N, Q^2/\mu^2\right). \tag{5.55}$$

Since we work at NLL accuracy at LP, we use the resummed partonic coefficient of eq. (5.44) with $g_0(\alpha_s) = 1$ and neglect the $g^{(3)}$ contribution in the exponent.

The results are shown in fig. 5.13, where we used a factorisation/renormalisation scale $\mu = Q/2$, which is the scale for which higher-order corrections are smallest [227]. We see that the LP NLL result gives a correction to the LO distribution of -3.2% to 4.7%, while the NLP LL terms cancel the partially negative LP correction, leading to a substantial enhancement of the LO distribution of $12.6 - 17.8\%$. Larger corrections are found for higher values of Q. The increase of the NLP LL + LP NLL result with respect to the LP NLL result is between 12.5% and 16.3%. As for the DY and single Higgs production processes, we find again that the NLP LL effect is sizeable. For comparison, the increase of going from LP LL (not shown here) to LP NLL is of the same order.

We now move on to W^+W^- and ZZ production. Threshold resummation up to NNLL was considered in the traditional QCD framework in ref. [228], and using the SCET framework in refs. [229, 230]. Transverse-momentum resummation for both processes has also been

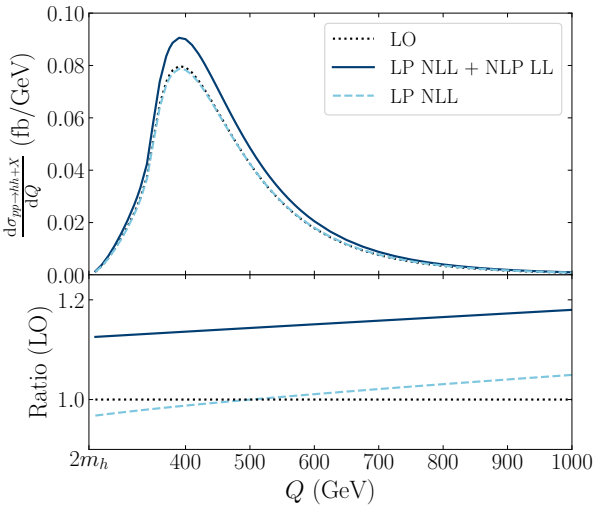

Figure 5.13: *Differential cross section for di-Higgs production showing the LO (black dotted), LP NLL (dashed light-blue), and NLP LL + LP NLL (solid dark-blue) results. The scale μ is set to $Q/2$. The bottom pannel shows the ratio with respect to the LO distribution.*

performed in ref. [231]. We use the LO expressions from refs. [232, 233].[14] We may write, similarly to eq. (5.52)

$$\frac{d\sigma_{pp\to VV}}{dQ} = \frac{2Q}{S}\sum_{i=\{q,\bar{q}\}}\int_\tau^1 \frac{dx}{x} f_i(x,\mu)\,\bar{f}_i\left(\frac{\tau}{x},\mu\right)\sigma_{q_i\bar{q}_i\to VV}(Q^2), \tag{5.56}$$

with the LO partonic cross sections given by

$$\sigma_{q_i\bar{q}_i\to W^+W^-}(Q^2) = \frac{1}{64\pi C_A Q^4}\left(c_i^{tt}\,\mathscr{F}_i(Q^2) - c_i^{ts}(Q^2)\mathscr{J}_i(Q^2) + c_i^{ss}(Q^2)\mathscr{K}_i(Q^2)\right), \tag{5.57}$$

$$\sigma_{q_i\bar{q}_i\to ZZ}(Q^2) = \frac{g_{V,i}^4 + g_{A,i}^4 + 6\left(g_{V,i}g_{A,i}\right)^2}{4\pi C_A Q^2}\left(\frac{1+4m_Z^4/Q^4}{1-2m_Z^2/Q^2}\log\left(\frac{1+\beta_Z}{1-\beta_Z}\right) - \beta_Z\right), \tag{5.58}$$

where $\beta_Z = \sqrt{1-4m_Z^2/Q^2}$. The expressions for the coefficients c_i^{tt}, c_i^{ts}, and c_i^{ss}, and the functions $\mathscr{F}_i$, $\mathscr{J}_i$ and $\mathscr{K}_i$ may be found in ref. [232]. Note that the partonic cross sections $\sigma_{q_i\bar{q}_i\to VV}$ depend on the left- and right-handed couplings of the quarks with the Z-boson, which are of course different for up-type quarks and down-type quarks. Following the same procedure as for the di-Higgs results, we obtain a resummed expression for both cases that reads

$$\frac{d\sigma_{pp\to VV+X}}{dQ} = \sigma_{q\bar{q}\to VV}(Q^2)\frac{2Q}{S}\int\frac{dN}{2\pi i}\,\tau^{-N} f_q(N,\mu)\,f_{\bar{q}}(N,\mu)\,\Delta_{q\bar{q}}^{\text{LP+NLP}}\left(N,Q^2/\mu^2\right). \tag{5.59}$$

The results are shown in fig. 5.14. The two processes are identical from a resummation

[14] Note that in ref. [232], there is a misprint in the LO integrated coefficients (eq. (3.12)). The second terms in the expressions for $\mathscr{F}_i(s)$ and $\mathscr{J}_i(s)$ need to be multiplied by a factor of 16.

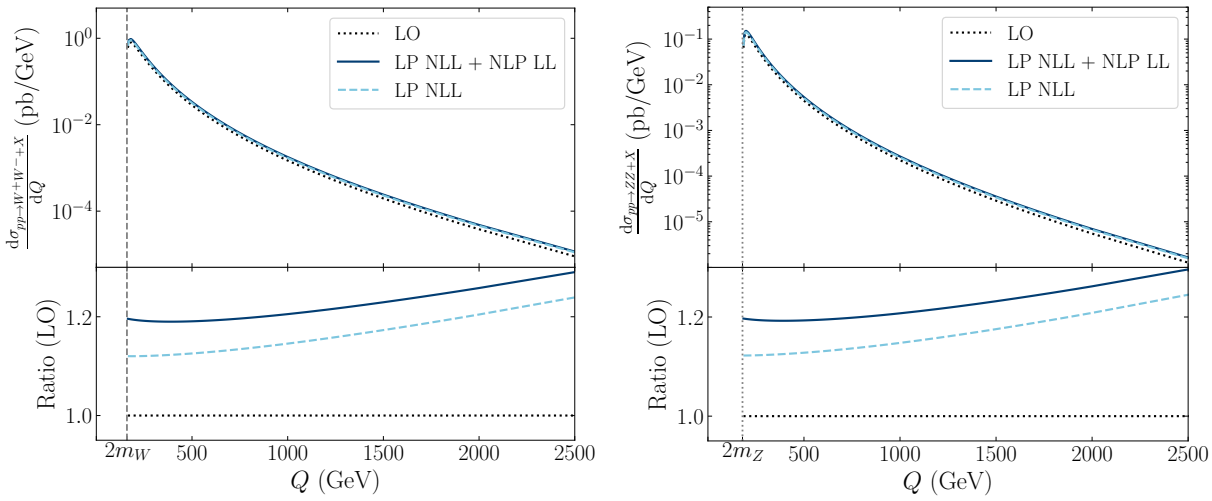

Figure 5.14: *Differential cross section for W^+W^- production **(a)** and ZZ production **(b)**, with the scale μ set to Q. Presentation is the same as in fig. 5.13.*

perspective, therefore, we find an LP NLL increase of the LO distribution between $12.2-20.8\%$ for both processes, whereas the NLP LL + LP NLL increases the LO distributions by $19.2-26.2\%$. As for the other processes, larger enhancements are found for higher values of Q. The increase induced by the NLP LL contributions with respect to the LP NLL result is between $4.5-6.8\%$, which is smaller than the correction that was found for di-Higgs production. This is not surprising: it is well known that gluon-initiated processes receive larger LL threshold corrections due to $C_A > C_F$. However, the difference between LP LL and LP NLL resummation for the VV production processes is only around 1%, once again underlining the importance of the NLP LL contribution.

5.3.4 A brief comparison of numerical NLP LL resummation studies

In this section we have explored the numerical effects of the NLP contribution $h_a^{(1)}$ to the resummed partonic coefficient function in eq. (5.44) on a selection of colour-singlet production processes. For all processes we reach a similar conclusion: NLP LL resummation has a non-negligible numerical effect. Here, we briefly comment on the relation between the work on NLP resummation presented in this study and in refs. [209, 234] for single Higgs production. The methods employed in this chapter may best be compared to their $\psi-\text{soft}_2$ prescription without exponentiation of the constant contributions.[15] The $\psi-\text{soft}_2$ prescription consists of replacing λ in the resummation exponents $g^{(i)}(\lambda)$ by the combination of di-gamma functions $\lambda = \alpha_s b_0(2\psi_0(N) - 3\psi_0(N+1) + 2\psi_0(N+2))$. Denoting their

[15] Another prescription, $A-\text{soft}_2$ in ref. [209] uses the Borel prescription [235, 236] to handle the asymptotic summation of the perturbative expansion. Numerical differences between $A-\text{soft}_2$ and $\psi-\text{soft}_2$ are shown to be small there.

resummation exponent at LP NLL with $\Delta_{aa}^{\psi-\text{soft}_2}$, the difference with our LP NLL + NLP LL resummation exponent (i.e. eq. (5.44) without $g_a^{(3)}$ and with $g_0(\alpha_s)=1$) may be evaluated at $\mathcal{O}(\alpha_s)$, where we obtain

$$\Delta_{aa}^{\psi-\text{soft}_2}(N)-\Delta_{aa}^{\text{LP+NLP}}(N)=\frac{\alpha_s}{\pi}\left[-A_a^{(1)}\left(2\gamma_E^2-2\gamma_E\ln\frac{Q^2}{\mu^2}\right)-\frac{A_a^{(1)}}{N}\ln\frac{Q^2}{\mu^2}+\mathcal{O}\left(\frac{1}{N^2}\right)\right]. \quad (5.60)$$

The difference at LP is of NNLL accuracy and is due to the resummation of $\log N$ rather than $\log\bar{N}$ terms in the $\psi-\text{soft}_2$ prescription. At NLP, the difference appears at NLL, such that the approaches are equivalent at the guaranteed accuracy. Note that the discrepancy continues beyond NLP, given that di-gamma functions generate power corrections to all orders in N at NLO, while our prescription, gives rise to at most $\mathcal{O}(1/N^n)$ terms at $\mathcal{O}(\alpha_s^n)$. They observe that the correction on the fixed-order single Higgs production cross section is increased with respect to standard resummation by making the $\psi-\text{soft}_2$ replacement, consistent with our observations on the effect of NLP LL resummation. No soft-quark contribution was considered in their work. To the best of our knowledge, a similar analysis for DY has not been performed.

5.4 Conclusions

In this chapter we studied the role and impact of NLP corrections in colour-singlet production processes, with a particular focus on DY and single Higgs production. In section 5.1 we assessed the quality of the threshold expansion for Higgs and DY, for both the dominant ($q\bar{q}$ and gg) and the subdominant (qg) partonic channels. The threshold expansion of the dominant Higgs production channel is less well-behaved than that of DY, due to a substantial part of the Higgs partonic cross section arising from the small-z region. The quality of the threshold expansion depends only marginally on the boson mass Q for DY, while the convergence for Higgs noticeably improves as Q increases. The threshold expansion of the off-diagonal qg-channel in Higgs production convergences only very slowly, whereas for DY convergence is already obtained after including the N^{4}LP contribution.

We subsequently reviewed the resummation of leading-logarithmic NLP corrections in QCD in section 5.2, and derived a slightly improved resummed expression involving a derivative with respect to the Mellin moment. We applied our resummation approach to a selection of colour-singlet production processes, revealing that the resummation of NLP LLs has a noticeable effect. Indeed, for single Higgs-production the central value of the LP NNLL$'$ + NLP LL resummed cross section lies outside the uncertainty band for the LP resummed (and matched) result. For the DY processes this is observed for $Q>1$ TeV. Both processes show that the numerical effect of resumming the NLP LL terms exceeds that of improving LP resummation to N^{3}LL accuracy. Scale uncertainties seem to slightly increase after the NLP LL result is included, and we expect that the scale uncertainty can be reduced only after the inclusion of the (unavailable) NLP NLL contributions. For di-boson production the

numerical enhancement of upgrading a LP NLL calculation to NLP LL rivals (in the case of di-Higgs) or exceeds (for W^+W^-/ZZ) that of going from LP LL to LP NLL, for central scale choices. In general, NLP LL effects originating from next-to-soft-gluon emissions are found to be larger for gg-induced processes than for $q\bar{q}$-induced processes. Lastly, we found that the DY process was (relatively) more sensitive to NLP LL contributions from the off-diagonal qg-channel than the Higgs process, owing to large NLO and NNLO contributions to $g_0(\alpha_s)$ for the latter process.

Our study of the numerical effects of NLP corrections in hadronic collisions is, we believe, a valuable addition to an area where most effort has so far been on the analytical side. It moreover validates these efforts by showing that NLP threshold corrections can have a notable impact, and should motivate further development of the understanding of NLP corrections.

5.A Fitted parton distribution functions

In this paper we rely on PDFs obtained from the LHAPDF library [237] and use the central member of the PDF4LHC15_NNLO_100 PDF set [216]. For our purposes these PDFs need to be converted to N-space to perform the resummation. To this end, we expand the PDFs on a basis of polynomials whose Mellin transforms may be computed directly. The functional form of the PDFs that we use is inspired by that used by the MMHT [238] collaboration, and reads

$$\begin{aligned} xf(x) &= A(1-x)^{a_1}x^{a_2}(1+by+c(2y^2-1))+B(1-x)^{a_3}x^{a_4}(1+Cx^{a_5}), \\ y &= 1-2\sqrt{x}, \end{aligned} \tag{5.61}$$

with 10 (real) fit parameters. We require that the fitted function lies within the 1σ error as given by the LHAPDF grid implementation of the PDFs in the entire domain. We have checked our set by comparing the fixed-order results obtained with the x-space form of the fitted PDFs with those obtained using the grid directly, and found that differences are smaller than the numerical integration error. A tabulated form in `C++` format of the resulting fit parameters is available at [239].

5.B Normalisation of the partonic cross section

In this appendix we discuss the normalisation of the partonic cross section $\Delta_{ij}(z)$, with the particular aim to highlight the origin of the additional factor of $1/z$ appearing in Higgs production relative to DY. We start from the definition of the invariant mass distribution

$$\frac{d\sigma}{dQ^2} = \sum_{i,j}\int_0^1 dx_1 \int_0^1 dx_2\, f_i(x_1) f_j(x_2)\, \hat{\sigma}_{ij}\left(\frac{Q^2}{x_1 x_2 S}\right), \tag{5.62}$$

where $\hat{\sigma}_{ij}(Q^2/(x_1x_2S))$ is the partonic cross section, and we drop the renormalisation/factorisation scale dependence for conciseness. For Higgs production an analogous equation holds, with the invariant mass distribution replaced by the total cross section.

We first rewrite the partonic cross section in terms of $z = Q^2/(x_1x_2S) = Q^2/s$. This can be done by inserting

$$1 = \int_0^1 dz\,\delta\left(z-\frac{\tau}{x_1x_2}\right) = \int_0^1 dz\, x_1x_2\,\delta(\tau-x_1x_2z) = \int_0^1 dz\,\frac{\tau}{z}\,\delta(\tau-x_1x_2z), \tag{5.63}$$

where we recall that $\tau = Q^2/S$. With this, eq. (5.62) becomes

$$\frac{d\sigma}{dQ^2} = \sum_{i,j}\int_0^1 dz \int_0^1 dx_1 \int_0^1 dx_2\, f_i(x_1) f_j(x_2)\,\delta(\tau-x_1x_2z)\,\frac{\tau}{z}\,\hat{\sigma}_{ij}(z). \tag{5.64}$$

This equation is then matched to eq. (5.12), which we repeat here

$$\frac{d\sigma}{dQ^2} = \sigma_0(Q^2) \sum_{i,j} \int_0^1 dz \int_0^1 dx_1 \int_0^1 dx_2 f_i(x_1) f_j(x_2) \delta(\tau - x_1 x_2 z) \Delta_{ij}(z). \tag{5.65}$$

The matching equation

$$\frac{\tau}{z} \hat{\sigma}_{ij}(z) = \sigma_0(Q^2) \Delta_{ij}(z), \tag{5.66}$$

is defined such that $\sigma_0(Q^2)$ contains the terms of the tree-level cross section which are z-independent, while $\Delta_{ab}(z)$ contains the z-dependent terms.

We are now in a position to perform the matching in eq. (5.66) for the DY and Higgs tree-level cross section. We start from the matrix element squared for the two processes, summed (averaged) over the final (initial) state partons

$$|\mathscr{M}_{\rm DY}^{(0)}|^2 = \frac{4\alpha_{\rm EM}^2}{3Q^2} \frac{s}{N_c}, \qquad |\mathscr{M}_{\rm h}^{(0)}|^2 = \left(\frac{\alpha_s}{3\pi v}\right)^2 \frac{s^2}{8(N_c^2-1)}. \tag{5.67}$$

The factor of s^2 in the Higgs matrix element squared is due to the derivative squared contained in the $G^a_{\mu\nu} G^{a,\mu\nu} H$ term of the effective Lagrangian. Given the one-particle phase space with the flux factor of $1/2s$

$$\frac{1}{2s} d\Phi_1 = \int d^4q \, 2\pi \, \delta^{(4)}(p_1 + p_2 - q) \delta^+\left(q^2 - Q^2\right) = \frac{\pi}{s^2} \delta(1-z), \tag{5.68}$$

the partonic cross section for the two processes reads

$$\hat{\sigma}_{\rm DY}^{(0)}(z) = \frac{4\pi\alpha_{\rm EM}^2}{3Q^2} \frac{1}{N_c} \frac{z}{Q^2} \delta(1-z), \qquad \hat{\sigma}_{\rm h}^{(0)}(z) = \frac{\alpha_s^2}{72\pi v^2} \frac{1}{N_c^2-1} \delta(1-z). \tag{5.69}$$

We see that the DY cross section has an additional factor of z compared to Higgs production, whose origin is ultimately related to the dimensionful effective ggH vertex versus the elementary $q\bar{q}\gamma$ vertex. The coefficient $\Delta_{aa}^{(0)}(z)$ is now obtained from eq. (5.66), where $\sigma_0^{\rm h}$ and $\sigma_0^{\rm DY}$ are taken as in eqs. (5.2) and (5.13), which implies

$$\Delta_{{\rm DY},q\bar{q}}^{(0)} = \delta(1-z), \qquad \Delta_{{\rm h},gg}^{(0)} = \frac{1}{z} \delta(1-z). \tag{5.70}$$

At tree level the additional factor of $1/z$ is of course harmless, given the overall $\delta(1-z)$. However, this factor is general, and it is present also at higher orders in perturbation theory, explaining the origin of the factor $1/z$ in eq. (5.7) (see also eq. (5.11)).

5.C Singular contributions at threshold

In order to asses how the parton flux weighs the partonic cross section, it is useful to consider the point-by-point multiplication of the partonic cross section and the parton luminosity factor $\mathscr{L}_{ij}(\tau/z)/z$. For non-singular terms beyond LP this is trivial, but the singular contributions at LP consist of plus-distributions which have the non-local definition

$$\int_0^1 dz\,[g(z)]_+ f(z) = \int_0^1 dz\, g(z)(f(z)-f(1))\,. \tag{5.71}$$

In this appendix we show explicitly how one obtains an equivalent point-by-point multiplication for the LP terms. Starting from the hadronic cross section

$$\frac{d\sigma_{ij}}{d\tau} = \int_\tau^1 dz\,\frac{\mathscr{L}_{ij}(\tau/z)}{z}\frac{d\hat{\sigma}_{ij}(z)}{dz}\,, \tag{5.72}$$

we express the partonic cross section, differential in z, as

$$\frac{d\hat{\sigma}(z)}{dz} = -\frac{\partial}{\partial z}\int_z^1 dz'\,\frac{d\hat{\sigma}(z')}{dz'}\,. \tag{5.73}$$

Upon integration by parts we find

$$\begin{aligned}\frac{d\sigma_{ij}}{d\tau} &= -\frac{\mathscr{L}_{ij}(\tau/z)}{z}\int_z^1 dz'\,\frac{d\hat{\sigma}_{ij}(z')}{dz'}\bigg|_\tau^1 + \int_\tau^1 dz\,\frac{\partial}{\partial z}\left[\frac{\mathscr{L}_{ij}(\tau/z)}{z}\right]\int_z^1 dz'\,\frac{d\hat{\sigma}_{ij}(z')}{dz'} \\ &= \int_\tau^1 dz\,\frac{\partial}{\partial z}\left[\frac{\mathscr{L}_{ij}(\tau/z)}{z}\right]\times\left(-\int_0^z dz'\,\frac{d\hat{\sigma}_{ij}(z')}{dz'}\right).\end{aligned} \tag{5.74}$$

The boundary term in the first line vanishes at $z=1$ by a vanishing domain for the integral over z', as well as at the lower boundary since $\lim_{z\to\tau}\mathscr{L}_{ij}(\tau/z)=0$. The plus-distributions in the remaining term on the first line of eq. (5.74) are now separately integrated, with the trivial test function $f(z')=1$, such that we could use

$$\int_z^1 dz'\,[g(z')]_+ = \int_0^1 dz'\,[g(z')]_+ - \int_0^z dz'\,g(z')\,. \tag{5.75}$$

to obtain the second line of eq. (5.74). Thus, the integrand of eq. (5.74) is indeed a point-by-point multiplication, consisting of the integrated plus-distributions weighted by the derivative of the parton luminosity function.

5.D Resummation coefficients

To evaluate the running of α_s we use the β-function as defined by

$$\frac{d\alpha_s(\mu^2)}{d\ln(\mu^2)} \equiv \beta(\alpha_s(\mu^2)) = -\alpha_s^2 \sum_{n=0} b_n \alpha_s^n \,. \tag{5.76}$$

With this definition, we have the one- [21, 22], two- [240–242] and three-loop [243, 244] coefficients

$$\begin{aligned} b_0 &= \frac{11C_A - 4T_R n_f}{12\pi}\,, \qquad b_1 = \frac{17C_A^2 - 10C_A T_R n_f - 6C_F T_R n_f}{24\pi^2}\,, \\ b_2 &= \frac{1}{(4\pi)^3}\Bigg[\frac{2857}{54}C_A^3 - \frac{1415}{27}C_A^2 T_R n_f - \frac{205}{9}C_A C_F T_R n_f + 2C_F^2 T_R n_f \\ &\qquad + \frac{158}{27}C_A T_R^2 n_f^2 + \frac{44}{9}C_F T_R^2 n_f^2\Bigg], \end{aligned} \tag{5.77}$$

and $T_R = 1/2$, $C_A = 3$ and $C_F = \frac{4}{3}$. The number of active flavours is denoted by n_f and is set equal to 5 in this study. At $\mathcal{O}(\alpha_s^2)$, the solution to the β-function reads

$$\alpha_s\left(k_T^2\right) = \frac{\alpha_s}{1 + b_0\alpha_s \ln\frac{k_T^2}{\mu_R^2}} - \frac{\alpha_s^2}{\left(1 + b_0\alpha_s \ln\frac{k_T^2}{\mu_R^2}\right)^2}\frac{b_1}{b_0}\ln\left(1 + b_0\alpha_s \ln\frac{k_T^2}{\mu_R^2}\right) + \mathcal{O}\left(\alpha_s^3\right). \tag{5.78}$$

The initial state exponents for the LP LL ($g_a^{(1)}$), NLL ($g_a^{(2)}$) and NNLL resummations ($g_a^{(3)}$) are given by [57, 245]

$$g_a^{(1)}(\lambda) = \frac{A_a^{(1)}}{2\pi b_0^2}\Big[2\lambda + (1-2\lambda)\ln(1-2\lambda)\Big], \tag{5.79a}$$

$$\begin{aligned} g_a^{(2)}(\lambda, Q^2/\mu_F^2, Q^2/\mu_R^2) &= \frac{1}{2\pi b_0}\left(-\frac{A_a^{(2)}}{\pi b_0} + A_a^{(1)}\ln\Big(\frac{Q^2}{\mu_R^2}\Big)\right)\Big[2\lambda + \ln(1-2\lambda)\Big] \\ &\quad + \frac{A_a^{(1)} b_1}{2\pi b_0^3}\Big[2\lambda + \ln(1-2\lambda) + \frac{1}{2}\ln^2(1-2\lambda)\Big] - \frac{A_a^{(1)}}{\pi b_0}\lambda\ln\Big(\frac{Q^2}{\mu_F^2}\Big), \end{aligned} \tag{5.79b}$$

$$\begin{aligned} g_a^{(3)}(\lambda, Q^2/\mu_F^2, Q^2/\mu_R^2) &= \frac{2A_a^{(1)}}{\pi}\frac{\zeta(2)\lambda}{1-2\lambda} + \frac{A_a^{(1)} b_2}{2\pi b_0^3}\left[2\lambda + \ln(1-2\lambda) + \frac{2\lambda^2}{1-2\lambda}\right] \\ &\quad + \frac{A_a^{(1)} b_1^2}{2\pi b_0^4(1-2\lambda)}\left[2\lambda^2 + 2\lambda\ln(1-2\lambda) + \frac{1}{2}\ln^2(1-2\lambda)\right] \\ &\quad - \frac{A_a^{(2)} b_1}{2\pi^2 b_0^3}\frac{1}{1-2\lambda}\left[2\lambda + \ln(1-2\lambda) + 2\lambda^2\right] - \frac{A_a^{(2)}}{\pi^2 b_0}\lambda\ln\frac{Q^2}{\mu_F^2} \\ &\quad - \frac{A_a^{(1)}}{2\pi}\lambda\ln^2\frac{Q^2}{\mu_F^2} + \frac{A_a^{(1)}}{\pi}\lambda\ln\frac{Q^2}{\mu_R^2}\ln\frac{Q^2}{\mu_F^2} + \frac{A_a^{(1)}}{\pi}\frac{\lambda^2}{1-2\lambda}\ln^2\frac{Q^2}{\mu_R^2} \end{aligned} \tag{5.79c}$$

$$+\frac{1}{1-2\lambda}\left(\frac{A_a^{(1)}b_1}{2\pi b_0^2}[2\lambda+\ln(1-2\lambda)]-\frac{2A_a^{(2)}}{\pi^2 b_0}\lambda^2\right)\ln\frac{Q^2}{\mu_R^2}$$
$$+\frac{A_a^{(3)}}{\pi^3 b_0^2}\frac{\lambda^2}{1-2\lambda}-\frac{D_{aa}^{(2)}}{2b_0\pi^2}\frac{\lambda}{1-2\lambda},$$

where $\lambda = b_0\alpha_s \ln\bar{N}$ and $\alpha_s \equiv \alpha_s(\mu_R^2)$. The N^{3}LL function $g_a^{(4)}(\lambda, Q^2/\mu_F^2, Q^2/\mu_R^2)$ is extracted from the TROLL code [209]. The function $h^{(1)}$, which is added to account for the NLP LL terms, reads

$$h_a^{(1)}(\lambda, N) = -\frac{A_a^{(1)}}{2\pi b_0}\frac{\ln(1-2\lambda)}{N}. \tag{5.80}$$

The coefficients $A_a^{(n)}$ are given by [49, 219, 220]

$$A_a^{(1)} = C_a, \qquad A_a^{(2)} = \frac{C_a}{2}\left[C_A\left(\frac{67}{18}-\zeta(2)\right)-\frac{10}{9}T_R n_f\right], \tag{5.81}$$
$$A_a^{(3)} = C_a\Bigg[\left(\frac{245}{96}-\frac{67}{36}\zeta(2)+\frac{11}{24}\zeta(3)+\frac{11}{8}\zeta(4)\right)C_A^2-\frac{1}{108}n_f^2$$
$$+\left(-\frac{209}{432}+\frac{5}{18}\zeta(2)-\frac{7}{12}\zeta(3)\right)C_A n_f+\left(-\frac{55}{96}+\frac{1}{2}\zeta(3)\right)C_F n_f\Bigg].$$

The first order coefficient $D_{aa}^{(1)} = 0$, while the second order coefficient reads [246, 247]

$$D_{aa}^{(2)} = C_a\left(C_A\left(-\frac{101}{27}+\frac{11}{18}\pi^2+\frac{7}{2}\zeta_3\right)+n_f\left(\frac{14}{27}-\frac{1}{9}\pi^2\right)\right), \tag{5.82}$$

with $C_q = C_F$ and $C_g = C_A$. The hard function $g_0(\alpha_s)$ is given by

$$g_0(\alpha_s) = \sigma_0\left[1+\alpha_s g_0^1+\alpha_s^2 g_0^2+\mathcal{O}\left(\alpha_s^3\right)\right], \tag{5.83}$$

where the various coefficients g_0^i are of course process dependent. We extract these from the TROLL code [209], but give their explicit form below for convenience. For DY one has

$$\sigma_0 = \sigma^{\mathrm{DY}}, \qquad g_0^{\mathrm{DY},1} = \frac{C_F}{\pi}\left(4\zeta_2-4+\frac{3}{2}\ln\frac{Q^2}{\mu_F^2}\right), \tag{5.84}$$
$$g_0^{\mathrm{DY},2} = -\frac{b_0 C_F}{\pi}\ln\frac{\mu_F^2}{\mu_R^2}\left(4\zeta(2)-4+\frac{3}{2}\ln\frac{Q^2}{\mu_F^2}\right)$$
$$+\frac{C_F}{16\pi^2}\Bigg[\ln^2\frac{Q^2}{\mu_F^2}(18C_F-11C_A+2n_F)+C_F\left(\frac{511}{4}-198\zeta(2)-60\zeta(3)+\frac{552}{5}\zeta(2)^2\right)$$
$$+C_A\left(-\frac{1535}{12}+\frac{376}{3}\zeta(2)+\frac{604}{9}\zeta(3)-\frac{92}{5}\zeta(2)^2\right)+n_f\left(\frac{127}{6}-\frac{64}{3}\zeta(2)+\frac{8}{9}\zeta(3)\right)$$
$$+\ln\frac{Q^2}{\mu_F^2}\left(C_F(48\zeta(3)+72\zeta(2)-93)+C_A\left(\frac{193}{3}-24\zeta(3)-\frac{88}{3}\zeta(2)\right)\right.$$

$$+ n_f \left(\frac{16}{3}\zeta(2) - \frac{34}{3} \right) \Bigg) \Bigg],$$

with $\sigma^{\rm DY}$ given in eq. (5.13). For single Higgs production the coefficients read

$$\sigma_0 = \sigma_0^{\rm h}, \qquad g_0^{\rm h,1} = \frac{C_A}{\pi}\left(4\zeta_2 + \frac{11}{6} + \frac{33-2n_f}{18}\ln\frac{\mu_R^2}{\mu_F^2} \right), \tag{5.85}$$

$$\begin{aligned} g_0^{\rm h,2} = {} & \frac{2A_g^{(2)}\zeta(2)}{\pi^2} + 3b_0^2\ln^2\frac{\mu_F^2}{\mu_R^2} + \ln\frac{Q^2}{m_t^2}\left(\frac{2}{3}\frac{n_f}{\pi^2} + \frac{19}{8\pi^2} \right) \\ & \frac{C_A}{\pi^2}\Bigg[\ln\frac{Q^2}{\mu_F^2}\left(8b_0\pi\zeta(2) + \frac{11}{3}b_0\pi + \frac{C_A}{6}(9\zeta(3)+8) - \frac{4n_f}{9} \right) \\ & - \ln\frac{Q^2}{\mu_R^2}\left(\frac{11}{2}b_0\pi + \frac{2}{3}b_1 + 12b_0\pi\zeta(2) \right) + n_f\left(-\frac{5}{9}\zeta(2) + \frac{5}{18}\zeta(3) - \frac{1189}{432} \right) \\ & + \frac{8}{3}\pi b_0\zeta(3) + 2C_A\left(\zeta(2)^2 + 6\zeta(4) \right) - \frac{9}{60}\zeta^2(2) + \frac{199}{6}\zeta(2) - \frac{55}{4}\zeta(3) + \frac{11399}{432} \Bigg], \end{aligned}$$

where σ_0^h is given in eq. (5.2), and we have used the infinite top mass limit for the effective ggh-coupling.

Chapter 6

Conclusions

In this thesis we studied various aspect of NLP threshold effects to improve our description of physics in this regime. By accounting for subleading effects in this kinematic limit, we hope to improve predictions for observables sensitive to soft radiation at (future) particle colliders in a systematic way. To this end, we studied the singular structure of scattering amplitudes and classified sources of NLP threshold logarithms, and made the first steps in extending the resummation of such terms from LP to NLP using diagrammatic techniques.

In chapter 2 we provided a systematic analysis of the all-order factorisation structure of non-radiative amplitudes in QED for massive and massless fermions. By means of power-counting techniques, inspired by a similar analysis for Yukawa theory [85], we constructed a factorisation formula involving new contributions with respect to earlier gauge-theory results at NLP [78,79,81]. While this formula also contains interactions between soft and hard or soft and collinear subdiagrams, we focused on new types of jet functions describing the exchange of multiple particles between a collinear blob and the hard scattering amplitude. We performed an explicit calculation of the so-called $f\gamma$- and $f\partial\gamma$-jet functions, which are the first non-trivial functions of this type. Subsequently, we performed one- and two-loop checks of the proposed factorisation formula by comparing the result of this particular contribution with a method of regions calculation of the relevant region. This analysis was carried out for non-radiative amplitudes in the case of fermions with a parametrically small but non-zero mass, and subsequently repeated for single-radiative amplitudes in the massless theory. In the latter case, we thus evaluated and tested one-loop radiative $f\gamma$- and $f\partial\gamma$-jet functions, allowing for direct comparison with factorisation in terms of the "standard" radiative jet function as discussed in refs. [78, 79], which has a more simplified factorisation structure with respect to our result, in that the ingredients factorise into a direct product rather than convolutions. However, a careful analysis of the one-loop amplitude reveals that the $f\gamma$- and $f\partial\gamma$-jet functions do capture all terms appearing in the collinear region, while the simplified factorisation approach does not. The difference, however, disappears upon contraction with the conjugate amplitude, such that the factorisation formulae of refs. [78, 79, 81] suffice to predict the NLP contributions to the cross section at this particular loop order. Our analysis

nevertheless reveals that one should expect additional NLP effects, and the systematic classification of contributions outlined in chapter 2 may provide a valuable starting point for the development of a general factorisation and resummation framework for NLP threshold logarithms at subleading logarithmic accuracy in QED. The subsequent generalisation of these results to QCD will be another interesting direction for future work, with potentially interesting phenomenological applications.

In chapter 3, we turned to the study of amplitudes involving multiple soft emissions in the presence of a single virtual loop. To gather detailed data to test future factorisation efforts for such corrections we computed the abelian-like 2R1V contribution to the DY K-factor, up to NLP in the threshold variable, by performing a full method of regions analysis [108–111]. We shed light on a particularly interesting contribution that may be overlooked if the regions expansion is applied too bluntly. It can be interpreted as one of the soft collinear interactions classified in chapter 2, as it arises in the limit that the two soft gluons are emitted from a soft quark line. Given that the associated energy scale is set by the invariant mass of the two-gluon system, and that a loop correction is required to generate the non-analytical dependence on this scale that allows one to identify it as a specific region, this is the first perturbative order at which such a contribution can be found. The correlation of these emissions at NLP led to rather involved phase space integrals, which could not be solved in closed form and required the application of Mellin-Barnes techniques. However, their eventual contribution to the N^{3}LO K-factor turned out to be highly suppressed, giving at most a N4LL at NLP. The collinear region contributes at NLL, also strictly at NLP, consistent with what was found in a similar analysis of the 1R1V part of the K-factor in ref. [122]. Parts of the result in the collinear region could be related to lower order information by dressing the 1R1V result, which is understood to be described entirely in terms of one-loop radiative jet function of ref. [79], with an eikonal emission. However, the remaining terms appeared to be generated by a doubly-radiative jet function in a factorisation approach, possibly affecting the resummation of such collinear contributions. Lastly, we noted that the hard function was solely responsible for the LLs at LP and NLP. These contributions are obtained from lower order information and have a clear interpretation in terms of the LBK theorem. This, together with earlier insights in the exponentiation properties of certain NLP contributions, inspired the resummation of NLP terms at LL accuracy as studied in chapter 4. Despite the calculation of the complete DY cross section at N3LO [33] since the publication of our study, we think a similar analysis of the 2R1V part of the K-factor would be valuable to further test the factorisation proposed in chapter 2, as (at least) contributions from the fff- and $f\gamma\gamma$-jet functions are expected at this perturbative order. In addition, one may think of extending the analysis presented in chapter 3 to include all colour structures that may arise in QCD, thereby providing data for the development of NLP factorisation formulae in non-abelian gauge theories.

In chapter 4 we studied the resummation of NLP threshold logarithms at LL accuracy, using diagrammatic methods. We argued that collinear contributions that are described by radiative jet functions (be it the traditional f-jet type or new functions such as the $f\gamma$-jet) give rise to at most NLLs at NLP and can be neglected for the purpose of LL resummation. In

addition, we showed that the NLP corrections that arise from correlations between the soft gluons in the final state phase space are of subleading logarithmic order as well. Therefore, all LLs at NLP arise from next-to-soft emissions, which are either described by the so-called next-to-soft function or associated to the orbital angular momentum of the initial state partons and thus expressed as derivative operators acting on the hard function. For the DY process, no derivative contribution is present due to the point-like structure of the DY amplitude at LO. Resummation of LLs at NLP then followed by the exponentiation of a NLP soft function in terms of next-to-soft webs [41, 83], confirming the conjecture of ref. [146] and the recent SCET result of ref. [167]. The LLs at both LP and NLP are found to be governed by the DGLAP splitting kernel, which dictates that the coefficients of the latter are identical but of opposite sign as those of the former. The NLP LL effects are then easily included in the standard framework for LP resummation at higher logarithmic accuracy, as proposed in ref. [162]. For general $q\bar{q}$-initiated colour-singlet production processes one should also account for the orbital angular momentum contribution. We did so by building on the fixed order result of ref. [84], which showed that a single next-to-soft emission is described by applying a kinematic shift to the squared matrix element, while dressing it with an eikonal emission factor. Since at NLP accuracy the NLP effects needs to be included only once, the replacement of the eikonal emission factor with the exponentiated LP soft function proved to be sufficient to obtain a general resummed result at NLP LL accuracy. This was subsequently generalised to gg-initiated processes, and applied to single Higgs production in the infinite top mass limit where we confirmed the conjecture of ref. [159] that the coefficients of the LP and NLP terms in the partonic coefficient follow from those for DY by Casimir scaling. This universality encourages us to take a less conservative approach in chapter 5, and assume that the NLP effects that stem from the orbital angular momentum operator may be exponentiated as well.

Chapter 5 focused on the numerical effects NLP contributions, both for fixed order and resummed results. We started by exploring the threshold behaviour of the partonic coefficient functions for single Higgs production and DY up to NNLO. We noted a better convergence of the threshold expansion in the DY process, due to the fact that the Higgs partonic coefficient function receives a sizeable contribution from the small z regime, which is not well described by the threshold expansion. This observation holds for both the dominant ($gg/q\bar{q}$) and off-diagonal (qg) partonic channels, while for each process the convergence is best in the dominant channel. We also found that the NLP correction in the dominant channel of either processes is sizeable and gives a small overestimation of the exact cross section, while the LP approximation recovers only a small part of it. Turning to the study of NLP effects in resummed cross sections, we briefly reviewed LP resummation and described how the NLP LL contribution $h_a^{(1)}$ to the resummation exponent can be expressed in terms of a derivative with respect to the Mellin moment acting on the LP LL function $g_a^{(1)}$. We applied our resummation prescription to DY and Higgs cross sections, yielding NLP LL + LP NNLL$'$ results, matched to NNLO. For the diagonal channel in either process we found that the NLP LL resummation has a notable numerical impact on the NNLL$'$ resummed result, especially when compared to the effect of the N^{3}LL correction. In addition, we explored off-diagonal qg NLP

LL contributions, by including the corresponding terms at N^{3}LO from refs. [160, 221]. This implied that off-diagonal contributions are more important for DY than for single-Higgs production given the large $\delta(1-z)$ contributions in the latter process at NLO and NNLO, which enter the resummation formula via the matching coefficient g_0 and inflate the resummation effects in the Higgs diagonal channel. Lastly, we performed similar numerical studies for di-Higgs and di-vector boson production, albeit at lower logarithmic accuracy, once again showing the importance of NLP LL contributions. We point out that in this study we kept all NLP LL effects in the exponent, thereby generating terms of $\mathcal{O}(1/N^n)$ upon expansion of the resummed coefficient function to order α_s^n, yielding a partial N^{n}LP result. Likewise, one would generate subleading logarithmic terms at NLP by the interplay of $h_a^{(1)}$ with the LP coefficients. Such terms beyond the guaranteed accuracy of the resummation formula are a mere byproduct but may require more careful handling for phenomenological applications.

To pursue these, understanding the resummation of NLP LLs in the off-diagonal channel remains, however, the highest priority (see e.g. refs. [104, 121, 160]). Once this is fully understood NLP LL resummation will provide a new versatile tool to account for all-order corrections for a range of Standard Model and BSM processes at the LHC and future colliders. Incorporating also (genuine) subleading logarithmic effects at NLP in resummation formulae, through knowledge about the rich structure of the amplitude at NLP, would provide an additional step towards the mastery of precision high-energy phenomenology. The results presented in this thesis should meaningfully contribute to this endeavour.

Bibliography

[1] N. Bahjat-Abbas, J. Sinninghe Damsté, L. Vernazza, and C. D. White, *On next-to-leading power threshold corrections in Drell-Yan production at N^3LO*, *JHEP* **10** (2018) 144, [arXiv:1807.09246].

[2] N. Bahjat-Abbas, D. Bonocore, J. Sinninghe Damsté, E. Laenen, L. Magnea, L. Vernazza, and C. White, *Diagrammatic resummation of leading-logarithmic threshold effects at next-to-leading power*, *JHEP* **11** (2019) 002, [arXiv:1905.13710].

[3] E. Laenen, J. Sinninghe Damsté, L. Vernazza, W. Waalewijn, and L. Zoppi, *Towards all-order factorization of QED amplitudes at next-to-leading power*, *Phys. Rev. D* **103** (2021) 034022, [arXiv:2008.01736].

[4] M. van Beekveld, E. Laenen, J. Sinninghe Damsté, and L. Vernazza, *Next-to-leading power threshold corrections for finite order and resummed colour-singlet cross sections*, *JHEP* **05** (2021) 114, [arXiv:2101.07270].

[5] S. Glashow, *Partial Symmetries of Weak Interactions*, *Nucl. Phys.* **22** (1961) 579–588.

[6] S. Weinberg, *A Model of Leptons*, *Phys. Rev. Lett.* **19** (1967) 1264–1266.

[7] A. Salam, *Weak and Electromagnetic Interactions*, *Conf. Proc. C* **680519** (1968) 367–377.

[8] G. 't Hooft and M. Veltman, *Regularization and Renormalization of Gauge Fields*, *Nucl. Phys. B* **44** (1972) 189–213.

[9] F. Englert and R. Brout, *Broken Symmetry and the Mass of Gauge Vector Mesons*, *Phys. Rev. Lett.* **13** (1964) 321–323.

[10] P. W. Higgs, *Broken symmetries, massless particles and gauge fields*, *Phys. Lett.* **12** (1964) 132–133.

[11] P. W. Higgs, *Broken Symmetries and the Masses of Gauge Bosons*, *Phys. Rev. Lett.* **13** (1964) 508–509.

[12] G. Guralnik, C. Hagen, and T. Kibble, *Global Conservation Laws and Massless Particles*, *Phys. Rev. Lett.* **13** (1964) 585–587.

[13] P. W. Higgs, *Spontaneous Symmetry Breakdown without Massless Bosons*, *Phys. Rev.* **145** (1966) 1156–1163.

[14] T. Kibble, *Symmetry breaking in nonAbelian gauge theories*, *Phys. Rev.* **155** (1967) 1554–1561.

[15] **ATLAS** Collaboration, G. Aad et al., *Observation of a new particle in the search for the Standard Model Higgs boson with the ATLAS detector at the LHC*, *Phys. Lett. B* **716** (2012) 1–29, [arXiv:1207.7214].

[16] **CMS** Collaboration, S. Chatrchyan et al., *Observation of a New Boson at a Mass of 125 GeV with the CMS Experiment at the LHC*, *Phys. Lett. B* **716** (2012) 30–61, [arXiv:1207.7235].

[17] **Particle Data Group** Collaboration, P. Zyla et al., *Review of Particle Physics*, *PTEP* **2020** (2020), no. 8 083C01.

[18] T. Aoyama, M. Hayakawa, T. Kinoshita, and M. Nio, *Tenth-Order QED Contribution to the Electron g-2 and an Improved Value of the Fine Structure Constant*, *Phys. Rev. Lett.* **109** (2012) 111807, [arXiv:1205.5368].

[19] D. Hanneke, S. Fogwell, and G. Gabrielse, *New Measurement of the Electron Magnetic Moment and the Fine Structure Constant*, *Phys. Rev. Lett.* **100** (2008) 120801, [arXiv:0801.1134].

[20] A. D. Sakharov, *Violation of CP Invariance, C asymmetry, and baryon asymmetry of the universe*, *Sov. Phys. Usp.* **34** (1991), no. 5 392–393.

[21] D. J. Gross and F. Wilczek, *Ultraviolet Behavior of Nonabelian Gauge Theories*, *Phys. Rev. Lett.* **30** (1973) 1343–1346.

[22] H. Politzer, *Reliable Perturbative Results for Strong Interactions?*, *Phys. Rev. Lett.* **30** (1973) 1346–1349.

[23] R. P. Feynman, *Very high-energy collisions of hadrons*, *Phys. Rev. Lett.* **23** (1969) 1415–1417.

[24] J. Bjorken and E. A. Paschos, *Inelastic Electron Proton and gamma Proton Scattering, and the Structure of the Nucleon*, *Phys. Rev.* **185** (1969) 1975–1982.

[25] G. T. Bodwin, *Factorization of the Drell-Yan Cross-Section in Perturbation Theory*, *Phys. Rev. D* **31** (1985) 2616. [Erratum: Phys.Rev.D 34, 3932 (1986)].

[26] J. C. Collins, D. E. Soper, and G. F. Sterman, *Factorization for Short Distance Hadron - Hadron Scattering*, *Nucl. Phys. B* **261** (1985) 104–142.

[27] J. C. Collins, D. E. Soper, and G. F. Sterman, *Soft Gluons and Factorization*, *Nucl. Phys. B* **308** (1988) 833–856.

[28] Y. L. Dokshitzer, *Calculation of the Structure Functions for Deep Inelastic Scattering and e+ e- Annihilation by Perturbation Theory in Quantum Chromodynamics.*, *Sov. Phys. JETP* **46** (1977) 641–653.

[29] V. Gribov and L. Lipatov, *Deep inelastic e p scattering in perturbation theory*, *Sov. J. Nucl. Phys.* **15** (1972) 438–450.

[30] G. Altarelli and G. Parisi, *Asymptotic Freedom in Parton Language*, *Nucl. Phys. B* **126** (1977) 298–318.

[31] C. Anastasiou, C. Duhr, F. Dulat, F. Herzog, and B. Mistlberger, *Higgs Boson Gluon-Fusion Production in QCD at Three Loops*, *Phys. Rev. Lett.* **114** (2015) 212001, [arXiv:1503.06056].

[32] B. Mistlberger, *Higgs boson production at hadron colliders at N^3LO in QCD*, *JHEP* **05** (2018) 028, [arXiv:1802.00833].

[33] C. Duhr, F. Dulat, and B. Mistlberger, *Drell-Yan Cross Section to Third Order in the Strong Coupling Constant*, *Phys. Rev. Lett.* **125** (2020), no. 17 172001, [arXiv:2001.07717].

[34] T. Kinoshita, *Mass singularities of Feynman amplitudes*, *J. Math. Phys.* **3** (1962) 650–677.

[35] T. Lee and M. Nauenberg, *Degenerate Systems and Mass Singularities*, *Phys. Rev.* **133** (1964) B1549–B1562.

[36] D. Yennie, S. C. Frautschi, and H. Suura, *The infrared divergence phenomena and high-energy processes*, *Annals Phys.* **13** (1961) 379–452.

[37] M. Levy and J. Sucher, *Eikonal approximation in quantum field theory*, *Phys. Rev.* **186** (1969) 1656–1670.

[38] G. F. Sterman, *Infrared divergences in perturbative QCD*, *AIP Conf. Proc.* **74** (1981) 22–40.

[39] J. Gatheral, *Exponentiation of Eikonal Cross-sections in Nonabelian Gauge Theories*, *Phys. Lett. B* **133** (1983) 90–94.

[40] J. Frenkel and J. Taylor, *Nonabelian Eikonal Exponentiation*, *Nucl. Phys. B* **246** (1984) 231–245.

[41] E. Laenen, G. Stavenga, and C. D. White, *Path integral approach to eikonal and next-to-eikonal exponentiation*, *JHEP* **03** (2009) 054, [arXiv:0811.2067].

[42] E. Gardi, E. Laenen, G. Stavenga, and C. D. White, *Webs in multiparton scattering using the replica trick*, *JHEP* **1011** (2010) 155, [arXiv:1008.0098].

[43] A. Mitov, G. Sterman, and I. Sung, *Diagrammatic Exponentiation for Products of Wilson Lines*, *Phys. Rev. D* **82** (2010) 096010, [arXiv:1008.0099].

[44] S. D. Drell and T.-M. Yan, *Massive Lepton Pair Production in Hadron-Hadron Collisions at High-Energies*, *Phys. Rev. Lett.* **25** (1970) 316–320.

[45] G. Altarelli, R. K. Ellis, and G. Martinelli, *Large perturbative corrections to the drell-yan process in qcd*, *Nucl. Phys. B* **157** (1979) 461.

[46] G. Parisi, *Summing Large Perturbative Corrections in QCD*, *Phys. Lett. B* **90** (1980) 295–296.

[47] G. Curci and M. Greco, *Large Infrared Corrections in QCD Processes*, *Phys. Lett. B* **92** (1980) 175–178.

[48] G. Sterman, *Summation of large corrections to short distance hadronic cross-sections*, *Nucl. Phys. B* **281** (1987) 310.

[49] S. Catani and L. Trentadue, *Resummation of the QCD Perturbative Series for Hard Processes*, *Nucl. Phys. B* **327** (1989) 323.

[50] G. Korchemsky and G. Marchesini, *Structure function for large x and renormalization of Wilson loop*, *Nucl. Phys. B* **406** (1993) 225–258, [hep-ph/9210281].

[51] G. P. Korchemsky and G. Marchesini, *Resummation of large infrared corrections using Wilson loops*, *Phys. Lett. B* **313** (1993) 433–440.

[52] H. Contopanagos, E. Laenen, and G. F. Sterman, *Sudakov factorization and resummation*, *Nucl. Phys. B* **484** (1997) 303–330, [hep-ph/9604313].

[53] S. Catani, M. L. Mangano, P. Nason, and L. Trentadue, *The resummation of soft gluons in hadronic collisions*, *Nucl. Phys. B* **478** (1996) 273–310, [hep-ph/9604351].

[54] N. Kidonakis and G. Sterman, *Resummation for qcd hard scattering*, *Nucl. Phys. B* **505** (1997) 321–348, [hep-ph/9705234].

[55] N. Kidonakis, G. Oderda, and G. Sterman, *Evolution of color exchange in QCD hard scattering*, *Nucl. Phys. B* **531** (1998) 365–402, [hep-ph/9803241].

[56] E. Laenen, G. Oderda, and G. Sterman, *Resummation of threshold corrections for single-particle inclusive cross sections*, *Phys. Lett. B* **438** (1998) 173–183, [hep-ph/9806467].

[57] S. Catani, D. de Florian, M. Grazzini, and P. Nason, *Soft-gluon resummation for Higgs boson production at hadron colliders*, *JHEP* **0307** (2003) 028, [hep-ph/0306211].

[58] S. Forte and G. Ridolfi, *Renormalization group approach to soft gluon resummation*, *Nucl. Phys. B* **650** (2003) 229–270, [hep-ph/0209154].

[59] V. Ravindran, *On Sudakov and soft resummations in QCD*, *Nucl. Phys. B* **746** (2006) 58–76, [hep-ph/0512249].

[60] V. Ravindran, *Higher-order threshold effects to inclusive processes in QCD*, *Nucl. Phys. B* **752** (2006) 173–196, [hep-ph/0603041].

[61] C. W. Bauer, S. Fleming, and M. E. Luke, *Summing Sudakov logarithms in B —> X(s gamma) in effective field theory*, *Phys. Rev. D* **63** (2000) 014006, [hep-ph/0005275].

[62] C. W. Bauer, S. Fleming, D. Pirjol, and I. W. Stewart, *An effective field theory for collinear and soft gluons: Heavy to light decays*, *Phys. Rev. D* **63** (2001) 114020, [hep-ph/0011336].

[63] C. W. Bauer and I. W. Stewart, *Invariant operators in collinear effective theory*, *Phys. Lett. B* **516** (2001) 134–142, [hep-ph/0107001].

[64] C. W. Bauer, D. Pirjol, and I. W. Stewart, *Soft collinear factorization in effective field theory*, *Phys. Rev. D* **65** (2002) 054022, [hep-ph/0109045].

[65] M. Beneke, A. Chapovsky, M. Diehl, and T. Feldmann, *Soft collinear effective theory and heavy to light currents beyond leading power*, *Nucl. Phys. B* **643** (2002) 431–476, [hep-ph/0206152].

[66] C. W. Bauer, S. Fleming, D. Pirjol, I. Z. Rothstein, and I. W. Stewart, *Hard scattering factorization from effective field theory*, *Phys. Rev. D* **66** (2002) 014017, [hep-ph/0202088].

[67] A. V. Manohar, *Deep inelastic scattering as $x \to 1$ using soft collinear effective theory*, *Phys. Rev. D* **68** (2003) 114019, [hep-ph/0309176].

[68] A. Idilbi and X.-d. Ji, *Threshold resummation for Drell-Yan process in soft-collinear effective theory*, *Phys. Rev. D* **72** (2005) 054016, [hep-ph/0501006].

[69] J. Chay and C. Kim, *Deep inelastic scattering near the endpoint in soft-collinear effective theory*, *Phys. Rev. D* **75** (2007) 016003, [hep-ph/0511066].

[70] T. Becher and M. Neubert, *Threshold resummation in momentum space from effective field theory*, *Phys. Rev. Lett.* **97** (2006) 082001, [hep-ph/0605050].

[71] T. Becher, M. Neubert, and B. D. Pecjak, *Factorization and Momentum-Space Resummation in Deep-Inelastic Scattering*, *JHEP* **01** (2007) 076, [hep-ph/0607228].

[72] T. Becher, M. Neubert, and G. Xu, *Dynamical Threshold Enhancement and Resummation in Drell-Yan Production*, *JHEP* **07** (2008) 030, [arXiv:0710.0680].

[73] V. Ahrens, A. Ferroglia, M. Neubert, B. D. Pecjak, and L. L. Yang, *Renormalization-Group Improved Predictions for Top-Quark Pair Production at Hadron Colliders*, *JHEP* **09** (2010) 097, [arXiv:1003.5827].

[74] J. C. Collins, *Sudakov form-factors*, *Adv.Ser.Direct.High Energy Phys.* **5** (1989) 573–614, [hep-ph/0312336].

[75] L. J. Dixon, L. Magnea, and G. F. Sterman, *Universal structure of subleading infrared poles in gauge theory amplitudes*, *JHEP* **0808** (2008) 022, [arXiv:0805.3515].

[76] F. Low, *Bremsstrahlung of very low-energy quanta in elementary particle collisions*, *Phys. Rev.* **110** (1958) 974–977.

[77] T. Burnett and N. M. Kroll, *Extension of the low soft photon theorem*, *Phys. Rev. Lett.* **20** (1968) 86.

[78] V. Del Duca, *High-energy Bremsstrahlung Theorems for Soft Photons*, *Nucl. Phys. B* **345** (1990) 369–388.

[79] D. Bonocore, E. Laenen, L. Magnea, S. Melville, L. Vernazza, and C. White, *A factorization approach to next-to-leading-power threshold logarithms*, *JHEP* **06** (2015) 008, [arXiv:1503.05156].

[80] J. Grammer, G. and D. Yennie, *Improved treatment for the infrared divergence problem in quantum electrodynamics*, *Phys. Rev. D* **8** (1973) 4332–4344.

[81] D. Bonocore, E. Laenen, L. Magnea, L. Vernazza, and C. D. White, *Non-abelian factorisation for next-to-leading-power threshold logarithms*, *JHEP* **12** (2016) 121, [arXiv:1610.06842].

[82] M. van Beekveld, W. Beenakker, E. Laenen, and C. D. White, *Next-to-leading power threshold effects for inclusive and exclusive processes with final state jets*, *JHEP* **03** (2020) 106, [arXiv:1905.08741].

[83] E. Laenen, L. Magnea, G. Stavenga, and C. D. White, *Next-to-eikonal corrections to soft gluon radiation: a diagrammatic approach*, *JHEP* **1101** (2011) 141, [arXiv:1010.1860].

[84] V. Del Duca, E. Laenen, L. Magnea, L. Vernazza, and C. D. White, *Universality of next-to-leading power threshold effects for colourless final states in hadronic collisions*, *JHEP* **11** (2017) 057, [arXiv:1706.04018].

[85] H. Gervais, *Soft Photon Theorem for High Energy Amplitudes in Yukawa and Scalar Theories*, *Phys. Rev. D* **95** (2017), no. 12 125009, [arXiv:1704.00806].

[86] A. J. Larkoski, D. Neill, and I. W. Stewart, *Soft Theorems from Effective Field Theory*, *JHEP* **06** (2015) 077, [arXiv:1412.3108].

[87] I. Moult, I. W. Stewart, and G. Vita, *Subleading Power Factorization with Radiative Functions*, *JHEP* **11** (2019) 153, [arXiv:1905.07411].

[88] M. Beneke, A. Broggio, S. Jaskiewicz, and L. Vernazza, *Threshold factorization of the Drell-Yan process at next-to-leading power*, *JHEP* **07** (2020) 078, [arXiv:1912.01585].

[89] M. Beneke, M. Garny, R. Szafron, and J. Wang, *Violation of the Kluberg-Stern-Zuber theorem in SCET*, *JHEP* **09** (2019) 101, [arXiv:1907.05463].

[90] M. Beneke, M. Garny, R. Szafron, and J. Wang, *Anomalous dimension of subleading-power N-jet operators*, *JHEP* **03** (2018) 001, [arXiv:1712.04416].

[91] M. Beneke, M. Garny, R. Szafron, and J. Wang, *Anomalous dimension of subleading-power N-jet operators. Part II*, *JHEP* **11** (2018) 112, [arXiv:1808.04742].

[92] D. W. Kolodrubetz, I. Moult, and I. W. Stewart, *Building Blocks for Subleading Helicity Operators*, *JHEP* **05** (2016) 139, [arXiv:1601.02607].

[93] I. Moult, I. W. Stewart, and G. Vita, *A subleading operator basis and matching for gg → H*, *JHEP* **07** (2017) 067, [arXiv:1703.03408].

[94] I. Feige, D. W. Kolodrubetz, I. Moult, and I. W. Stewart, *A Complete Basis of Helicity Operators for Subleading Factorization*, *JHEP* **11** (2017) 142, [arXiv:1703.03411].

[95] C.-H. Chang, I. W. Stewart, and G. Vita, *A Subleading Power Operator Basis for the Scalar Quark Current*, *JHEP* **04** (2018) 041, [arXiv:1712.04343].

[96] I. Moult, L. Rothen, I. W. Stewart, F. J. Tackmann, and H. X. Zhu, *Subleading Power Corrections for N-Jettiness Subtractions*, *Phys. Rev. D* **95** (2017), no. 7 074023, [arXiv:1612.00450].

[97] R. Boughezal, X. Liu, and F. Petriello, *Power Corrections in the N-jettiness Subtraction Scheme*, *JHEP* **03** (2017) 160, [arXiv:1612.02911].

[98] I. Moult, L. Rothen, I. W. Stewart, F. J. Tackmann, and H. X. Zhu, *N -jettiness subtractions for $gg \to H$ at subleading power*, *Phys. Rev. D* **97** (2018), no. 1 014013, [arXiv:1710.03227].

[99] R. Boughezal, A. Isgrò, and F. Petriello, *Next-to-leading-logarithmic power corrections for N-jettiness subtraction in color-singlet production*, *Phys. Rev. D* **97** (2018), no. 7 076006, [arXiv:1802.00456].

[100] M. A. Ebert, I. Moult, I. W. Stewart, F. J. Tackmann, G. Vita, and H. X. Zhu, *Power Corrections for N-Jettiness Subtractions at $\mathcal{O}(\alpha_s)$*, *JHEP* **12** (2018) 084, [arXiv:1807.10764].

[101] R. Boughezal, A. Isgrò, and F. Petriello, *Next-to-leading power corrections to $V + 1$ jet production in N-jettiness subtraction*, *Phys. Rev. D* **101** (2020), no. 1 016005, [arXiv:1907.12213].

[102] M. A. Ebert, I. Moult, I. W. Stewart, F. J. Tackmann, G. Vita, and H. X. Zhu, *Subleading power rapidity divergences and power corrections for q_T*, *JHEP* **04** (2019) 123, [arXiv:1812.08189].

[103] Z. L. Liu and M. Neubert, *Factorization at subleading power and endpoint-divergent convolutions in $h \to \gamma\gamma$ decay*, *JHEP* **04** (2020) 033, [arXiv:1912.08818].

[104] M. Beneke, M. Garny, S. Jaskiewicz, R. Szafron, L. Vernazza, and J. Wang, *Large-x resummation of off-diagonal deep-inelastic parton scattering from d-dimensional refactorization*, *JHEP* **10** (2020) 196, [arXiv:2008.04943].

[105] Z. L. Liu, B. Mecaj, M. Neubert, and X. Wang, *Factorization at Subleading Power and Endpoint Divergences in Soft-Collinear Effective Theory*, arXiv:2009.04456.

[106] L. Landau, *On analytic properties of vertex parts in quantum field theory*, *Nucl. Phys.* **13** (1960), no. 1 181–192.

[107] S. Coleman and R. Norton, *Singularities in the physical region*, *Nuovo Cim.* **38** (1965) 438–442.

[108] M. Beneke and V. A. Smirnov, *Asymptotic expansion of Feynman integrals near threshold*, *Nucl. Phys. B* **522** (1998) 321–344, [hep-ph/9711391].

[109] V. A. Smirnov, *Applied asymptotic expansions in momenta and masses*, *Springer Tracts Mod. Phys.* **177** (2002) 1–262.

[110] A. Pak and A. Smirnov, *Geometric approach to asymptotic expansion of Feynman integrals*, *Eur. Phys. J. C* **71** (2011) 1626, [arXiv:1011.4863].

[111] B. Jantzen, *Foundation and generalization of the expansion by regions*, *JHEP* **12** (2011) 076, [arXiv:1111.2589].

[112] G. F. Sterman, *Mass Divergences in Annihilation Processes. 1. Origin and Nature of Divergences in Cut Vacuum Polarization Diagrams*, *Phys. Rev. D* **17** (1978) 2773.

[113] R. Akhoury, *Mass Divergences of Wide Angle Scattering Amplitudes*, *Phys. Rev. D* **19** (1979) 1250.

[114] E. Bagan, P. Ball, V. M. Braun, and P. Gosdzinsky, *Charm quark mass dependence of QCD corrections to nonleptonic inclusive B decays*, *Nucl. Phys. B* **432** (1994) 3–38, [hep-ph/9408306].

[115] M. Aivazis, J. C. Collins, F. I. Olness, and W.-K. Tung, *Leptoproduction of heavy quarks. 2. A Unified QCD formulation of charged and neutral current processes from fixed target to collider energies*, *Phys. Rev. D* **50** (1994) 3102–3118, [hep-ph/9312319].

[116] R. Thorne and R. Roberts, *An Ordered analysis of heavy flavor production in deep inelastic scattering*, *Phys. Rev. D* **57** (1998) 6871–6898, [hep-ph/9709442].

[117] S. Forte, E. Laenen, P. Nason, and J. Rojo, *Heavy quarks in deep-inelastic scattering*, *Nucl. Phys. B* **834** (2010) 116–162, [arXiv:1001.2312].

[118] T. Liu and A. A. Penin, *High-Energy Limit of QCD beyond the Sudakov Approximation*, *Phys. Rev. Lett.* **119** (2017), no. 26 262001, [arXiv:1709.01092].

[119] R. Mertig, M. Bohm, and A. Denner, *FEYN CALC: Computer algebraic calculation of Feynman amplitudes*, *Comput. Phys. Commun.* **64** (1991) 345–359.

[120] V. Shtabovenko, R. Mertig, and F. Orellana, *New Developments in FeynCalc 9.0*, *Comput. Phys. Commun.* **207** (2016) 432–444, [arXiv:1601.01167].

[121] I. Moult, I. W. Stewart, G. Vita, and H. X. Zhu, *The Soft Quark Sudakov*, *JHEP* **05** (2020) 089, [arXiv:1910.14038].

[122] D. Bonocore, E. Laenen, L. Magnea, L. Vernazza, and C. D. White, *The method of regions and next-to-soft corrections in Drell-Yan production*, *Phys. Lett. B* **742** (2015) 375–382, [arXiv:1410.6406].

[123] J. C. Collins, D. E. Soper, and G. F. Sterman, *Factorization of Hard Processes in QCD*, in *Advanced Series on Directions in High Energy Physics*, vol. 5, pp. 1–91. World Scientific, 1989. hep-ph/0409313.

[124] T. Huber and D. Maitre, *HypExp: A Mathematica package for expanding hypergeometric functions around integer-valued parameters*, *Comput. Phys. Commun.* **175** (2006) 122–144, [hep-ph/0507094].

[125] T. Huber and D. Maitre, *HypExp 2, Expanding Hypergeometric Functions about Half-Integer Parameters*, *Comput. Phys. Commun.* **178** (2008) 755–776, [arXiv:0708.2443].

[126] T. Matsuura, S. C. van der Marck, and W. L. van Neerven, *The order α_s^2 contribution to the K factor of the Drell-Yan process*, *Phys. Lett. B* **211** (1988) 171.

[127] T. Matsuura, S. van der Marck, and W. van Neerven, *The Calculation of the Second Order Soft and Virtual Contributions to the Drell-Yan Cross-Section*, *Nucl. Phys. B* **319** (1989) 570–622.

[128] T. Matsuura, R. Hamberg, and W. L. van Neerven, *The contribution of the gluon-gluon subprocess to the drell-yan k factor*, *Nucl. Phys. B* **345** (1990) 331–368.

[129] R. Hamberg, W. van Neerven, and T. Matsuura, *A Complete calculation of the order α_s^2 correction to the Drell-Yan K factor*, *Nucl.Phys. B* **359** (1991) 343–405.

[130] R. Hamberg, W. van Neerven, and T. Matsuura, *Erratum to: A complete calculation of the order α_s^2 correction to the Drell-Yan K-factor: [Nucl. Phys. B 359 (1991) 343]*, *Nucl. Phys. B* **644** (2002), no. 1-2 403 – 404.

[131] S. Dawson, *Radiative corrections to Higgs boson production*, *Nucl. Phys. B* **359** (1991) 283–300.

[132] C. Anastasiou and K. Melnikov, *Higgs boson production at hadron colliders in NNLO QCD*, *Nucl. Phys. B* **646** (2002) 220–256, [hep-ph/0207004].

[133] R. V. Harlander and W. B. Kilgore, *Next-to-next-to-leading order Higgs production at hadron colliders*, *Phys. Rev. Lett.* **88** (2002) 201801, [hep-ph/0201206].

[134] C. Anastasiou, C. Duhr, F. Dulat, and B. Mistlberger, *Soft triple-real radiation for Higgs production at N3LO*, *JHEP* **07** (2013) 003, [arXiv:1302.4379].

[135] C. Anastasiou, C. Duhr, F. Dulat, F. Herzog, and B. Mistlberger, *Real-virtual contributions to the inclusive Higgs cross-section at N^3LO*, *JHEP* **12** (2013) 088, [arXiv:1311.1425].

[136] C. Anastasiou, C. Duhr, F. Dulat, E. Furlan, T. Gehrmann, F. Herzog, and B. Mistlberger, *Higgs boson gluon-fusion production at threshold in N^3LO QCD*, *Phys. Lett. B* **737** (2014) 325–328, [arXiv:1403.4616].

[137] C. Anastasiou, C. Duhr, F. Dulat, E. Furlan, T. Gehrmann, F. Herzog, and B. Mistlberger, *Higgs boson gluon-fusion production beyond threshold in N^3LO QCD*, *JHEP* **03** (2015) 091, [arXiv:1411.3584].

[138] Y. Li, A. von Manteuffel, R. M. Schabinger, and H. X. Zhu, *Soft-virtual corrections to Higgs production at N^3LO*, *Phys. Rev. D* **91** (2015) 036008, [arXiv:1412.2771].

[139] Y. Li, A. von Manteuffel, R. M. Schabinger, and H. X. Zhu, *N^3LO Higgs boson and Drell-Yan production at threshold: The one-loop two-emission contribution*, *Phys. Rev. D* **90** (2014), no. 5 053006, [arXiv:1404.5839].

[140] T. Ahmed, M. Mahakhud, N. Rana, and V. Ravindran, *Drell-Yan Production at Threshold to Third Order in QCD*, *Phys. Rev. Lett.* **113** (2014), no. 11 112002, [arXiv:1404.0366].

[141] P. Nogueira, *Automatic Feynman graph generation*, *J. Comput. Phys.* **105** (1993) 279–289.

[142] C. Studerus, *Reduze-Feynman Integral Reduction in C++*, *Comput. Phys. Commun.* **181** (2010) 1293–1300, [arXiv:0912.2546].

[143] A. von Manteuffel and C. Studerus, *Reduze 2 - Distributed Feynman Integral Reduction*, arXiv:1201.4330.

[144] B. Jantzen, A. V. Smirnov, and V. A. Smirnov, *Expansion by regions: revealing potential and Glauber regions automatically*, *Eur. Phys. J. C* **72** (2012) 2139, [arXiv:1206.0546].

[145] C. Anastasiou, C. Duhr, F. Dulat, E. Furlan, F. Herzog, and B. Mistlberger, *Soft expansion of double-real-virtual corrections to Higgs production at N^3LO*, *JHEP* **08** (2015) 051, [arXiv:1505.04110].

[146] S. Moch and A. Vogt, *On non-singlet physical evolution kernels and large-x coefficient functions in perturbative QCD*, *JHEP* **11** (2009) 099, [arXiv:0909.2124].

[147] W. van Neerven, *Dimensional Regularization of Mass and Infrared Singularities in Two Loop On-shell Vertex Functions*, *Nucl. Phys. B* **268** (1986) 453–488.

[148] V. A. Smirnov, *Evaluating Feynman integrals*, *Springer Tracts Mod. Phys.* **211** (2004) 1–244.

[149] G. Somogyi, *Angular integrals in d dimensions*, *J. Math. Phys.* **52** (2011) 083501, [arXiv:1101.3557].

[150] A. Smirnov and V. Smirnov, *On the Resolution of Singularities of Multiple Mellin-Barnes Integrals*, *Eur. Phys. J. C* **62** (2009) 445–449, [arXiv:0901.0386].

[151] M. Czakon, *Automatized analytic continuation of Mellin-Barnes integrals*, *Comput. Phys. Commun.* **175** (2006) 559–571, [hep-ph/0511200].

[152] M. Ochman and T. Riemann, *MBsums - a Mathematica package for the representation of Mellin-Barnes integrals by multiple sums*, *Acta Phys. Polon. B* **46** (2015), no. 11 2117, [arXiv:1511.01323].

[153] S. Moch and P. Uwer, *XSummer: Transcendental functions and symbolic summation in form*, *Comput. Phys. Commun.* **174** (2006) 759–770, [math-ph/0508008].

[154] J. Vermaseren, *New features of FORM*, math-ph/0010025.

[155] M. Kramer, E. Laenen, and M. Spira, *Soft gluon radiation in Higgs boson production at the LHC*, *Nucl. Phys. B* **511** (1998) 523–549, [hep-ph/9611272].

[156] F. Herzog and B. Mistlberger, *The Soft-Virtual Higgs Cross-section at N3LO and the Convergence of the Threshold Expansion*, in *49th Rencontres de Moriond on QCD and High Energy Interactions*, pp. 57–60, 2014. arXiv:1405.5685.

[157] G. Soar, S. Moch, J. Vermaseren, and A. Vogt, *On Higgs-exchange DIS, physical evolution kernels and fourth-order splitting functions at large x*, *Nucl. Phys. B* **832** (2010) 152–227, [arXiv:0912.0369].

[158] S. Moch and A. Vogt, *Threshold Resummation of the Structure Function F(L)*, *JHEP* **04** (2009) 081, [arXiv:0902.2342].

[159] D. de Florian, J. Mazzitelli, S. Moch, and A. Vogt, *Approximate N^3LO Higgs-boson production cross section using physical-kernel constraints*, *JHEP* **10** (2014) 176, [arXiv:1408.6277].

[160] N. Lo Presti, A. Almasy, and A. Vogt, *Leading large-x logarithms of the quark–gluon contributions to inclusive Higgs-boson and lepton-pair production*, *Phys. Lett. B* **737** (2014) 120–123, [arXiv:1407.1553].

[161] R. Akhoury, M. G. Sotiropoulos, and G. F. Sterman, *An Operator expansion for the elastic limit*, *Phys. Rev. Lett.* **81** (1998) 3819–3822, [hep-ph/9807330].

[162] E. Laenen, L. Magnea, and G. Stavenga, *On next-to-eikonal corrections to threshold resummation for the Drell-Yan and DIS cross sections*, *Phys. Lett. B* **669** (2008) 173–179, [arXiv:0807.4412].

[163] G. Grunberg, *Threshold resummation to any order in (1-x)*, arXiv:0710.5693.

[164] G. Grunberg and V. Ravindran, *On threshold resummation beyond leading 1-x order*, *JHEP* **10** (2009) 055, [arXiv:0902.2702].

[165] G. Grunberg, *Large-x structure of physical evolution kernels in Deep Inelastic Scattering*, *Phys. Lett. B* **687** (2010) 405–409, [arXiv:0911.4471].

[166] I. Moult, I. W. Stewart, G. Vita, and H. X. Zhu, *First Subleading Power Resummation for Event Shapes*, *JHEP* **08** (2018) 013, [arXiv:1804.04665].

[167] M. Beneke, A. Broggio, M. Garny, S. Jaskiewicz, R. Szafron, L. Vernazza, and J. Wang, *Leading-logarithmic threshold resummation of the Drell-Yan process at next-to-leading power*, *JHEP* **03** (2019) 043, [arXiv:1809.10631].

[168] M. Beneke, M. Garny, S. Jaskiewicz, R. Szafron, L. Vernazza, and J. Wang, *Leading-logarithmic threshold resummation of Higgs production in gluon fusion at next-to-leading power*, *JHEP* **01** (2020) 094, [arXiv:1910.12685].

[169] J. Wang, *Resummation of double logarithms in loop-induced processes with effective field theory*, arXiv:1912.09920.

[170] Z. L. Liu and M. Neubert, *Two-Loop Radiative Jet Function for Exclusive B-Meson and Higgs Decays*, *JHEP* **06** (2020) 060, [arXiv:2003.03393].

[171] Z. L. Liu, B. Mecaj, M. Neubert, X. Wang, and S. Fleming, *Renormalization and Scale Evolution of the Soft-Quark Soft Function*, *JHEP* **07** (2020) 104, [arXiv:2005.03013].

[172] A. M. Polyakov, *Gauge Fields as Rings of Glue*, *Nucl. Phys. B* **164** (1980) 171–188.

[173] I. Arefeva, *Quantum Contour Field Equations*, *Phys. Lett. B* **93** (1980) 347–353.

[174] V. Dotsenko and S. Vergeles, *Renormalizability of Phase Factors in the Nonabelian Gauge Theory*, *Nucl. Phys. B* **169** (1980) 527–546.

[175] R. A. Brandt, F. Neri, and M.-a. Sato, *Renormalization of Loop Functions for All Loops*, *Phys. Rev. D* **24** (1981) 879.

[176] G. Korchemsky and A. Radyushkin, *Loop Space Formalism and Renormalization Group for the Infrared Asymptotics of QCD*, *Phys. Lett. B* **171** (1986) 459–467.

[177] G. Korchemsky and A. Radyushkin, *Renormalization of the Wilson Loops Beyond the Leading Order*, *Nucl. Phys. B* **283** (1987) 342–364.

[178] E. Gardi, J. M. Smillie, and C. D. White, *On the renormalization of multiparton webs*, *JHEP* **09** (2011) 114, [arXiv:1108.1357].

[179] E. Gardi, J. M. Smillie, and C. D. White, *The Non-Abelian Exponentiation theorem for multiple Wilson lines*, *JHEP* **06** (2013) 088, [arXiv:1304.7040].

[180] E. Gardi and C. D. White, *General properties of multiparton webs: Proofs from combinatorics*, *JHEP* **03** (2011) 079, [arXiv:1102.0756].

[181] M. Dukes, E. Gardi, E. Steingrimsson, and C. D. White, *Web worlds, web-colouring matrices, and web-mixing matrices*, *J. Comb. Theor. A* **A120** (2013) 1012–1037, [arXiv:1301.6576].

[182] M. Dukes, E. Gardi, H. McAslan, D. J. Scott, and C. D. White, *Webs and Posets*, *JHEP* **01** (2014) 024, [arXiv:1310.3127].

[183] E. Gardi, *From Webs to Polylogarithms*, *JHEP* **04** (2014) 044, [arXiv:1310.5268].

[184] G. Falcioni, E. Gardi, M. Harley, L. Magnea, and C. D. White, *Multiple Gluon Exchange Webs*, *JHEP* **10** (2014) 010, [arXiv:1407.3477].

[185] M. Dukes and C. D. White, *Web matrices: structural properties and generating combinatorial identities*, arXiv:1603.01589.

[186] A. A. Vladimirov, *Exponentiation for products of Wilson lines within the generating function approach*, *JHEP* **06** (2015) 120, [arXiv:1501.03316].

[187] C. White, *An Introduction to Webs*, *J. Phys. G* **43** (2016), no. 3 033002, [arXiv:1507.02167].

[188] E. Casali, *Soft sub-leading divergences in Yang-Mills amplitudes*, *JHEP* **08** (2014) 077, [arXiv:1404.5551].

[189] F. Cachazo and A. Strominger, *Evidence for a New Soft Graviton Theorem*, arXiv:1404.4091.

[190] A. Bhattacharya, I. Moult, I. W. Stewart, and G. Vita, *Helicity Methods for High Multiplicity Subleading Soft and Collinear Limits*, *JHEP* **05** (2019) 192, [arXiv:1812.06950].

[191] G. F. Sterman, *Partons, factorization and resummation, TASI 95*, in *Theoretical Advanced Study Institute in Elementary Particle Physics (TASI 95): QCD and Beyond*, pp. 327–408, 6, 1995. hep-ph/9606312.

[192] Y. L. Dokshitzer, D. Diakonov, and S. Troian, *Hard Processes in Quantum Chromodynamics*, *Phys. Rept.* **58** (1980) 269–395.

[193] D. Amati, R. Petronzio, and G. Veneziano, *Relating Hard QCD Processes Through Universality of Mass Singularities. 2.*, *Nucl. Phys. B* **146** (1978) 29–49.

[194] V. Del Duca, *An introduction to the perturbative QCD pomeron and to jet physics at large rapidities*, hep-ph/9503226.

[195] R. Ellis, W. Stirling, and B. Webber, *QCD and collider physics*, vol. 8. Cambridge University Press, 2, 2011.

[196] S. Catani and L. Trentadue, *Comment on QCD exponentiation at large x*, *Nucl. Phys. B* **353** (1991) 183–186.

[197] S. Moch and A. Vogt, *Higher-order soft corrections to lepton pair and Higgs boson production*, *Phys. Lett. B* **631** (2005) 48–57, [hep-ph/0508265].

[198] E. Laenen and L. Magnea, *Threshold resummation for electroweak annihilation from DIS data*, *Phys. Lett. B* **632** (2006) 270–276, [hep-ph/0508284].

[199] A. Idilbi, X.-d. Ji, J.-P. Ma, and F. Yuan, *Threshold resummation for Higgs production in effective field theory*, *Phys. Rev. D* **73** (2006) 077501, [hep-ph/0509294].

[200] T. O. Eynck, E. Laenen, and L. Magnea, *Exponentiation of the Drell-Yan cross-section near partonic threshold in the DIS and MS-bar schemes*, *JHEP* **06** (2003) 057, [hep-ph/0305179].

[201] Y. Dokshitzer, G. Marchesini, and G. Salam, *Revisiting parton evolution and the large-x limit*, *Phys. Lett. B* **634** (2006) 504–507, [hep-ph/0511302].

[202] M. van Beekveld, W. Beenakker, R. Basu, E. Laenen, A. Misra, and P. Motylinski, *Next-to-leading power threshold effects for resummed prompt photon production*, *Phys. Rev. D* **100** (2019), no. 5 056009, [arXiv:1905.11771].

[203] A. Ajjath, P. Mukherjee, and V. Ravindran, *On next to soft corrections to Drell-Yan and Higgs Boson productions*, arXiv:2006.06726.

[204] D. Appell, G. Sterman, and P. Mackenzie, *Soft gluons and the normalization of the drell-yan cross- section*, *Nucl. Phys. B* **309** (1988) 259.

[205] L. Magnea, *All Order Summation and Two Loop Results for the Drell-Yan Cross-section*, *Nucl. Phys. B* **349** (1991) 703–713.

[206] C. Anastasiou, C. Duhr, F. Dulat, E. Furlan, T. Gehrmann, F. Herzog, A. Lazopoulos, and B. Mistlberger, *High precision determination of the gluon fusion Higgs boson cross-section at the LHC*, *JHEP* **05** (2016) 058, [arXiv:1602.00695].

[207] M. Bonvini, S. Forte, and G. Ridolfi, *Soft gluon resummation of Drell-Yan rapidity distributions: Theory and phenomenology*, *Nucl. Phys. B* **847** (2011) 93–159, [arXiv:1009.5691].

[208] M. Bonvini, S. Forte, G. Ridolfi, and L. Rottoli, *Resummation prescriptions and ambiguities in SCET vs. direct QCD: Higgs production as a case study*, *JHEP* **01** (2015) 046, [arXiv:1409.0864].

[209] M. Bonvini and S. Marzani, *Resummed Higgs cross section at N^3LL*, *JHEP* **09** (2014) 007, [arXiv:1405.3654].

[210] M. Bonvini, S. Marzani, C. Muselli, and L. Rottoli, *On the Higgs cross section at N^3LO+N^3LL and its uncertainty*, *JHEP* **08** (2016) 105, [arXiv:1603.08000].

[211] A. H. Ajjath, G. Das, M. C. Kumar, P. Mukherjee, V. Ravindran, and K. Samanta, *Resummed Drell-Yan cross-section at N^3LL*, *JHEP* **10** (2020) 153, [arXiv:2001.11377].

[212] R. Basu, E. Laenen, A. Misra, and P. Motylinski, *Soft-collinear effects in prompt photon production*, *Phys. Rev. D* **76** (2007) 014010, [arXiv:0704.3180].

[213] A. Djouadi, M. Spira, and P. Zerwas, *Production of Higgs bosons in proton colliders: QCD corrections*, *Phys. Lett. B* **264** (1991) 440–446.

[214] M. Spira, A. Djouadi, D. Graudenz, and P. M. Zerwas, *Higgs boson production at the LHC*, *Nucl. Phys. B* **453** (1995) 17–82, [http://arXiv.org/abs/hep-ph/9504378].

[215] V. Ravindran, J. Smith, and W. L. van Neerven, *Nnlo corrections to the total cross section for higgs boson production in hadron hadron collisions*, *Nucl. Phys. B* **665** (2003) 325–366, [hep-ph/0302135].

[216] J. Butterworth et al., *PDF4LHC recommendations for LHC Run II*, *J. Phys. G* **43** (2016) 023001, [arXiv:1510.03865].

[217] S. Catani, D. de Florian, and M. Grazzini, *Direct higgs production and jet veto at the tevatron and the lhc in nnlo qcd*, *JHEP* **01** (2002) 015, [http://arXiv.org/abs/hep-ph/0111164].

[218] A. Vogt, F. Herzog, S. Moch, B. Ruijl, T. Ueda, and J. A. M. Vermaseren, *Anomalous dimensions and splitting functions beyond the next-to-next-to-leading order*, *PoS* **LL2018** (2018) 050, [arXiv:1808.08981].

[219] S. Moch, J. A. M. Vermaseren, and A. Vogt, *The three-loop splitting functions in qcd: The non-singlet case*, *Nucl. Phys. B* **688** (2004) 101–134, [hep-ph/0403192].

[220] A. Vogt, S. Moch, and J. A. M. Vermaseren, *The three-loop splitting functions in qcd: The singlet case*, *Nucl. Phys. B* **691** (2004) 129–181, [hep-ph/0404111].

[221] F. Dulat, A. Lazopoulos, and B. Mistlberger, *iHixs 2 — Inclusive Higgs cross sections*, *Comput. Phys. Commun.* **233** (2018) 243–260, [arXiv:1802.00827].

[222] D. Y. Shao, C. S. Li, H. T. Li, and J. Wang, *Threshold resummation effects in Higgs boson pair production at the LHC*, *JHEP* **07** (2013) 169, [arXiv:1301.1245].

[223] D. de Florian and J. Mazzitelli, *Higgs pair production at next-to-next-to-leading logarithmic accuracy at the LHC*, *JHEP* **09** (2015) 053, [arXiv:1505.07122].

[224] D. De Florian and J. Mazzitelli, *Soft gluon resummation for Higgs boson pair production including finite M_t effects*, *JHEP* **08** (2018) 156, [arXiv:1807.03704].

[225] T. Plehn, M. Spira, and P. M. Zerwas, *Pair production of neutral Higgs particles in gluon-gluon collisions*, *Nucl. Phys. B* **479** (1996) 46–64, [hep-ph/9603205]. [Erratum: Nucl.Phys.B 531, 655–655 (1998)].

[226] S. Catani, L. Cieri, D. de Florian, G. Ferrera, and M. Grazzini, *Threshold resummation at N^3LL accuracy and soft-virtual cross sections at N^3LO*, *Nucl. Phys. B* **888** (2014) 75–91, [arXiv:1405.4827].

[227] J. Alison et al., *Higgs boson potential at colliders: Status and perspectives*, *Rev. Phys.* **5** (2020) 100045, [arXiv:1910.00012].

[228] S. Dawson, I. M. Lewis, and M. Zeng, *Threshold resummed and approximate next-to-next-to-leading order results for W^+W^- pair production at the LHC*, *Phys. Rev. D* **88** (2013), no. 5 054028, [arXiv:1307.3249].

[229] Y. Wang, C. S. Li, Z. L. Liu, and D. Y. Shao, *Threshold resummation for $W^\pm Z$ and ZZ pair production at the LHC*, *Phys. Rev. D* **90** (2014), no. 3 034008, [arXiv:1406.1417].

[230] Y. Wang, C. S. Li, and Z. L. Liu, *Resummation prediction on gauge boson pair production with a jet veto*, *Phys. Rev. D* **93** (2016), no. 9 094020, [arXiv:1504.00509].

[231] M. Grazzini, S. Kallweit, D. Rathlev, and M. Wiesemann, *Transverse-momentum resummation for vector-boson pair production at NNLL+NNLO*, *JHEP* **08** (2015) 154, [arXiv:1507.02565].

[232] S. Frixione, *A Next-to-leading order calculation of the cross-section for the production of W+ W- pairs in hadronic collisions*, *Nucl. Phys. B* **410** (1993) 280–324.

[233] R. W. Brown and K. O. Mikaelian, *W^+W^- and Z^0Z^0 Pair Production in $e^+e^-, pp, p\bar{p}$ Colliding Beams*, *Phys. Rev. D* **19** (1979) 922.

[234] M. Bonvini, S. Forte, M. Ghezzi, and G. Ridolfi, *The scale of soft resummation in SCET vs perturbative QCD*, *Nucl. Phys. B Proc. Suppl.* **241-242** (2013) 121–126, [arXiv:1301.4502].

[235] R. Abbate, S. Forte, and G. Ridolfi, *A New prescription for soft gluon resummation*, *Phys. Lett. B* **657** (2007) 55–63, [arXiv:0707.2452].

[236] S. Forte, G. Ridolfi, J. Rojo, and M. Ubiali, *Borel resummation of soft gluon radiation and higher twists*, *Phys. Lett. B* **635** (2006) 313–319, [hep-ph/0601048].

[237] A. Buckley, J. Ferrando, S. Lloyd, K. Nordström, B. Page, M. Rüfenacht, M. Schönherr, and G. Watt, *LHAPDF6: parton density access in the LHC precision era*, *Eur. Phys. J. C* **75** (2015) 132, [arXiv:1412.7420].

[238] L. Harland-Lang, A. Martin, P. Motylinski, and R. Thorne, *Parton distributions in the LHC era: MMHT 2014 PDFs*, *Eur. Phys. J. C* **75** (2015), no. 5 204, [arXiv:1412.3989].

[239] https://github.com/melli1992/resummation/tree/master/src.

[240] W. E. Caswell, *Asymptotic Behavior of Nonabelian Gauge Theories to Two Loop Order*, *Phys. Rev. Lett.* **33** (1974) 244.

[241] D. Jones, *Two Loop Diagrams in Yang-Mills Theory*, *Nucl. Phys. B* **75** (1974) 531.

[242] E. Egorian and O. Tarasov, *Two Loop Renormalization of the {QCD} in an Arbitrary Gauge*, *Teor. Mat. Fiz.* **41** (1979) 26–32.

[243] O. Tarasov, A. Vladimirov, and A. Zharkov, *The Gell-Mann-Low Function of QCD in the Three Loop Approximation*, *Phys. Lett. B* **93** (1980) 429–432.

[244] S. A. Larin and J. A. M. Vermaseren, *The three loop qcd beta function and anomalous dimensions*, *Phys. Lett. B* **303** (1993) 334–336, [hep-ph/9302208].

[245] S. Catani, M. L. Mangano, and P. Nason, *Sudakov resummation for prompt photon production in hadron collisions*, *JHEP* **07** (1998) 024, [hep-ph/9806484].

[246] A. Vogt, *Next-to-next-to-leading logarithmic threshold resummation for deep inelastic scattering and the Drell-Yan process*, *Phys. Lett. B* **497** (2001) 228–234, [hep-ph/0010146].

[247] S. Catani, D. de Florian, and M. Grazzini, *Higgs production in hadron collisions: Soft and virtual QCD corrections at NNLO*, *JHEP* **05** (2001) 025, [hep-ph/0102227].

Summary

In this summary I will explain the topic of this thesis for a broader audience, trying to convey the essence of the research I conducted in the past years without too much technical detail.

The work presented in this thesis is a theoretical study in the field of particle physics, the realm of physics that describes the fundamental building blocks of nature and their interactions. From our everyday perspective, this *quantum* world at length scales much, much smaller than the size of molecules and even atoms may seem very remote. However, using advanced machinery such as the Large Hadron Collider (LHC) at CERN, we can study the properties and behaviour of these particles nonetheless. This is primarily done by carefully analysing the remnants of highly energetic collisions between protons that move at nearly the speed of light. While protons and neutrons are the constituents of atomic nuclei, they are comprised of yet smaller particles themselves: the up- and down quarks. Together with the electron and an associated neutral particle that barely interacts (the neutrino), these are what we call the fundamental particles of matter.[1] They are supplemented by four force carriers that govern their interactions, of which the photon is most familiar: the particle interpretation of light. The final link is the Higgs field, which determines the masses of the other particles. The Higgs *boson* is the observable excitation of this field and was discovered in 2012 in the ATLAS and CMS experiments at the LHC, which completed the so-called Standard Model (SM) of particle physics. The properties of these particles and their interactions are being tested extensively in many experiments and so far the SM agrees very well with the data.

Even though the SM provides an extremely accurate description of that quantum world in many aspects, some phenomena cannot be explained in this framework. A notable example is the apparent existence of a type of matter in the universe that we cannot see with our present detectors: dark matter. We observe, for example, a higher than expected speed at which stars orbit the centre of their galaxy. This is best explained by the presence of matter

[1] In fact there are two additional, more exotic copies of this set of particles containing heavier siblings. Moreover, there exists for almost all particles an *antiparticle* which has opposite charges, e.g. an electron with a *positive* electric charge that is aptly called the positron.

that has gravitational pull but barely interacts otherwise. In almost all models that try to explain such puzzling observations, newly proposed particles are the ideal candidate. This is what is often called *new* physics or Beyond the Standard Model (BSM) physics. While new particles with a small mass might show up in experiments as a clear signal, heavier particles would only give rise to very subtle effects in measured quantities that are dominated by familiar SM processes. The discovery of such a particle thus hinges on excellent experimental precision, as well as on an equally good understanding of what contribution is expected from SM physics alone. To this end, theorists try to make very precise predictions of the latter. Discovery of new physics then happens if the discrepancy between the SM prediction and the measured value of some observable is significant.

Such predictions are made by calculating probabilities (called cross sections) that certain particles are created in the scattering process of the initial state particles. We do so by diagrammatically representing the scattering, as in fig. S.1a, and accounting for increasingly complex interactions that give rise to the same reaction product or final state. To each of the lines drawn in such *Feynman diagrams*, certain mathematical expressions are associated. Together, upon evaluation, they give the quantum mechanical *scattering amplitude*, from which the cross section follows. In fig. S.1a we "calculate" the probability that a quark (denoted by q) from one proton, and an anti-quark ($\bar{q}$) from a proton in the opposite beam collide and produce an electron (e^-) and a positron (its antiparticle, e^+). In this process the quark and antiquark cancel one another due to their exact opposite properties (called annihilation), leaving only a large amount of energy in the form of a photon (indicated by γ^*). The energy stored in this photon renders it unstable, such that it subsequently decays into the electron-positron pair. This relatively simple interaction is called the Drell-Yan process and is denoted by $q + \bar{q} \to e^- + e^+$. We often use it in this thesis as a testing ground for the development of new theoretical tools.

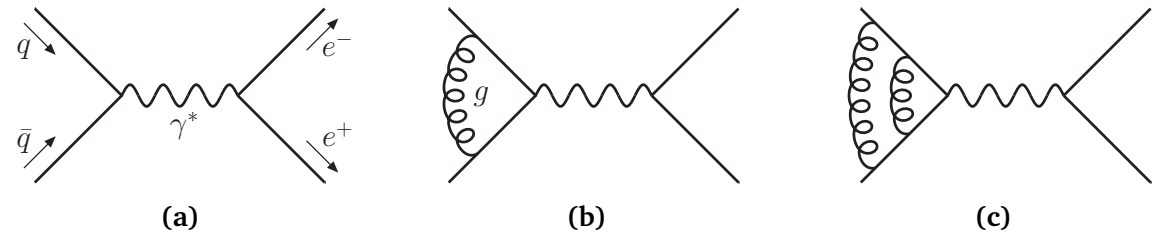

Figure S.1: *Contributions to the Drell-Yan process at the lowest order in perturbation theory* ***(a)****, at the one-loop level* ***(b)*** *and at the two-loop level* ***(c)****. Time progresses from left to right.*

An additional contribution to this process is given by fig. S.1b, where the colliding quark and antiquark exchange a gluon (g) first, meaning that they perceive each others presence prior to their annihilation, as magnets that are brought together. Such an additional contribution is what we call a *loop-correction*, and is already quite a bit harder to calculate since the closed loop requires one to sum (or in fact, integrate) over the various ways in which energy may now flow through the particles that are part of that loop. Typically, one shall find that the contribution to the cross section from such a loop-correction is smaller than that

from the leading-order approximation of fig. S.1a. This is due to the fact that the coupling of the gluon to the quark is rather weak for such a collision, such that each coupling suppresses the probability even further. We would find that the one-loop diagram in fig. S.1b contributes about one tenth of the leading-order cross section in fig. S.1a, while the even more complicated interaction involving two loops in fig. S.1c gives an enhancement of the total probability at the percent level. One can thus improve a prediction step-by-step, by calculating more and more involved diagrams that yield increasingly smaller corrections. This approach is called *perturbation theory*. At the same time the number of diagrams that contribute at a particular order grows enormously. For both the Drell-Yan process and Higgs production, the state-of-the-art calculation is at an impressive three-loop order, requiring the computation of millions of diagrams.

A complication is that, in addition to the loop effects we just discussed, these cross sections also receive corrections from the *emission* of gluons that end up in the final state, as shown in fig. S.2. If this gluon is low-energetic, or as we say *soft*, it is not identified by the detector, such that this event is also regarded as electron-positron production, rather than electron-positron-gluon production. One might expect these contributions to get smaller with increasing number of emissions, given that there is again powers of the coupling involved. In spite of this effect, such corrections turn out to be large *at every order* in the coupling (so approximately the same size for one, two, three, etc. soft emissions) because they give rise to logarithms in the energy (ζ) carried by the emitted gluon(s), which become large if the gluons are soft. Given that this occurs if the original final state particles (in this case the electron-positron pair) are produced near *threshold*, that is when the colliding quark-antiquark pair has just a little bit more energy than needed to produce them, we often speak of threshold effects in the context of soft emissions. In this case perturbation theory is of little help, and good predictions are only obtained by summing these *threshold logarithms* to all orders in the coupling, effectively accounting for the possibility of a single gluon up to an infinite amount of such soft emissions. This is what we call *resummation*. In order to make such bold statements about the all-order cross section, we must make some approximations to simplify the calculational rules.

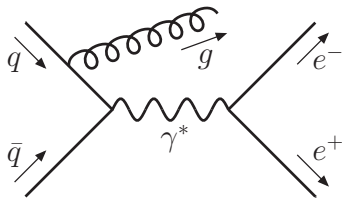

Figure S.2: *Correction to the Drell-Yan process involving an emitted gluon.*

Such threshold corrections are historically studied in the leading power (LP) soft limit, which is the simplest approximation one can make for soft emissions. In that case, all subsequent emissions are largely independent of one another and the resummation is easily obtained. Despite the crude nature of the approximation, the resummation of resulting LP threshold logarithms has proven to be very valuable for many theory predictions. As an improvement, one may retain the effect of the first subleading term in this soft expansion. These are what

we call next-to-leading power (NLP) threshold corrections, in which important physical effects such as recoil and spin (a quantum number associated to each particle) are included for the first time, thus retaining more information of the soft gluon and the particle that emits it. Describing scattering processes at this level of accuracy should therefore improve predictions based on resummation even further.

In this thesis, we study various aspects of such NLP threshold corrections. In chapter 2 we focus on the NLP *factorisation* structure of scattering amplitudes up to arbitrary loop orders in case a single soft photon is emitted.[2] Factorisation means the division of scattering processes into sub-amplitudes, that contain particles that behave similarly (e.g. all moving in the same direction, or all being soft). Such a categorisation aids in deriving resummation since it allows one to systematically organise the various sources of the threshold logarithms. In this chapter we give a first exhaustive classification at NLP in a diagrammatic way for Quantum Electrodynamics (QED), revealing interesting new contributions. We calculate some of these new ingredients and test part of the factorisation formula at one- and two-loop order, explicitly showing how it accounts for nontrivial effects. In chapter 3 we explore the NLP effects for the Drell-Yan process, in case of a single loop correction and in presence of two soft gluon emissions. We come across a new contribution, which is understood to originate from a term in the factorisation formula presented in chapter 2. This study, aimed to provide detailed theoretical data to test future multi-emission factorisation approaches, thereby underlines the rich structure of scattering amplitudes at NLP. Only part of terms are directly relatable to lower order factorisation ingredients, however, the most important threshold contributions at NLP (the highest power of the threshold logarithm) are fully understood. We then show in chapter 4 how these *leading logarithms* can be resummed at the NLP level, for various processes. Finally, we study the numerical impact of NLP terms in chapter 5, on both fixed-order and resummed cross sections for Drell-Yan and Higgs production.[3] We observe that the resummation of NLP leading logarithms has a clear effect on the overall result, especially compared to further upgrading the logarithmic accuracy of LP resummation, which has been the primary way of improving resummed predictions historically. We thus conclude that NLP effects of soft emissions are sizeable, justifying the current interest in this field, and motivating further study.

It is my hope that the advances presented in this thesis may contribute to future theory predictions for collider experiments, and thereby help to further shape our understanding of nature.

[2] In addition, we study the structure of non-radiative amplitudes in case the mass of matter particles is kept small but non-zero.

[3] We also study resummation effects for the production of two Higgs bosons or two force carriers (ZZ and W^+W^-), albeit in less detail.

Samenvatting

In deze samenvatting zal ik het onderwerp van dit proefschrift uitleggen voor een breder publiek en proberen de essentie van het onderzoek dat ik in de afgelopen jaren heb uitgevoerd over te brengen zonder al te veel technische aspecten te bespreken.

Het werk dat in dit proefschrift wordt beschreven is een theoretische studie in het veld van de deeltjesfysica, het deelgebied van de natuurkunde dat de fundamentele bouwstenen van de natuur en hun interacties beschrijft. Vanuit ons alledaagse perspectief lijkt deze *quantum* wereld, op lengteschalen heel veel kleiner dan het formaat van moleculen en zelfs atomen, wellicht erg ver weg. Desalniettemin kunnen we met geavanceerde apparatuur zoals de deeltjesversneller bij CERN, de *Large Hadron Collider* (LHC), de eigenschappen en het gedrag van deze deeltjes bestuderen. Dit wordt voornamelijk gedaan door het aandachtig analyseren van de restanten van hoog energetische botsingen tussen protonen die haast met de lichtsnelheid bewegen. Terwijl protonen en neutronen de onderdelen zijn van atoomkernen, bestaan zij zelf uit nog kleinere deeltjes: de up- en down-quarks. Tezamen met het elektron en een bijbehorend neutraal deeltje dat nauwelijks interacteert (het neutrino), vormen zij de fundamentele materiedeeltjes.[4] Zij worden aangevuld met vier krachtdeeltjes die hun interacties bepalen, waarvan het foton als lichtdeeltje het bekendste is. De laatste schakel is het Higgs veld, welke de massa van alle andere deeltjes bepaalt. Het Higgs *deeltje* is de waarneembare excitatie van dit veld en is in 2012 ontdekt in de ATLAS en CMS experimenten bij de LHC, die het zogeheten Standaard Model (SM) van de deeltjesfysica completeert. De eigenschappen en interacties van deze deeltjes worden uitgebreid getest in tal van experimenten en vooralsnog komt het SM uitstekend overeen met de data.

Ondanks dat het SM veel aspecten van deze quantum wereld uitstekend beschrijft, zijn er fenomenen die niet verklaard kunnen worden middels dit kader. Een noemenswaardig voorbeeld is het klaarblijkelijke bestaan van een soort materie in het universum die we

[4] Er zijn in feite nog twee, meer exotische kopieën van deze set deeltjes die zwaardere varianten bevatten. Bovendien bestaat er voor bijna elk deeltje een *antideeltje* met tegenovergestelde ladingen, bijvoorbeeld een elektron met *positieve* elektrische lading welke de toepasselijke naam positron draagt.

niet kunnen zien met onze huidige detectoren: donkere materie. We observeren bijvoorbeeld een hoger dan verwachte snelheid waarmee sterren om het centrum van hun sterrenstelsel cirkelen. Dit kan het beste verklaard worden door de aanwezigheid van materie die wel zwaartekrachtswerking heeft, maar verder nauwelijks interacties ondergaat. In bijna alle modellen die zulke raadselachtige observaties proberen te verklaren zijn nieuw geïntroduceerde deeltjes de beste kandidaat. Dit is wat *nieuwe* fysica genoemd wordt of natuurkunde *voorbij* het Standaard Model. Terwijl lichte nieuwe deeltjes eventueel in experimenten kunnen verschijnen als een duidelijk signaal, zouden zwaardere deeltjes enkel een subtiel effect geven op meetbare grootheden die gedomineerd worden door bekende processen uit het SM. De ontdekking van een nieuw deeltje hangt dus af van uitstekende experimentele precisie én een evengoed begrip van welke bijdrage verwacht kan worden op basis van SM fysica. Daarom proberen theoretici hier zo precies mogelijke voorspellingen van te maken. De ontdekking van nieuwe fysica volgt dan indien de discrepantie tussen de SM voorspelling en de gemeten waarde van een relevante observabele significant is.

Deze voorspellingen worden gemaakt door het berekenen van kansen (ofwel botsingsdoorsneden) dat bepaalde deeltjes gecreëerd worden in het verstrooiingsproces van de deeltjes in de initiële toestand. Dat doen we door het diagrammatisch weergeven van de verstrooiing zoals in fig. S.1a, en het meenemen van steeds ingewikkeldere interacties die leiden tot dezelfde uiteindelijke toestand (het reactie product). Aan elk van de getekende lijnen in zulke *Feynman diagrammen* zijn wiskundige uitdrukkingen verbonden. Wanneer deze tezamen geëvalueerd worden geeft dat de quantum mechanische *verstrooiingsamplitude*, waaruit de botsingsdoorsnede voortkomt. In fig. S.1a "berekenen" we de kans dat een quark (weergegeven als q) uit het ene proton botst met een antiquark ($\bar{q}$) uit een tegemoetkomend proton, en samen een elektron (e^-) en een positron (zijn antideeltje, e^+) produceren. In dit proces heffen het quark en het antiquark elkaar op vanwege hun tegengestelde eigenschappen (annihilatie genoemd) en blijft enkel een grote hoeveelheid energie achter in de vorm van een foton (aangegeven met γ^*). De opgeslagen energie maakt het foton instabiel, zodat het vervolgens vervalt in het elektron-positron paar. Deze relatief eenvoudige interactie heet het Drell-Yan proces en wordt weergegeven als $q + \bar{q} \to e^- + e^+$. We gebruiken het in dit proefschrift regelmatig als een proeftuin voor de ontwikkeling van nieuwe theoretische inzichten en rekenkundige technieken.

Een extra bijdrage aan dit proces is weergegeven in fig. S.1b, waar het botsende quark en antiquark eerst een gluon (g) uitwisselen. Dit betekent dat zij elkaars aanwezigheid voelen alvorens zij annihileren, als magneten die samen gebracht worden. Deze extra bijdrage is wat we een *lus-correctie* noemen en is al een stuk lastiger om uit te rekenen, doordat de gesloten lus impliceert dat we moeten sommeren (in feite integreren) over alle mogelijke manieren waarop de energie door de deeltjes in die lus kan vloeien. Doorgaans zal men vinden dat de bijdrage aan de botsingsdoorsnede van een dergelijke lus-correctie kleiner is dan die van de laagste-orde benadering in fig. S.1a. Dit komt doordat de koppeling van het gluon aan het quark relatief zwak is voor een typische botsing, zodat iedere extra koppeling de kans verder drukt. We zouden vinden dat het één-lus diagram in fig. S.1b ongeveer een tiende bijdraagt van de laagste-orde botsingsdoorsnede uit fig. S.1a, terwijl de nog

ingewikkeldere interactie met twee lussen in fig. S.1c een bijdrage geeft aan de totale kans op het procent niveau. Men kan voorspellingen zodoende stap voor stap verbeteren, door steeds ingewikkeldere diagrammen uit te rekenen die steeds kleinere correcties geven. Deze aanpak heet *storingstheorie*. Tegelijkertijd groeit het aantal diagrammen dat bijdraagt op een bepaalde orde enorm. Voor zowel het Drell-Yan proces als voor Higgs productie is de meest geavanceerde berekening op een indrukwekkend drie-lus niveau, wat het uitrekenen van miljoenen diagrammen vereist.

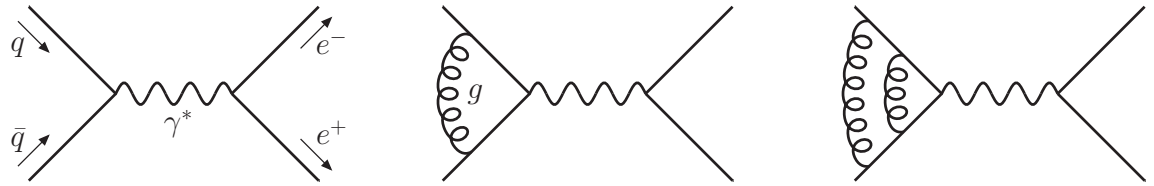

Figuur S.1: *Bijdragen aan het Drell-Yan proces op de laagste orde in storingstheorie **(a)**, op het één-lus niveau **(b)** en op het twee-lus niveau **(c)**. De tijd verstrijkt van links naar rechts.*

Een complicatie is dat, bovenop de lus-effecten die we zojuist besproken hebben, de botsingsdoorsneden ook bijdragen ontvangen van de *emissie* van gluonen die onderdeel worden van de uiteindelijke toestand, zoals weergegeven in fig. S.2. Wanneer dit gluon laag energetisch is, of *zacht*, wordt het niet geïdentificeerd in de detector, met als resultaat dat dit proces ook als elektron-positron productie wordt geoormerkt in plaats van als elektron-positron-gluon productie. Men zou wellicht verwachten dat deze bijdragen ook kleiner worden met toenemend aantal emissies, gegeven dat er wederom machten van de koppeling in het spel zijn. Desondanks blijken zulke correcties groot te zijn *op iedere orde* in de koppeling (dus ongeveer even groot voor één, twee, drie, etc. zachte emissies), omdat ze leiden tot logaritmen in de energie (ζ) van de geëmitteerde gluonen, welke groot worden indien de gluonen zacht zijn. Dit gebeurt wanneer het botsende quark-antiquark paar net meer energie heeft dan de *drempelwaarde*: de minimale energie die nodig is om de deeltjes in de uiteindelijke toestand op laagste orde (in dit geval het elektron-positron paar) te produceren. Zodoende spreken we vaak van *drempel-effecten* als het gaat over zachte emissies. In dit geval is storingstheorie niet goed toepasbaar en kunnen goede voorspellingen alleen worden verkregen door deze *drempel-logaritmen* tot op alle ordes in de koppeling te sommeren, daarmee tegelijkertijd rekening houdend met de mogelijkheid van één tot een oneindige hoeveelheid van dergelijke zachte emissies. Dit wordt *hersommatie* genoemd. Om zulke gewaagde uitspraken te kunnen doen over de botsingsdoorsnede tot op alle ordes moeten we wel wat benaderingen maken om de rekenregels te versimpelen.

Van oudsher werden deze drempel-correcties bestudeerd in de leidende-macht (*leading power*, LP) zachte limiet, hetgeen de simpelste benadering is die men kan maken voor zachte emissies. In dat geval zijn alle opeenvolgende emissies grotendeels onafhankelijk van elkaar en volgt hersommatie gemakkelijk. Ondanks de ruwe aard van deze benadering heeft de hersommatie van de bijpassende LP drempel-logaritmen bewezen van groot belang te zijn

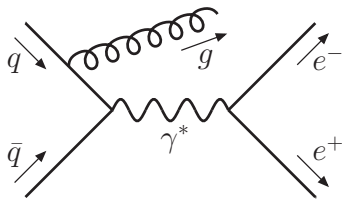

Figuur S.2: *Bijdrage aan het Drell-Yan proces met een enkele gluon-emissie.*

voor vele theoretische voorspellingen. Als verbetering kan men het effect van de eerste subdominante term in deze zachte benadering behouden. Dit is wat we op-één-na-leidende macht (*next-to-leading power*, NLP) drempel-correcties noemen, waarin belangrijke fysische effecten zoals terugslag en spin (een quantum getal dat ieder deeltje draagt) voor de eerste keer worden meegenomen en zodoende meer informatie over het zachte gluon en het deeltje dat het emitteert behouden blijft. Het beschrijven van verstrooiingsprocessen met deze precisie zou daarom op hersommatie gebaseerde voorspellingen verder moeten verbeteren.

In dit proefschrift bestuderen we verschillende aspecten van deze NLP drempel-correcties. In hoofdstuk 2 focussen we op de NLP factorisatie-structuur van verstrooiingsamplitudes met een willekeurig aantal lussen in het geval een enkel zacht foton wordt geëmitteerd.[5] Factorisatie betekent het opdelen van een verstrooiingsproces in sub-amplitudes die enkel deeltjes bevatten die gelijk gedrag vertonen (bijvoorbeeld allemaal in dezelfde richting bewegend, of allemaal zacht zijn). Deze categorisatie helpt in het afleiden van hersommatie aangezien het de mogelijkheid biedt om op systematische wijze de verschillende bronnen van drempel-logaritmen te organiseren. In dit hoofdstuk geven we voor het eerst een uitputtende diagrammatische classificatie op NLP niveau voor Quantum Elektrodynamica (QED), en leggen we interessante nieuwe bijdragen bloot. We berekenen enkele van deze nieuwe ingrediënten en testen een deel van de factorisatie-formule op één- en twee-lus niveau, wat laat zien dat de factorisatie niet-triviale effecten correct beschrijft. In hoofdstuk 3 verkennen we de NLP effecten voor het Drell-Yan proces, in het geval van een enkele lus-correctie en met twee zachte gluon-emissies. We vinden hier een nieuwe bijdrage, waarvan we de oorsprong kunnen toeschrijven aan een term in onze factorisatie-formule uit hoofdstuk 2. Deze studie, bedoeld om gedetailleerde theoretische data te produceren waarmee een toekomstige factorisatie-aanpak voor multi-emissie amplitudes getest kan worden, onderstreept daarmee de rijke structuur van verstrooiingsamplitudes op NLP niveau. Enkel een gedeelte van het resultaat is direct te relateren aan lagere-orde factorisatie-ingrediënten, maar de belangrijkste drempel-bijdragen op NLP (de hoogste macht van het drempel-logaritme) zijn volledig begrepen. We laten vervolgens in hoofdstuk 4 zien hoe deze *leidende logaritmen* gehersommeerd kunnen worden op het NLP niveau, voor diverse processen. Tot slot bestuderen we de numerieke impact van NLP termen in hoofdstuk 5, op zowel eindige-orde als gehersommeerde botsingsdoorsneden voor Drell-Yan en Higgs productie.[6] We vinden

[5] Daarnaast bestuderen we de structuur van amplitudes zonder extra emissie in het geval de massa van materie deeltjes klein, maar niet nul, gekozen wordt.

[6] We beschouwen ook hersommatie effecten voor de productie van twee Higgs deeltjes of twee krachtdeeltjes (ZZ en W^+W^-), zij het in minder detail.

dat de hersommatie van de leidende logaritmen op NLP een duidelijk effect heeft op het totale resultaat, in het bijzonder vergeleken met het verhogen van de logaritmische precisie van de LP hersommatie, wat van oudsher de voornaamste manier is om gehersommeerde voorspellingen te verbeteren. We concluderen dat NLP effecten van zachte emissies omvangrijk zijn, hetgeen de huidige interesse in dit veld verantwoordt en motivatie biedt voor vervolgstudies.

Het is mijn hoop dat de in dit proefschrift gepresenteerde bevindingen zullen bijdragen aan toekomstige theoretische voorspellingen voor deeltjesfysica experimenten, en daarmee helpen om ons begrip van de wereld om ons heen verder vorm te geven.

Dankwoord

Allereerst wil ik graag mijn promotor Eric Laenen bedanken voor zijn wijze advies en enthousiaste begeleiding gedurende de voorbije jaren. Ik heb onze samenwerking als erg plezierig ervaren en waardeer de vrijheid die je mij hebt gegeven om te groeien als zelfstandig onderzoeker. Uiteraard ook mijn dank aan Wouter Waalewijn, wiens betrokkenheid als co-promotor van belang geweest is voor het tot stand komen van dit proefschrift en wiens initiatieven hebben geleid tot een prettige en saamhorige onderzoeksgroep.

Ik dank de leescommissie, bestaande uit Stan Bentvelsen, Wim Beenakker, Piet Mulders, Lorenzo Magnea, Marieke Postma en Jordy de Vries, voor de tijd en inspanning die in het beoordelen van het manuscript zijn gaan zitten.

A big thanks to my collaborators, without whom this thesis may not have seen the light of day. In particular to Leonardo Vernazza, with whom I have had countless enthusiastic blackboard sessions in which we tackled problems and posed new questions. That's how progress is made! In addition, I am grateful for Chris White's wisdom and dedication which were instrumental to parts of the work presented here. I also thank Lorenzo Magnea, for both his deep insights and great stories. Visting any of you in Edinburgh, London or Turin was very enjoyable! Of course, a special word of thanks to Melissa van Beekveld and Lorenzo Zoppi, my fellow PhD students. Working side by side, as foot soldiers at the frontiers of physics, has been a pleasure!

I should also mention my office mates: Darren, Eleftheria, Ruben, Jorinde and Solange, who provided the necessary distraction and office banter. I would also like to thank the other members of the Nikhef theory group, for creating such a stimulating yet friendly workspace.

Ik wil ook graag mijn dierbare vrienden bedanken. Zowel diegenen met wie ik de fascinatie voor de natuurkunde heb kunnen delen gedurende onze studie, waaronder mijn paranimfen Jaap en Thom, als diegenen met wie ik zoveel mooie herinneringen aan onze jeugd in Schagen deel en wie gelukkig nog steeds een grote rol in mijn leven spelen. Jullie hebben geholpen een juiste balans te behouden tussen werk en ontspanning, en hebben steun geboden wanneer nodig. Jullie zijn fantastisch!

Dank gaat ook uit naar mijn (schoon)familie voor hun interesse in mijn vakgebied. In grote lijnen uitleggen wat mijn onderzoek behelst bleek altijd een bron van hernieuwd enthousiasme. Ik wil mijn lieve zus danken daar zij immer tijd weet te maken voor mij, zo ook om mee te denken over mijn kaftontwerp. En natuurlijk mijn ouders, wiens liefde, betrokkenheid en vertrouwen het fundament vormen onder dit proefschrift. Ik ben dankbaar uit een hecht gezin te komen waarin hoogte- en dieptepunten met elkaar worden gevierd en doorstaan. Ik hoop nog lang van jullie te mogen genieten.

Bovenal wil ik jou bedanken, lieve Roos. Al zoveel jaren mijn stralende vriendin en metgezel, diegene die mijn leven verlicht en extra kleur geeft. Altijd even lief, begripvol en relativerend, een baken van rust in woelige tijden. Ik ben ontzettend blij met jou!